

STATUS OF THESIS

Title of thesis

IMAGING FOR SKIN ROUGHNESS ANALYSIS

I, ESA PRAKASA

hereby allow my thesis to be placed at the Information Resource Centre (IRC) of Universiti Teknologi PETRONAS (UTP) with the following conditions:

- 1. The thesis becomes the property of UTP
- 2. The IRC of UTP may make copies of the thesis for academic purposes only.
- 3. This thesis is classified as

Confidential

Non-confidential

If this thesis is confidential, please state the reason:

\_\_\_\_\_  
\_\_\_\_\_  
\_\_\_\_\_

The contents of the thesis will remain confidential for \_\_\_\_\_ years.

Remarks on disclosure:

\_\_\_\_\_  
\_\_\_\_\_  
\_\_\_\_\_

Signature of Author

Permanent address:  
Pusat Penelitian Informatika  
Lembaga Ilmu Pengetahuan Indonesia  
Jalan Sangkuriang, Cisitua, Bandung  
Indonesia 40135

Date: 3/9/2013

Endorsed by

Signature of Supervisor

Prof. Ir. Dr. Ahmad Fadzil Mohamad Hani, FASc, FIEE,  
Deputy Vice-Chancellor (Academic)  
Universiti-Teknologi PETRONAS

Name of Supervisor  
Prof. Ir. Dr. Ahmad Fadzil  
Bin Mohamad Hani

Date: 3/9/13

UNIVERSITI TEKNOLOGI PETRONAS  
IMAGING FOR SKIN ROUGHNESS ANALYSIS

by

ESA PRAKASA

The undersigned certify that they have read, and recommend to the Postgraduate Studies Programme for acceptance this thesis for the fulfilment of the requirements for the degree stated.

Signature:

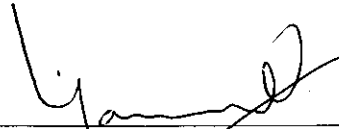


Prof. Ir. Dr. Ahmad Fadzil Bin Mohamad Hani, FASc, FIEM  
Deputy Vice-Chancellor (Academic)  
Universiti Teknologi PETRONAS

Main Supervisor:

Prof. Ir. Dr. Ahmad Fadzil Bin Mohamad Hani

Signature:

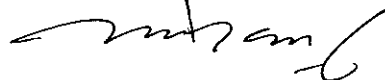


Dr. Vijanth Sagayan Asirvadam  
Associate Professor  
Electrical and Electronic Engineering Dept  
Universiti Teknologi PETRONAS  
31750 Tronoh Perak

Co Supervisor:

Assoc. Prof. Dr. Vijanth Sagayan Asirvadam

Signature:



Head of Department:

Dr. Rosdiazli Bin Ibrahim

Assoc. Prof. Dr. Rosdiazli Bin Ibrahim  
Head of Department  
Electrical and Electronic Engineering Department  
Universiti Teknologi PETRONAS

Date:

06/09/13

IMAGING FOR SKIN ROUGHNESS ANALYSIS

by

EŞA PRAKASA

A Thesis

Submitted to the Postgraduate Studies Programme

as a Requirement for the Degree of

DOCTOR OF PHILOSOPHY

ELECTRICAL AND ELECTRONIC ENGINEERING DEPARTMENT

UNIVERSITI TEKNOLOGI PETRONAS

BANDAR SERI ISKANDAR,

PERAK

AUGUST 2013

## ABSTRAK

Kebanyakan kaedah penilaian kulit digunakan dalam amalan klinikal menggunakan deria visual dan sentuhan pakar dermatologi untuk menilai ciri-ciri dan syarat-syarat penyakit kulit. Walau bagaimanapun, penilaian bersifat subjektif dan menyebabkan perbezaan hasil penilaian antara penilai. Kajian ini menyiasat masalah ukuran kekasaran kulit untuk penilaian luka psoriasis. Psoriasis adalah penyakit kulit yang tidak boleh diubati, menjejaskan 2-3% penduduk dunia. Psoriasis *scaliness* adalah parameter penilaian utama daripada Psoriasis Area and Severity Index (PASI) yang bersifat subjektif. PASI *scaliness* menentukan jumlah sisik pada permukaan luka. Kajian ini mencadangkan penggabungan algoritma 3D *surface roughness* dan teknik *clustering* untuk menentukan markah PASI *scaliness* secara objektif. *High order polynomial surface fitting* digunakan untuk menganggarkan 3D *waviness surface*. Algoritma ini telah disahkan pada kekasaran berstandard dan permukaan melengkung menggunakan 390 model luka dan patung medik. Kekasaran permukaan yang diukur sangat bresesuaian (0,989) kepada model luka dengan pelbagai gred kekasaran dan algoritma juga telah disahkan di permukaan patung medik dengan ketepatan 94,12 %. Algoritma pengukur kekasaran digabungkan dengan algoritma *unsupervised clustering* bagi membolehkan penilaian objektif untuk pemarkahan PASI *scaliness*. Sistem pengklasifikasi ini dibuat dengan menggunakan 1,999 luka psoriasis yang dikumpulkan daripada kajian klinikal melibatkan 204 pesakit di Jabatan Dermatologi, Hospital Kuala Lumpur. Dua kaedah *unsupervised clustering*, *k-means* dan *fuzzy c-means* (FCM) telah digunakan untuk membuat empat kelompok yang ditakrifkan untuk mewakili empat set markah PASI *scaliness*. Teknik statistik kualitatif menggunakan pekali Kappa digunakan dalam kerja-kerja penyelidikan ini untuk menilai variasi penilaian antara dua pakar dermatologi dan dua imbasan pengukuran 3D berturutan pada 324 luka. Pekali Kappa antara dua pakar dermatologi didapati 0.55 (dengan itu tidak boleh dianggap sebagai *ground truth*) manakala pekali Kappa antara dua imbasan pengukuran 3D secara berturutan adalah 0.8473 (*k-means*) dan 0,8708 (FCM). Kesesuaian hasil penilaian ini dianggap sempurna ( $> 0.81$ ) dan dapat mengurangkan isu subjektiviti. Hasil kajian tesis ini menunjukkan bahawa algoritma yang dibangun membolehkan sistem pengukuran objektif untuk penilaian PASI *scaliness* luka psoriasis dalam amalan klinikal.

In compliance with the terms of the Copyright Act 1987 and the IP Policy of the university, the copyright of this thesis has been reassigned by the author to the legal entity of the university.

Institute of Technology PETRONAS Sdn Bhd.

Due acknowledgement shall always be made of the use of any material contained in, or derived from, this thesis.

© Esa Prakasa, 2013

Institute of Technology PETRONAS Sdn Bhd

All rights reserved

## TABLE OF CONTENTS

STATUS OF THESIS .....	i
APPROVAL PAGE .....	iv
TITLE PAGE .....	iii
DECLARATION OF THESIS .....	iv
ABSTRACT .....	v
ABSTRAK .....	vi
COPY RIGHT PAGE .....	vii
TABLE OF CONTENTS .....	viii
LIST OF TABLES .....	xi
LIST OF FIGURES .....	xiii
CHAPTER 1 INTRODUCTION .....	1
1.1 Background and Motivation of Research .....	1
1.2 Problem Statements .....	6
1.3 Research Hypothesis .....	10
1.4 Research Objectives .....	11
1.5 Scope of Work .....	12
1.6 Organisation of the Thesis .....	13
CHAPTER 2 MEDICAL LITERATURE REVIEW .....	15
2.1 Skin Structure .....	15
2.2 Clinical Features of Psoriasis .....	16
2.2.1 Plaque psoriasis .....	20
2.2.2 Guttate psoriasis .....	20
2.2.3 Flexural (inverse) psoriasis .....	21
2.2.4 Generalised pustular psoriasis .....	21
2.2.5 Erythrodermic psoriasis .....	22
2.3 Skin Assessment and Analysis .....	23
2.3.1 Subjectivity of Skin Assessment .....	25
2.3.2 PASI Scoring for Psoriasis Assessment .....	27
2.4 Summary .....	30
CHAPTER 3 SURFACE MEASUREMENT METHODS .....	31

3.1 Surface Roughness Analysis .....	32
3.2 Mechanical Surface Profilometry .....	32
3.3 Imaging Technologies for Surface Analysis .....	33
3.3.1 Laser Profilometry Method .....	35
3.3.2 Light Scattering and Speckle Imaging Methods .....	36
3.3.3 Structured Light Projection Method .....	38
3.4 Surface Profile Characterisation .....	42
3.4.1 Fourier Transform .....	44
3.4.2 Gaussian Filter .....	44
3.4.3 Wavelet Filter .....	44
3.4.4 Polynomial Surface Fitting .....	45
3.5 Surface Roughness Parameter .....	46
3.6 Imaging Methods for Skin Surface Roughness Measurement .....	48
3.7 Summary .....	52
CHAPTER 4 DEVELOPMENT ON SURFACE ROUGHNESS ALGORITHM .....	56
4.1 Surface Roughness as Scaliness Parameter for PASI Scoring .....	56
4.2 Surface Roughness Algorithm .....	57
4.2.1 Polynomial Surface Fitting .....	58
4.2.2 Surface Roughness Calculation .....	59
4.3 Validation Study .....	67
4.3.1 Surface Roughness Measurement: Abrasive Paper .....	67
4.3.2 Surface Roughness on Curve Surface: Mannequin Surface .....	69
4.4 Performance Analysis .....	74
4.4.1 Determination on Measurement Accuracy .....	74
4.4.2 Evaluation on Rotational Invariance .....	75
4.4.3 Sample Area for Surface Roughness Determination .....	77
4.5 Summary .....	85
CHAPTER 5 DEVELOPMENT ON SURFACE ROUGHNESS ALGORITHM .....	87
5.1 Study Set-up and Data Collection .....	87
5.1.1 Sample Size Measurement .....	87
5.1.2 Data Collection Procedure .....	90
5.1.3 Data Profile of Recruited Patients in Clinical Study .....	94

5.2 Clustering Algorithm Classifying Surface Roughness .....	97
5.3 The Agreement Analysis of Psoriasis Assessment .....	118
5.4 Summary .....	122
CHAPTER 6 CONCLUSION AND RECOMMENDATION .....	126
6.1 Conclusion .....	126
6.2 Recommendations for Further Work .....	130
REFERENCES .....	132
APPENDIX A: SURFACE ROUGHNESS OF LESION MODEL AT FLAT SURFACES .....	144
APPENDIX B: SURFACE ROUGHNESS OF LESION MODEL AT CURVE SURFACES .....	147
APPENDIX C: TRAINING DATASET OF PSORIASIS LESION .....	157
APPENDIX D: SCORING RESULTS BY APPLYING CLUSTERING ALGORITHM ON TESTING DATASET .....	188
APPENDIX E: APPROVAL OF OBSERVATIONAL CLINICAL STUDY (NMRR-09-1098-4863) .....	197
APPENDIX F: SOURCE CODE OF SURFACE ROUGHNESS DETERMINATION (MATLAB CODE) .....	198
APPENDIX G: SOURCE CODE OF CLUSTERING (FCM) IMPLEMENTATION FOR SCORING SCALINESS (MATLAB CODE) .....	205
APPENDIX H: LIST OF PUBLICATIONS : .....	211
APPENDIX I: PATENT DOCUMENT OF SCALINESS ALGORITHM .....	215
APPENDIX J: CERTIFICATE OF AWARD (ITEX 2009) .....	216
APPENDIX K: CERTIFICATE OF AWARD (INNOVA 2010) .....	217
APPENDIX L: CERTIFICATE OF AWARD (MTE 2012) .....	218

## LIST OF TABLES

Table 2.1 Features for PASI scaliness scoring used by dermatologists.....	29
Table 3.1 Comparison of 3D acquisition methods for surface measurement.....	52
Table 4.1 The surface roughness of abrasive paper.....	68
Table 4.2 The surface roughness of lesion models at a flat surface .....	70
Table 4.3 The distribution of lesion models on the body regions of mannequin .....	72
Table 4.4 The surface roughness of lesion models at a flat surface .....	73
Table 4.5 Performance evaluation of the surface roughness algorithm.....	75
Table 4.6 The normal skin surface roughness of 9 subjects with a size variation.....	81
Table 4.7 The threshold points of minimum sampling area. ....	84
Table 5.1 Statistics of the scaliness value for each score. ....	89
Table 5.2 Sample sizes of scaliness score 1 with $\alpha=0.05$ (confidence level 95%) and maximum difference variations.....	90
Table 5.3 Distribution of PASI Scaliness Score (N=1,892). ....	96
Table 5.4 Centroid of PASI scaliness scores. ....	103
Table 5.5 Score centroids of subset 1 and 2. ....	104
Table 5.6 Score centroids of subset 1, 2, and 3. ....	104
Table 5.7 Boundary levels of surface roughness for PASI scaliness score. ....	104
Table 5.8 Average of Euclidean distances of surface roughness and boundary levels of $k$ -means classification algorithm.....	107
Table 5.9 Average of Euclidean distances of surface roughness and boundary levels determined from correct classification cases of $k$ -means algorithm. ....	107
Table 5.10 The surface roughness ranges near the boundary levels of $k$ -means classification algorithm. ....	107
Table 5.11 Coefficients of Gaussian functions for the roughness classification of PASI scaliness scores. ....	113
Table 5.12 Calculations of PASI scaliness scores by applying FCM algorithm ....	114
Table 5.13 Average of Euclidean distances of surface roughness and boundary levels of FCM classification algorithm.....	117
Table 5.14 Average of Euclidean distances of surface roughness and boundary levels determined from correct classification cases of FCM algorithm. ....	117
Table 5.15 The surface roughness ranges near the boundary levels of FCM classification algorithm. ....	118
Table 5.16 Scoring results of two observers, $O1$ and $O2$ . ....	119

Table 5.17 Summary of agreement from scoring by two observers. ....	119
Table 5.18 Agreement interpretation of Kappa coefficient. ....	120
Table 5.19 Summary of agreement from scoring by dermatologists. ....	121
Table 5.20 Summary of agreement from scoring by applying <i>k</i> -means algorithm. ....	121
Table 5.21 Summary of agreement from scoring by applying FCM algorithm. ....	121
Table 5.22 Comparison of Kappa coefficients using <i>k</i> -means and FCM. ....	121
Table 6.1 Comparison of skin surface roughness measurements. ....	129

## LIST OF FIGURES

Figure 1.1 Plaque psoriasis lesions grow on several body regions (left to right): head, upper limb, trunk, and lower limb regions.....	2
Figure 1.2 Human skin is composed by several skin layers [11]. .....	3
Figure 1.3 The stages of skin growing at epidermis layers. The picture is reproduced from [15], [16], [17]. .....	5
Figure 1.4 Psoriasis lesions are found in various parts of the body such as trunk (1), upper limb (2), lower limb, elbow (4), and forehead (5).....	5
Figure 1.5 Patterns of rosacea blood vessels are acquired by (a) digital camera and (b) microscope.....	8
Figure 1.6 Cross-sectional view of a skin lesion on normal skin surface.....	11
Figure 1.7 An example of 3D lesion surface obtained from psoriasis patient.....	12
Figure 2.1 Skin histology of (a) normal skin and (b) skin affected by psoriasis [36]. .....	18
Figure 2.2 Common locations of psoriasis lesions growing on human skin. The picture is created by combining graphic materials and description from [40] [41] [42]. .....	19
Figure 2.3 Plaque psoriasis lesions appear at several body regions such as (a) elbow, (b) upper back, and (c) trunk. ....	20
Figure 2.4 Example of guttate psoriasis lesions. These lesions are spread at several body regions such as (a) chest and arm [44], (b) forearm [45] and (c) back region [45]. .....	21
Figure 2.5 Flexural psoriasis growths lesions are appeared at folded skin areas. The areas such as (a) armpit [37], (b) ear [46], and (c) umbilicus. ....	21
Figure 2.6 Many pustules scatter on the inflamed skin affected by generalised pustular psoriasis at (a) palm [47], (b) upper back [48], and (c) neck [49] regions. ....	22
Figure 2.7 Erythrodermic psoriasis covers most of body surfaces at areas such as (a) trunk [51], (b) lower limbs [52], and (c) hand including wrist area [53]. .....	23
Figure 2.8 Two dermatologists are assessing psoriasis lesions. ....	26
Figure 2.9 An example of PASI scores summary obtained from dermatologist assessment to a psoriasis patient.....	28
Figure 2.10 Psoriasis lesions and its PASI scaliness scores given by human visual and tactile perceptions [75]. .....	29
Figure 3.1 Stylus and optical measurements. ....	34
Figure 3.2 Laser triangulation of laser camera. ....	35

Figure 3.3 (a) 2D image of psoriasis lesions (b). 3D surface of psoriasis lesions is scanned by a 3D laser scanner. ....	36
Figure 3.4 The light is uniformly reflected at (a) smooth surface whereas (b) the rough surfaces will scatter the light to various directions. ....	37
Figure 3.5 Intensity distributions of reflected light from (a) smoother surface and (b) rougher surfaces. ....	38
Figure 3.6 Diagram for depth calculation based on phase differences. ....	41
Figure 3.7 Surface profile is composed by three major components - roughness, waviness, and form [89] [90] [78]. ....	42
Figure 3.8 Wavelength distributions of roughness and waviness [78]. ....	43
Figure 3.9 Wavelength distributions of roughness and waviness [91]. ....	45
Figure 3.10 Sample categorisation based on the coverage area of the sample. ....	46
Figure 3.11 Three main groups of surface roughness parameters. ....	47
Figure 4.1 3D surfaces of (a) normal skin, psoriasis lesion (b) score 1, and (c) score 4; (d) Rough profiles of normal skin (solid line), lesion score 1 (dotted line), and lesion score 4 (dashed line). ....	57
Figure 4.2 The cross-sectional view of a skin lesion on normal skin surface .....	57
Figure 4.3 Flowchart of the surface roughness algorithm. ....	60
Figure 4.4 The segmented rough surface of the lesion model and its 4×4 subdivided surfaces. ....	61
Figure 4.5 The 3D surfaces involved in surface roughness determination: (a) lesion surface, (b) estimated waviness, and (c) deviation surface. ....	65
Figure 4.6 Rough surface and fitted profiles of a lesion model. The first, second, third and fourth orders are applied to determine the fitted profiles. ....	66
Figure 4.7 (a) 3D surface of a lesion model. (b) – (e) The estimated waviness and deviation surfaces that are determined by applying several different fitting orders. ....	67
Figure 4.8 The 2D and 3D images of abrasive papers used in the surface roughness validation: The roughness grades are (a) 16, (b) 24, (c) 60, (d) 80, and (e) 280. ....	68
Figure 4.9 Plot of surface roughness vs. 1G (CAMI grade) obtained from measurement on abrasive papers. ....	69
Figure 4.10 (a) Lesion models made of surgical tape are pasted on the flat surfaces of paperboard. (b) A 3D surface of lesion model. ....	70
Figure 4.11 The histogram of lesion models pasted on flat surfaces. ....	71
Figure 4.12 Lesion model (20×11.5 mm <sup>2</sup> ) is made of surgical tape (left) and a psoriasis lesion (right). The images are photographed by PRIMOS camera. ....	71

Figure 4.13 Lesion models are pasted onto life-size mannequin to simulate the lesions. A 2D image and 3D surface of lesion model are shown in the figure. .	72
Figure 4.14 Histogram of lesion models pasted on curved surfaces. ....	73
Figure 4.15 Rotated surfaces of lesion models by applying 12 rotation angles. ....	75
Figure 4.16 $S_a$ of lesion models with a variation on rotation angles. The values of $S_a$ are within acceptable accuracy (>95%). ....	76
Figure 4.17 Lesion surfaces are obtained from two successive scans. Lesion (a) is from the first scan and lesion (b) is from the following scan. ....	77
Figure 4.18 The 2D image and height map of lesion surfaces from the first (a) and the second (b) measurements. ....	77
Figure 4.19 Psoriasis lesions differentiation based on its size: (1) small, (2) medium, (3) large, and (4) huge. ....	79
Figure 4.20 2D image (a) and 3D surface (b) of normal skin surface. ....	80
Figure 4.21 Scanned image is cropped to obtain evaluated surface. Subdivided surfaces are obtained by performing mesh division on an evaluated surface. ....	80
Figure 4.22 The surface roughness of normal skin samples from 9 subjects with a sampling area variation. The sampling area is a square of sampling length. ....	82
Figure 4.23 (a) Surface roughness ( $S_a$ ) depends on sampling size variations. Figure (b) and (c) are the plot of the first and the second derivative functions, respectively. ....	83
Figure 5.1 An area with a certain confidence level bounded by $\pm Z\alpha/2$ . ....	89
Figure 5.2 (a) A projected pattern of PRIMOS 3D optical scanner. (b) A scanning process for acquiring the data for a scaliness measurement. ....	92
Figure 5.3 (a) Dermatologist selects and labels the lesion. (b) An example of a labelled lesion on lower limb region of Patient 184. ....	93
Figure 5.4 Data acquisition for determining PASI parameters: (a) area (b) erythema, and (c) lesion thickness and scaliness. ....	94
Figure 5.5 Charts of patient demography based on (a) gender, (b) race, (c) age, and (d) psoriasis duration. ....	95
Figure 5.6 Histogram of surface roughness of collected lesions. ....	96
Figure 5.7 Comparison of classification methods used in (a) hard and (b) soft clustering algorithms. ....	99
Figure 5.8 Clustering results of $k$ -means algorithm on test dataset. ....	105
Figure 5.9 Surface roughness intervals of score groups. ....	109
Figure 5.10 Predefined membership degrees of score groups. ....	111
Figure 5.11 Iteration of FCM clustering with random (dotted line) and predefined (solid line) membership degrees. ....	111

Figure 5.12 Membership degrees scattering of clustered dataset. ....	112
Figure 5.13 Membership functions of PASI scaliness scores. ....	113
Figure 5.14 Clustering results of FCM algorithm on test dataset. ....	114
Figure 5.15 Deviation surfaces of psoriasis lesions: (a) score 1, (b) score 2, (c) score 3, and (d) score 4, determined by the surface roughness algorithm and classified by the FCM algorithm. ....	115
Figure 5.16 A boundary level (white circle) splits membership functions of score 1 (dot-dashed line) and score 2 (dashed line). ....	116
Figure 5.17 Clustering of the <i>k</i> -means and ECM at the boundary of two clusters - score 1 and score 2. A boundary level of the <i>k</i> -means clustering (dotted-line) crosses the membership functions of score 1 (dot-dashed line) and score 2 (solid line). ....	122
Figure 6.1 Multiple scans for a single large lesion: (a) Large lesion covering part of the region and (b) Single large lesion covering the whole region. ....	131

## CHAPTER 1

### INTRODUCTION

This chapter discusses related research areas namely skin assessment and analysis, subjectivity of skin assessment, and skin roughness measurement, in formulating research problems of the thesis. The research objectives and hypotheses, and scope of work are discussed in the subsequent sections. The chapter ends with a summary of the thesis organisation.

#### **1.1 Background and Motivation of Research**

Various skin assessment methods are available for skin analysis in clinical practice. Most of these methods employ visual and tactile senses. Features of skin disease and their conditions such as colour, thickness, volume, or surface roughness are used as physical characteristics in these methods. These skin features which are regarded as assessment parameters are then observed, perceived and scored by dermatologists in determining severity of a particular skin condition. However, such assessments could lead to intra- and inter-rater variations due to subjectivity element in the dermatologists' assessments.

The need to analyse the severity of various skin diseases or disorders and their conditions (severity) through visual and tactile senses has resulted in the development of various skin disease-scoring methods. Skin disease assessment by quantifying the disease severity is common in clinical diagnosis as reported in the Medal website, listing 65 skin disorders that apply scoring method for its assessment. Many scoring methods have been developed; in the Medal website alone, a total of 313 methods are listed [1]. Disease severity is characterised by a score derived from the scores of observed parameters.

In this research, the problems of skin roughness measurement for psoriasis assessment are investigated in order to develop practical solution for daily practice. Psoriasis refers to a common chronic skin disease that affects about 2 - 3% of world population [2][3]. Neimann *et al.* summarised the psoriasis prevalences from epidemiological studies around the world. The prevalence varies from 0.6 to 4.8% [4]. In a recent study, Chandran *et al.* also reported the variety of psoriasis prevalence among regions. The variation of psoriasis prevalence from several countries is 0.60-6.50% in Europe, 0.70-3.15% in North and South America and 0.08-4.00% in Africa. In Asia and Australia the psoriasis prevalence of observed countries is reported to be 0.05-5.30% and 2.30%-2.57%, respectively [5]. The Dermatological Society of Malaysia reported a psoriasis prevalence of 3% in Malaysia [6]. In the period of 2005-2010, the Dermatology Department of Hospital Kuala Lumpur registered 3,906 psoriasis patients of a total of 75,883 hospital's patients, giving an incidence of 5.2% [7].

Psoriasis is characterised by red plaques that can occur in a localised area of the body or it can be widespread all over the body. Psoriasis itself refers to an incurable but treatable skin disease in which the immune system sends wrong signals that accelerate the cycle of skin cells' growth. In normal conditions, skin cells grow in a cycle of about 28 days but for psoriasis new skin cells grow faster, taking about 4 days to produce as many skin cells as in normal skin [8]. This disease is distressful to the patient as the skin is itchy all over and the condition can last for a long durations [9]. Even though psoriasis is not a contagious disease, recent studies have shown that psoriasis can significantly impact on quality of life with many psoriasis patients experience social and psychological problems with their environment [10]. Figure 1.1 shows examples of plaque psoriasis lesions on several body regions.

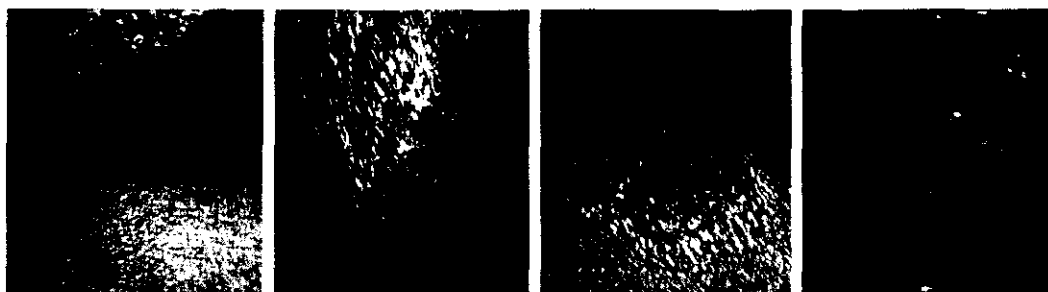


**Figure 1.1** Plaque psoriasis lesions grow on several body regions (left to right): head, upper limb, trunk, and lower limb regions.

The skin is comprised of several main skin layers. The epidermis is the outer layer and the dermis at the inner part. The next layer located under the epidermis is subcutaneous layer. The epidermis is made by stacking of skin cells. The living cells in the inner layer and the dead cells at the outer layer. In this layer, the skin cells are produced and matured to replace the dead skin cells. The dead skin cells at the outermost epidermis layer form a tough, flexible, and waterproof mantle on the skin surface. These cells are shed periodically from the skin surface as keratinous scales.

The dermis forms skin characteristics such as resistance from tearing and its elasticity. This layer contains a thick network of collagen and elastic fibres. Blood vessels (artery and vein), lymphatics, nerve fibres, connective tissue cells, and immune cells are also compacted in the dermis layer. The deepest layer, subcutaneous tissue or hypodermis is not considered the real part of human skin. However, this layer has significant contributions to enable protective functions of human skin. The hypodermis comprises mainly of adipose tissue and some areolar connective tissues. This layer fixes the skin to the body, stores fat reserve, and works as thermal and mechanical insulations. Excessive amount of the adipose can thicken the hypodermis layer. The arrangement of these three main layers - epidermis, dermis, and subcutaneous layer - are depicted in Figure 1.2.

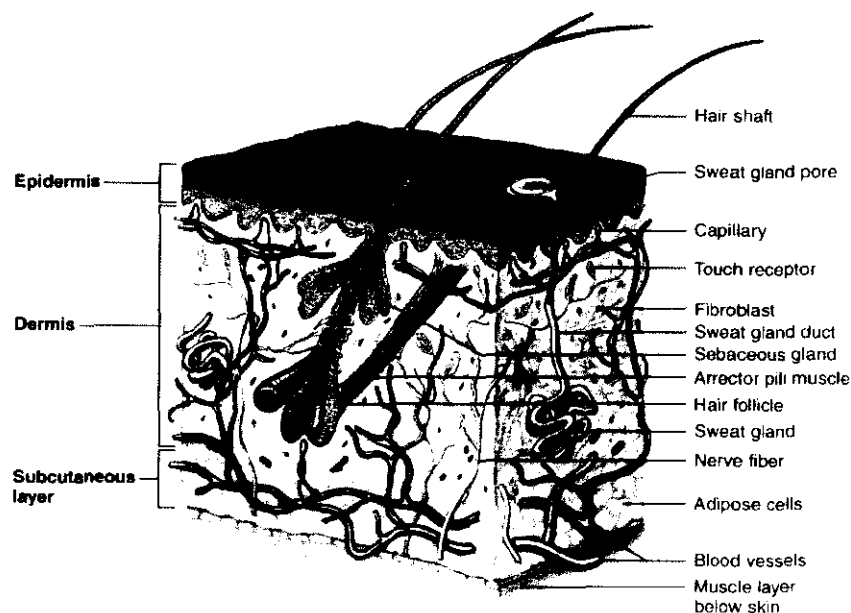


**Figure 1.2** Human skin is composed by several skin layers [11].

Stratum corneum is considered as the outermost layer of the skin structure and located at epidermis layer. It protects the living skin layers from the environmental harmfulness and is constructed by around twenty layers of densely packed keratinocytes, the main cell of the epidermis layer forming 95% of the skin cells [12]. The other skin cells are merkel, melanocytes, and langerhans. These cells are interlocked each other to construct some brick-like layers. In the inner part, several new keratinocytes are created to replace the older cells at the outer layers. Once created, a keratinocyte will gradually migrate from the inner to the outer layer. With this migration, the old and the dead keratinocytes at outer layer can be replaced by the keratinocytes from the inner layers [13]. The keratinocyte will transform its shape during the layer migration, from a round shape into a plate shape. This transformation process is known as differentiation. In the end of skin cell cycle, the dead keratinocyte will automatically flake away from skin surface. This final stage is known as the desquamation process. Human body can shed 30,000 to 40,000 dead skin cells from its surface every minute. This shedding amount equals 4.08 kg of cells annually [14]

The growing process of skin cell, including keratinocyte, occurs through several layers of skin epidermis. The migration process of keratinocyte through the layers within epidermis is considered as a lifetime cycle of skin cell in which a cycle normally spends 28 days approximately. The process of skin cell regeneration is divided into four stages.

First stage, a new cell is generated from cell division in the lowest layer of the subcutis, *i.e.* the basal layer. In second stage, the cell shape is flattened following the cell migration to the outer layers. The cells are now located in stratum spinosum layer. This layer contains large cells with prickle contour on the surface profile. For the third stage, skin cells move to stratum granulosum layer above the stratum spinosum layer. In this stage, the cell size becomes smaller compared to its previous size. Lastly, in the fourth stage, the cells will perish at stratum corneum and fall off from the skin surface. Figure 1.3 depicts the life stages of skin cell.

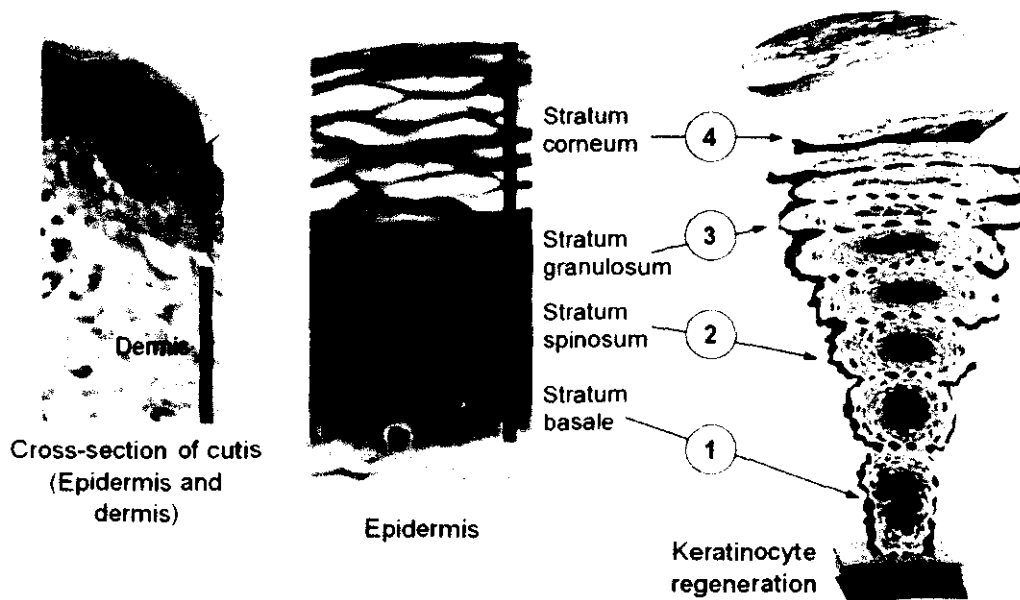


**Figure 1.3** The stages of skin growing at epidermis layers. The picture is reproduced from [15], [16], [17].

At higher severity of psoriasis, the lesion gets thicker with coarse white scales. The psoriasis lesions can affect any part of skin particularly on the elbows, knees, scalp, palm of the hand, chest, lower back, leg, soles and nails [18]. A periodic medical treatment for psoriatic patient is important, as the disease cannot be completely cured. Figure 1.4 shows several body parts affected by psoriasis lesions. The images are acquired from data collection sessions at Dermatology Department, Hospital Kuala Lumpur from 2007 to 2010.

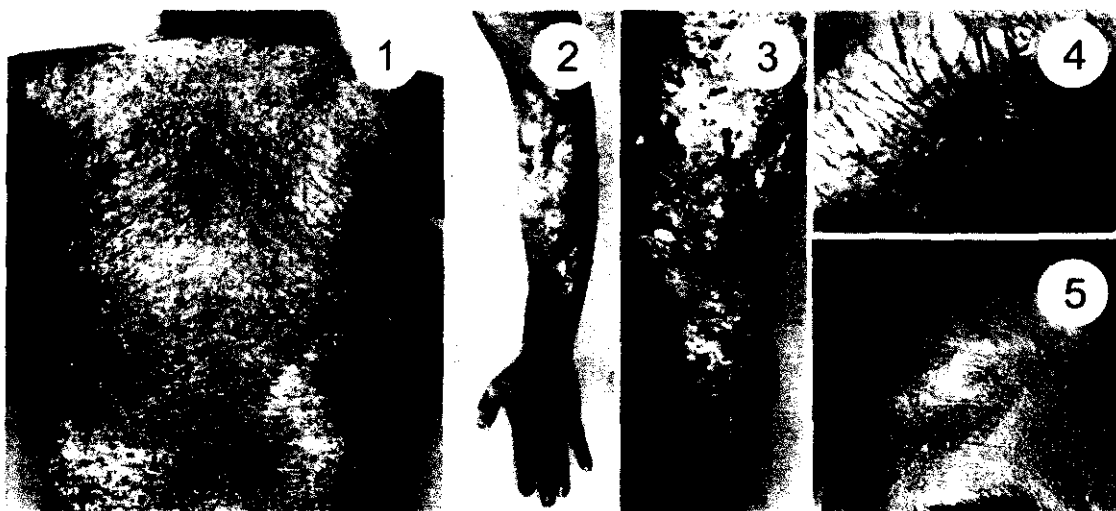


**Figure 1.4** Psoriasis lesions are found in various parts of the body such as trunk (1), upper limb (2), lower limb, elbow (4), and forehead (5).

## 1.2 Problem Statements

The PASI (Psoriasis Area and Severity Index) scoring method is known as gold standard for the severity assessment [19]. Six clinical severity scores i.e. PASI, BSA, PGA, LS-PGA, SPI, and SAPASI for psoriasis assessment has been systematically reviewed by Bonsard *et al.* [20]. Based on the review, there is no psoriasis severity scoring that meets all of the required validation criteria. Nevertheless, PASI scoring has been recommended for clinical study. Thus, PASI is considered the reference for having been widely applied in clinical studies and being the most validated among the psoriasis scoring methods [20].

PASI scoring method was introduced by Fredriksson and Pettersson in 1978. The method was proposed to evaluate a clinical efficacy of a new anti psoriatic drug [21]. To determine total PASI score, four parameters, i.e. area (ratio of lesion area to total body surface area), erythema (colour of lesion inflammation), lesion thickness, and scaliness of the lesion are required. In PASI assessment, the human body is divided into four regions namely, head, trunk, upper limbs and lower limbs. The PASI parameters of the psoriasis lesions are determined for each body region. Dermatologists use their visual and tactile senses to score the PASI parameter. The parameter scores from each region are weighted and totalled to provide a PASI score ranging from 0 – 72. For the treatment efficacy, dermatologist refers at least a 75% reduction in PASI score is considered to be a clinically meaningful improvement [19]. The PASI score is calculated from following equation:

$$\begin{aligned} \text{PASI} = & 0.1 \times (E_h + T_h + S_h)A_h + 0.2 \times (E_u + T_u + S_u)A_u + \\ & 0.3 \times (E_t + T_t + S_t)A_t + 0.4 \times (E_l + T_l + S_l)A_l \end{aligned} \quad (1-1)$$

Score ranges for PASI erythema ( $E$ ), thickness ( $T$ ), and scaliness ( $S$ ) are from 0 to 4 whereas the range for PASI area ( $A$ ) is from 0 to 6. Four body regions namely, head, upper limb, trunk, and lower limb are denoted by subscripting  $h$ ,  $u$ ,  $t$ , and  $l$  respectively for each PASI parameter. Variable  $E_h$  for instance is used to represent PASI erythema score at the head region.

The scaliness parameter is selected as PASI parameter studied in this research. For PASI scaliness assessment, dermatologists observe several lesions that are appeared on an examined body region. The PASI scaliness scores are then given to these lesions. Dermatologists assign a scaliness score of the examined body region based on the commonest score of the lesions. To minimise tediousness in PASI scaliness assessment, a simplified procedure is performed by dermatologists by selecting a representative lesion for the examined body region. The score obtained from a representative lesion is then considered as scaliness score for the body region.

Although the PASI scoring has been accepted as the gold standard for psoriasis assessment, it is not used in daily practice. PASI scoring is tedious, time-consuming ( $\pm 30$  minutes/patient) and subjective. Four parameters must be determined at four body regions (a total of 16 assessments). The subjectivity of the scores is influenced by intra and inter-rater variation of dermatologists. Reliability and agreement of dermatologist assessments are of concerned in many studies. Assessment agreements between self assessment and dermatologist on benign melanocytic nevi patients are studied in [22]. Agreement study is also conducted to evaluate a new method for burn scar assessment [23]. A better assessment method can be decided based on the results of agreement analysis. Therefore, an objective and reliable system is required to deal with these problems.

An imaging approach to overcome the aforementioned problem is proposed to assess PASI scaliness objectively. Imaging technology is also advantageous as it is can be designed to recognise skin diseases in their early stages known as the pre-disease diagnosis. As seen in chronic dermatoses, the disease is preceded by some changes. The changes may occur - even for years prior to the disorder being clinically observed [24]. This achievement can be illustrated by prevention of rosacea skin disease. This disease is characterised by reddening on facial area. The dilated blood vessels cause increasing the redness of the skin. It can occur especially in the central face region - across the cheeks, nose, and forehead. Most of rosacea cases occur in adult ages (30 to 50) and people with fair skin [25]. However, in early stages, the reddening symptoms on face area cannot be visually observed.

Video microscope with polarised light has been used to reveal a network of invisible dilated blood vessels underneath the skin surface. Subsurface structures can be clearly observed by applying polarised light imaging whereas finer details of blood vessels are obtained by microscope [26]. The method can detect the vessels at early stages, e.g. when the patient age is less than 10 years old. Since the method enables to detect early stages, mild topical treatments may be applied to slow down progression of rosacea [24].

Images of rosacea patterns obtained from digital camera and microscope are shown in Figure 1.5 (a) and Figure 1.5 (b) respectively. Polarising filters on both acquisitions can reveal the vessels patterns even though they are located in underneath skin surface. Microscopic magnification  $100\times$  is used to obtain Figure 1.5 (b). Higher magnification -  $200\times$  - is applied to see the details as show in the inset image of Figure 1.5 (b) [27] [28].



**Figure 1.5** Patterns of rosacea blood vessels are acquired by (a) digital camera and (b) microscope.

To achieve objective assessment, the PASI scaliness visual descriptors are studied and defined in terms on surface roughness, a measurable feature that can be used to differentiate PASI scaliness scores. Abnormality of skin can be identified through several skin symptoms, such as itching skin, skin lesion, mole symptoms, acne, skin colour changes, redness, etc [29]. Skin lesions can be caused by various diseases. A total of 422 diseases that can cause skin lesions are listed in RightDiagnosis website [30]. A skin lesion is a superficial growth or patch of the skin that does not appear as surrounding normal skin [31]. Skin lesion appearance is specified by visual and tactile descriptions based on primary morphology (size, shape and thickness), secondary morphology (clustered or distributed), surface texture

(roughness), location and colour [32]. A texture determination of normal and abnormal skin surface is crucial in the field of dermatology measurements, particularly in the evaluation of therapeutic or cosmetic treatments. Skin surface can be characterised by physical features, such as dryness, smoothness, thickness, and roughness.

Dermatologists conduct PASI scaliness assessment based on some descriptions of a visual appearance. These descriptions are used as a standard guidance for determining the PASI scaliness scores. In the proposed approach, surface roughness features are required to represent scaliness severity. The correspondence between surface roughness of psoriasis lesion and severity stages needs to be investigated and defined by surface roughness parameter(s) that can be measured from digital surface image data.

The current problems of PASI scaliness assessment and surface roughness measurement are formulated as follows:

- Dermatologist assessment can be subjective due to intra- and inter-rater variability of human assessment. The subjectivity depends on the perception and the clinical experience of the dermatologist.
- Objective skin assessment might be performed objectively but the available methods require an invasive treatment on the measured skin. A tiny skin cut is sampled from the patient and then analysed using a scanning electron microscopy. Trained and experienced medical personnel are required to properly prepare and analyse the skin sample.
- A non-invasive method can be applied to obtain a high accuracy measurement on surface roughness. However, several methods need a skin replica as a representation of the actual skin surface. The skin replica is required because the measuring process uses a precise profilometer (sharp needle or laser beam) to extract the profile of skin surface. Though being able to provide measurement results with high accuracy, this method in clinical practice is not so practical. In addition, well-trained personnel are required to build qualified skin replica and operate the profilometer system.

Digital image analysis of skin surface roughness for scaliness classification is proposed to resolve the aforementioned problems. 3D imaging algorithm and clustering algorithm can be applied in the proposed approach. However, there are challenges that need to be overcome in this approach. The challenges are as follows:

- Difficulty in an assessment of lesion surface roughness on curved skin surfaces. The roughness assessment should be able to measure the vertical deviation of the lesion surface at various points on human body surface.
- To determine vertical deviations on lesion surface, a reference surface is required to be a zero point of vertical distance measurement as commonly applied in industrial applications. However, there are no such surfaces on the skin that can be referred as the zero point. The reference surface needs to be determined before the vertical deviations can be computed.
- Dermatologists' assessment results cannot be considered as a ground truth for evaluating algorithm performance due to subjectivity influences on assessment results.

### **1.3 Research Hypothesis**

In this research work, two primary hypotheses are defined. The hypotheses can be described as follows:

- a. The first hypothesis is a lesion surface is a superimposed surface between two surfaces - curved and rough surfaces. To prepare surface roughness determination, these surfaces need to be extracted from the lesion surface. Surface roughness of lesion is calculated by averaging the vertical deviations of the rough surface. Vertical deviation due to the lesion is determined by subtracting lesion surface from an estimated waviness obtained by fitting a polynomial surface to lesion surface. Most of the estimated waviness surfaces have the form of curved surfaces.
- b. The second hypothesis defines that surface roughness of the lesions can be used to build clustering algorithm for PASI scaliness scoring. With availability of large datasets, an unsupervised clustering algorithm can be

applied to obtain the boundary levels of lesion surface roughness for PASI scaliness scoring.

Figure 1.6 depicts the cross-sectional view of a skin lesion on normal skin surface. Vertical deviations of lesion surface can be either positive or negative and the average of deviation magnitudes is used to represent surface roughness of the lesion.

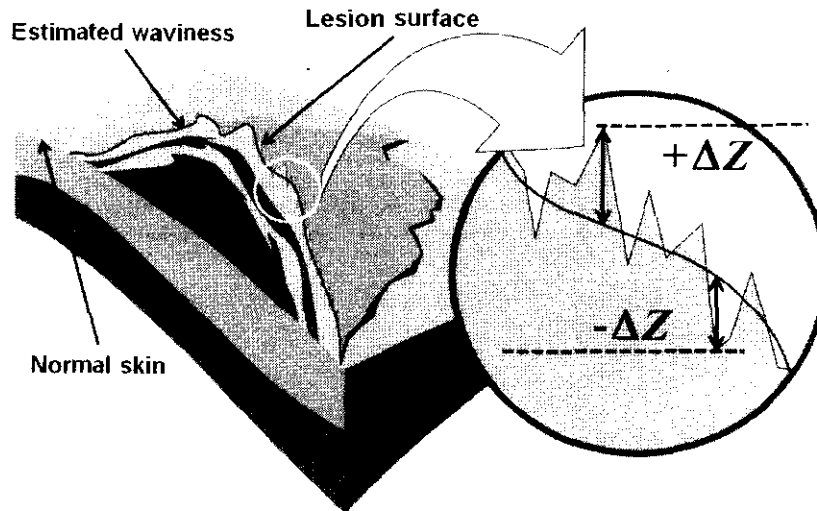


**Figure 1.6** Cross-sectional view of a skin lesion on normal skin surface.

#### 1.4 Research Objectives

Two research objectives are specified for the thesis. These objectives are described as follows:

- a. The first research objective is to develop 3D imaging algorithm for accurately measuring the surface roughness of skin lesions. The algorithm must be valid for all skin lesions that appear at any body parts.
- b. The second objective is to develop an objective and reliable PASI scaliness scoring using an unsupervised clustering technique on surface roughness of skin lesions.

## 1.5 Scope of Work

Three items in the scope of work have been identified that limits the coverage of the research. The limitations are defined for the type of skin disease, PASI parameter, and the size of acquired images. The type of psoriasis lesion in the research work is limited to plaque psoriasis. This is the commonest types of psoriasis accounting around 80% of psoriasis cases. Other psoriasis types are flexural, guttate, pustular, nail psoriasis, psoriatic arthritis and erythrodermic [4]. The Malaysian Psoriasis Registry found that the percentage of plaque psoriasis in Malaysia reaches 80.9% [33]. Surface roughness of psoriasis lesion is determined by applying 3D image analysis on scanned lesion surface. The PASI parameter studied in this research is limited only to PASI scaliness. The other parameters – area, erythema, thickness - are not considered since the surface roughness is not involved in the scoring process of the parameters.

The measured area is limited to the maximum area of 3D scanner used in this research. The maximum measured area is  $40 \times 30 \text{ mm}^2$  and the vertical heights are stored as a matrix with  $640 \times 480$  data points in size. Figure 1.7 shows an example of 3D lesion surface taken by using 3D optical scanner. This image is a second sample of psoriasis lesion. The image is acquired from upper limb region of a psoriasis patient at Dermatology Department, Hospital Kuala Lumpur.



**Figure 1.7** An example of 3D lesion surface obtained from psoriasis patient.

This localised measurement is not contrary with the clinical procedure of PASI assessment. In real situations, the dermatologist scores several representative lesions one by one even though there are several lesions at the same body region (head,

upper limb, trunk, or lower limb). The score given for a body region is determined by selecting the commonest PASI scores of psoriasis lesions at the same body region. The same procedure can be conducted by applying the proposed method. The surface measurement can be conducted repeatedly to another lesion located at the same region. Patient data profile, such as gender, age, ethnic, and medical history would not be considered in this study. There is no significant difference on scale surface appearances based on those parameters.

## **1.6 Organisation of the Thesis**

The thesis is organised into six chapters including the first chapter. Chapter 1 introduces background of the research work, initially by illustrating the current method on skin assessment and analysis. The method can suffer from an assessment inconsistency due to human subjectivity. Skin roughness is one of the common features used in the skin assessment. The feature is intensively studied in this work for having a relationship with the scaliness characteristic of psoriasis lesion. Research problems and objectives are formulated in this chapter as well as a research hypothesis on imaging method for skin roughness analysis. Scopes of work, such as the type of skin disease, studied PASI parameter and acquired image are defined afterward. In the final section, organisation of the thesis details the thesis content started from chapter 1 to 6.

Chapter 2 presents a medical review of the skin structure and the clinical features of skin disease. This chapter begins by describing the physical structure of human skin. Layers types and its function are mentioned as well. Psoriasis, a well-known skin disease, is studied in this research work.

Chapter 3 furthermore describes related methods that are used for surface roughness analysis. Surface roughness initially is determined by drawing a stylus on the measured surface known as mechanical surface profilometry method. Several imaging technologies for surface analysis, such as laser profilometry, speckle imaging, microscopy imaging, and structured light projection are developed to enable 3D surface acquisition. Surface roughness is determined from the extracted roughness component of surface profile. To extract roughness components from the

unwanted components, surface filtering methods have been developed. This section presents the commonest filters for surface filtering *i.e.* Fourier transform, Gaussian filter, wavelet filtering, and polynomial surface fitting. Calculation of surface roughness parameter is then performed on filtered surface to obtain measured surface roughness. In this section, three roughness parameters; those are frequency-based parameter, amplitude-based parameter, and fractal parameter are reviewed. Applications of surface roughness measurement for manufacturing and medical purposes are provided in this chapter.

Chapter 4 describes the development of surface roughness algorithm. In the first stage, surface roughness is simulated as a computational model of lesion surface. Estimated waviness is extracted from the computed model for testing the performance of polynomial surface fitting. Validation study of surface roughness algorithm on abrasive paper, as a rough surface, and curved surface are reported in this chapter. From the validation study, accuracy and total standard deviation are determined.

Chapter 5 discusses a surface roughness analysis for a psoriasis assessment. A clinical study has been conducted to collect 3D surfaces of psoriasis lesions. Experiment set-up and procedures for data collection are detailed in the first section. Development and validation study of clustering algorithms are described in the following sections. Two unsupervised clustering algorithms -  $k$ -means and fuzzy  $c$ -means clustering algorithms are applied to determine PASI scaliness score based on lesion surface roughness. Objectivity of the scoring algorithm is evaluated by performing agreement analysis between the first and the second assessment.

Chapter 6 finally summarises the findings on this research work into a conclusion section. This is followed by some recommendations and suggestions for future work. Some potential applications for implementing the developed skin roughness algorithm are mentioned in the end of this chapter.

## CHAPTER 2

### MEDICAL LITERATURE REVIEW

Chapter 2 presents both general information on human skin structure comprising several skin layers and a number of related diseases including the assessment. It begins from Section 2.1 that describes the characteristics of skin layers and their functions. Section 2.2, provides a detailed discussion about psoriasis, a chronic skin disease which is the object of study in the research work. This section also includes a discussion on various psoriasis types and its treatment methods for reducing the effects of psoriasis. Following this, Section 2.3 presents the PASI (Psoriasis Area and Severity Index) scoring method as a gold standard for psoriasis assessment in order to obtain the treatment efficacy for the dermatologist in quantifying the psoriasis severity. The contents of Chapter 2 are finally summarised in Section 2.4.

#### 2.1 Skin Structure

Skin is considered one of the largest organs of human body [34]; in adult, its weight is about 4 to 5 kg or 7% of total body weight covering almost 1.7 m<sup>2</sup> of body surface area [13]. The skin area between male and female will be different in size. For male, it ranges from 1.39 to 2.10 m<sup>2</sup> and for female the area interval is 1.19 to 1.88 m<sup>2</sup> [35]. Based on its structure, skin is divided into two parts namely actual skin (*cutis*) and subcutaneous tissue (*tela subcutanea*) [13]. The actual skin layer comprises of two layers - epidermis and dermis. Epidermis is a stratified squamous keratinous epithelium whereas dermis is a dense network of collagen and elastic fibres. Epidermis is located in outer layer of 0.1 - 0.2 mm in thickness. This thickness range is observed at most of body areas. Exceptions are found at the hand palms and soles of the feet, the epidermis layer in these areas is thicker compared to other body areas ranging from 0.8 to 1.5 mm. The research is focused on the outer

surface of epidermis since most of the skin diseases affect and appear on this layer.

The skin organ is composed by four main tissue types - epithelial, connective, muscle, and nervous. These tissue types are also mostly found in the other organs. The tissues are combined to perform specific function of the organ. Skin organ has multiple functions [13] such as: (1) To protect the skin from mechanical, thermal and chemical damage; (2) To regulate body temperature; (3) To maintain skin moisture from dryness; (4) To sense physical stimulus through the skin receptors; (5) To build immune system from pathogenic threats; (6) To communicate an expression by changing the skin colour of face area. These functions can be obtained for normal skin but for the diseased skin, one or more functions would not be performed normally. Skin organ, derivatives of skin (sweat glands, oil glands, hair, and nails) and accessory structures (blood vessels and nerves) are integrated to form an integumentary system. The function of this system is to protect the human body from harmful interactions with the outer substances and environment [34].

## 2.2 Clinical Features of Psoriasis

The psoriasis prevalences in several countries from 1964 to 2005 have been studied by Neimann *et al.* Their study found that the psoriasis prevalence around the world is in the range of 0.6 to 4.8% [4]. In a recent review, Chandran *et al.* reported psoriasis prevalence varies among the regions. The prevalences of psoriasis are 0.60-6.50% in Europe, 0.70-3.15% in North and South America and 0.08-4.00% in Africa. In Asia and Australia, psoriasis prevalences of 0.05-5.30% and 2.30%-2.57%, respectively have been reported [5]. These prevalence data are obtained from clinical based and field survey from 1998 to 2009. However, if the worldwide population is used as the prevalence base then the psoriasis prevalence around the world is about 2 to 3% [2][3]. The Dermatological Society of Malaysia studied that the psoriasis prevalence in Malaysia is 3% [6]. The Dermatology Department of Hospital Kuala Lumpur registered 3,906 psoriasis patients of a total of 75,883 hospital's patients for the years 2005-2010, giving a prevalence of 5.2% [7]. Periodical medical treatment for psoriatic patient is important, as the disease cannot be cured. The treatment for psoriasis can be grouped into three types - topical,

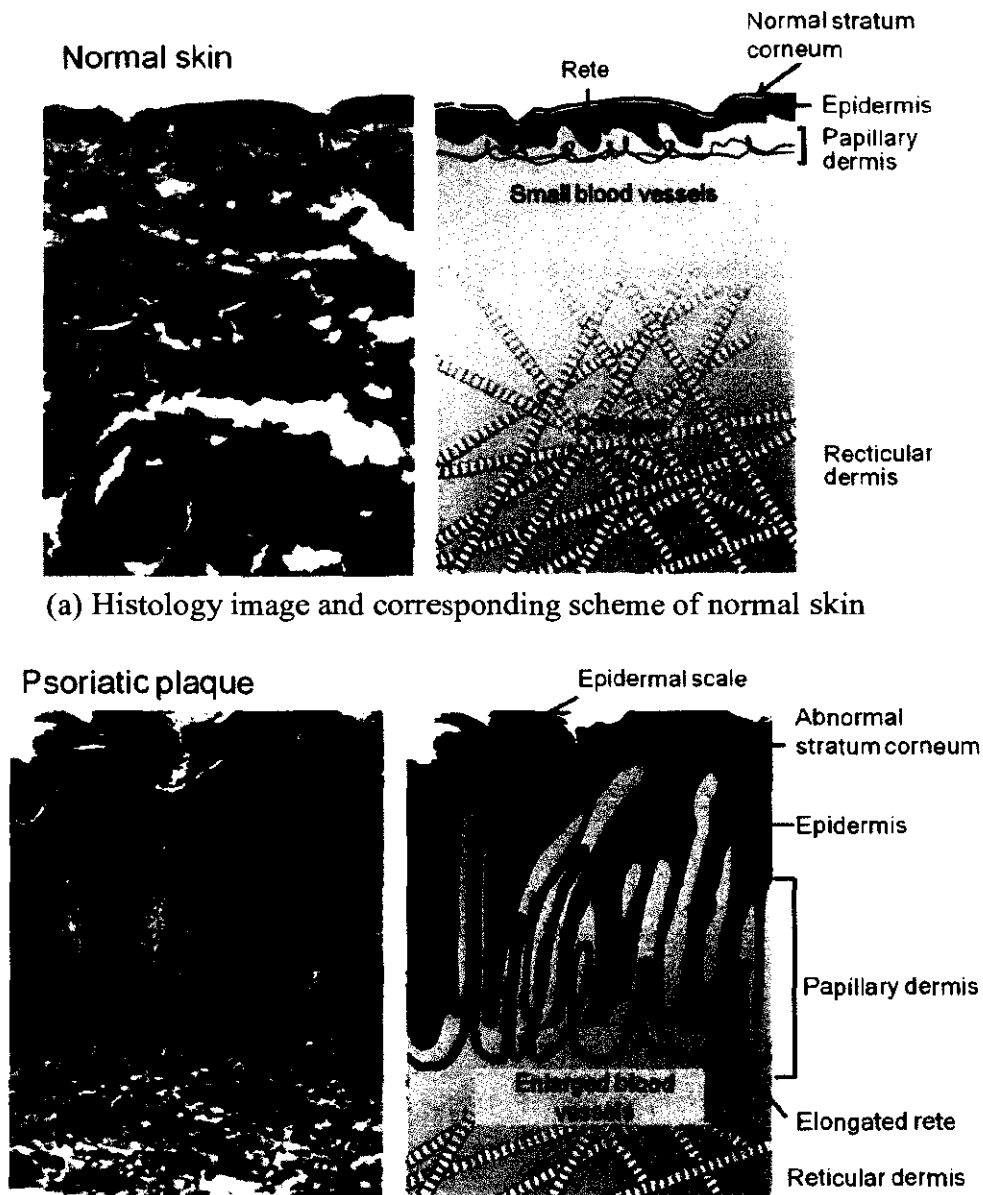
phototherapy, and systemic medications. The treatment is specific for each patient. It is decided based on both disease progression and medical response of treated patient. Topical method is usually used for handling psoriasis at mild levels. The second treatment is phototherapy that uses a UV light emission to control the growth of psoriasis lesions. The third treatment is systemic method applied when the two previous methods are not considered effective to deal with psoriasis.

For adults, psoriasis is believed to be the most prevalent immune-mediated skin disease, which is initiated by an activated cellular immune system. Therefore, the psoriasis is also considered as an organ-specific autoimmune disease [36]. The most common form of psoriasis is psoriasis vulgaris reaching 90% of all psoriasis cases. In psoriasis vulgaris, scaly papules and plaques are well-defined from surrounding normal skin [37].

Pathogenesis of psoriasis has not been being completely understood until recently. The immune system and T lymphocytes so far are considered as the initiator for psoriasis. In response, the epidermal cell cycle is then shortened resulting in silvery scale lesions [38]. The psoriasis scales are formed from a number of abnormally stacked cells on the stratum corneum - an outermost surface of epidermis layer. The granular layer of the epidermis is much reduced by increasing the size of cells stacking. Clinical features and severities of psoriasis are not only varying in time but also specific for each individual.

In characterizing psoriasis, four abnormalities can be used. The first abnormality is vascular changes that are shown by dilatation and tortuosity of the papillary blood vessels. At this point, there will be elongation and enlargement of epidermal blood vessels [39]. In such condition, the skin becomes reddish and this is widely known as psoriasis erythema. The second condition is inflammation in which polymorphonuclear leukocytes from the dermal vessels move into the epidermis. Here, the number of leukocyte of psoriatic lesion significantly increases and many immune-related pathways are activated [39]. In turn, lesions with a large amount of activated T helper cells ( $CD4^+$  and  $CD8^+$ ) will release proinflammatory cytokines. The cytokines cell is signalling cell that can activate body immune system result in skin inflammation. The third abnormality is hyperproliferation (high rate on cells

regeneration) of the keratinocytic layer. This layer protects the body from pathogens, heat, light radiation, and water losses. The last abnormality is the altered epidermal differentiation. Keratinocytes keep their nuclei in the protected layer (parakeratosis) and lose the granular layer. They grow excessively with different appearance compared to normal skin. Comparison between normal skin and skin affected by psoriasis is shown Figure 2.1.



(a) Histology image and corresponding scheme of normal skin

(b) Histology image and corresponding scheme of skin affected by psoriasis

**Figure 2.1** Skin histology of (a) normal skin and (b) skin affected by psoriasis [36].

These progressions in the epidermis layer will introduce skin scales on the lesion locations [39]. The epidermal rete is extended and the papillary blood vessels of

psoriatic plaque are dilated. Epidermal rete is ridge profiles located at boundary area between epidermis and dermis layers. The epidermal rate enables epidermis and dermis to be interlocked into a unified skin layer. These enlarged blood vessels, as shown by psoriatic plaque cross-section in Figure 2.1 (b), make the affected skin become reddish which is defined as lesion erythema. Hyperpoliferation of keratinocyte is also depicted by changing on the stratum corneum layer. Previously, its thickness is slimmer but after affected by psoriasis, the layer goes very thick and irregular.

Psoriasis lesions typically appears in certain locations such as scalp, ears, elbows, umbilicus (belly button), buttocks (gluteal cleft) and genitalia areas, knees, soles of the feet, fingers and toes. It is possible for the lesions to grow at moist areas; for examples in armpits, under breasts, and groins [40]. Figure 2.2 describes the lesion locations that are commonly found in psoriasis cases.

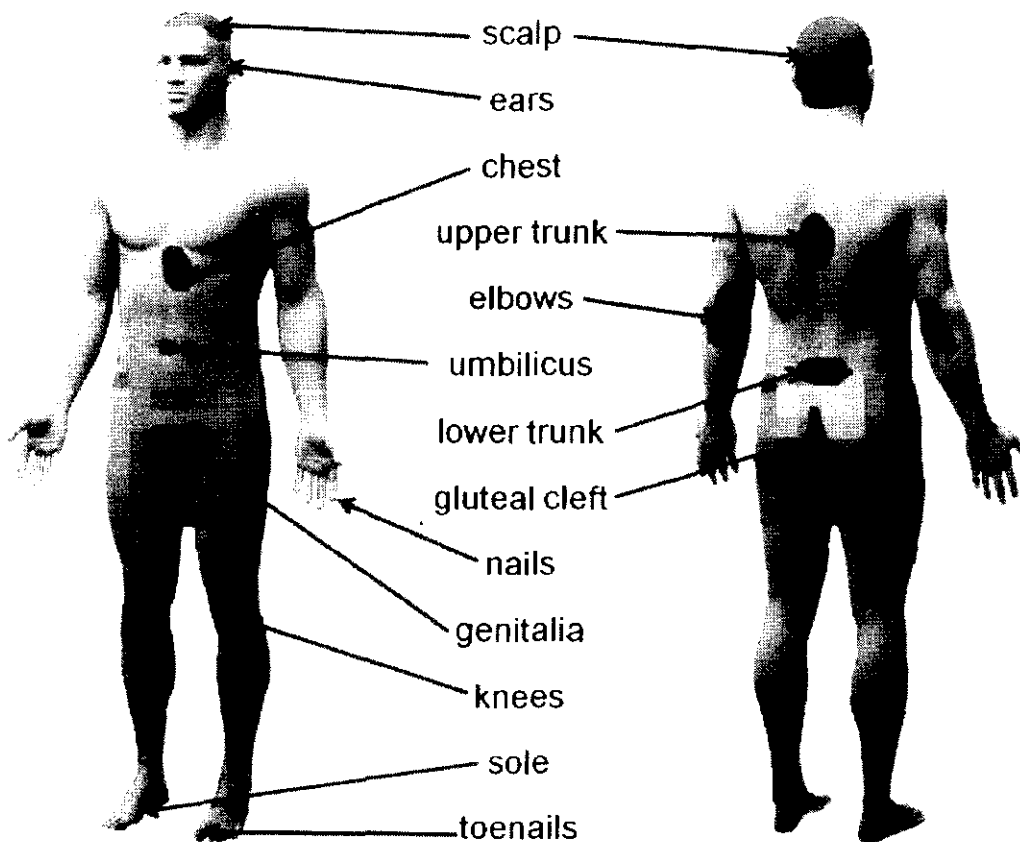


**Figure 2.2** Common locations of psoriasis lesions growing on human skin. The picture is created by combining graphic materials and description from [40] [41] [42].

Based on the appearance and characteristic, psoriasis could be categorised several types that are presented in the following sections.

### 2.2.1 Plaque psoriasis

Psoriasis lesion typically is covered by silvery white scales with varying thicknesses. Plaque psoriasis usually starts in early adulthood and will generally persist for a long time. Plaque psoriasis lesions frequently occur on certain areas such as elbows, knees, and the scalp [36].

The amount of scales may vary among the psoriatic patients and also at different parts of the same patient [43]. The lesion is usually clumped as a single skin patch. However, due to improper treatment, the lesion size could be enlarged. The enlarged lesion can be merged with another neighbour lesion to create a larger lesion. Some images of plaque psoriasis lesions from clinical study at Hospital Kuala Lumpur are shown in Figure 2.3. From these examples, it can be shown that the large lesions are formed by merging some smaller adjacent lesions.

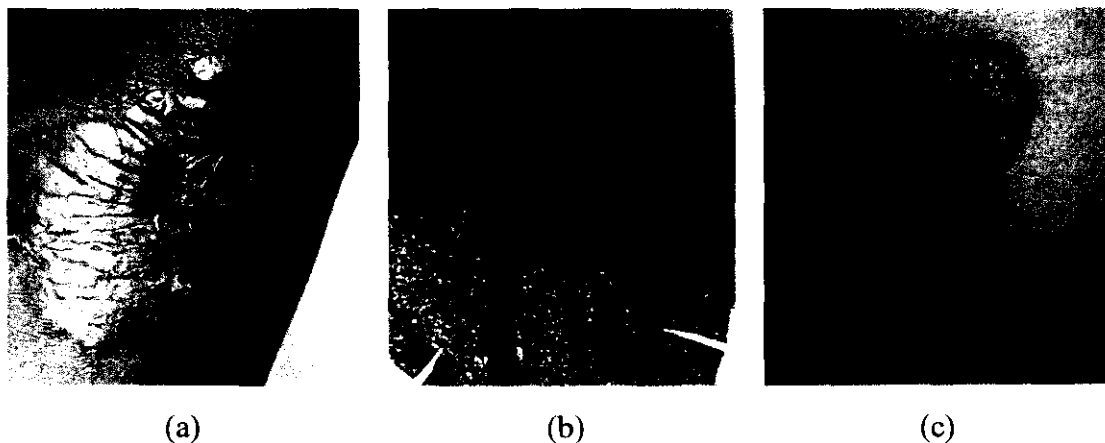


**Figure 2.3** Plaque psoriasis lesions appear at several body regions such as (a) elbow, (b) upper back, and (c) trunk.

### 2.2.2 Guttate psoriasis

Guttate psoriasis originated from Greek *gutta* meaning a tiny drop. The drop gives a description of the acute onset of unnumbered tiny psoriasis lesions with diameter 2 - 10 mm. A total of five to hundreds lesions can appear at certain affected regions, such as head and limbs. Guttate psoriasis occurs in 2% of total psoriasis cases. Plaque psoriasis can be initiated by suffering guttate psoriasis at younger ages [43]. Figure 2.4 shows guttate psoriasis lesions at several body regions.

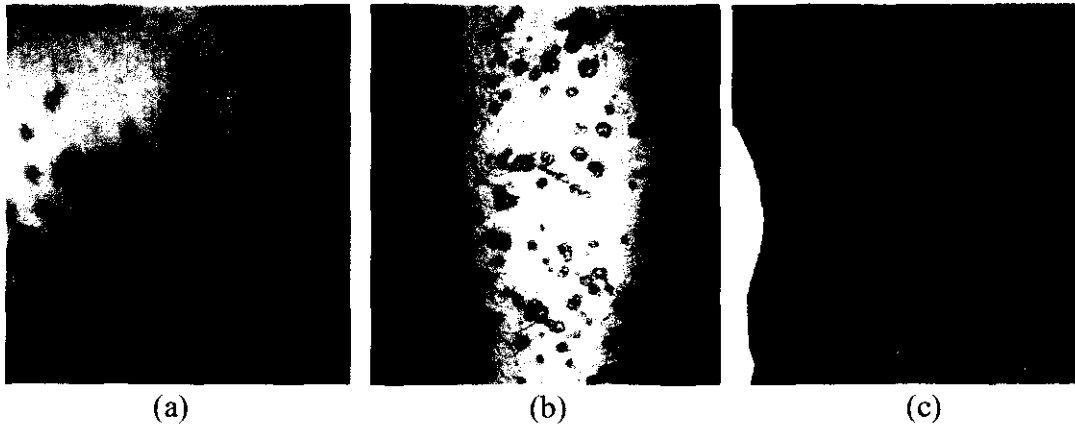


**Figure 2.4** Example of guttate psoriasis lesions. These lesions are spread at several body regions such as (a) chest and arm [44], (b) forearm [45] and (c) back region [45].

### 2.2.3 Flexural (inverse) psoriasis

Flexural psoriasis occurs at the flexural areas. These areas are located between two body parts such as at the folding areas of breast, genital, and armpit. The flexural lesions appear as red and shiny lesions. Its plaque boundaries are also easily to pronounce from the surrounding normal skin. However, the disease sometimes is misidentified as candidal, intertrigo, or dermatophyte infections [43]. Figure 2.5 shows the folded skin areas that are affected by psoriasis.

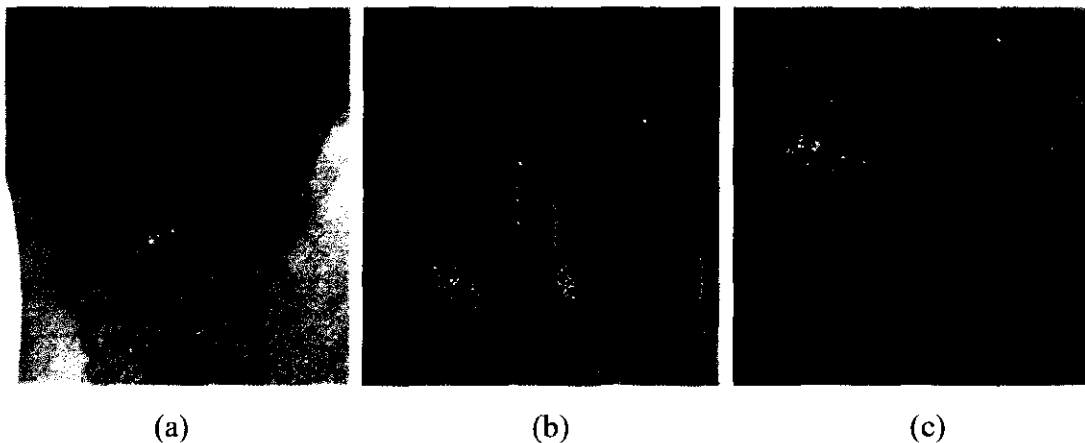


**Figure 2.5** Flexural psoriasis growths lesions are appeared at folded skin areas. The areas such as (a) armpit [37] (b) ear [46], and (c) umbilicus.

### 2.2.4 Generalised pustular psoriasis

Pustular type is characterised by red skin on the affected area and scattered by many pustules. These pustules contain white blood cells that can dry and peel causing the

skin to be glazed. Moreover, this type also can cause a fever to the patients. In many cases, the adult patients need to be hospitalised [43]. Figure 2.6 illustrates the examples of skin affected by pustular psoriasis.

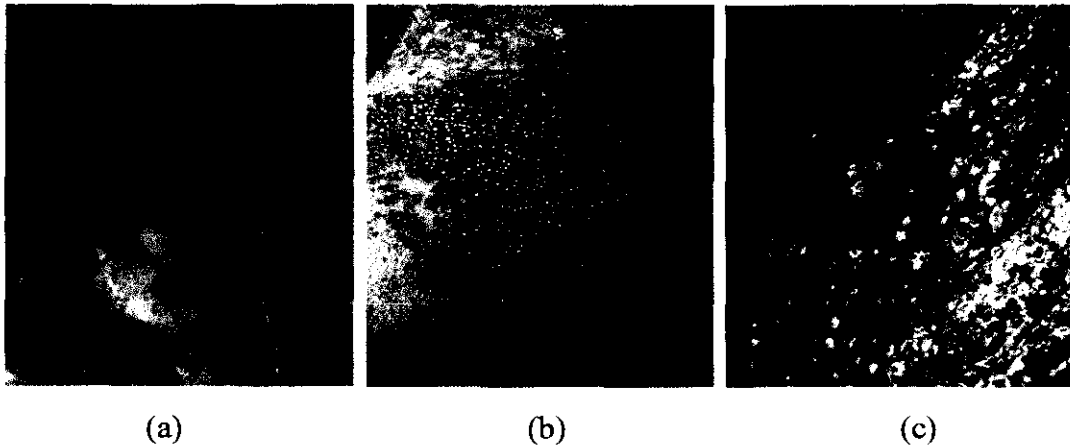


**Figure 2.6** Many pustules scatter on the inflamed skin affected by generalised pustular psoriasis at (a) palm [47], (b) upper back [48], and (c) neck [49] regions.

### **2.2.5 Erythrodermic psoriasis**

Erythrodermic psoriasis can affect the body skin surface, either partially or completely affected. This psoriasis type might be developed from the gradual enlargement of chronic psoriasis plaques. It is also triggered by an abrupt termination on a systemic psoriasis treatment, infections, or allergic reaction to the medicines. This psoriasis type is characterised by several symptoms, such as periodical and widespread appearance, inflaming skin surface, and lesion scales in the form of sheets. Patients with erythrodermic psoriasis will experience severe itching and pain, increasing heat rate, and unpredictable body temperature. Abnormality in skin temperature regulation can lead hypothermia, high output cardiac failure, and change in blood metabolism. Once the symptoms have been detected, hospitalised treatments need to be given immediately to the patients [43] [50]. Figure 2.7 depicts the example of erythrodermic psoriasis.

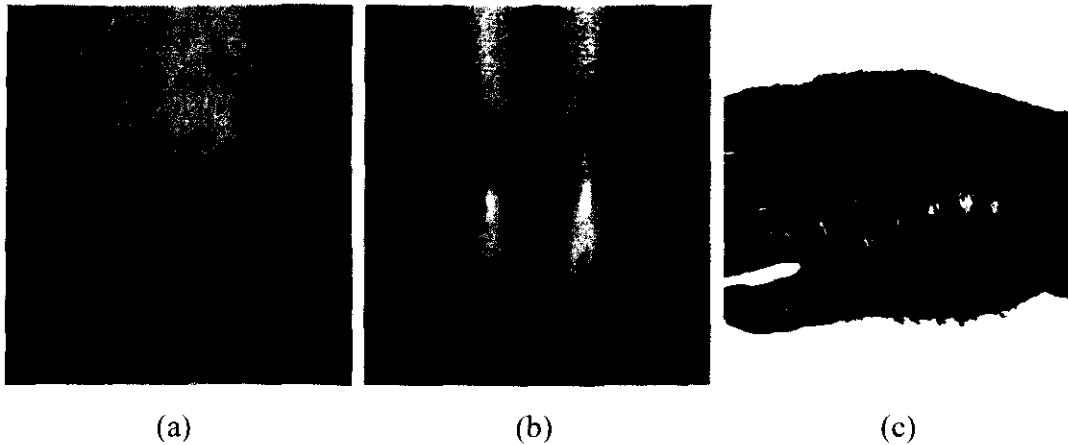


**Figure 2.7** Erythrodermic psoriasis covers most of body surfaces at areas such as (a) trunk [51], (b) lower limbs [52], and (c) hand including wrist area [53].

Psoriasis treatments can be categorised into three therapeutic modalities, namely topical agents, phototherapy using appropriate ultra violet wavelength, and systemic medications. Topical agents are used for treating mild psoriasis and resistant lesions at higher severity. Phototherapy is applied for psoriasis at moderate level. Meanwhile, the systemic treatment is implemented for treating severe cases. This treatment includes photo chemotherapy, oral medicine consumption, and biological injection [54]. In topical category coal tar, vitamin D analogues, steroids, and dithranol are applied to the skin surface. On the other hand, through phototherapy, Narrow-band Ultraviolet-B (NBUVB, 315 – 280 nm) and Psoralen Ultraviolet-A (PUVA, 400 – 315 nm) treatments are aimed to improve the patient condition. In systemic treatment, various medicines, such as methotrexate, retinoids, sulphasalazine, cyclophosphamide, and cyclosporine can be given. All of these psoriasis treatments are discussed in the following sections [55].

### **2.3 Skin Assessment and Analysis**

In the 1950s, skin assessment was relatively simple based on the direct accessibility of the skin surface using visual and tactile senses. Dermatologists are able to assess and diagnose using only their perception of the physical appearances of skin. In contrast to other medical specialists, such as internists, surgeons, and radiologists, equipments or modalities such as electroencephalography (EEG), magnetic resonance imaging (MRI), x-ray, and medical ultrasonography are used to observe

affected human body parts [24]. Nowadays, many advanced equipments have been used to examine and measure skin abnormalities. These equipments such as digital single-lens reflex camera (DSLR) [56], dermatoscopy [28][57], video dermatoscopy also known as video microscopic [28][58], optical coherence tomography [59], confocal scanning laser microscopy [60], stylus and laser profilometries on skin replicas [61][62], and tribo-acoustic system [63] have been used in skin assessment. However, most of them are only available for clinical studies and not for clinical practice.

In clinical practice, the skin diseases are commonly analysed and assessed through visual and tactile senses using skin disease-scoring methods. Many scoring methods are available to determine severity of various skin diseases. For example, eczema area and severity index (EASI) is used to grade atopic dermatitis [64]. EASI defines four parameters which are erythema, thickness, scratching and lichenification (lined skin). The intensities of these parameters are obtained from four regions of body (head and neck, upper limbs, trunk, and lower limbs). Patient age and affected body surface area are considered as the weighting factors in a final score calculation. The EASI score ranges from 0 to 72.

SCORAD (SCORing Atopic Dermatitis) is another example of well known skin disease assessment. SCORAD is used to grade atopic dermatitis severity. There are three parameters need to be assessed. The parameters are lesion existence on body regions, disease severities, and subjective symptoms. The first and second parameters are scored by dermatologists. The third parameter - subjective symptoms - is scored by patient based on his or her subjective perception and experience.

The combination of assessment results by dermatologists and patient represent the patient condition [65]. The SCORAD score ranges from 0 to 103. Both scoring methods purposively are to standardise the atopic dermatitis assessment and to evaluate therapeutic response [66].

The *Cutaneous Lupus Erythematosus* Disease Area and Severity Index (CLASI) scoring is performed on the patient to determine the severity of *cutaneous lupus erythematosus*. This method assesses four parameters (erythema, scale,

dyspigmentation, and scarring) at 16 anatomical locations, such as scalp, ears, nose, back, arms, hands, legs, etc. CLASI scoring is applied to evaluate treatment efficacy on *cutaneous lupus erythematosus* disease [67].

Several scoring methods have also been developed for psoriasis assessment such as National Psoriasis Foundation (NPF), Psoriasis Score (NPF-PS), Physician static global assessment (PSGA), Overall lesion assessment (OLA), Lattice System Physician's Global Assessment (LS-PGA) Psoriasis Global Assessment (PGA), Copenhagen Psoriasis Severity Index (CoPSI), and Psoriasis Area and Severity Index (PASI) [19], [68], [69].

Among the existing psoriasis scoring methods, PASI is considered the gold standard for psoriasis assessment. However, new scoring methods developed are motivated to simplify assessment procedures, accommodate new parameters, and possibly minimise the score variations among the raters. However, due to the inherent subjectivity of human assessment most of these scoring methods suffer from intra- and inter-rater score variations. The subjectivity on assessment in turn can result in treatment inefficacy, as seen in psoriasis cases [24].

### **2.3.1 Subjectivity of Skin Assessment**

Most assessment methods are performed by using visual and tactile senses. A standard guide based on physical characteristics of the disease is used by dermatologists to score disease severities; perception will be significant in the physical interpretation of the disease. In many cases, subjective clinical assessments by dermatologist produce intra- and inter-rater variation.

Figure 2.8 illustrates two dermatologists assessing psoriasis lesions in a session of clinical trial using visual and tactile senses. Numerous studies have reported the intra and inter-rater variation problem on scoring methods of skin diseases. Chen *et al.* studied inter-rater reliability in leprosy assessment in which pain sensations of the skin lesion and peripheral nerve enlargement were assessed. It was found that the agreements among the raters were less than 0.53. In this study, leprologist, medical students, and leprosy staff were considered as the raters and involved to examine the

disease [70]. Forbes-Duchart *et al.* investigated an inter-rater reliability in paediatric burn scar assessment. Three raters are involved in the study.



**Figure 2.8** Two dermatologists are assessing psoriasis lesions.

Modified Version of the Vancouver Scar Scale (MVSS) is used to score the scar severities. MVSS defines four parameters for scar assessment, such as pigmentation level, vascularity, pliability (skin elasticity), and height (scar thickness). In the analysis of  $\kappa$  agreement between two raters, it is found that all MVSS parameters have a low inter-rater reliability. The maximum  $\kappa$  coefficients for pigmentation, vascularity, pliability, and height parameters are 0.16, 0.25, 0.38, and 0.58 respectively. The research suggested the use of MVSS total scores rather than that of individual parameters [71].

Berth-Jones J. *et al.* reported that intra-rater reliability of three scoring methods for psoriasis (PASI, CoPASI, and PGA) cannot be categorised as a perfect agreement. In the inter-rater reliability evaluation, agreements of PASI and CoPASI are considered only substantial and become lower for PGA assessment (moderate agreement). In this regard, CoPASI might be better than PASI and PGA, particularly for assessment of milder cases [69].

Principally, the development of objective assessments and measurements is continuously improving to reduce subjectivity and introduce objectivity in skin assessment [72]. Although the scoring parameters have been simplified, the intra and inter-rater variations problem remain. To eliminate the aforementioned

problems, it is pertinent to develop techniques to measure and quantify the parameters in order to obtain objective scores for skin assessment.

### **2.3.2 PASI Scoring for Psoriasis Assessment**

Psoriasis assessment using PASI scoring method was proposed by Fredriksson and Pettersson in 1978. This new assessment is used to evaluate efficacy of Ro 10-9359, a retinoic acid derivative, for treating the psoriatic patients. In their study, more than 90% reduction of psoriatic lesions in 10 patients out of 20 after 4 to 8 weeks of medical treatment has been found. Total PASI score functionally is used to indicate the reduction of psoriasis severity [21].

As mentioned in previous chapter, there are four PASI parameters - area, erythema, thickness, and scaliness - that need to be assessed in a round PASI assessment. Dermatologists carefully select the representative lesions from each body region for scoring (head, upper limb, trunk, and lower limb). The head incorporates face, scalp, ear, and neck. Meanwhile, chest, stomach, back, armpits and genital are considered as the parts of the trunk. The upper limbs comprise the arms, hands, and palms whereas the legs, buttocks, feet, and soles are belong to the lower limbs [73]. In this research work, the patients are required to wear their underwear during the assessment sessions. It implies that the psoriasis condition on breast, buttock, and genital regions are not assessed during the clinical study.

The following description is an example of a psoriasis patient that has been involved in clinical study (Patient 052, male, 35 years old). He has been assessed by dermatologist (Dermatologist 1). Figure 2.9 shows a summary of the PASI score from the assessment.

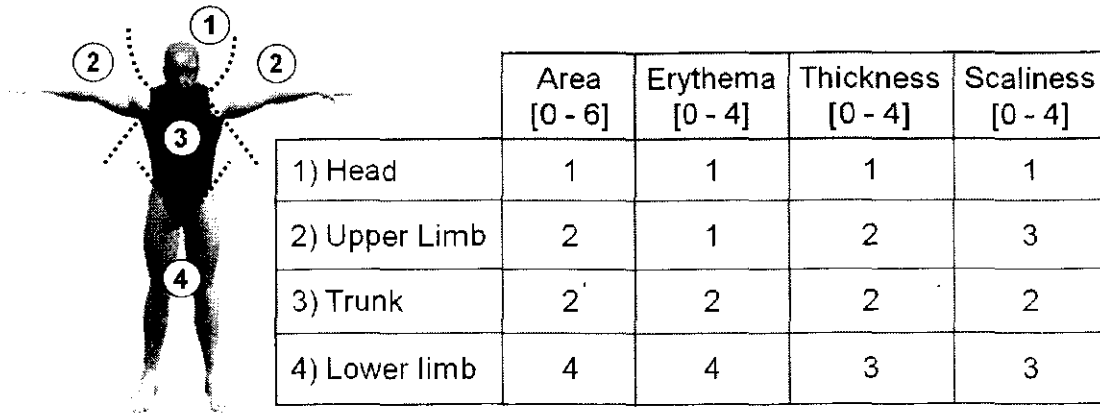


**Figure 2.9** An example of PASI scores summary obtained from dermatologist assessment to a psoriasis patient.

The total PASI score for this patient is calculated using the scores to Equation (1-1) (Chapter 1). The detail of calculation is explained as follows:

$$\text{PASI} = 0.1 \times (E_h + T_h + S_h)A_h + 0.2 \times (E_u + T_u + S_u)A_u + 0.3 \times (E_t + T_t + S_t)A_t + 0.4 \times (E_l + T_l + S_l)A_l \quad (2-1)$$

$$\text{PASI} = 0.1 \times (1 + 1 + 1)1 + 0.2 \times (1 + 2 + 3)2 + 0.3 \times (2 + 2 + 2)2 + 0.4 \times (4 + 3 + 3)4 \quad (2-2)$$

$$\text{PASI} = 0.3 + 2.4 + 3.6 + 16.0 = 22.3 \quad (2-3)$$

The result shows that the total PASI score for the observed patient is 22.3. This total value is important for dermatologist, especially to determine the treatment efficacy. In this case, the given treatment is considered significant if total PASI score after treatment can achieve at least 5.5 (75% reduction from initial total PASI score). According to maximum scores for each parameter and total PASI score equation, the score can achieve 72 for a maximum score. In real situation, a maximum score is uncommon since the patients are being treated to reduce the psoriasis severity. The high total PASI scores usually are not more than 40 [74].

PASI scaliness assessment is conducted by dermatologist based on certain physical descriptions as listed in Table 2.1. These descriptions are referred by dermatologists as a standard guidance for determining PASI scaliness scores.

**Table 2.1** Features for PASI scaliness scoring used by dermatologists

PASI Score	PASI scaliness visual descriptors
0	No scale
1	Fine scale, some of lesion covered by scale
2	Coarse scale with most lesion partially covered by scale
3	Coarse scale almost all lesions covered by a rough surface
4	Very coarse thick scales covering all lesions, very rough surface

Dermatologists score the lesions based on their visual and tactile perceptions. Figure 2.10 shows the psoriasis lesions for PASI scaliness scores 0 to 4. These images are used to provide training on PASI assessment. The high score lesion is rougher compared to the lesion with low scores. It is clear that the lesion roughness is related to the scale appearance on the lesion surfaces. As shown in Figure 2.10, no scales appear on lesion score 0 and only fine scales at lesion score 1. However, at score 4, a large amount of rough scales can spread over lesion surfaces.

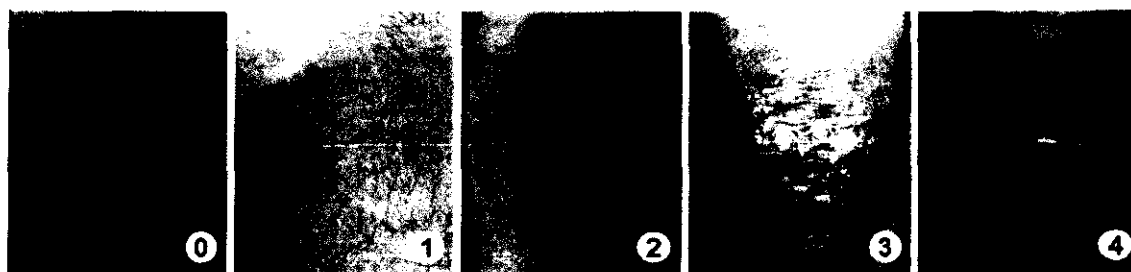


**Figure 2.10** Psoriasis lesions and its PASI scaliness scores given by human visual and tactile perceptions [75].

In its application, it is found that PASI assessment is subjective, time-consuming and requires trained physician. Thus, it leads the assessment to be difficult to be applied in either daily practice or a large-scale epidemiologic research. In addition, the self-assessment by the patients or clinical study participants are not included in PASI scoring but all parameter scores are obtained only from dermatologists' observation and assessment [76]. Regardless of those drawbacks, the PASI scoring, however, is still considered as the gold standard in a psoriasis assessment.

## 2.4 Summary

This chapter presents the information about human skin, psoriasis skin disease, severity assessment, and its treatments. These descriptions describe the significance of the study on skin disease assessment, especially for psoriasis skin disease. The disease brings some effects on the largest part of human body and cannot be totally cured. In response, an accurate and objective assessment is highly required to evaluate the treatment efficacy given by the dermatologist.

Psoriasis is a common skin disorder that affects about 2 - 3% of world population. It is known as the most prevalent immune-mediated skin disease for adults. Until recently, the initial process of psoriasis has been being in research and not totally discovered yet. The psoriasis lesions can affect at any body parts. Psoriasis is categorised into several types based on its specific appearance. The types include plaque, guttate, flexural, and erythrodermic psoriasis. Plaque psoriasis is the commonest case among the psoriasis types. Considering that psoriasis cannot be totally cured, a long term treatment for this disease is highly needed.

Psoriasis assessment using PASI (Psoriasis Area Severity Index) scoring method was proposed by Fredriksson and Pettersson in 1978. The scoring method defines four assessment parameters, namely area, erythema, thickness, and scaliness. The parameters are scored by dermatologists for each defined body regions (head, upper limb, trunk, and lower limb). The scores are given based on visual and tactile descriptions of the psoriasis lesions. Total PASI score is used to indicate the reduction of psoriasis severity.

PASI scaliness assessment is conducted by dermatologists based on their visual and tactile perceptions. The PASI scaliness scores are ranging from 0 to 4. The scores are used to represent the amount of scale on the lesion surface. It is found that PASI assessment is subjective, time-consuming and requires trained physician. Although these disadvantages are permanently extant in PASI scoring method, the scoring method is still considered gold standard for psoriasis assessment.

## CHAPTER 3

### SURFACE MEASUREMENT METHODS

Chapter 3 describes about the background information of the methods for measuring surface roughness and analysing the measurement results using a clustering algorithm. Section 3.1 reviews the methods of the surface roughness analysis. In the initial section, a long history of the surface roughness implementation is presented. Since the beginning era, mechanical surface profilometry has been commonly used to measure the surface texture of manufacturing and metallurgical products. Here, a sharp needle is drawn along a line on the measured surface to acquire height information. Although being able to provide a high resolution, this method in fact still has the very restricted scan area and scanning time. In response to this restriction, the imaging technologies then provide a light profiling medium to extract the height profile of the measured surfaces. Three imaging methods for 3D surface measurements are presented in this subsection; those are laser profilometry, light scattering and structured light projection. To enable surface roughness measurement, surface filtering and surface roughness parameters have to be defined. Surface filtering is a method aimed to extract a roughness component from certain unsuitable components of surface profile. Such methods include Fourier transform, Gaussian filter, wavelet filtering, and polynomial surface fitting. The following subsection discusses the surface roughness parameters that dominate the current standard in a surface roughness measurement. Section 3.2, on the other hand, shows some applications of imaging methods for skin surface roughness measurement. At last, the summary of the materials that have been described in Chapter 3 is briefly described in Section 3.4.

### 3.1 Surface Roughness Analysis

The main problem of assessing surfaces is related to the small size of the machining marks. Surface roughness is one of important quality parameter in many industrial applications such as manufacturing process of metals, semiconductors, ceramics, paper, and plastic products [77]. Until in the end of 1920s there was no any effort to create a surface measurement system. The metallurgists at that time merely examined the surfaces by their visual and tactile perceptions. This examination might be sufficient in one factory but not for further examination outside to the factory [78]. To standardise the assessment, several samples with certain roughness were provided to be used as the references to compare with the assessed surface. By comparing with these reference samples, the metallurgists were able to classify the assessed surface according its roughness levels.

### 3.2 Mechanical Surface Profilometry

Mechanical surface profilometry is a conventional method for measuring surface roughness. It uses a sharp stylus made of diamond for sweeping along the measured surface. Here, the stylus tip, which has a few micrometers of radius size, is drawn on the surface. During the movement, the stylus body will move up and down following the profile variations of scanned surface. In common, the recommended length for stylus scanning is 5 mm [79]. The vertical variations of the stylus are automatically interpreted as the roughness profile of the surface. The scan resolution of stylus profilometer is limited by the diameter size of stylus tip [79]. To obtain a reliable measurement, ridge valleys of the surface profile should be wider than the diameter size. If the valley is narrower than the stylus tip diameter, the profilometer will not extract the actual elevation of the surface. This problem can be solved by applying a finer probe to replace the stylus tip, as applied by Atomic Force Microscopy (AFM). However, the tiny scan area and the long scanning time become the drawbacks of AFM. For example, to measure an area of  $70 \times 70 \mu\text{m}^2$  it requires at least 1 to 2 hours for each scan [79]. The advantages of mechanical surface profilometry are listed as follows [80]:

- Measurement is performed to the measured object without any prior

treatment.

- The measurement can cover a wide range from tens of microns to ten of millimetres. In addition, the vertical sensitivity can be increased less than 10 nm.

Despite these advantages, the mechanical surface profilometry has several drawbacks:

- Contact stress of stylus tip can damage the scanned surface. The stylus also could scratch the surface especially for the soft materials. Although the stylus load is low, it can cause a high stress for being applied and centred to a very small area of stylus tip.
- A number of vertical points might not correctly be profiled by the stylus tip. It occurs when the size of stylus tip is bigger than the vertical gaps. As a consequence, the stylus tip is not able to enter deeply to the point location.
- To obtain two-dimensional topographical information, a number of the consecutive line scans are required. This scanning process can be time-consuming. Based on this constraint, the sample area is typically limited to a small size only.

The drawbacks founded on mechanical surface profilometry motivate the researchers to develop non-contact techniques for surface roughness determination.

### **3.3 Imaging Technologies for Surface Analysis**

After established for hundred years, mechanical stylus profiling has been proposed to be replaced with several optical techniques. These optical techniques give some advantages in measuring surface roughness as follows [80]:

- Scanning process is not going to damage the scanned surface. Additionally, profiling process can be performed without applying any direct contact between the sensor and the scanned surface.
- Physical stylus is not longer used as a profiling sensor. The function has been replaced by applying a light medium that can omit the probe breakage problems.

- The scan using the light as the measurement medium can have a very fast completion.
- The light beam as the probe medium is able to penetrate the vertical profile deeper than the probe stylus. In the mechanical stylus, the probe cannot measure an actual surface that is located in small gap – smaller than the stylus.
- Measurement is able to cover a large area. The light also can be directed to perform measurement on a large area.

Beside those advantages, the optical methods have several challenges, such as:

- The light coming from a certain angle might be covered by the surface profiles in which the reflected light in this condition will not give any depth information correctly.
- The measurement results can be influenced by the optical characteristic of the surface material. In this case, the reflected light might come from the unwanted surface resulting errors for a depth measurement. As shown in Figure 3.1, the  $n_1$  and  $n_2$  are made of the distinct materials. Stylus profiling is able to measure the surfaces correctly since the stylus sweep is not reliant on the optical characteristics of the materials. However, for the optical measurement it may obtain inaccurate results.

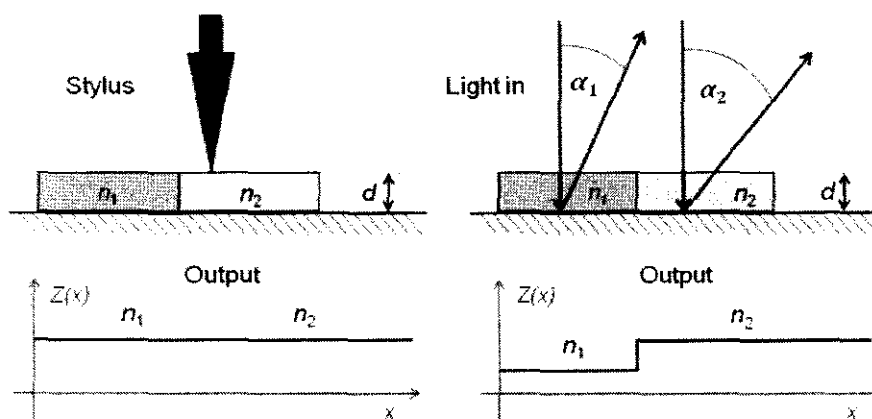


**Figure 3.1** Stylus and optical measurements.

Imaging technology is applied for measuring surface roughness. This implementation is motivated by two main objectives: to provide high resolution (depth and lateral resolutions) measurement and to perform high speed scanning. In

this case, the earliest technology is laser profilometry.

### 3.3.1 Laser Profilometry Method

In laser profilometry, a laser beam is emitted and line by line directed to a scanned surface. The laser beam is used to profile the elevation points of the surface. The elevation points are determined by applying triangulation method to the reflected light. The reflected light is focused by an optical lens to a light sensitive detector. A surface topography, afterward, is interpreted from the projection of the reflected laser on light sensitive detector. Figure 3.2 describes the triangulation principle of a laser camera in extracting the elevation profiles of the scanned surface. The laser light is exactly reflected to the centre of light sensitive detector if the light is projected onto a reference plane. Once the surface is located either upper or below the reference plane, the reflected laser light would be deviated from the centre of the detector. Depth information is then determined from the deviations of reflected laser light on the light detector. A higher deviation represents a farther location from the reference plane.

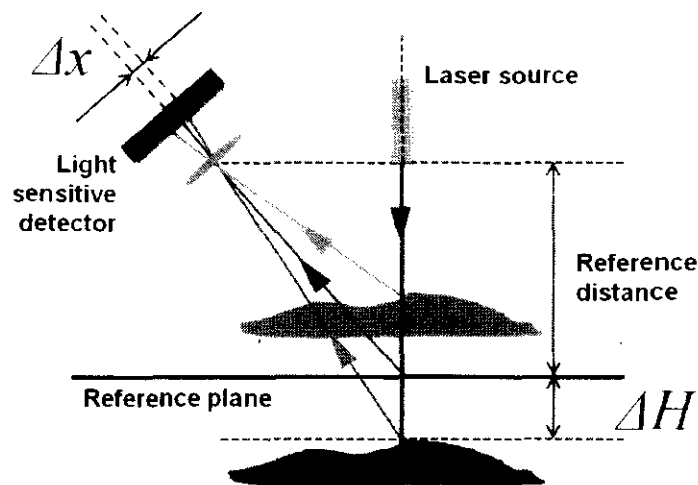


**Figure 3.2** Laser triangulation of laser camera.

The laser profilometry has some advantages such as providing high resolution scan, being able to penetrate and scan deep surfaces and being adapted with any kinds of materials. However, this also has some drawbacks, for example the scanning process that cannot be performed as a fast measurement. By using a laser scanner, the surface information obtained is not a grid matrix of elevation data. The

information is recorded by a laser system as a point of cloud. To construct a 3D surface, these measured points need to be connected using an interconnection of small triangular meshes. In order to enable practical linear calculation, these meshes are then converted to a grid of XYZ coordinates. The data obtained from laser profilometry has been applied for measuring skin disease treatments. In this research, a laser scanner, Konica Minolta Vivid 910, has been used to scan the surface of the psoriasis lesions.

The laser scanner can properly scan the skin surface if the surface is stable. Conversely, the scanning cannot be properly performed for the regions with some vibrations on the surface such as at the chest regions. The vibrations are caused by a periodical breathing movement. For having no stability on the scanned surface, a focused surface is difficult to be obtained. Figure 3.3 shows the example of psoriasis lesions obtained from the laser scanner. Figure 3.3 (a) shows 2D image of plaque psoriasis lesions at lower back region. The surface vibrates are continuously caused by the breathing movement. Figure 3.3 (b) displays the blurriness of the scanned lesion at a vibrated surface. Some parts of the scanned surfaces are overlaid due to the surface movement during the scanning process. These overlying edges are found at the edges of tape 3 (pointed by arrow 1) and the lesion edges (shown by arrow 2).

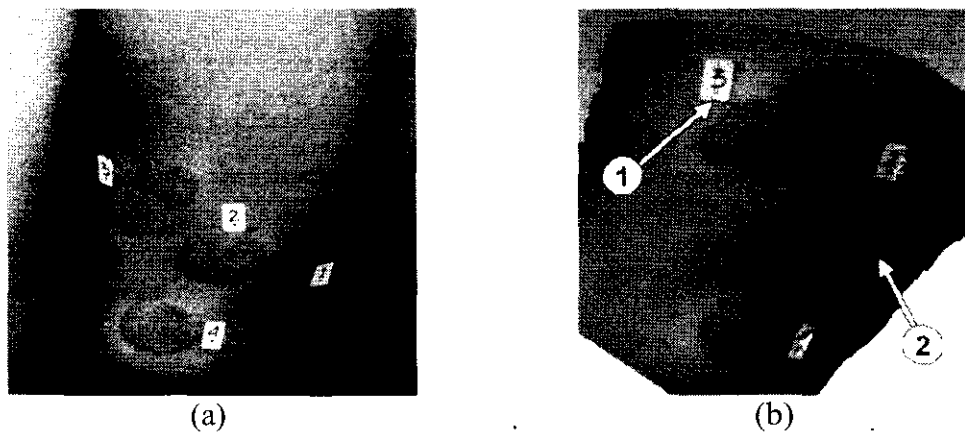


**Figure 3.3** (a) 2D image of psoriasis lesions (b). 3D surface of psoriasis lesions is scanned by a 3D laser scanner.

### 3.3.2 Light Scattering and Speckle Imaging Methods

Another technology implemented for surface roughness measurement is light scattering and speckle imaging. In these technologies, a light beam is projected to

the scanned surface. The beam consists of many light paths. The reflected lights are then photographed by a 2D camera. The roughness differences are determined based on the characteristic of reflected lights. Figure 3.6 shows the reflected light of two surfaces with different roughness.

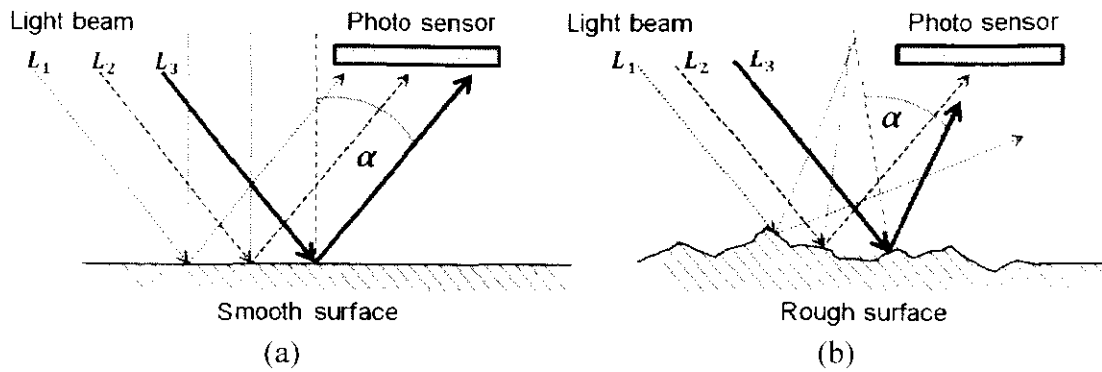


**Figure 3.4** The light is uniformly reflected at (a) smooth surface whereas (b) the rough surfaces will scatter the light to various directions.

In the light scattering method, the smooth surface reflects the lights in uniform direction to the camera. In the other hand, rough surface will return back the projected lights at unordered manner. The intensity of reflected light from smooth surface will be higher than the rough surface. Photo sensor at smooth surface can receive reflected light at higher intensity. It can occur because all of the lights are reflected by smooth surface with the same reflection angles. The intensity received by photo sensor at rough surface will be lower. The reflected lights are scattered due to unordered normal direction of the rough surface. Surface roughness is then interpreted based on these reflected light characteristics.

Persson illustrates the distribution of reflected light from different surface roughness - smoother and rougher surfaces [81]. The light is emitted perpendicular onto the measured surfaces. The reflection angles and reflected light intensities are then recorded. To provide a reference value, surface roughness of the observed subject is determined by rms-roughness. The rms-roughness of smoother surface is 50 nm whereas the rms-roughness of rougher surfaces is 300 nm. The surface is made of stainless steel and it is illuminated with laser light  $\lambda=700$  nm. From the experiment, it can be found that reflected light dispersion of the rough surface is higher than the smoother surface. The rough surface will scatter the reflected light to

more various directions. Histogram of reflection light intensity against reflection angles are created to find the light dispersion characteristics. The intensities of reflected light from smoother surface are accumulated in a certain angle. For the rougher surface, the reflected light are scattered at various angles. Therefore a certain amount of light intensity can be found at all angles. The histograms of both surfaces are presented in Figure 3.5 (a) and (b).

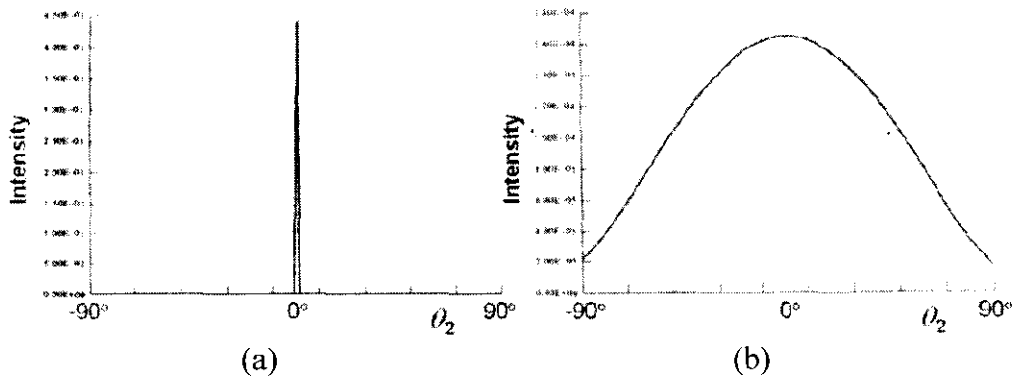


**Figure 3.5** Intensity distributions of reflected light from (a) smoother surface and (b) rougher surfaces.

As performed by light scattering, speckle imaging method also interprets surface roughness based on reflected illumination on the measured surface. However, in the speckle imaging, the speckles amount in the image. Average contrast of the speckle is also found related with the surface roughness [82]. Speckle is considered a random pattern region of bright and dark which is obtained when a surface is illuminated by a highly or partially coherent light beam [77]. Both methods, light scattering and speckle imaging can provide advantages on non-contact measurement and fast scanning [77]. Despite these advantages, the method has drawbacks in the 3D surface measurement. The drawbacks of this method are sophisticated system arrangement and standardised environment lighting. The measurement surface is usually limited to the small size area.

### 3.3.3 Structured Light Projection Method

Another available method for acquiring 3D surface is the structured light projection. This 3D measurement method has been used for many years in various researches and industrial applications [83]. The method utilises the projection of some

particular structured patterns onto the measured surface. A series of the structured patterns can also be applied for the measurement. 2D images of the surface with several projected patterns are computed to reconstruct 3D surface. Depth information is interpreted from deviations of the projected patterns on the surface. Currently, some pixel-wise addressable projection systems on the basis of micro mirror projectors have been being used to create certain projected patterns. These projector systems in their application are able to generate various types of the pattern with high resolution. Furthermore, the application scope of the method has been expanded from measuring small size area to the large coverage area [83].

Principally, the structured light projection also uses a triangulation process as applied in the laser profilometry. This method also projects a light beam to the scanned surface, as conducted by scattering method. However, the structured projected light illuminates a structured pattern, rather than speckle imaging that illuminates random of lights. A difference between both of methods lies on the way of implementing the light profiling. Laser triangulation, as aforementioned in the previous section, uses a single beam to profile the surface. By applying this method, the surface elevations are able to be measured point by point. However, the structured light projection measures the surface elevations of the whole area at once. The area of projected pattern is composed by an equidistant of several line triangulations. The scanning is simplified by projecting the lines at the same time. Therefore, the movement of either the optical sensor and the measured object are not needed [83].

In this research, a 3D optical scanner is built by applying a structured light projection method. Thus, the details of this method are more widely elaborated. Figure 3.6 shows the basic diagram of camera and projector arrangement in the structured light projection. The projector and the camera are adjusted at fixed positions. These positions are indicated by the projection angle  $\alpha$ , the distance of the projector to the camera, and the distance of the camera to the reference measured surface. The principle of 3D surface acquisition is mentioned in the following section as mentioned in [84] [85]. Phase-shifting method has been widely applied in 3D surface measurement in consideration of its scanning speed and high accuracy.

Initially, three images are required to apply a phase-shifting algorithm, which therefore is called as the single three-step phase-shifting algorithm. These images are obtained from some projected fringe patterns on the measured surfaces and differentiated with a phase shift angle  $\theta$ . These three images can be expressed by following equations.

$$I_1(x, y) = I_0(x, y) + I_{mod}(x, y) \cos(\phi(x, y) - \theta) \quad (3-1)$$

$$I_2(x, y) = I_0(x, y) + I_{mod}(x, y) \cos(\phi(x, y)) \quad (3-2)$$

$$I_3(x, y) = I_0(x, y) + I_{mod}(x, y) \cos(\phi(x, y) + \theta) \quad (3-3)$$

Variables  $I_1(x, y)$ ,  $I_2(x, y)$ , and  $I_3(x, y)$  denote the intensities of three fringe patterns.  $I_0(x, y)$  represents the background intensity and  $I_{mod}(x, y)$  represents the modulation signal amplitude. Meanwhile, variables  $\phi(x, y)$  and  $\theta$  are the phase and the constant phase-shift angle, respectively. The phase map  $\phi(x, y)$  is calculated by applying three fringe images as written in the following equation.

$$\phi(x, y) = \tan^{-1} \left[ \sqrt{3} \frac{I_1(x, y) - I_3(x, y)}{2I_2(x, y) - I_1(x, y) - I_3(x, y)} \right] \quad (3-4)$$

The phase  $\phi(x, y)$  calculated in (3-5) will have a range from  $-\pi$  to  $+\pi$  and discontinuity points at multiples of  $2\pi$ . These discontinuities are located and then discarded by adding or subtracting the phase  $\phi(x, y)$  with multiples of  $2\pi$ . The equation for removing discontinuity is given by

$$\Phi(x, y) = \phi(x, y) + 2k\pi \quad (3-5)$$

The  $\phi(x, y)$  and  $\Phi(x, y)$  are known as the unwrapped and wrapped images, respectively and variable  $k$  denotes the projection period. The elevation map in 3D coordinates is determined based on the phase difference between the measured surface  $\Phi(x, y)$  and reference surface  $\Phi_0(x, y)$ . The phase of reference surface  $\Phi_0(x, y)$  is obtained from the projected pattern images on the flat surface. From Figure 3.6, it can be derived an equation for determining height  $Z$  as described in (3-6)

$$\frac{Z}{L-Z} = \frac{d}{B} \quad (3-6)$$

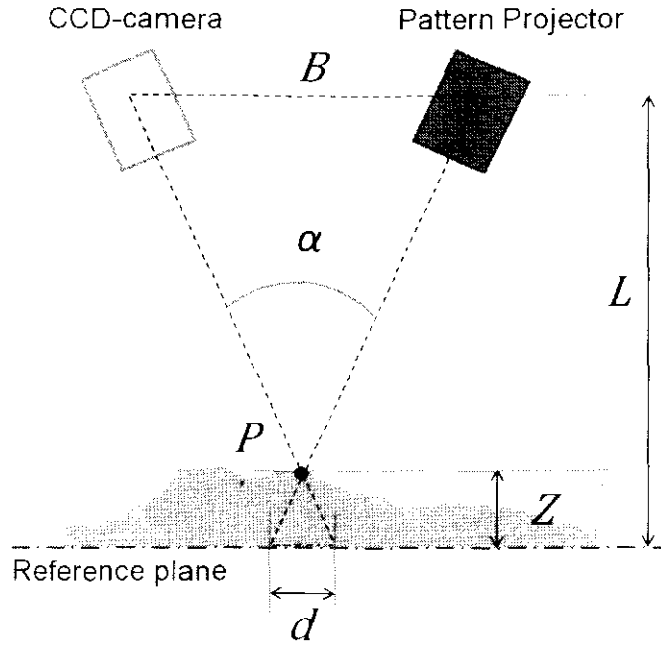


**Figure 3.6** Diagram for depth calculation based on phase differences.

Equation (3-6) is then simplified to obtain the following equations:

$$Z = \frac{L-Z}{B} d \quad (3-7)$$

$$Z = \left( \frac{L}{B} - \frac{Z}{B} \right) d \quad (3-8)$$

Since  $Z \ll B$ , it can be considered that  $\frac{Z}{B} \approx 0$ . This simplification can give

$$Z \approx \frac{L}{B} d \quad (3-9)$$

It is known that  $d$  is directly proportional to the phase difference,  $d \propto (\Phi - \Phi_0)$ , and then the equation (3-9) is modified to obtain a new expression (3-10).

$$Z \approx \frac{L}{B} (\Phi - \Phi_0) \quad (3-10)$$

According to this method, the measured skin surface is exposed by a structured fringe-shaped light projection. The light is projected by applying projection angle  $\alpha$  from the vertical axis. Since the scan process is quite fast, it can deal with the

constant vibration of skin surface. This movement is caused by the vibration of the autonomous nervous system. Despite the method advantages, there are some limitations in the 3D surface acquisition. These limitations can be described such as measurement resolution and shadow problems. The measurement resolution depends on the projector resolution and the CCD density of the camera [86]. The method also cannot measure accurately the shadowed area and isolated surfaces [87]. These locations are usually found either as deep pit or localised peak surfaces.

### 3.4 Surface Profile Characterisation

The surface characterisation has been widely used in diverse application fields, such as road monitoring, material industry, remote sensing, and medical engineering. ISO 14460-1 defines the surface as a set of features which physically exist and separate the entire work piece from the surrounding medium [88]. A surface can be considered as a boundary layer between object and its environment. Normal profile, perpendicular to the reference surface, is used to extract the vertical variations of surface profile. The profile can be classified into three main components; namely roughness, waviness and form [88], as depicted in Figure 3.7 [89].

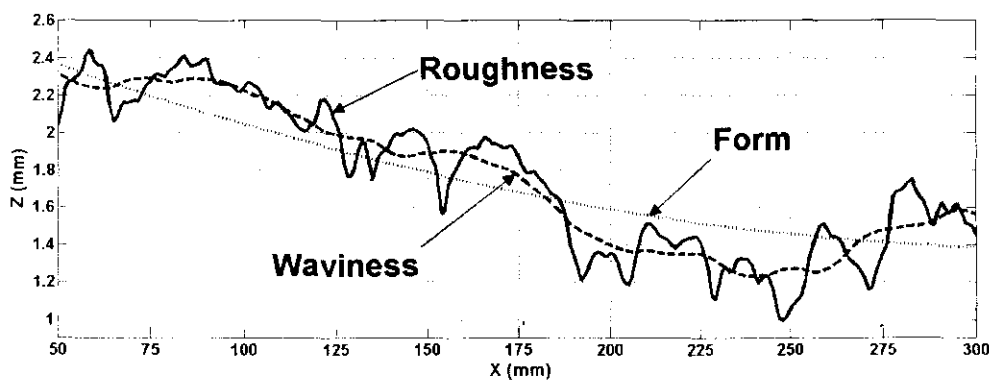


**Figure 3.7** Surface profile is composed by three major components - roughness, waviness, and form [89] [90] [78].

These components are superimposed to form a surface profile. The surface wavelength or peak-to-peak spacing is used to differentiate a number of surface profile components [88]. Roughness has the finer texture and ridges compared to waviness, which is smoother than the roughness. Form, meanwhile, is a curved surface with a very long-range deviation.

The profile components are distinguished based on their wavelength. The roughness is the component with short wavelengths whereas the longer ones belong to the waviness and form [90]. ISO 115621, a standard for the manufacturing application, defines the separation point between roughness and waviness based on its wavelengths. Figure 3.8 depicts this component separation. The distribution of the roughness wavelength is denoted by  $R$  whereas waviness wavelength is represented by  $W$ . The wavelengths of roughness profile range from  $\lambda_1$  to  $\lambda_2$  in which the shorter wavelengths ( $\lambda < \lambda_1$ ) exist in the surface. However, its quantity is not significant and can be neglected. The waviness profile has longer wavelengths ranging from  $\lambda_2$  to  $\lambda_3$  in which wavelength  $\lambda_2$  is assigned to a wavelength that has the proportion of 50:50 for its roughness and waviness. The  $\lambda_3$ , meanwhile, is used to separate the waviness and form profiles [78].

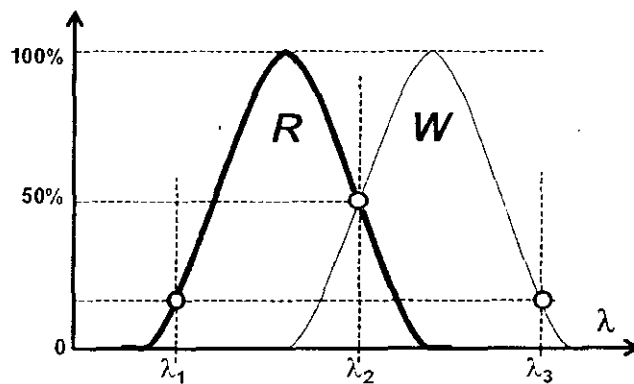


**Figure 3.8** Wavelength distributions of roughness and waviness [78].

The characterization and separation methods of surface profile are therefore important in a surface determination. These methods are implemented as a filtering process to the measured data. There are several filtering methods that can be applied to separate the surface components [90] such as Fourier transform, Gaussian filter, wavelet, and polynomial surface fitting.

In the earliest years, surface roughness filtering was performed manually based on a graphical plot on the 2-dimensional coordinates. In this case, the plot is divided equally into several segments. A mean line is subsequently created for each segment. The line is drawn to represent the gradient between the segment intervals. Vertical deviations are then determined by subtracting the actual profile to the gradient line. Nowadays, some computational methods are widely applied to

separate the profile components. The main objective of surface characterisation is to extract and to eliminate the waviness component. This waviness can be filtered by applying some methods such as Fourier transform, Gaussian filter, wavelet filtering, and polynomial surface fitting.

### **3.4.1 Fourier Transform**

Digital Fourier transform is used to filter the components of a surface profile. The method was initially explored by Raja and Radhakrishnan [91]. In a surface engineering, the surface is considered to be formed by certain sinusoidal functions with various amplitudes and frequencies. From aforementioned discussion, it is known that the surface profiles – roughness, waviness, and form – are differentiated based on their frequencies. A number of cut-offs frequencies are defined by a user to enable a surface profiles differentiation [91]. In this case, this power spectral density analysis has been applied to determine surface roughness of metal surface [92].

### **3.4.2 Gaussian Filter**

Gaussian filter is one of the surface characterisation methods widely used in recent years. A single filter here can be applied to extract roughness and waviness components [91]. However, Gaussian filter possesses some drawbacks in its implementation. The first drawback is edge distortion that can be found in the edges of the filtered data. In addition, Gaussian filter cannot properly perform to filter a surface dominated by a large form. Even, it is not robust to deal with outliers [91].

### **3.4.3 Wavelet Filter**

Principally, the aim of wavelet filtering is similar with Gaussian filter. Both filters are used to characterise the surface profile components based on their wavelengths. Compared with Gaussian filter, the wavelet filter, however, has more advance capabilities. This filter can be used to analyze data at various resolution levels. For this, its filter is also known as the multi-scale filters. Figure 3.9 depicts the decomposed signals of a surface profile [91]. Diff1 is a signal component with the shortest wavelength (the highest frequency). The advantage of wavelet filter is its

ability to decompose the profile component, specifically at certain wavelength. Used in many works on surface roughness determinations, the wavelet filtering method also has a drawback in which its process requires a high computational cost. Also, it finds difficult to define the required number of level in the filtering process.

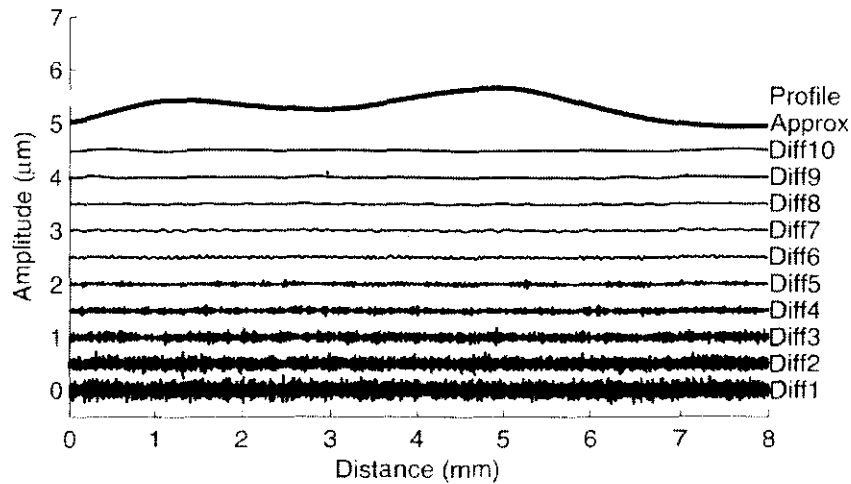


**Figure 3.9** Wavelength distributions of roughness and waviness [91].

#### 3.4.4 Polynomial Surface Fitting

Polynomial surface fitting has been widely used in the 3D surface characterisation of various applications. The surface fitting determines a least square mean plane. The plane here represents the nominal direction of a surface. A quadratic polynomial surface is the suitable approximation of common geometrical shapes in a small area. Further, the polynomial surface fitting is widely used to fit various surface shapes, such as partial cylindrical forms, partial spheres, and any arbitrary curved forms. Determination on a suitable polynomial order, however, can result in a problem. This problem occurs when the surface fitting is applied to a surface containing some different curvatures [93] [94]. Polynomial surface fitting is usually fitted into a rectangular mesh of XYZ coordinates. Buxton *et al.* have found that the whole human body curvature can be constructed using interconnection of rectangular meshes [95]. This fact shows that polynomial surface fitting is suitable to be applied to any part of human body surfaces.

In the early roughness measurement by using stylus profilometer, there are three terms to define the sample [78] including traversing, assessment, and sampling

length. Traversing length is the crossing distance of the stylus over the measured surface. Assessment length is only a part of traversing length that would be assessed. Another shorter sample is then measured from the assessment length. This shorter part is called as the sampling length. Figure 3.10 shows this sample categorisation in term of one dimensional sampling.

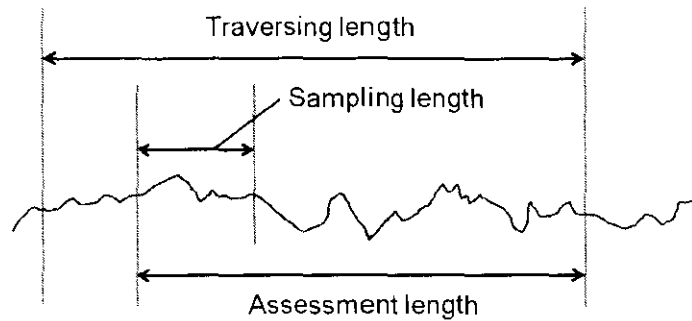


**Figure 3.10** Sample categorisation based on the coverage area of the sample.

In the research, this categorisation is also implemented. The traversing length corresponds to a maximum scanned area by the camera. Meanwhile, assessment length is similar with the ROI of the image. In the research, ROI is defined as a lesion area in the scanned image. In this research, sampling length, additionally, can be considered as the smallest subdivided area of the developed algorithm. The next chapter of this thesis will present the determination of the optimum sampling area for surface roughness algorithm.

### 3.5 Surface Roughness Parameter

Most of 3D surface parameters are extended from the earlier 2D parameters of surface roughness. These 3D parameters were initially proposed and listed in 1990s. The parameters consist of 14 parameters leading it to be known as "Birmingham 14" [88]. New parameters were included to the list afterward. The ASME B46.1 has also included some 3D parameters in their standard. Currently, several 3D parameters are being viewed to be adopted as the international standards [90].

Surface parameter is divided into three main groups, each of which is differentiated based on the direction of the measured unit. The groups are including amplitude, frequency, and combination of amplitude-frequency based parameters.

Meanwhile, the calculation of the amplitude parameter has applied the vertical distances of the surface data points. The frequency parameter is calculated based on the distances at horizontal direction. To accommodate a measurement from both directions, these two parameters are combined in order to provide an amplitude-frequency parameter. Figure 3.11 displays the distances used for surface roughness determination.

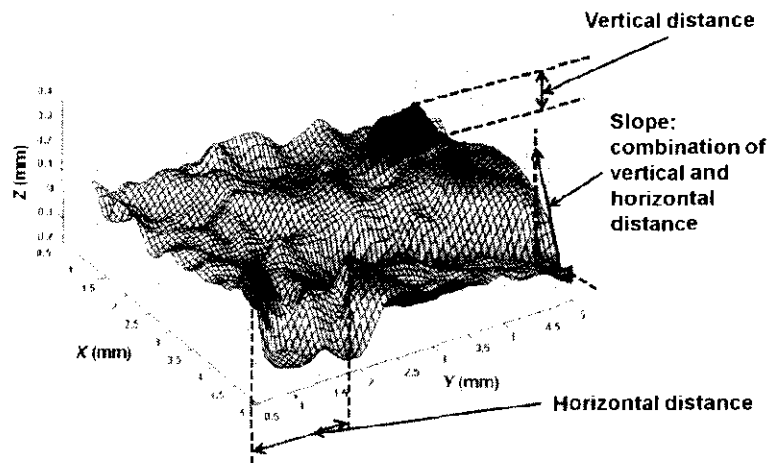


**Figure 3.11** Three main groups of surface roughness parameters.

Several roughness parameters are classified as amplitude parameters such as average roughness ( $S_a$ ), root mean square roughness ( $S_q$ ), maximum profile peak height ( $S_p$ ), maximum profile valley height ( $S_v$ ), maximum height of the profile ( $S_t$ ), and average maximum height of the profile ( $S_z$ ). Here, average roughness ( $S_a$ ) is defined as the average of the absolute vertical deviations measured from the mean surface. Root mean square roughness ( $S_q$ ), meanwhile, is determined by applying root mean square to the profile measured from the mean surface. Maximum profile peak height ( $S_p$ ) additionally refers to the distance to the highest point of the profile measured from the reference surface. Maximum profile valley height ( $S_v$ ) and maximum height of the profile ( $S_t$ ) are determined as the distance of the lowest point to the reference surface and the distance between the highest and lowest points of the surface profile, respectively. Lastly, the average maximum height of the profile refers to the average of the successive values of  $S_{t,i}$  which is calculated over the area of the profile. The  $S_{t,i}$  in this case is the maximum height of the profile within the sampling length of  $i$ -th. Usually, the measured area is segmented into several

sampling areas. If the measurement is applied to the whole areas,  $S_z$  will be equal to  $S_t$ .

Furthermore, the mean peak spacing can be used to determine the surface roughness based on a horizontal distance. This parameter is denoted by variable of  $SS_m$ , which is calculated by averaging the distance between zero crossings of the profile. At this point, two conditions need to be satisfied to specify a crossing as zero crossing. The first condition is the greater maximum profile height between two zero crossings compared to a threshold. The threshold is usually set at 10% of  $S_z$ . The second condition is that the spacing between two zero crossings is greater than a threshold; typically it is 1% of the sampling area. Furthermore, a slope is used as a hybrid parameter that combines the amplitude and frequency parameters. The value is determined as the ratio of the vertical to the horizontal distances of two consecutive data points. To increase sensitivity on the spacing of data points, six consecutive points are used in the slope determination. The average roughness is mostly used among the amplitude parameters that can represent the actual vertical deviation of surface, minimise impulse noises, and consider all data points in roughness determination. A research on tactile perception also shows that perceived coarseness by human on several paper surfaces is correlated ( $R^2=0.73$ ) with the surface roughness of the papers [96].

### **3.6 Imaging Methods for Skin Surface Roughness Measurement**

As mentioned in the earlier section, the skin assessment based on human senses and perception can result in a subjective assessment. To obtain objective results, a system of assessment and measurement based on imaging technologies has been developed. This research is focused on skin surface roughness as a characterisation parameter of skin lesion. Objective measurements of skin surface roughness have been attempted by several methods. The method of the skin roughness measurement can be grouped into invasive and non invasive method [97].

In invasive method, an incision procedure is required to provide sample data. For skin roughness measurement, a piece of skin sample is cut from the patient body. The measurement will be performed separately from the human body. This

procedure is widely known as skin biopsy. High resolution and tiny details of skin sample surface can be acquired by microscopic camera. The skin sample preparation is conducted by a plastic surgeon or dermatologist. A pathologist will handle the analysis part of the skin sample. Both processes require well trained medical personnel and may take 3 to 10 days for the results of the analysis [98]. For instance, the skin surface topography of wrinkles on elderly people is measured by light microscopy and scanning electron microscopy. Here, the measurement will detect the loss skin elasticity at wrinkled area. The skin sample is obtained by performing skin biopsy on the skin sample [99]. Scanning Electron Microscopy [100] on skin sample is considered as an invasive method. The texture impression is then observed using microscope to photograph the microscopic pattern of skin ridges and furrows. In this case, the 3D features cannot be analysed through the microscope observation.

Non-invasive method does not require skin cutting to obtain the sample. This method is preferred by most of the patient. Measurement can be performed as either non-direct or direct measurement. In non-direct measurement, the equipment is not applied directly to the skin surface. The process requires a skin surface replica to represent the actual surface. Conversely, the direct measurement does not need skin replica. The equipment can be applied directly to the skin surface of the living person. This method is also known as *in-vivo* measurement.

Direct measurement method is applied in early developments of surface roughness measurement. A high precision profilometer using sharp stylus is used to obtain profile lines of skin surface replica [101] [102] [103]. Since 1962 the silicon rubber plastic has been used to make an impression of skin texture by Sarkany [104] [105]. The process of replica preparation is not simple. Two mould steps using silicon materials have to be completed to obtain a skin replica. The first step is to create negative impression of skin surfaces. The negative impression is then used to cast a positive print of the evaluated surface. Since the process is performed manually, significant errors can be introduced in both replication steps. An experienced technician is required to prepare skin replica accurately. To complete the replication process, it can take few minutes (3 to 15 minutes) for the first step and several hours (3 to 5 hours) for the second step [106]. For another impression

material, it can take 24 hours to harden the skin replica [101]. Even though profilometer machines can measure with high resolution, the measurement process itself is very slow. Therefore this method cannot be adapted in daily practice that requires simple, reliable, and fast procedures. For instance, scan speed of stylus profilometer as used by Gassmueller *et al.* [107] ranging from 0.15 to 1.00 mm/s [108].

Light medium is applied to improve scan speed in surface roughness determination [109]. Three-dimensional (3D) imaging and computer vision algorithms are applied to enable a fast scanning and measurement at high resolutions. By using imaging technologies, characterisation of surface components will not be limited by the dimension of the profilometer stylus; instead, surface characterisation and filtering process of imaging technologies can be performed through computational operations.

By using a laser profilometer, light profiling can speed up the scanning process. Scan speed of optical profilometer used in [110] can be increased until 250 mm/s [111], 250× greater than scan speed of stylus profilometer. By applying light profiling, either a direct or non-direct surface measurement can be performed on skin surface [112]. Skin replica can be provided for light profiling to ensure the scanned surface is firm and stable. The measurement of laser scanner is initially applied in cosmetic industry – in which, as mentioned in [113], it is used to measure skin surface indicators. The cosmetic efficacy is evaluated based on skin surface indicators, such as fold reduction, skin smoothness, and skin tightness. Skin surface roughness is measured to evaluate those skin indicators. Laser profilometry has been used to determine surface roughness. In the research, the laser does not scan the skin surface directly but it scans the skin impressions of the actual skin surface. These impressions are made of silicon materials and measured at size 3 mm × 3 mm [113]. Skin roughness analysis is also performed to quantify skin aging. Initially, a skin replica is required to extract the skin texture. The skin replica, made of an araldite casting resin, is scanned to provide several quantitative parameters such as  $R_a$ ,  $R_p$ ,  $R_t$ ,  $R_{max}$ , and others [114].

Stripe projection method has been applied to determine *in vivo* skin surface

roughness [115]. By measuring *in vivo* skin surface roughness, inaccuracy caused by skin replica is investigated [116]. A 3D optical scanner using fringe projection method is used to acquire 3D surfaces from the actual skin surface and skin replica. Both scans are compared to find the 3D surface with better quality. It is found that fringe projection method on the actual skin surface can extract surface profiles more detail. Fine structures of skin surfaces cannot be represented during the process of replica making.

In the research, the skin roughness parameter of a psoriasis lesion is measured by analysing a number of digital images of lesion samples. The roughness parameter of healthy and unhealthy skin can be characterised by roughness parameters such as  $R_a$ ,  $R_q$ , and peak-peak height ( $R_y$ ) [117]. These parameters are extended to measure the 3D surface roughness.

Surface roughness also can be measured from the speckle texture of the surface. The image of speckle texture is projected from scattering of coherent light in a rough surface. The contrast of the speckle is found to be related to the surface roughness [118]. A number of the texture analysis methods, such as co-occurrence matrix [119] and fractal analysis [120], have been applied to determine the roughness from the speckle images. In a recent research, Tchvialeva *et al.* [109] proposed a speckle contrast method in order to determine the surface roughness. The results, afterward, have been validated with the results obtained from a fringe projection method.

Several methods are available for skin roughness determination. However, there are uncertainties in the methods that have not been defined yet. The methods have not been validated at various locations of the body surface. The reported studies have been selective in the location of the body surface such as cheek [121], back hand & upper buttock [122], facial area [123], volar forearm, lower back, thigh and lower leg [124]. It is pertinent that the measurement is reliable at any location of the body surface. In addition, it is found that most of the reported researches do not focus on surface roughness of marked lesion [121] [124] [123] whereas in clinical practice, surface roughness is not only measured to normal area but also to skin lesions. Table 3.1 summarises the comparison of 3D acquisition methods -

mechanical surface profilometry, laser profilometry, light scattering, and structured light projection - that currently used for surface measurement.

**Table 3.1** Comparison of 3D acquisition methods for surface measurement.

Methods	Advantages	Disadvantages
Mechanical surface profilometry	<ul style="list-style-type: none"> <li>▪ Measurement is performed to the object without any prior treatment [80]</li> <li>▪ The measurement can cover a wide range from tens of microns to ten of mm [80]</li> </ul>	<ul style="list-style-type: none"> <li>▪ The scan resolution of stylus profilometer is limited by the stylus size [79]. If the size of stylus tip is bigger than the vertical gaps then a number of vertical points might not correctly be profiled by the stylus tip [80].</li> <li>▪ The scanning process can be time-consuming. To obtain topographical information, a number of the consecutive line scans are required. To reduce scanning time, the sample area is limited to a small size only [79] [80]</li> <li>▪ Contact stress of stylus tip can damage and scratch the surface especially for the soft materials [80]</li> </ul>
Laser Profilometry	<ul style="list-style-type: none"> <li>▪ Provides high resolution scan</li> <li>▪ It has ability to scan deep surfaces</li> <li>▪ The laser light can adapt with any kinds of materials</li> </ul>	<ul style="list-style-type: none"> <li>▪ The scanning process that cannot be performed as a fast measurement</li> <li>▪ The surface information obtained is not a grid matrix of elevation data. An algorithm for converting coordinate system is required to construct the grid matrix</li> <li>▪ The scanning cannot be properly performed for the regions with some vibrations on the surface such as skin surfaces at the chest regions</li> </ul>
Light Scattering and Speckle Imaging	<ul style="list-style-type: none"> <li>▪ The methods can provide non-contact measurement and fast scanning [77]</li> </ul>	<ul style="list-style-type: none"> <li>▪ The method requires sophisticated system arrangement and standardised environment lighting.</li> <li>▪ The measurement surface is usually limited to the small size area.</li> </ul>
Structured Light Projection	<ul style="list-style-type: none"> <li>▪ By performing fast scanning, the method overcomes the scan problem on constant vibration of skin surface</li> <li>▪ Scanned surface is acquired as a grid matrix at high resolution</li> </ul>	<ul style="list-style-type: none"> <li>▪ The resolution of the measurement is limited by the resolution of the projection</li> <li>▪ And the imaging CCD arrays. Multiple projections and multiple viewing cameras can be used to improve the resolution of the measurement.[86]</li> <li>▪ Elevation cannot be measured accurately at local shadows and isolated surfaces[87]</li> </ul>

### 3.7 Summary

Chapter 3 presents a comprehensive description on surface roughness measurement methods. A surface roughness analysis in early years has been described in the beginning sections. Manufacturing and metallurgical process applies a mechanical surface profilometry to quantify the product surfaces. The profilometer system, at this point, has utilised a sharp needle to extract the profile

elevation at a high resolution. However, there are drawbacks in the method related to the physical size of the needle. A small needle tip might damage the surface whereas the bigger tip might lose the profile details with narrow gaps. Some imaging technologies are proposed to overcome these problems. Here, the imaging system measures the surface directly without any physical contact. In this chapter, well-known surface imaging methods are reviewed. The methods are laser profilometry, light scattering, speckle imaging, and structured light projection.

A laser beam is emitted and directed line by line to the scanned surface. The laser triangulation is used to determine the position of a target based on the reflected light. The surface elevation is linearly proportional to the reflected light deviations. Although the laser system can provide high resolution images, the process is considered to be time-consuming. Light scattering and speckle imaging are another methods applied to measure surface roughness. In these methods, a light beam is projected to the scanned surface. Both methods utilise its reflection to interpret the surface roughness. These methods can provide non-contact measurement and fast scanning but they require sophisticated system arrangement and standardised environment lighting. A more advanced method of 3D surface measurement is the structured light projection. The method projects some particular structured patterns onto the measured surface. The surface elevation of the scanned surface is determined from the deviated patterns on the surface. This method can perform high resolution scanning at high speed scan.

Surface filtering and surface roughness parameters are defined to enable a surface roughness determination. Surface filtering, in this case, is performed to extract roughness profile from the waviness and form components. The filtering methods are available, such as Fourier transform, Gaussian filter, wavelet filtering, and polynomial surface fitting. Digital Fourier transform is applied to identify the roughness from its frequency domains. Furthermore, Gaussian filter is applied in order to smooth the surface profile. However, Gaussian filter also has some drawbacks such as edge distortion, unable to filter a surface with a large form, and unreliable to deal with the surface outliers. Wavelet filter is used to analyze data at multi-resolution levels. However, the filtering process not only requires high

computational costs but also is difficult to define the number of decomposition levels. The polynomial surface fitting as the last filtering method has been widely used in 3D surface characterisation. The surface fitting determines the mean plane that represents the nominal direction of a surface. The fitting can any arbitrary curved forms including cylindrical and spheres. Several roughness parameters are defined to determine the surface roughness. The parameters are classified into three groups: amplitude, frequency, and combination of amplitude-frequency. Average roughness – an amplitude parameter – is considered as the most reliable parameter and can adopt the characteristics of the natural surfaces.

The skin assessment based on human senses and perception can result in a subjective assessment. Imaging technologies have been developed to enable objective assessment. The method of skin roughness measurement is grouped into invasive and non invasive methods. In invasive method, an incision procedure is required and the measurement is performed separately from the human body. High resolution and tiny details of skin sample surface can be acquired by microscopic camera. The process requires well trained medical personnel and may several days for the results of the analysis. Non-invasive method does not require skin cutting to obtain the sample. This method is preferred by most of the patient. Measurement can be performed as either non-direct or direct measurement. In non-direct measurement, the process requires a skin surface replica to represent the actual surface. Conversely, the direct measurement can be applied directly to the skin surface of the living person. Direct measurement method is applied in early developments of surface roughness measurement. A high precision profilometer using sharp stylus is used to obtain profile lines of skin surface replica. The replica making process is not simple. Significant errors can be introduced in the skin replica due to manual preparation. Light medium is applied to improve scan speed and profiling accuracy in surface roughness determination. The light profiling can be applied as either direct or non-direct surface measurement. The measurement of laser scanner is initially applied in cosmetic industry to evaluate the cosmetic efficacy. Several quantitative parameters such as  $R_a$ ,  $R_p$ ,  $R_t$ , and  $R_{max}$  are used to represent surface roughness. Stripe projection method has been applied to determine in vivo skin surface roughness. By applying in vivo measurement, inaccuracy

caused by skin replica can be minimised. Skin surface roughness is also measured from the speckle texture of the surface. The speckle contrast is related to the surface roughness. The texture analysis method is also used to determine the surface roughness from the speckle images. These mentioned methods have been applied for skin roughness determination. However, the methods have not been validated at various locations of the body surface. It is pertinent that the measurement is reliable at any location of the body surface. In addition, it is found that most of the previous works do not focus on surface roughness of marked lesion. In the research, a surface roughness algorithm based on polynomial surface fitting has been developed to enable objective measurement. The development of this surface roughness algorithm is elaborated in the next chapter.

## CHAPTER 4

### DEVELOPMENT ON SURFACE ROUGHNESS ALGORITHM

Chapter 4 is to describe the development of surface roughness algorithm. This chapter consists of several sections. The first section discusses in detail about the developed surface roughness algorithm by applying a high order polynomial surface fitting. In this case, a surface waviness is filtered out from a rough curved surface using the application of this polynomial surface fitting. The rough surface will afterward be flattened and the remaining vertical deviations are used to determine surface roughness. The following section describes a validation study on the surface roughness algorithm that is conducted to determine the accuracy and total standard deviation. In the next section, these values are used to analyse the system performance. This chapter also includes an evaluation on the rotational invariance and the sample area determination. These studies aim to evaluate and to define the algorithm limitations. The final section of this chapter summarises all of the materials presented.

#### **4.1 Surface Roughness as Scaliness Parameter for PASI Scoring**

As mentioned in the earlier chapter, surface roughness is used as the measurable features to grading the psoriasis scaliness. These features are selected based on the surface appearances of the lesion with different scaliness scores. Rougher surfaces, which are caused by irregular stack of dead skin cells, are found at a psoriasis lesion with higher severities. Imaging modalities *i.e.* 3D optical scanner is now available to perform fast surface scan at high resolution.

Figure 4.1(a)-(c) describes the 3D correspondence between skin surface roughness and scaliness severities (scores). Figure 4.1(d) illustrates the roughness profiles of normal skin; *i.e.*, lesions with score 1 and score 4. In lesions with score 4,

large vertical deviations have been observed that are caused by excessive coarse scales irregularly stacked on the lesion surfaces. The scores are provided based on dermatologists' visual and tactile perceptions. In this research, an imaging method is developed to assess scaliness objectively and accurately.

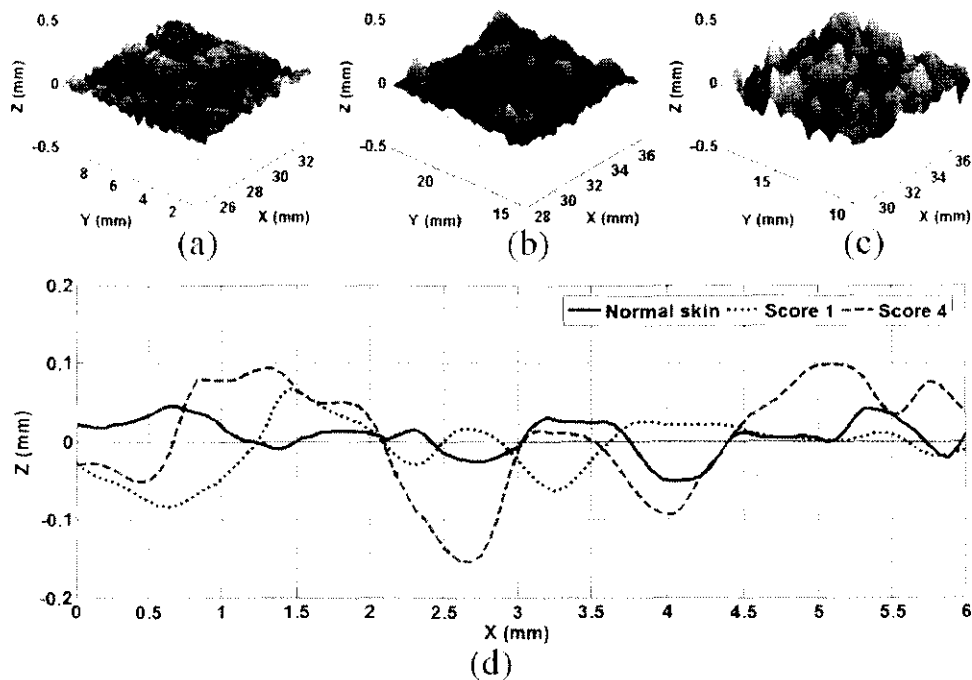


**Figure 4.1** 3D surfaces of (a) normal skin, psoriasis lesion (b) score 1, and (c) score 4; (d) Rough profiles of normal skin (solid line), lesion score 1 (dotted line), and lesion score 4 (dashed line).

## 4.2 Surface Roughness Algorithm

The 3D surface roughness is determined by averaging the vertical deviations of the lesion surface. Because lesions appear on 3D curved surface (human body), the vertical deviations due to the lesion is determined by subtracting a lesion surface from an estimated waviness surface as shown in cross-sectional view in Figure 4.2.

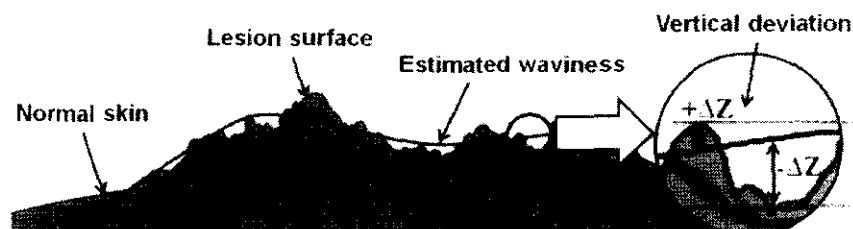


**Figure 4.2** The cross-sectional view of a skin lesion on normal skin surface

A 3D optical scanner with a structured light projection method, namely PRIMOS (Phase shift Rapid In vivo Measurement of Skin) portable, is used to acquire some lesion surface images. This optical scanner is designed for 3D in vivo measurements of a microscopic and macroscopic skin surface structure [125]. The structured light projection method is applied by PRIMOS camera to obtain the 3D surface image. The method provides a number of advantages such as standardised capture distance and high-speed scan (<63 ms). A high-speed capture is important for a skin surface measurement due to the inevitable movements of the subject. The PRIMOS has a high-resolution 3D surface (spatial resolution: 0.0062 mm and depth resolution: 0.0040 mm) in which its image is used as the input to the developed algorithm to determine the surface roughness.

A higher-order polynomial surface fitting is applied to the rough lesion surface to extract an estimated 3D waviness surface from the rough lesion surface. By subtracting the rough lesion surface from an estimated waviness surface, the vertical deviations of lesion surface can be exactly determined. The vertical deviations of a lesion surface are known as the deviation surface. The second and third order polynomials are applied in this work. These polynomial orders are suitable for the small surface areas in that the vertical undulation of the waviness surface is lesser [93].

#### 4.2.1 Polynomial Surface Fitting

As the lesion surface is not always flat, a polynomial surface fitting is required to fit a lesion surface. The second and third order polynomials are applied in this work. These polynomial orders are suitable for some small surface areas [93] such as lesion. In the small area, the vertical undulation of the estimated waviness is less and can be accurately fitted with the second and third order polynomials. The general form of polynomials can be written within the following equations [126]:

The second order polynomial:

$$z_2(x, y) = (a_1x^2 + a_2x + a_3)y^2 + (a_4x^2 + a_5x + a_6)y + (a_7x^2 + a_8x + a_9) \quad (4-1)$$

The third order polynomial:

$$\begin{aligned}
z_3(x, y) = & (a_1x^3 + a_2x^2 + a_3x + a_4)y^3 + (a_5x^3 + a_6x^2 + a_7x + a_8)y^2 \\
& + (a_9x^3 + a_{10}x^2 + a_{11}x + a_{12})y \\
& + (a_{13}x^3 + a_{14}x^2 + a_{15}x + a_{16})
\end{aligned} \tag{4-2}$$

To create a surface based on a polynomial equation, 9 and 16 polynomial coefficients are required for the second and third polynomials, respectively. The coefficient of determination ( $R^2$ ) is used to measure fittingness of polynomial fitting [127]. A good fit can be obtained if  $R^2$  is in interval [0.9, 1.0]. The best fitting result of the polynomial orders is selected based on the highest  $R^2$ . The equation of  $R^2$  is expressed in following equation:

$$R^2 = 1 - \frac{\sum_{i=1}^M \sum_{j=1}^N (z(x_i, y_j) - w_k(x_i, y_j))^2}{\sum_{i=1}^M \sum_{j=1}^N (z(x_i, y_j) - \bar{z})^2} \tag{4-3}$$

where  $z(x_i, y_j)$  represents the elevation of lesion surface.  $\bar{z}$  represents the elevation average and  $w_k(x_i, y_j)$  is fitted value at  $(x_i, y_j)$  using  $k$ -th order polynomial. The surface roughness is determined by using average roughness ( $S_a$ ) equation [128]. In this equation, the surface roughness is calculated by averaging the absolute vertical deviation of all data points. The average roughness,  $S_a$ , is defined as equation below. Variable  $e(x_i, y_j)$  denotes the vertical deviation of lesion surface at  $(x_i, y_j)$ .

$$S_a = \frac{1}{MN} \sum_{i=1}^M \sum_{j=1}^N |z(x_i, y_j) - w_k(x_i, y_j)| = \frac{1}{MN} \sum_{i=1}^M \sum_{j=1}^N |e(x_i, y_j)| \tag{4-4}$$

#### 4.2.2 Surface Roughness Calculation

The surface roughness algorithm is described by the flow chart shown in Figure 4.3. In this flow chart, the fitting process of the second and the third orders are performed separately in order to get the best fit based on  $R^2$ .

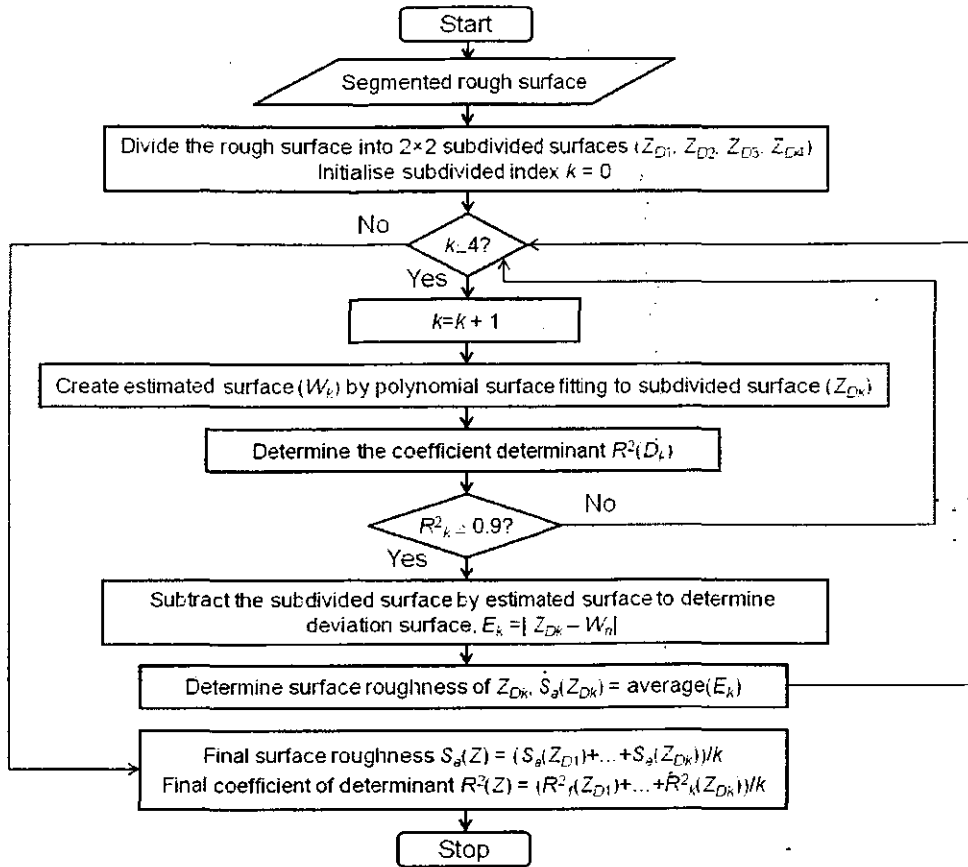


**Figure 4.3** Flowchart of the surface roughness algorithm.

The detail explanation on surface roughness algorithm is described as follows:

- Input a 3D lesion surface matrix,  $Z_0(x, y)$ , with size  $M \times N$  (see Figure 4.4). The coordinates  $x$ ,  $y$ , and its value  $z(x, y)$  are then used to calculate some polynomial coefficients. The total data point in lesion surface is  $M \times N$ .
- Divide the lesion surface into  $2 \times 2$  subdivided surfaces that gives four subdivided surfaces, namely  $D_1$ ,  $D_2$ ,  $D_3$ , and  $D_4$ , as shown in Figure 4.4. Half division is applied symmetrically to each side of the lesion area, thus the size of each subdivided surface becomes  $\frac{M}{2} \times \frac{N}{2} = L$ .
- For each subdivided surface,  $D_1$  to  $D_4$ , determine the polynomial coefficients of the selected order from coordinates  $x$ ,  $y$ , and  $z(x, y)$  through a matrix inversion. This inversion is performed separately for all subdivided surfaces. As described in (4-5), matrix  $V$  contains the elements of the polynomial equation, the coefficients of polynomial equation are stored in matrix  $A$ , and matrix  $Z$

represents the subdivided lesion surface.

$$VA = Z \quad A = V^{-1}Z \quad (4-5)$$

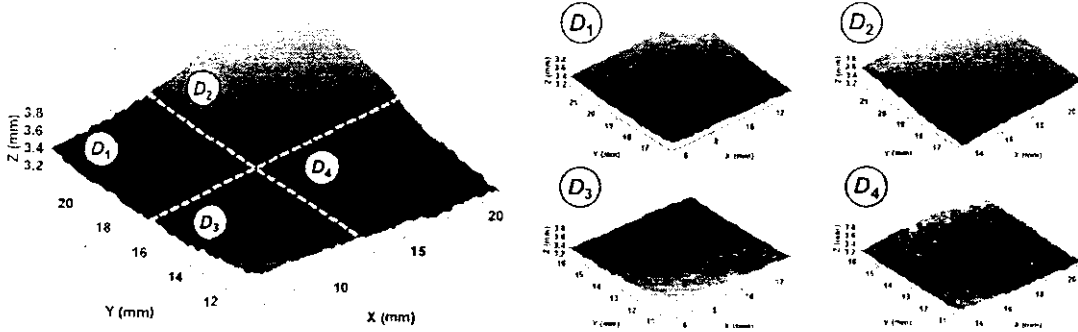


**Figure 4.4** The segmented rough surface of the lesion model and its 4x4 subdivided surfaces.

- d) For the first stage, the second order polynomial is selected to find polynomial coefficients  $A$ . Once the coefficients have been determined, the estimated waviness surface can be constructed. The waviness is obtained by applying calculated polynomial equation with polynomial coefficients  $A$  at the evaluated coordinate points  $(x, y)$ . The matrix equation (4-5) can be written as  $V_2 A_2 = Z_{D_1}$  to denote a second order polynomial fitting at subdivided surface  $D_1$ .
- e) The matrices elements of  $V_2$ ,  $A_2$  and  $Z_{D_1}$  are given by the following forms. Here, variable  $L$  refers to the total number of data points at a subdivided surface.

$$V_2 = \begin{bmatrix} x_1^2 y_1^2 & x_1 y_1^2 & y_1^2 & x_1^2 y_1 & x_1 y_1 & y_1 & x_1^2 & x_1 & 1 \\ x_2^2 y_2^2 & x_2 y_2^2 & y_2^2 & x_2^2 y_2 & x_2 y_2 & y_2 & x_2^2 & x_2 & 1 \\ x_3^2 y_3^2 & x_3 y_3^2 & y_3^2 & x_3^2 y_3 & x_3 y_3 & y_3 & x_3^2 & x_3 & 1 \\ x_4^2 y_4^2 & x_4 y_4^2 & y_4^2 & x_4^2 y_4 & x_4 y_4 & y_4 & x_4^2 & x_4 & 1 \\ \dots & \dots \\ x_L^2 y_L^2 & x_L y_L^2 & y_L^2 & x_L^2 y_L & x_L y_L & y_L & x_L^2 & x_L & 1 \end{bmatrix} \quad (4-6)$$

$$A_2 = [a_1 \quad a_2 \quad a_3 \quad \dots \quad a_8 \quad a_9]^T \quad (4-7)$$

$$Z_{D_1} = [z_{D_1}(x_1, y_1) \quad z_{D_1}(x_2, y_2) \quad z_{D_1}(x_3, y_3) \quad \dots \quad z_{D_1}(x_L, y_L)]^T \quad (4-8)$$

- f) The matrix of polynomial coefficients  $A_2$  is unknown and inversion  $A_2 = V_2^{-1} Z_{D_1}$  is applied to determine its values then. The polynomial coefficients of

$A_2$  are determined by applying the equation below.

$$\begin{bmatrix} a_1 \\ a_2 \\ a_3 \\ \dots \\ a_8 \\ a_9 \end{bmatrix} = \begin{bmatrix} x_1^2 y_1^2 & x_1 y_1^2 & y_1^2 & \dots & x_1^2 & x_1 & 1 \\ x_2^2 y_2^2 & x_2 y_2^2 & y_2^2 & \dots & x_2^2 & x_2 & 1 \\ x_3^2 y_3^2 & x_3 y_3^2 & y_3^2 & \dots & x_3^2 & x_3 & 1 \\ \dots & \dots & \dots & \dots & \dots & \dots & \dots \\ x_4^2 y_4^2 & x_4 y_4^2 & y_4^2 & \dots & x_4^2 & x_4 & 1 \\ \dots & \dots & \dots & \dots & \dots & \dots & \dots \\ x_L^2 y_L^2 & x_L y_L^2 & y_L^2 & \dots & x_L^2 & x_L & 1 \end{bmatrix}^{-1} \times \begin{bmatrix} z_{D_1}(x_1, y_1) \\ z_{D_1}(x_2, y_2) \\ z_{D_1}(x_3, y_3) \\ z_{D_1}(x_4, y_4) \\ \dots \\ z_{D_1}(x_L, y_L) \end{bmatrix} \quad (4-9)$$

g) Waviness surface  $W_2(x, y)$  (Figure 4.5-b) is estimated by applying the second order polynomial surface fitting with coefficients  $A_2$ . The estimation is limited for  $(x, y)$  coordinates at  $D_1$  area. An equation for determining  $W_2(x, y)$  is shown by following expression.

$$W_2 = V_2 A_2 \quad (4-10)$$

$$\begin{bmatrix} w_2(x_1, y_1) \\ w_2(x_2, y_2) \\ w_2(x_3, y_3) \\ w_2(x_4, y_4) \\ \dots \\ w_2(x_L, y_L) \end{bmatrix} = \begin{bmatrix} x_1^2 y_1^2 & x_1 y_1^2 & y_1^2 & \dots & x_1^2 & x_1 & 1 \\ x_2^2 y_2^2 & x_2 y_2^2 & y_2^2 & \dots & x_2^2 & x_2 & 1 \\ x_3^2 y_3^2 & x_3 y_3^2 & y_3^2 & \dots & x_3^2 & x_3 & 1 \\ x_4^2 y_4^2 & x_4 y_4^2 & y_4^2 & \dots & x_4^2 & x_4 & 1 \\ \dots & \dots & \dots & \dots & \dots & \dots & \dots \\ x_L^2 y_L^2 & x_L y_L^2 & y_L^2 & \dots & x_L^2 & x_L & 1 \end{bmatrix} \times \begin{bmatrix} a_1 \\ a_2 \\ a_3 \\ \dots \\ a_8 \\ a_9 \end{bmatrix} \quad (4-11)$$

h) Deviation surface,  $E_2(x, y)$  (Figure 4.5-c), is determined by subtracting the estimated waviness,  $W_2(x, y)$ , from the lesion surface  $Z_{D_1}(x, y)$ . The equation is  $E_2(x, y) = |Z_{D_1}(x, y) - W_2(x, y)|$ .

i) The coefficient of determination ( $R^2$ ) is calculated to evaluate the fitting result. Here,  $W_2(x, y)$  is accepted if  $R^2$  is within [0.9, 1.0]. The equation for determining  $R^2$  is provided in (4-3). Notation  $R_2^2(D_1)$  is used to denote the  $R^2$  of the second order polynomial surface fitting at the subdivided surface  $D_1$ . Equation (4-3) is used to determine this coefficient.

$$R_2^2(D_1) = 1 - \frac{\sum_{i=1}^M \sum_{j=1}^N (z_{D_1}(x_i, y_j) - w_2(x_i, y_j))^2}{\sum_{i=1}^M \sum_{j=1}^N (z_{D_1}(x_i, y_j) - \bar{z}_{D_1})^2} \quad (4-12)$$

j) Equation (4-4) is used to determine the surface roughness  $S_a$  at the subdivided surface  $D_1$ . The input variables for this equation are deviation surface  $E_2(x, y)$

with matrix size  $\frac{M}{2} \times \frac{N}{2}$ .

$$S_{a,2}(D_1) = \frac{1}{\left(\frac{M}{2} \times \frac{N}{2}\right)} \sum_{i=1}^{\frac{M}{2}} \sum_{j=1}^{\frac{N}{2}} |z_{D_1}(x_i, y_j) - w_2(x_i, y_j)| \quad (4-13)$$

Notation  $S_{a,2}(D_1)$  is used to represent the surface roughness of the subdivided surface  $D_1$  that is determined by the second order polynomial surface fitting.

- k) Repeat step 4 to 10 to compute the surface roughness values for other subdivided surfaces,  $D_2$  to  $D_4$ . These computations are performed separately for each subdivided surface. The overall surface roughness of lesion surface is obtained by averaging the surface roughness of subdivided surfaces. Here, the surface roughness of a subdivided surface will not be included in final calculation if  $R^2$  of polynomial surface fitting is not within an acceptable interval [0.9, 1.0]. Thus, the overall surface roughness of lesion surface can be expressed as

$$\overline{S_{a,2}} = \frac{\sum_{i=1}^{N_D} S_{a,2}(D_i)}{N_D}, \text{ if } 0.9 \leq R_2^2(D_i) \leq 1.0, N_D \leq 4 \quad (4-14)$$

The overall coefficient of determination  $R^2$  is computed as well by using the equation below.

$$\overline{R_2^2} = \frac{\sum_{i=1}^{N_D} R_2^2(D_i)}{N_D}, \text{ if } 0.9 \leq R_2^2(D_i) \leq 1.0, N_D \leq 4 \quad (4-15)$$

- l) Perform some similar steps as step 3 to step 11 but, instead of by fitting to a second order polynomial, use the third order polynomial surface fitting to estimate a waviness surface. For the implementation of third order polynomial to the subdivided surface  $D_1$ , equation (4-5) can be updated as  $V_3 A_3 = Z_{D_1}$ .
- m) Matrices elements of  $V_3$  and  $A_3$  are arranged as in the following forms. There is no any difference in the input data  $Z_{D_1}$  compared to the previous steps. Variable  $L$  here represents the total number of data points of the subdivided surface  $D_1$ .

$$V_3 = \begin{bmatrix} x_1^3 y_1^3 & x_1^2 y_1^3 & x_1 y_1^3 & y_1^3 & \cdots & x_1^3 y_1 & x_1^2 y_1 & x_1 y_1 & y_1 & x_1^3 & x_1^2 & x_1 & 1 \\ x_2^3 y_2^3 & x_2^2 y_2^3 & x_2 y_2^3 & y_2^3 & \cdots & x_2^3 y_2 & x_2^2 y_2 & x_2 y_2 & y_2 & x_2^3 & x_2^2 & x_2 & 1 \\ x_3^3 y_3^3 & x_3^2 y_3^3 & x_3 y_3^3 & y_3^3 & \cdots & x_3^3 y_3 & x_3^2 y_3 & x_3 y_3 & y_3 & x_3^3 & x_3^2 & x_3 & 1 \\ x_4^3 y_4^3 & x_4^2 y_4^3 & x_4 y_4^3 & y_4^3 & \cdots & x_4^3 y_4 & x_4^2 y_4 & x_4 y_4 & y_4 & x_4^3 & x_4^2 & x_4 & 1 \\ \cdots & \cdots \\ x_N^3 y_N^3 & x_N^2 y_N^3 & x_N y_N^3 & y_N^3 & \cdots & x_N^3 y_N & x_N^2 y_N & x_N y_N & y_N & x_N^3 & x_N^2 & x_N & 1 \end{bmatrix} \quad (4-16)$$

$$A_3 = [a_1 \ a_2 \ a_3 \ \cdots \ a_{15} \ a_{16}]^T \quad (4-17)$$

n) The inversion of  $A_3 = V_3^{-1}Z_{D_1}$  is applied to determine the polynomial coefficients  $A_3$  and its equation is given as follows:

$$\begin{bmatrix} a_1 \\ a_2 \\ a_3 \\ \cdots \\ a_{15} \\ a_{16} \end{bmatrix} = \begin{bmatrix} x_1^3 y_1^3 & x_1^2 y_1^3 & x_1 y_1^3 & y_1^3 & \cdots & x_1^3 & x_1^2 & x_1 & 1 \\ x_2^3 y_2^3 & x_2^2 y_2^3 & x_2 y_2^3 & y_2^3 & \cdots & x_2^3 & x_2^2 & x_2 & 1 \\ x_3^3 y_3^3 & x_3^2 y_3^3 & x_3 y_3^3 & y_3^3 & \cdots & x_3^3 & x_3^2 & x_3 & 1 \\ x_4^3 y_4^3 & x_4^2 y_4^3 & x_4 y_4^3 & y_4^3 & \cdots & x_4^3 & x_4^2 & x_4 & 1 \\ \cdots & \cdots \\ x_N^3 y_N^3 & x_N^2 y_N^3 & x_N y_N^3 & y_N^3 & \cdots & x_N^3 & x_N^2 & x_N & 1 \end{bmatrix}^{-1} \times \begin{bmatrix} Z_{D_1}(x_1, y_1) \\ Z_{D_1}(x_2, y_2) \\ Z_{D_1}(x_3, y_3) \\ Z_{D_1}(x_4, y_4) \\ \cdots \\ Z_{D_1}(x_L, y_L) \end{bmatrix} \quad (4-18)$$

o) Estimated waviness surface  $W_3(x, y)$  is obtained by the substitution of coefficients  $A_3$  into the following equation.

$$W_3 = V_3 A_3 \quad (4-19)$$

$$\begin{bmatrix} w_3(x_1, y_1) \\ w_3(x_2, y_2) \\ w_3(x_3, y_3) \\ w_4(x_4, y_4) \\ \cdots \\ w_{16}(x_L, y_L) \end{bmatrix} = \begin{bmatrix} x_1^3 y_1^3 & x_1^2 y_1^3 & x_1 y_1^3 & y_1^3 & \cdots & x_1^3 & x_1^2 & x_1 & 1 \\ x_2^3 y_2^3 & x_2^2 y_2^3 & x_2 y_2^3 & y_2^3 & \cdots & x_2^3 & x_2^2 & x_2 & 1 \\ x_3^3 y_3^3 & x_3^2 y_3^3 & x_3 y_3^3 & y_3^3 & \cdots & x_3^3 & x_3^2 & x_3 & 1 \\ x_4^3 y_4^3 & x_4^2 y_4^3 & x_4 y_4^3 & y_4^3 & \cdots & x_4^3 & x_4^2 & x_4 & 1 \\ \cdots & \cdots \\ x_N^3 y_N^3 & x_N^2 y_N^3 & x_N y_N^3 & y_N^3 & \cdots & x_N^3 & x_N^2 & x_N & 1 \end{bmatrix} \times \begin{bmatrix} a_1 \\ a_2 \\ a_3 \\ \cdots \\ a_{15} \\ a_{16} \end{bmatrix} \quad (4-20)$$

p) By subtracting the estimated waviness  $W_2(x, y)$  from the lesion surface  $Z_{D_1}(x, y)$ , the deviation surface  $E_3(x, y)$  is determined. The equation of this subtraction is  $E_3(x, y) = |Z_{D_1}(x, y) - W_3(x, y)|$ .

q) The coefficient of the determinant and surface roughness of the measured subdivided surface  $D_1$  can be given by following equations.

$$R_3^2(D_1) = 1 - \frac{\sum_{i=1}^M \sum_{j=1}^N (Z_{D_1}(x_i, y_j) - w_3(x_i, y_j))^2}{\sum_{i=1}^M \sum_{j=1}^N (Z_{D_1}(x_i, y_j) - \bar{Z}_{D_1})^2} \quad (4-21)$$

$$S_{a,3}(D_1) = \frac{1}{\left(\frac{M}{2} \times \frac{N}{2}\right)} \sum_{i=1}^{\frac{M}{2}} \sum_{j=1}^{\frac{N}{2}} |z_{D_1}(x_i, y_j) - w_3(x_i, y_j)| \quad (4-22)$$

- r) Determine  $S_{a,3}$  and  $R_3^2$  for the remain subdivided surfaces,  $D_2$ ,  $D_3$ , and  $D_4$ . Hence, the overall surface roughness and coefficient of determination are determined by

$$\overline{S_{a,3}} = \frac{\sum_{i=1}^{N_D} S_{a,3}(D_i)}{N_D}, \text{ if } 0.9 \leq R_3^2(D_i) \leq 1.0, N_D \leq 4 \quad (4-23)$$

$$\overline{R_3^2} = \frac{\sum_{i=1}^{N_D} R_3^2(D_i)}{N_D}, \text{ if } 0.9 \leq R_3^2(D_i) \leq 1.0, N_D \leq 4 \quad (4-24)$$

- s) Coefficient  $\overline{R_2^2}$  and  $\overline{R_3^2}$  are compared to decide the best order of the polynomial surface fitting. The overall surface roughness  $\overline{S_a}$  is obtained from the calculation that can give a higher  $\overline{R^2}$  value. For example, if  $\overline{R_2^2}$  is found to be higher than  $\overline{R_3^2}$ ,  $\overline{S_{a,2}}$  is considered as the overall surface roughness. Consequently, the surface roughness of  $\overline{S_{a,3}}$  would be discarded. A subtraction between a lesion surface and an estimated waviness is shown in Figure 4.5. This subtraction yields deviation surface. The average roughness equation is applied to the deviation surface to compute the lesion surface roughness.

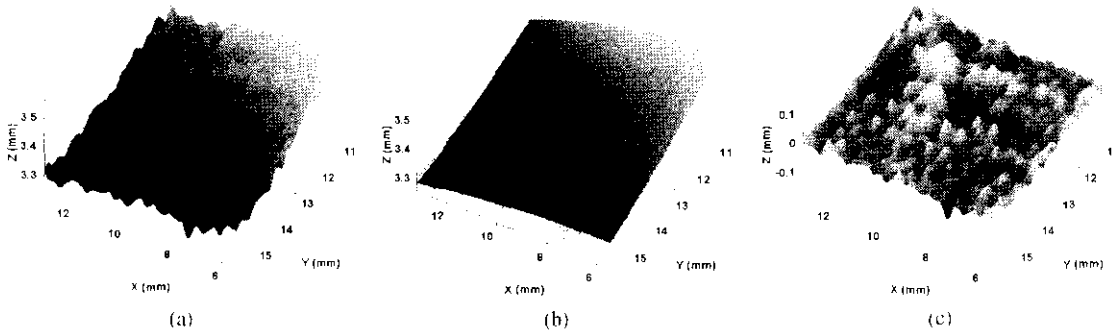


**Figure 4.5** The 3D surfaces involved in surface roughness determination: (a) lesion surface, (b) estimated waviness, and (c) deviation surface.

Higher polynomial orders (higher than 3rd order) are not selected in estimating waviness surface. This limitation aims to avoid over fitting on rough profile of the lesion surface [129]. In over fitting condition, the estimated waviness tends to follow

the actual profile of lesion surface. Therefore, the fitted surface does not measure the vertical deviations accurately. Figure 4.6 shows comparison of the waviness profiles that have been estimated by applying surface fitting with several orders. It can be shown that fitting lines of second (red line) and third orders (green line) are able to follow the rough profile curvature better than fourth and fifth orders.

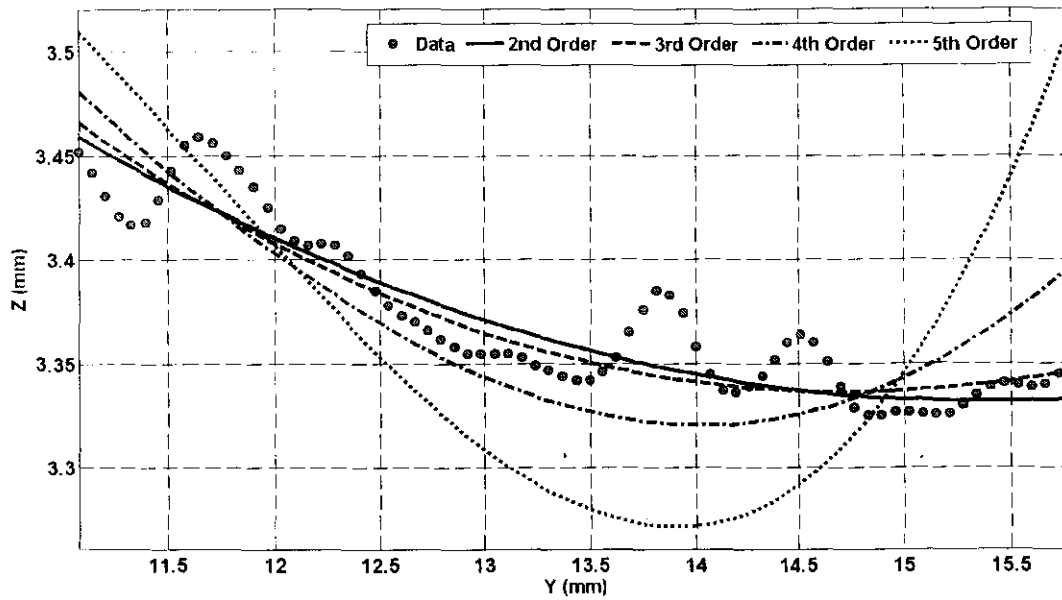


**Figure 4.6** Rough surface and fitted profiles of a lesion model. The first, second, third and fourth orders are applied to determine the fitted profiles.

These surface and fitted profiles are extracted from a lesion surface. The size of lesion surface is  $75 \times 69$  pixels representing  $4.710 \times 4.326 \text{ mm}^2$ . The profile line is located parallel with Y-axis at point  $x$  equals 50 pixel (3.150 mm from the vertical edge of the 3D surface). The fourth and the fifth orders are not able to fit properly on the lesion surface. The fitting process is trying to fit undulated profiles at centre area. Therefore, the edges of fitted surface are released freely and not set to follow the lesion curvature. Finally, the fitting error are minimised at centre area but it becomes very large at the edges. Figure 4.7 (a) and (b) demonstrate the success of the second and third order polynomial surface fitting implementations. The lesion in this figure is the same lesion that has been mentioned in previous plot (Figure 4.8). The estimated and deviation surfaces are shown for each fitting order implementation. The fitting results of fourth and fifth orders are shown in Figure 4.7 (c) and (d). Their waviness estimation cannot be used in surface roughness determination because the the estimated waviness does not follow mean curvature of

the lesion surface. The coefficient of determinant ( $R^2$ ) of both calculations are less than 0.90.

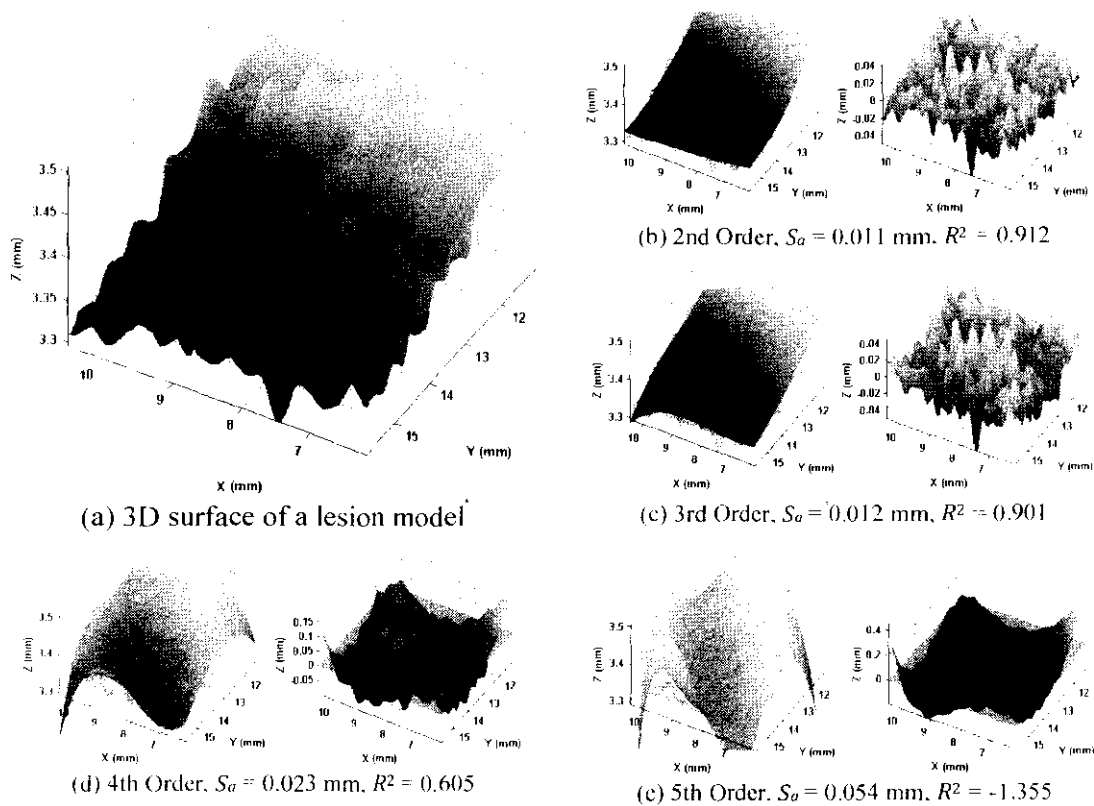


**Figure 4.7** (a) 3D surface of a lesion model. (b) – (e) The estimated waviness and deviation surfaces that are determined by applying several different fitting orders.

### 4.3 Validation Study

#### 4.3.1 Surface Roughness Measurement: Abrasive Paper

Several abrasive papers with several different roughness grades have been tested to validate the surface roughness measurement on various rough surfaces. There are five grades here used for the validation, those are 16, 24, 60, 80, and 280. Grade value ( $G$ ) follows the standard of United States CAMI (Coated Abrasive Manufacturers Institute) [130]. The grade is inversely proportional with the surface roughness. Rougher surfaces are valued by smaller grades. Notation  $1/G$  is usually used to relate linearly proportional to the surface roughness.

A total of 72 3D surfaces are scanned for each grade. Since there are five grades

evaluated in this study, the acquisition finally gives a total of 280 surfaces. A surface roughness algorithm is applied to the collected 3D surfaces. Table 4.1 lists surface roughness and its standard deviation for each abrasive grade. As listed in this table, the surface roughness increases proportionally with  $1/G$ . Average diameter is an average size of the abrading particles embedded in the abrasive paper. Figure 4.8, meanwhile, shows 3D surfaces of the abrasive papers. The surface images are ordered from the less rough to the very rough surfaces. Subsequently, several impulse noises appear in the rough surfaces as a result of the reflectivity of the abrasive particles. The scanner could not scan correctly on the shiny surface.

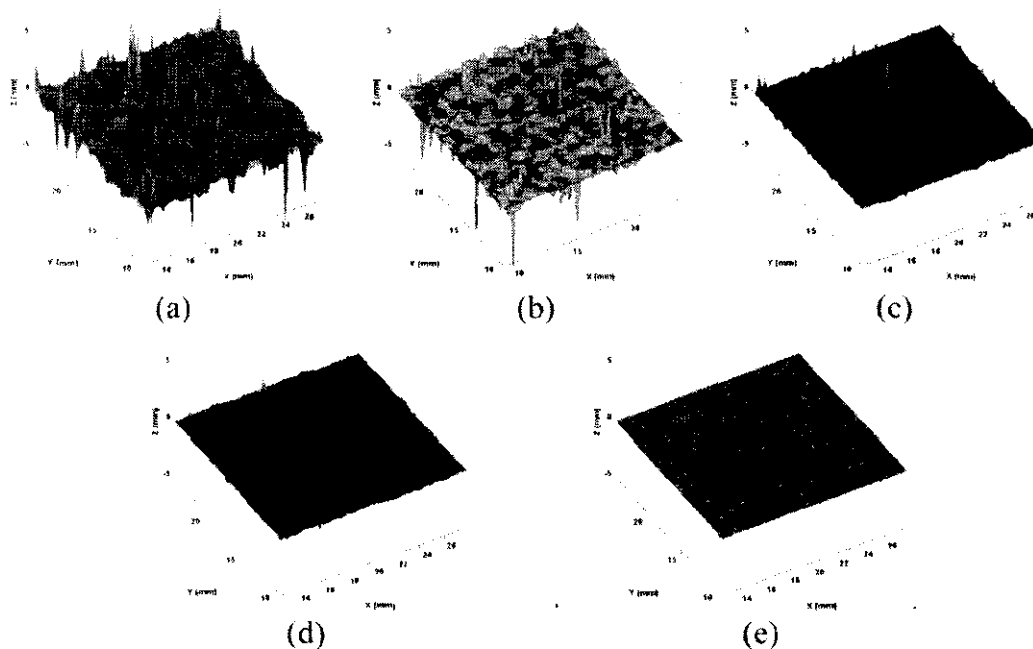


**Figure 4.8** The 2D and 3D images of abrasive papers used in the surface roughness validation. The roughness grades are (a) 16, (b) 24, (c) 60, (d) 80, and (e) 280.

**Table 4.1** The surface roughness of abrasive paper

Grade Values ( $G$ )	Average diameter (mm)	$1/G$	$\bar{S}_a$ (mm)	$\sigma$ (mm)	$\bar{S}_a + \sigma$ (mm)	$\bar{S}_a - \sigma$ (mm)
280	0.044	0.004	0.0122	0.0007	0.0115	0.0128
80	0.192	0.013	0.0856	0.0090	0.0766	0.0946
60	0.268	0.017	0.1101	0.0380	0.0722	0.1481
24	0.715	0.042	0.2552	0.0336	0.2216	0.2888
16	1.320	0.063	0.4517	0.0555	0.3962	0.5072

The results of Table 4.1 are then plotted, as displayed in Figure 4.9. The relation between  $1/G$  and  $S_a$  is proven by using Pearson's correlation coefficient. The

correlation value of  $S_a$  and  $1/G$  is 0.989 showing a strong relation between them. A positive sign furthermore represents a linear relationship, which means that the smoother surface (small  $S_a$  value) is represented by a small number of  $1/G$ . This value proves that roughness algorithm can be used to determine a roughness grading. Since the surface roughness is an amplitude parameter, its value will relate to a particle size. The rougher surface is composed by particles with a bigger diameter size and results in a number of higher amplitude deviations. Therefore,  $1/G$ , which is given based on particle size and the surface roughness, is linearly correlated.

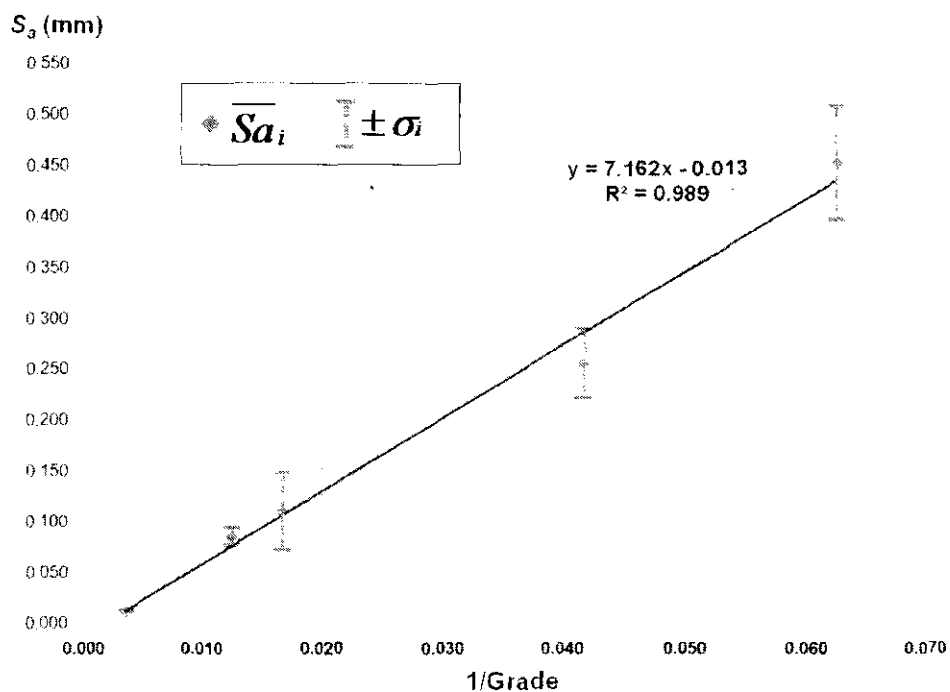


**Figure 4.9** Plot of surface roughness vs.  $1/G$  (CAMI grade) obtained from measurement on abrasive papers.

#### 4.3.2 Surface Roughness on Curve Surface: Mannequin Surface

To model a skin lesion, a medical tape that has regular and uniform texture on its surface is used. The tape has regular and uniform texture on its surface. It is made from an elastic material. Therefore, the tape can adapt the surface curvature when located onto any surfaces. However, to preserve its texture characteristics, the medical tape has to be pasted onto a smooth surface only. The average surface roughnesses  $\overline{S_a}$  of 33 lesion models are used as the reference. These reference models are pasted at a hard paperboard flat surface. By applying lesion models on

the flat surface, some vertical undulations caused by a curved surface would not contribute to the surface roughness measurement. Then, it could be ensured that only vertical deviations of the lesion model contribute to the roughness calculation. Figure 4.10 shows the lesion models at flat surface.

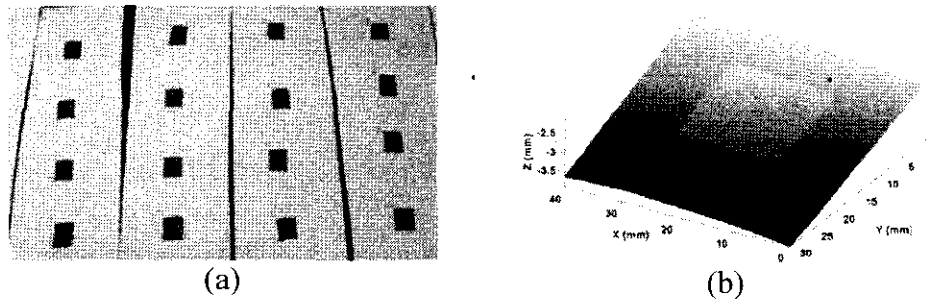


**Figure 4.10** (a) Lesion models made of surgical tape are pasted on the flat surfaces of paperboard. (b) A 3D surface of lesion model.

In this experiment, the lesion model is scanned three times by applying a series of scans on the scanner mode. The scanning process of 33 lesion models has then given a total of 99 3D surface images. The surface roughness of a lesion model is represented by the average of surface roughness from these three consecutive scans. Additionally, the algorithm is applied separately for each 3D surface to obtain the surface roughness of the lesion models. Since the model preparation is manually performed, it results in a variety of sizes on the area of the lesion model. Table 4.2 shows the first 12 of 99 surface roughness measurements. In this case, the smallest and the largest areas are  $10.06 \times 9.93 \text{ mm}^2$  and  $14.14 \times 10.69 \text{ mm}^2$ , respectively.

**Table 4.2** The surface roughness of lesion models at a flat surface

Lesion model	Scan index	$S_{a,2}$	$R_2^2$	$S_{a,3}$	$R_3^2$	$S_{final}$	$R_{final}^2$	$\overline{S_{final}}$
1	1	0.0142	0.997	0.0138	0.997	0.0138	0.997	0.0139
	2	0.0146	0.996	0.0142	0.997	0.0142	0.997	
	3	0.0140	0.996	0.0137	0.997	0.0137	0.997	
2	1	0.0123	0.998	0.0120	0.998	0.0120	0.998	0.0130
	2	0.0122	0.998	0.0119	0.998	0.0119	0.998	
	3	0.0151	0.997	0.0149	0.997	0.0149	0.997	
3	1	0.0124	0.994	0.0122	0.994	0.0122	0.994	0.0122
	2	0.0125	0.994	0.0122	0.994	0.0122	0.994	
	3	0.0123	0.994	0.0121	0.994	0.0121	0.994	
4	1	0.0123	0.994	0.0119	0.994	0.0119	0.994	0.0118
	2	0.0122	0.994	0.0118	0.994	0.0118	0.994	
	3	0.0123	0.994	0.0118	0.994	0.0118	0.994	

The surface roughness of lesion models are summarised in a histogram as shown in Figure 4.11. From the histogram, average surface roughness  $\bar{S}_a$  and its standard deviation are found to be  $0.0122 \pm 0.0011$  mm ( $\bar{x}_{Ref} \pm \sigma_{Ref}$ ).

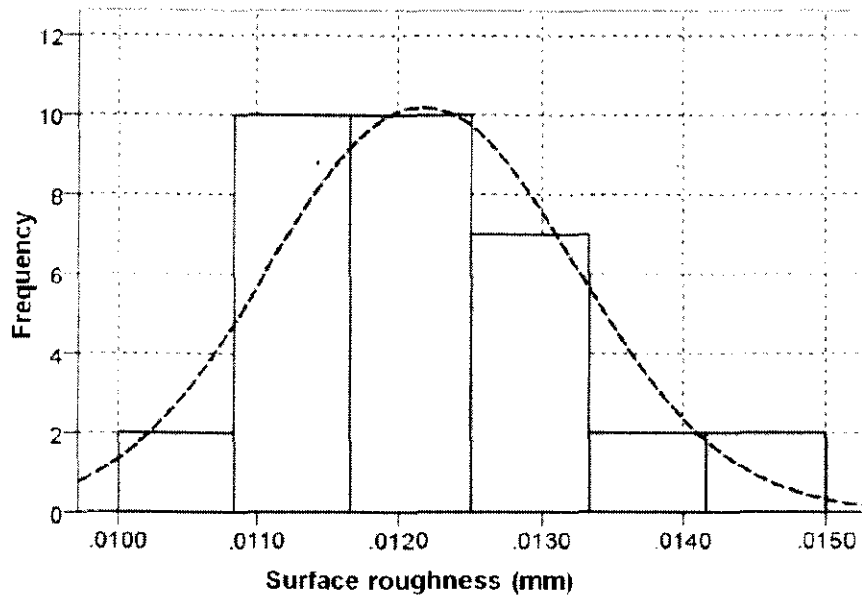


**Figure 4.11** The histogram of lesion models pasted on flat surfaces.

To validate the surface roughness algorithm on the curved surfaces of human skin, the lesion models are placed on surfaces of mannequin that is made based on the body size of human at adult ages. In common, mannequin is used for medical purposes. The validation on mannequin uses a similar tape material with the validation on the flat surface. As comparison, Figure 4.12 displays a lesion model in which Figure 4.12 (a) shows a lesion model made of a surgical tape and Figure 4.12 (b) shows the actual psoriasis lesion. Both of the objects are photographed at the same resolution.

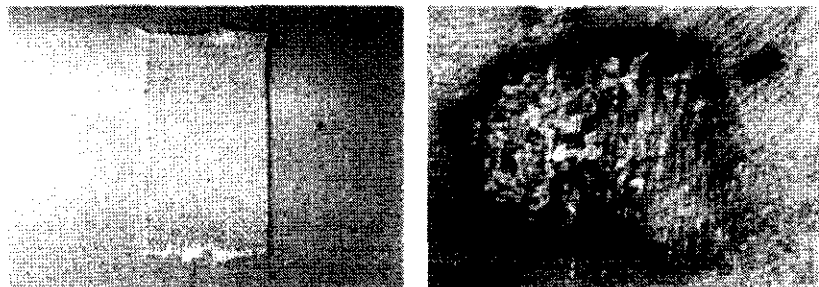


**Figure 4.12** Lesion model ( $20 \times 11.5$  mm<sup>2</sup>) is made of surgical tape (left) and a psoriasis lesion (right). The images are photographed by PRIMOS camera.

A total of 390 lesion models are pasted and distributed onto several locations of the mannequin body. The lesion models are placed in the centre point of grid arrangement with size  $40 \times 30 \text{ mm}^2$ . The centre point is selected to provide an accurate image because the highly focused area is located in this point. The region of the lesion models are defined following four regions (head, upper limb, trunk, and lower limb) of PASI scoring. Table 4.3 presents a list of the distribution of lesion models on body regions. Since each model requires a certain rectangular space, the number of lesions is limited by the available areas for each body region. Figure 4.13 shows the mannequin used in the validation study and a 3D surface of lesion model.

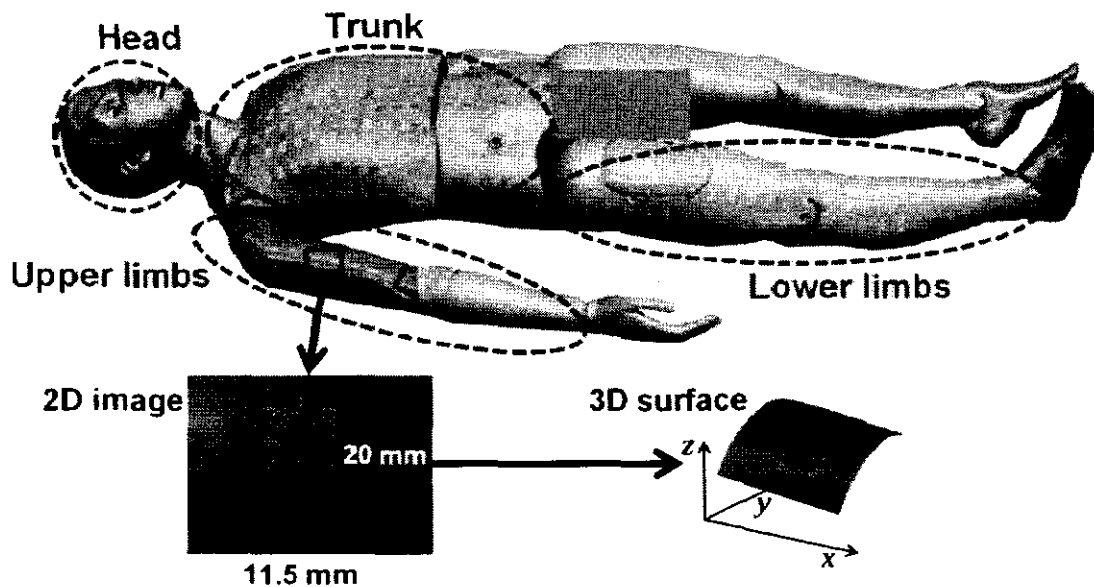


**Figure 4.13** Lesion models are pasted onto life-size mannequin to simulate the lesions. A 2D image and 3D surface of lesion model are shown in the figure.

**Table 4.3** The distribution of lesion models on the body regions of mannequin

Body region	Number of lesions
Head	6
Upper limb	87
Trunk	159
Lower limb	138

The validation process determines the accuracy and total standard deviation of a roughness measurement on a 3D curved skin surface. The algorithm is considered valid if the measured surface roughness of tapes (lesion model) is constant at any locations on the skin surfaces. In this study, a surface of mannequin's skin is used to simulate the human skin surfaces. Table 4.4 presents several surface roughness

values of the lesion models.

**Table 4.4** The surface roughness of lesion models at a flat surface

Lesion Index	Body Region	Width (mm)	Height (mm)	$S_{a,2}$	$R_2^2$	$S_{a,3}$	$R_3^2$	$S_{final}$	Pct. Error (%)
2	Head	10.05	9.04	0.014	0.996	0.015	0.995	0.014	14.8%
6	Head	13.49	8.40	0.013	0.996	0.013	0.996	0.013	6.6%
7	Head	9.54	7.64	0.014	0.998	0.014	0.998	0.014	14.8%
4	Upper Limb	9.80	4.84	0.012	0.971	0.013	0.964	0.012	1.6%
5	Upper Limb	9.67	16.42	0.012	0.998	0.012	0.998	0.012	1.6%
6	Upper Limb	10.18	3.82	0.011	0.996	0.013	0.994	0.011	9.8%
3	Trunk	15.01	7.77	0.012	0.944	0.015	0.905	0.012	1.6%
4	Trunk	9.93	6.49	0.013	0.992	0.013	0.992	0.013	6.6%
8	Trunk	12.22	7.51	0.012	0.977	0.016	0.962	0.012	1.6%
2	Lower Limb	9.29	12.48	0.012	0.982	0.014	0.984	0.014	14.8%
7	Lower Limb	10.18	5.73	0.013	0.959	0.014	0.950	0.013	6.6%
8	Lower Limb	9.67	14.51	0.011	0.970	0.011	0.975	0.011	9.8%

The surface roughness of lesion models on curve surfaces are then summarised in a histogram as depicted in Figure 4.14. The average surface roughness  $\bar{S}_a$  and the standard deviation of lesion models are found to be  $0.0130 \pm 0.0013$  mm ( $\bar{x}_{Curve} \pm \sigma_{Curve}$ ).

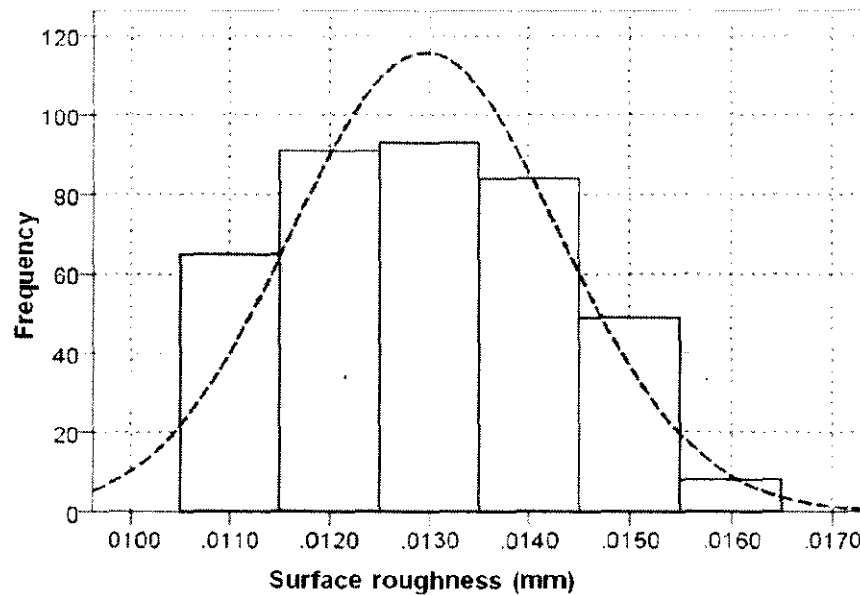


**Figure 4.14** Histogram of lesion models pasted on curved surfaces.

## 4.4 Performance Analysis

### 4.4.1 Determination on Measurement Accuracy

To determine accuracy and total standard deviation of a surface roughness measurement, the average  $S_a$  of lesion models (33) on a flat surface is used as a reference ( $S_{aRef}$ ). The  $S_{aRef}$  value is found to be  $0.0122 \pm 0.0011$  mm ( $\bar{x}_{Ref} \pm \sigma_{Ref}$ ). Meanwhile, the  $S_a$  of lesion models on the mannequin surface ( $S_{aCurve}$ ) is found to be  $0.0130 \pm 0.0013$  mm ( $\bar{x}_{Curve} \pm \sigma_{Curve}$ ). The following equations are used for the error analysis of the algorithm. The calculation results of these equations are described in Table 4.5.

$$Error = |\bar{x}_{Curve} - \bar{x}_{Ref}| \quad (4-25)$$

$$\sigma_{Total} = \sqrt{\sigma_{Ref}^2 + \sigma_{Curve}^2} \quad (4-26)$$

$$Accuracy = \left[ 1 - \frac{|\bar{x}_{Curve} - \bar{x}_{Ref}|}{\bar{x}_{Ref}} \right] \times 100\% \quad (4-27)$$

From the equation (4-25) and (4-26), it is found that the error is  $|0.0130 - 0.0122| = 0.0008$  mm and the total standard deviation is  $(0.0011^2 + 0.0013^2)^{1/2} = 0.0017$  mm. Afterwards, the algorithm accuracy is computed by applying (4-27) that gives  $(1 - |0.0130 - 0.0122|/0.0122) \times 100\% = 94.12\%$ . In this case, the computed accuracy is the minimum accuracy. It implies that the algorithm accuracy is not less than 94.12%. Based on the calculated standard deviation ( $\sigma_{Total} = 0.0017$  mm), the 95% confidence interval ( $Z_{\alpha/2} = 1.96$ ) for the calculated values were in the range of  $\pm 0.0019$  mm for the sample provided. This measurement range showed that it lay within the depth resolution of the PRIMOS camera (0.0040 mm) [131].

**Table 4.5** Performance evaluation of the surface roughness algorithm.

Surfaces	Surface Roughness Parameter		
	$\bar{x}$ (mm)	$\sigma$ (mm)	Accuracy (%)
Reference	0.0122	0.0011	
Curve	0.0130	0.0013	
Absolute Error	$ 0.0130 - 0.0122  =$ 0.0008	$\sqrt{0.0011^2 + 0.0013^2} =$ 0.0017	$(1 - \frac{0.0008}{0.0122}) \times 100\% =$ 94.12 %

#### 4.4.2 Evaluation on Rotational Invariance

The rotation invariance of the algorithm with the second and third order polynomials are tested at the rotated surfaces of lesion model. Another surgical tape on a flat surface with size more than 40 mm × 30 mm is used as the object. The rotation angles are varied from 0° to 330° with the increment of 30°. Thus, 12 rotation angles are applied to evaluate rotation invariance characteristics. Figure 4.15 shows the rotated surfaces of lesion model.

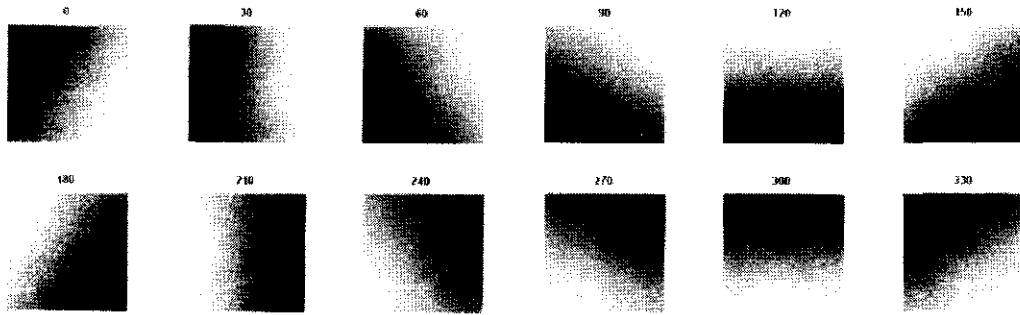


**Figure 4.15** Rotated surfaces of lesion models by applying 12 rotation angles.

Five measurements are conducted for each angle variation. The  $S_a$  of lesion models with various rotation angles is obtained to be  $0.0128 \pm 0.0003$  mm ( $\bar{x} \pm \sigma$ ). Figure 4.16 shows the  $S_a$  of the rotated lesions within the acceptable accuracy (>95%). The results then show that the algorithm is invariant to the rotation of the measured surface. This is made possible because the matrix inversion in a polynomial coefficients determination does not depend on the element sequence of matrices  $V$  and  $Z$ . A surface rotation will change the element sequence of these matrices.

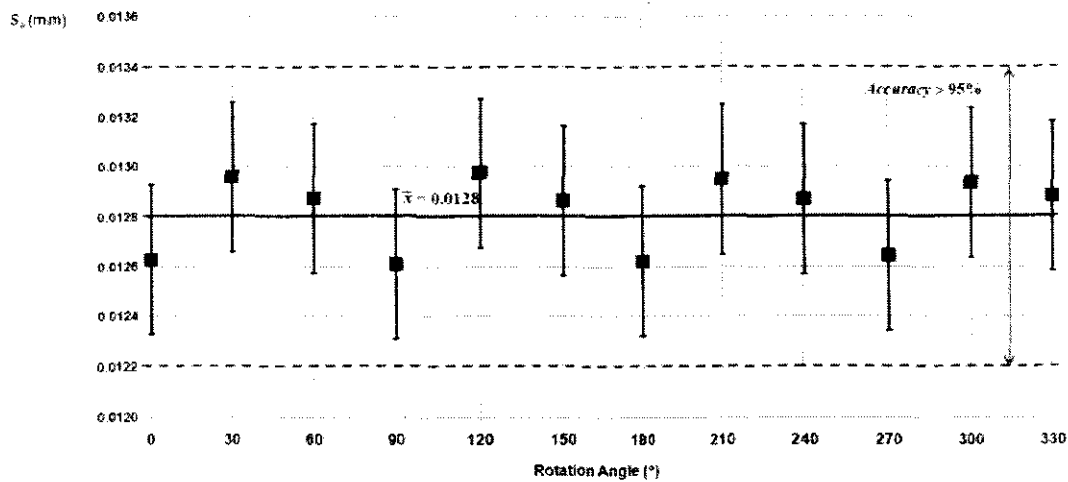


**Figure 4.16**  $S_a$  of lesion models with a variation on rotation angles. The values of  $S_a$  are within acceptable accuracy (>95%).

To test the rotation invariance of a surface roughness algorithm, a lesion surface obtained in two successive scans will be measured. The surface roughness of the lesion images are then determined by a same user in separated calculation. Here, there are 465 samples of the lesions (930 images). The lesion surface between the first and the second scan are made slightly different. As an example (see Figure 4.17), the lesion surface of the second scan has been tilted in a clockwise direction compared to the first scan. By applying a surface roughness algorithm to the lesions (Figure 4.17), the measured  $S_a$  for the first and the second scans are to be 0.0371 mm ( $R^2 = 0.9804$ ) and 0.0511 mm ( $R^2 = 0.9587$ ), respectively.

Further, to prove that the algorithm is invariant to the rotation of the measured surface, the repeatability of the successive scan is evaluated. The definition of repeatability is a closeness between independent results that are obtained through the same method on an identical object, same operator, same conditions, and performed in the short time interval [132]. The absolute differences between the two measurements are used to determine the system repeatability. The repeatability itself can be accepted if 95% of the absolute of measurement differences are less than two standard deviations of the measurement difference ( $2\sigma_{Diff}$ ). This rule has been presented by Bland and Altman in [133].

From the data of successive measurements, the standard deviation of measurement differences ( $\sigma_{Diff}$ ) is found to be 0.011 mm. Therefore, the system repeatability of surface roughness algorithm can be accepted since 95.27% of the measurement differences (443 of 465 lesions) are within the acceptable repeatability ( $2\sigma_{Diff} = 0.021$  mm).

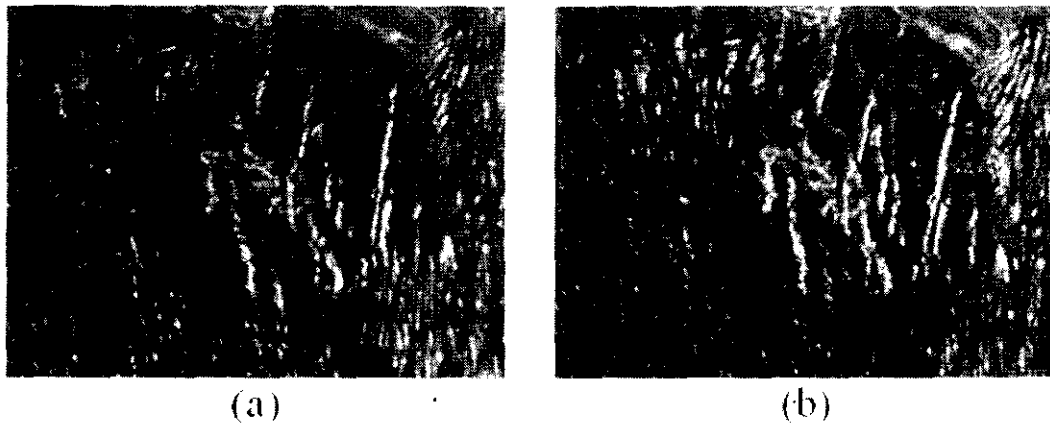


**Figure 4.17** Lesion surfaces are obtained from two successive scans. Lesion (a) is from the first scan and lesion (b) is from the following scan.

The measurement differences can be due to manual segmentation of the lesion ROI as seen in an example in Figure 4.18. The ROI of lesion (a) is larger than the lesion (b). This problem might occur in a segmentation process – particularly in the case of a very large lesion. As a consequence, the lesion boundary cannot be clearly defined.

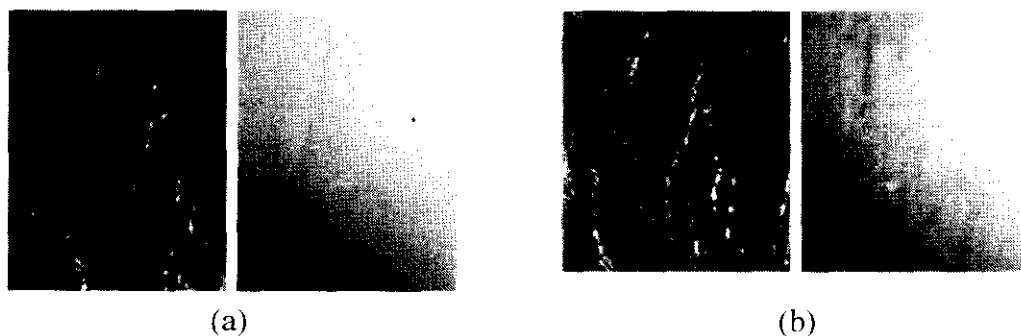


**Figure 4.18** The 2D image and height map of lesion surfaces from the first (a) and the second (b) measurements.

#### 4.4.3 Sample Area for Surface Roughness Determination

In the developed surface roughness, the measured lesion surface is divided into several smaller subdivided surfaces in order to minimise over fitting by a polynomial

surface fitting. The overall surface roughness of lesion surface is obtained by averaging the surface roughness of subdivided surfaces, which have been separately calculated. In this algorithm, the surface division is performed without any consideration of the lesion size. The algorithm does not define minimum area of lesion surface for the optimal performance of the algorithm.

Stout and Blunt have reviewed several 3D surface measurement methods in bioengineering [134]. The review describes that the sampled area is dependent on the machine resolution, measuring time requirement and sample availability. For example, in measuring the surface roughness of tooth root surface, the sampled area is set to be  $0.610 \times 0.610 \text{ mm}^2$ . This method is also applied in determining the surface roughness of blood vessel where a sample area of  $6.400 \times 2.720 \text{ mm}^2$  is used. In this case, a topography measurement on a fingerprint replica with size  $1.020 \times 1.540 \text{ mm}^2$  is performed using a focus detection method.

In a comparative study of two profiling methods (diamond and laser stylus methods), tracing length of 5.6 mm is defined in extracting the roughness profile of dental material [135]. In a larger scale, the landscape surface roughness varies according to the sample area of terrain images. In every landscape type (glacial, upland fluvial, and lowland fluvial), there is a threshold sample area to the extent that there is no any surface roughness variation at the sample area bigger than the threshold [136]. By determining the surface roughness on a bigger area, it can be ensured that all roughness components from low to high frequencies are accounted in a surface roughness determination. The roughness components that have low and medium frequencies might not be accounted if the sample area is too small. As reported in [137] the surface roughness of terrain surface is varying with the spatial resolution (spatial frequency) of the acquired images. Therefore, a large enough sample area, in this case larger than certain threshold size, needs to be acquired in obtaining a representative measurement.

A study on the surface roughness similarity of a large rough surface is reported in [138]. In this study, the threshold for the sampled area in computing surface roughness is determined by plotting two parameters, *i.e.* fractal dimension and amplitude parameter, against the variation of sample area. Fractal dimension and

amplitude parameter are found to be scale-dependent. Its values decrease along with the increase of the sample area. However, the decreasing trend stops at a particular area size. This area is considered as a stationary threshold. Fractal area and amplitude values become constant at sample area sizes larger than the stationary threshold.

The objective of this section is to determine the minimum surface area in determining skin surface roughness. To make the algorithm working properly, the lesion surface must contain all significant roughness components. The above method [137] is adopted in this thesis but only the surface roughness - not the fractal dimension - is used as an indicator. In a developed algorithm, the calculation of surface roughness is based on the vertical deviations of the rough profiles. The amplitude parameter is used to represent the actual vertical deviations of the rough surface, whereas the fractal dimension is used to describe the rough surface irregularity. In the clinical study at the Dermatology Department, Hospital Kuala Lumpur, 2,202 lesion images have been obtained from 204 patients. The lesion sizes vary according to the psoriasis severity as shown in Figure 4.19. This figure shows some lesion examples that are differentiated based on its size: (1) small,  $1.66 \times 2.55 \text{ mm}^2$ , (2) medium  $10.44 \times 10.05 \text{ mm}^2$ , (3) large  $26.78 \times 20.29 \text{ mm}^2$ , and (4) huge  $>40 \times 30 \text{ mm}^2$ . Some of the lesions are larger than the maximum scanned area ( $40 \times 30 \text{ mm}^2$ ) leading the normal skin area not to be acquired in the image. Most of the collected lesions are smaller than the maximum scanning area of the PRIMOS 3D optical scanner since normal skin is required for a lesion thickness determination (lesion thickness is another parameter studied in the clinical study).

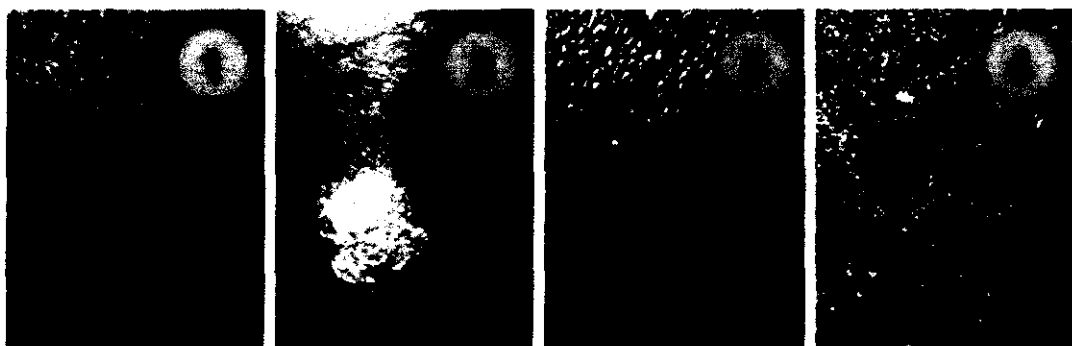


**Figure 4.19** Psoriasis lesions differentiation based on its size: (1) small, (2) medium, (3) large, and (4) huge.

To find a minimum area for a sampled area, skin surface roughness has been determined using different numbers of sampled area. In this evaluation, normal skin surfaces are used as the input data. Figure 4.20 shows the examples of 2D and 3D images of a scanned normal skin surface. The texture of normal skin at the scanned area is assumed to be uniform. Therefore, it can be used in observing the surface roughness variations on several different sampled areas.

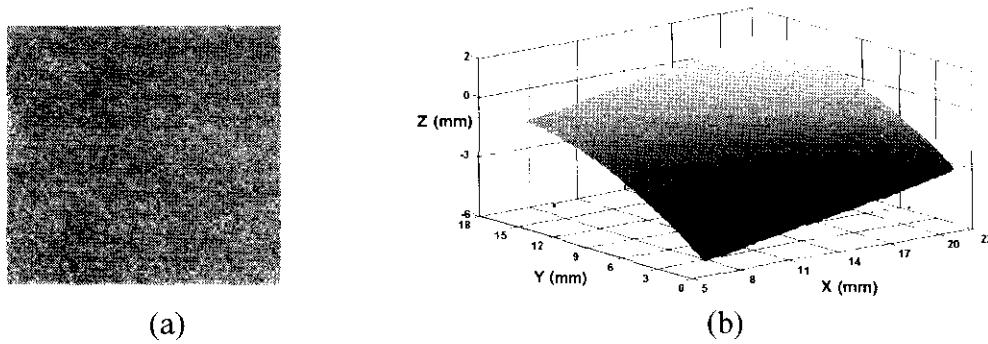


**Figure 4.20** 2D image (a) and 3D surface (b) of normal skin surface.

Nine normal skin images acquired from nine subjects are evaluated in this stage. Three surface images are acquired from forearm region of three volunteers with no psoriasis and six images are obtained from psoriasis patients. The images are then cropped from the surrounding normal skin of the psoriasis lesions. These images are divided into a number of smaller subdivided surfaces with size  $n \times n \text{ mm}^2$ , as shown in Figure 4.21.

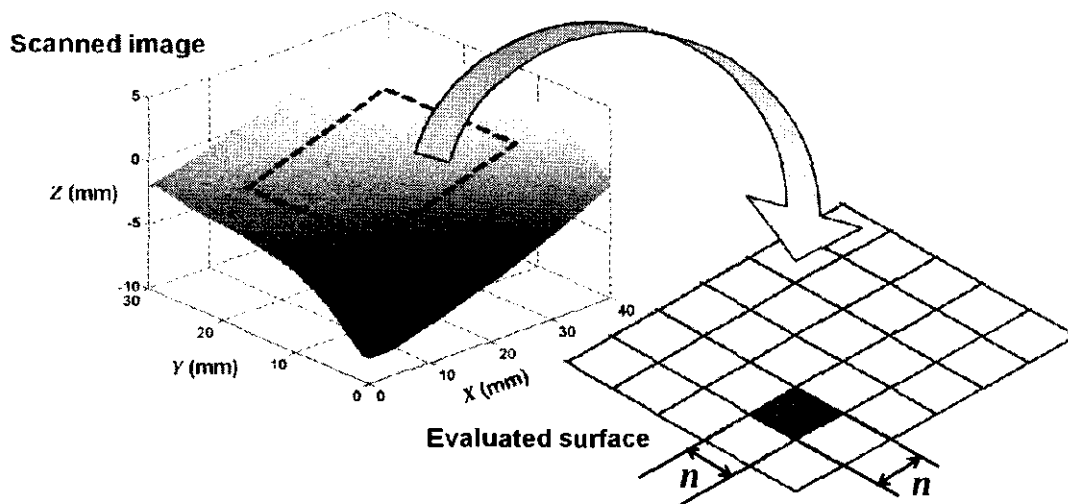


**Figure 4.21** Scanned image is cropped to obtain evaluated surface. Subdivided surfaces are obtained by performing mesh division on an evaluated surface.

These subdivided surfaces are considered as the evaluated surfaces. For this evaluation, the determination of surface roughness is performed for 7 size variations. In this case, the smallest area of subdivided area is  $1 \times 1 \text{ mm}^2$  whereas the largest one is  $7 \times 7 \text{ mm}^2$ . The sizes are varied at increments of 1 mm on both sides. The second, third, and fourth order polynomials are applied to these subdivided surfaces. In previous section, only the second and third orders have been applied. Similarly, the fourth order polynomial is also applied to figure out some fitting problems on a larger area. A larger curved surface may have more undulations than the smaller surface. Therefore, a polynomial with a higher order is required to fit this surface. The equation of fourth order polynomial can be expressed as in (4-28).

$$\begin{aligned}
z_4(x, y) = & (a_1x^4 + a_2x^3 + a_3x^2 + a_4x + a_5)y^4 + \\
& (a_6x^4 + a_7x^3 + a_8x^2 + a_9x + a_{10})y^3 + \\
& (a_{11}x^4 + a_{12}x^3 + a_{13}x^2 + a_{14}x + a_{15})y^2 + \\
& (a_{16}x^4 + a_{17}x^3 + a_{18}x^2 + a_{19}x + a_{20})y + \\
& (a_{21}x^4 + a_{22}x^3 + a_{23}x^2 + a_{24}x + a_{25})
\end{aligned} \tag{4-28}$$

A polynomial surface fitting can fit a surface properly if the fitting order is not less than the actual order of the surface. On the other hand, the actual order of the surface can be characterised by the number of peaks and valleys of the undulated surfaces. Table 4.6 below shows the obtained surface roughness values. Here, the cases of the fitting results at  $R^2 < 0.90$  are not included. Figure 4.22 shows the surface roughness of normal skin samples from 9 subjects with a sampling area variation. The sampling areas are varied from  $1 \times 1 \text{ mm}^2$  to  $7 \times 7 \text{ mm}^2$ .

**Table 4.6** The normal skin surface roughness of 9 subjects with a size variation

Sampling length (mm)	Surface roughness (mm)								
	$S_1$	$S_2$	$S_3$	$S_4$	$S_5$	$S_6$	$S_7$	$S_8$	$S_9$
1.0	0.015	0.008	0.011	0.014	0.013	0.015	0.014	0.013	0.020
2.0	0.018	0.011	0.014	0.019	0.018	0.024	0.018	0.018	0.030
3.0	0.020	0.011	0.015	0.022	0.019	0.032	0.019	0.022	0.035
4.0	0.021	0.012	0.016	0.024	0.020	0.035	0.019	0.023	0.036
5.0	0.022	0.012	0.016	0.025	0.020	0.034	0.019	0.024	0.038
6.0	0.024	0.013	0.016	0.031	0.020	0.036	0.020	0.024	0.040
7.0	0.025	0.013	0.017	0.031	0.021	0.034	0.021	0.026	0.045

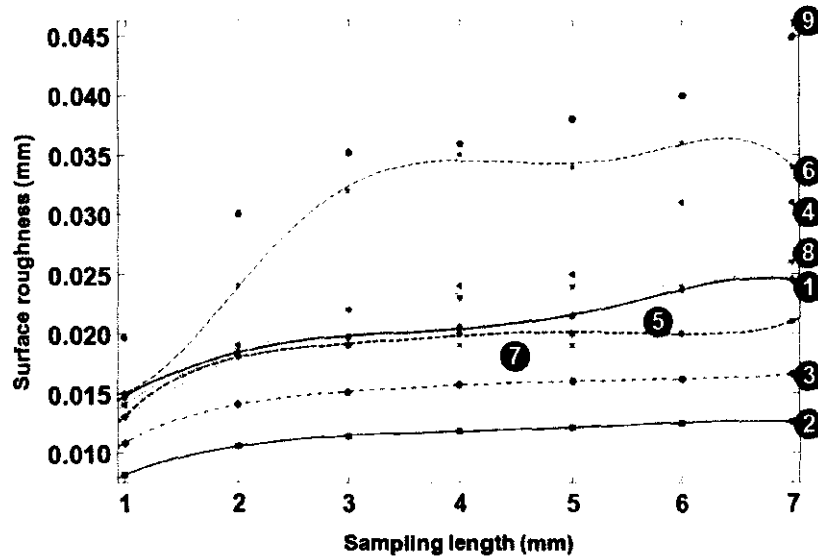


**Figure 4.22** The surface roughness of normal skin samples from 9 subjects with a sampling area variation. The sampling area is a square of sampling length.

Surface roughness ( $S_a$ ) versus sampling length is then fitted to a polynomial function in order to find a stationary threshold for the skin roughness determination.  $R^2$  of these fittings is found to be greater than 0.9957. Subjects  $S_2$  and  $S_7$  are then fitted with the fifth order polynomial. The sixth order polynomial, furthermore, is used to fit the subjects  $S_1, S_3, S_4, S_5, S_6,$  and  $S_8$ , while the seventh order polynomial is only applied to fit subject  $S_9$ . The polynomial equation can be written as follows.

$$f(n) = c_1n^6 + c_2n^5 + c_3n^4 + c_4n^3 + c_5n^2 + c_6n + c_7 \quad (4-29)$$

A fitting result is considered good if  $R^2$  is greater than 0.9 and close to 1.0. At  $R^2 \geq 0.9$ , the difference between the actual data points and the fitted data points are approaching a minimum value. All  $R^2$  of these nine fitting equations are greater than 0.9. The order of polynomial equation is selected from the highest  $R^2$  that can be obtained from the polynomial fitting.

By referring the plots in Figure 4.22, it is possible to determine the threshold of the surface roughness stability. This threshold defines the minimum sampled area for measuring skin surface roughness. The threshold point can be determined from the first inflection point of the plot. To find this inflection point, the second derivative of the fitting equation (2) needs to be determined. The first inflection point occurs when the plot of the second derivative crosses the axis  $Y = 0$ . Figure 4.23 depicts the plot of surface roughness dependency on a sampling size variation. Here, its first derivative and second derivative for the data are taken from subject  $S_3$ .

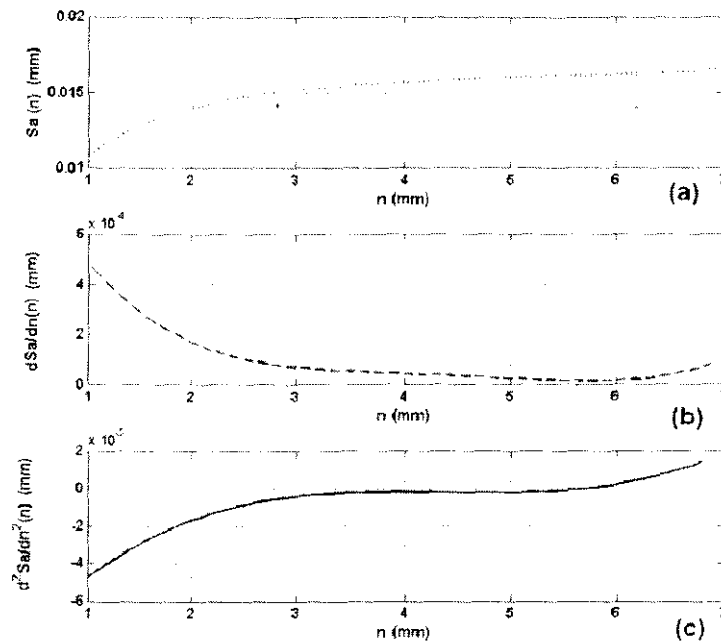


**Figure 4.23** (a) Surface roughness'( $S_a$ ) depends on sampling size variations. Figure (b) and (c) are the plot of the first and the second derivative functions, respectively.

As shown in Figure 4.23 (c), the first inflection point is found at  $n = 4$  mm with  $d^2S_a/dn^2|_{n=4} = -1.73 \times 10^{-6}$  mm. It can be stated here that the roughness components are totally covered within a sampling area if its size is not less than  $4 \times 4$  mm<sup>2</sup>. Surface roughness is increasing for  $n < 4$  mm because the roughness components are not totally included within the sampled area. To determine a threshold value applicable for all skin surfaces, the highest value has to be determined from several skin samples. The threshold points of 9 evaluated skin samples are shown in Table 4.7.

As seen in Table 4.7, the highest threshold point is found to be 4.9 mm. This size can be considered as a minimum sampled area that can be used in a skin surface

roughness determination. The aim of this area setting is to ensure that all of roughness components are accounted in the calculation. From the findings, the surface roughness measurement on normal skin needs a sampled area not less than  $3.8 \times 3.8 \text{ mm}^2$ . It is also recommended to measure a lesion surface with a sampled area greater than  $4.9 \times 4.9 \text{ mm}^2$ . Moreover, its texture is less regular than the texture of normal skin. Therefore, a small lesion as shown in Figure 4.19 would not be correctly measured with the current algorithm.

**Table 4.7** The threshold points of minimum sampling area.

Subject	Threshold point (mm)	Minimum Sampling Area ( $\text{mm}^2$ )	$d^2 S_a / dn^2_i$ (mm)
$S_1$	3.4	11.56	$9.75 \times 10^{-8}$
$S_2$	3.9	15.21	$-4.89 \times 10^{-8}$
$S_3$	4.0	16.00	$-1.73 \times 10^{-6}$
$S_4$	3.6	12.96	$-1.08 \times 10^{-6}$
$S_5$	3.4	11.56	$-7.81 \times 10^{-7}$
$S_6$	4.3	18.49	$3.57 \times 10^{-7}$
$S_7$	3.6	12.96	$7.96 \times 10^{-8}$
$S_8$	4.9	24.01	$1.91 \times 10^{-7}$
$S_9$	3.5	12.25	$1.91 \times 10^{-6}$

In the developed surface roughness algorithm, an input 3D surface is divided into several  $2 \times 2$  subdivided surfaces. By using 4.9 mm as the minimum subdivided area, it can be defined that the minimum size of 3D surface is  $(2 \times 4.9) \text{ mm} \times (2 \times 4.9) \text{ mm} = 9.8 \text{ mm} \times 9.8 \text{ mm}$ . Generally, a surface roughness variation is less for the sample area that is higher than the threshold. However, there is a small surface roughness increment related to the sample size enlargement. As illustrated in Figure 4.23 (c), the surface roughness increment is started from sample size ( $n$ ) equal to 6 mm ( $dS_a/dn|_{n=6\text{mm}} = 0.0004 \text{ mm}$ ). This fact is initiated due to the polynomial surface fitting properties. In a polynomial surface fitting, the errors near the borders are increasing.

A data point can be estimated properly if the estimated data point is located in the centre of the actual data points. The fitting iteration of its neighbour data points can minimise the fitting error at the centre data point. This ideal condition cannot be obtained at the border areas where an estimated data point is fitted with the less

neighbour data points. Similarly, the location of estimated data point also cannot be considered as a centre point since only a half of neighbour data points are available.

Through this condition, the polynomial function cannot fit the mean curvature accurately. To fit a data point accurately, a number of surrounding data points from all sides is required in a surface fitting determination [139]. The increasing sampled size in fact can increase the error between the fitted surface and the original surface.

#### **4.5 Summary**

Chapter 4 details the development of surface roughness algorithm. Surface roughness is used as the measurable features to represent the severity of psoriasis scaliness. A 3D optical scanner is used to acquire some lesion surface images. The estimated 3D waviness surface is extracted from the rough lesion surface by applying a high order polynomial surface fitting. The rough lesion surface is subtracted from the estimated waviness to obtain the vertical deviations of lesion surface. Surface roughness is calculated by averaging the absolute values of the vertical deviations.

This chapter additionally presents the validation study of surface roughness algorithm on the standardised rough surface and curved surfaces. This validation is conducted in order to determine the accuracy and total standard deviation of the developed algorithm. A set of abrasive papers with different roughness grades are evaluated to perform algorithm validation on several various rough surfaces. From the validation, it can be found that the measured surface roughness of the developed algorithm is linearly related to the standardised roughness grade.

Medical tape is used to model skin lesions. The tape is elastic and can adapt with the surface curvature. To validate the surface roughness algorithm on human skin, the lesion models are placed on the curved surfaces of a life-size medical mannequin. The validation process calculates the accuracy and total standard deviation of a roughness measurement on 3D curved skin surfaces. Surface roughness of lesion models is considered valid if surface roughness of lesion model is constant at any locations. The algorithm accuracy is high and can be accepted.

The rotation invariance of the algorithm is tested at the rotated surfaces of lesion model. A lesion model is rotated at varying rotation angles. Surface roughnesses of rotated lesion models are determined. The results prove the rotation invariance characteristic of the surface roughness algorithm. The rotation invariance of a surface roughness algorithm is also tested to psoriasis lesion surface obtained from two successive scans. Due to the rotation and translation, the lesion surface between the first and the second scan is made slightly different. From the measured data, it can be found the system repeatability is within the acceptable repeatability.

Furthermore, the minimum surface area for surface roughness algorithm is determined to define the algorithm limitations. The sizes of psoriasis lesions vary according to the severity. To calculate a minimum sample area, skin surface roughness has been determined using a different number of sampled areas. These images are divided into smaller subdivided surfaces. In the evaluation, the surface roughness determination is applied to the images with several size variations. A sample area threshold defines the minimum sampled area for the surface roughness algorithm. The area threshold is determined from the plot of surface roughness against sampling length. Sample area enlargement does not change the determined surface roughness if the sample area is greater than the threshold level.

From the materials presented in this chapter, it can be shown that the developed algorithm has been validated at a significant level. In its last part, this chapter also clearly describes the algorithm performance and limitations. These remarkable results provide the high level of confidence to build a system for objective clinical assessment. The system is built by combining the developed surface roughness algorithm with the clustering algorithm. This part is elaborated in the following chapter.

## CHAPTER 5

### DEVELOPMENT ON SURFACE ROUGHNESS ALGORITHM

Chapter 5 describes the study set-up, data collection, result and analysis of the developed computerised psoriasis (PASI) scaliness assessment. For a statically representative data collection, a proper sampling size needs to be determined. Dermatologists assess the PASI scaliness of all collected data. Section 5.1 of this chapter presents the data collection requirements and procedures. The developed surface roughness algorithm (presented in Chapter 4) is applied to measure the skin roughness of psoriasis lesions. It is then followed by Section 5.2 that discusses about unsupervised clustering methods. Two clustering methods, *k*-means and fuzzy *c*-means (FCM) algorithms, are used to obtain the PASI scaliness score of psoriasis lesion. These methods are presented to classify the measurement result of skin surface roughness to be next interpreted in PASI scaliness score. The results of these clustering algorithms are described in this section. Following this, Section 5.3 describes an agreement analysis related to the PASI scaliness scoring performance that is evaluated by determining kappa agreement coefficients between the first and the second assessment of the developed algorithm. The results of agreement analysis are later used to determine the assessment objectivity. Section 5.4 recaps all findings and analyses of the Chapter 5.

#### **5.1 Study Set-up and Data Collection**

##### **5.1.1 Sample Size Measurement**

A sample data is used to represent the uncounted size of population data. The problem is about how to determine the sample size correctly. The size should be

well optimised to represent the population characteristics. A very large sample size might make the data representation better but it can be costly and time-consuming. Lowering the sample size, can reduce the amount of the resources needed. Nevertheless, this can potentially make the sample characteristics dissociated from the actual population.

The determination of the sample size can be done based on the margin error equation [140]. The margin error equation is used to determine a maximum error between the population mean  $\mu$  (true value) and the sample mean  $\bar{x}$  (observed from the collected data). The population data is assumed normally distributed. Only the population standard deviation can be provided to the equation whereas the population mean is unknown. The equation is given as follows,

$$E = Z_{\alpha/2} \frac{\sigma}{\sqrt{n}} \quad (5-1)$$

Variable  $E$  represents the margin of the error of the unknown population mean. The error is determined from the sample mean  $\bar{x}$  of sample data. If the mean of sample  $\bar{x}$  has the same value with the population mean,  $\mu$ , then  $E$  will be equal to zero. Variable  $Z_{\alpha/2}$  refers to the critical value of normal distribution table (the bell curve). The term  $\alpha$  is used to define the level of confidence. Any positive value less than 1 can be applied but in order to have meaningful results, the value of  $\alpha$  should be close to 1. The level of confidence is usually set at 90%, 95%, and 99%. For instance, to obtain an area with the level of confidence 95%,  $\pm Z_{\alpha/2}$  values need to be determined. Here, it is calculated by  $\alpha = 1 - 0.95 = 0.05$ . This remaining area ( $\alpha = 0.05$ ) is then divided by 2 and distributed to the left and the right tails of the normal distribution, as shown in Figure 5.1. The observed area (95%) is located in the middle of normal distribution and bounded by  $\pm Z_{\alpha/2}$ . From the standard normal distribution table, it can be found that  $\pm Z_{\alpha/2} = \pm 1.96$ . The term  $\sigma$  is the population standard deviation whereas  $n$  is the sample size.

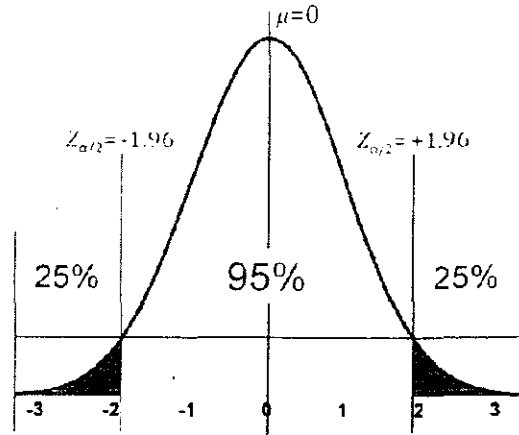


**Figure 5.1** An area with a certain confidence level bounded by  $\pm Z_{\alpha/2}$ .

Equation (5.1) is rewritten as follows to obtain the sample size:

$$n = \left[ \frac{Z_{\alpha/2} \times \sigma}{E} \right]^2 \quad (5-2)$$

The population standard deviation  $\sigma$  is considered similar to the sample standard deviation. As in the aforementioned example, the  $Z_{\alpha/2}$  is found based on the required accuracy  $(1-\alpha)$  in the sampling process.

The required sample size of PASI scaliness is calculated by using the data of lesion scaliness from a previous study [14]. In this study, the data is acquired by a 3D laser scanner (Konica Minolta Vivid 910) with a focal length,  $f = 14$  mm. The object distance is set around 1 meter from the scanner and the depth accuracy of the 3D laser scanner is up to 0.10 mm to the reference surface. The scaliness data is grouped into four different scores by applying an unsupervised clustering algorithm *i.e.*  $k$ -means clustering. Table 5.1 below lists the statistical values of PASI scaliness.

**Table 5.1** Statistics of the scaliness value for each score.

Scaliness Score	Samples	Minimum (mm)	Maximum (mm)	Interval (mm)	Mean (mm)	Standard Deviation
1	37	0.024	0.078	0.054	0.057	0.014
2	21	0.083	0.133	0.050	0.104	0.014
3	14	0.140	0.206	0.066	0.172	0.021
4	11	0.221	0.328	0.108	0.256	0.038

From Table 5.1, score 1 is the only data that would be used for the sample size determination. This score is statistically reliable because it has more than 30 samples. The significant level ( $\alpha$ ) of 0.05 corresponding to confidence level 95% is

assigned in the determination. To compare some options, the margin of error  $E$  is varied for 5%, 10%, and 15% and the sample mean is used as the base for determining the  $E$  value. For example, a maximum difference with error 10% is determined by  $10\% \times \bar{x}_1 = 10\% \times 0.057 = 0.006$  mm.

**Table 5.2** Sample sizes of scaliness score 1 with  $\alpha=0.05$  (confidence level 95%) and maximum difference variations.

Confidence Level ( $Z$ )	Error (%)	Maximum Difference ( $E$ ) (mm)	Required Sample Size
95%	5	0.003	83.66 $\approx$ 84
	10	0.006	20.92 $\approx$ 21
	15	0.009	9.30 $\approx$ 10

The sample size with error 5% is used to provide sample size with acceptable mean difference from the actual value. Four scaliness scores need to be analysed. Hence, to cover all scores, the total sample size required is 4 scores  $\times$  84 samples = 336 samples. A scaliness sample is obtained from a scaliness calculation of a single psoriasis lesion. Based on this calculation approach, 336 psoriasis lesions are required to achieve a confidence level of 95% for all scaliness scores.

The lesion data were acquired in a clinical study involving 204 registered psoriasis patients at Department of Dermatology, Hospital Kuala Lumpur. The number of patient is defined based on a sample size determination for the PASI area parameter. Naturally, more than one lesion can be obtained from a patient. The clinical study NMRR-09-1098-4863 for data collection has been approved by the Clinical Research Centre, Ministry of Health, Malaysia. In this study, the data collection for scaliness parameter is part of the data collection for other PASI parameters (area, erythema, and thickness).

### 5.1.2 Data Collection Procedure

The patients involved are referred as participants in the study. Two criteria – inclusion and exclusion – are applied in recruiting participants in the clinical study. The details for these criteria are described in the following lists.

Inclusion criteria:

- Participant has been informed regarding the nature and the aims of the study

and has given their written informed consent.

- Male and female participants can be involved in the study.
- The age of participant is not less than 18 years.
- Participant has been clinically diagnosed to have plaque psoriasis.

Exclusion criteria:

- Participant refuses consent to be involved in the study.
- Participant with other forms of psoriasis, such as erythrodermic, pustular, flexural, palmoplantar, or guttate psoriasis.
- Presence of other dermatological diseases that can interfere with the interpretation of the photographs (*e.g.* eczema, vitiligo).
- Participant who is unfit and is unable to stand for a long time.

A PRIMOS 3D optical scanner in this procedure is also used to acquire 3D surface images of the plaque psoriasis lesion of patients. The scanner gives the maximum depth resolution of 4  $\mu\text{m}$  and the lateral resolution of 63  $\mu\text{m}$ . The image size obtained at this resolution is 640 by 480 pixels. The dermatologists subsequently select a representative lesion for each body region (head, trunk, upper and lower limbs). All four representative lesions are scanned in order to obtain 3D surfaces. The collected lesions are also being applied for another measurement (lesion thickness). Hence, the selection requires a lesion, which has an area less than the total scanned area ( $40 \times 30 \text{ mm}^2$ ). For patients with severe psoriasis condition, additional lesions are collected from the patient without lesion area limitation.

The 3D scanning of psoriasis lesions requires certain conditions and room settings. These requirements are described as follows:

- a. The illumination of the projected pattern of PRIMOS 3D optical scanner should be higher than the ambient illumination, as shown in Figure 5.2 (a). The illumination of the projected pattern produced by the optical scanner is measured to be  $1,435 \pm 29 \text{ Lux}$ . The lights in the room are switched off to lower the ambient illumination below the projector illumination. The ambient illumination during data collection is  $249 \pm 11 \text{ Lux}$ .
- b. The distance between the optical scanner and the object (lesion surface) is fixed at 220 mm. The measured surface must be parallel with the surface of

the scanner lens. On the other hand, a fixed distance is required to scale a surface pixel to an actual size in length unit. A parallel and fixed distance arrangement is to ensure the surface is within the area of depth of field.

- c. Two persons are required during the scanning process. The first person handles the camera and scans the lesion. The second person operates the PRIMOS software running on the laptop. Figure 5.2 (b) shows the data acquisition method for 3D surface of skin lesion.

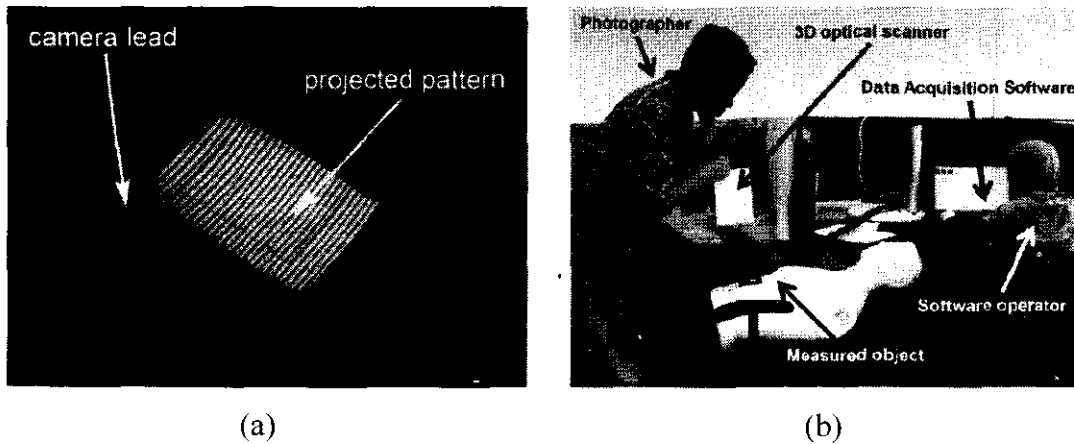


**Figure 5.2** (a) A projected pattern of PRIMOS 3D optical scanner. (b) A scanning process for acquiring the data for a scaliness measurement.

The process flow during the data collection involves several steps such as patient's preparation, PASI assessment by dermatologists, and data acquisition. It takes 28 minutes to complete the whole process; 12 minutes are required by dermatologists to assess PASI scores and another 16 minutes for the computerised PASI assessment. The detailed steps are as follows:

- a. Dermatologist briefs patient on the procedures of data collection.
- b. Patient takes off clothes and then put on underwear. The underwear is used to cover genital area for all patients and chest area for female patient.
- c. Dermatologist performs the PASI assessment to score area, erythema, thickness, and scaliness, as depicted in Chapter 1 by Figure 1.1. For erythema, thickness, and scaliness assessment, the first dermatologist selects a representative lesion for each body region (head, upper limbs, trunk, and

lower limbs). After being labelled using a pen marker, the lesions are scored by the first and the second dermatologists consecutively. Figure 5.3 (a) shows the dermatologist gives label on a representative lesion. An example of a labelled lesion (Lesion 2268 obtained from lower limb region of Patient 184) is shown in Figure 5.3 (b). Number 2 indicates the lesion is the second lesion to be assessed at particular body region. This label is written on the surrounding normal skin surfaces and it would not affect the process of surface measurement. The labels are used to help the dermatologists to differentiate the assessed lesions. Another one or two additional lesions can be collected and assessed for each patient. Therefore, the number of lesions that can be obtained from a patient is 12 lesions, 3 lesions from each four body regions.



**Figure 5.3** (a) Dermatologist selects and labels the lesion. (b) An example of a labelled lesion on lower limb region of Patient 184.

- d. Patient is asked to move from the medical examination room to the photography room. In this room, some investigators will perform a computerised PASI assessment. In this assessment, three imaging modalities - 2D camera, chromameter, and 3D optical scanner - are integrated to the computer with PASI software. Male patients are handled by male investigators. For handling the female patients, only female investigator is allowed to enter the photography room.
- e. PASI area assessment is carried out by acquiring 2D images of the whole body of the patient. The images are photographed from four different views - front, back, right, and left. PASI area algorithm uses these 2D images to

determine PASI area score.

- f. PASI erythema assessment is performed by measuring the CIE Lab data of selected lesions and surrounding normal skin. A chromameter CR-400 is used to measure the colour data.
- g. The last step of data collection is 3D surface measurement. The optical scanner is used to acquire the lesion surfaces. The 3D surfaces obtained in this step are used to determine PASI thickness and scaliness scores. Figure 5.4 displays acquisition processes for PASI area, erythema, and thickness-scaliness parameters, as mentioned in step 5, 6, and 7.

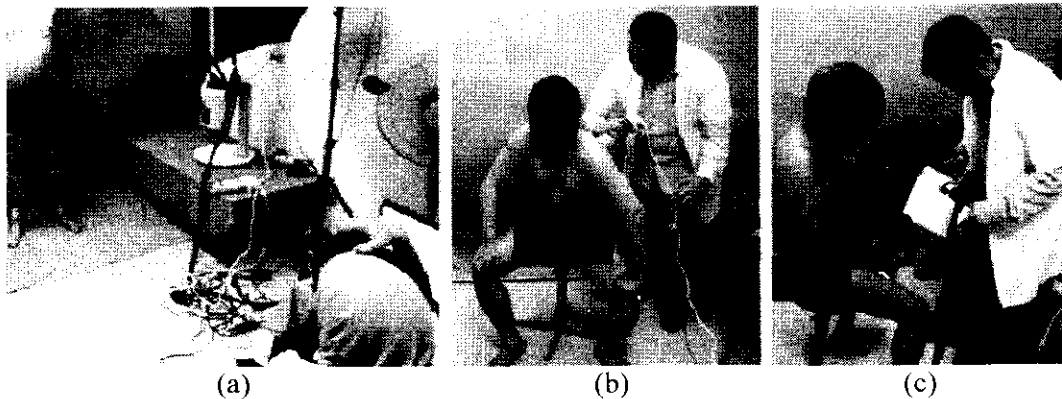


**Figure 5.4** Data acquisition for determining PASI parameters: (a) area (b) erythema, and (c) lesion thickness and scaliness.

- h. In performing a double assessment, the acquisition steps are repeated from step 4 to step 6. This session is performed after step 6 has been completed in the earlier session. In this research, the double assessment is applied to the last 43 patients. 161 patients earlier are assessed in one session only. Not all of patients are assessed twice because double assessment was only proposed during the later stages of the study.

### **5.1.3 Data Profile of Recruited Patients in Clinical Study**

In this research, the psoriasis lesions dataset is applied to the surface roughness algorithm. The data have been acquired from a number of the registered psoriasis patients of Dermatology Department, Hospital Kuala Lumpur. The data collection was conducted from 10 March to 5 October 2010 (10 months) involving 204 patients

(163 males and 41 females) with ages ranging from 19 to 82 years. The average psoriasis duration of the recruited patients is 14.05 years. Therefore, most of the patients have been affected by psoriasis more than 10 years.

The demographic data might not be complete enough to represent the actual condition of psoriasis - especially at gender category. The number of male patients is higher than that of female patients. A population-based study has shown that the male and female patients can suffer psoriasis with a male to female prevalence ratio almost 1:1, except for younger females (*i.e.* age <20 years) whereas the female prevalence is higher with ratio of 1:1.3 [142]. In this study however, more male patients were recruited due to the lack of consenting female patients. They worry about the assessment procedure, especially in taking 2D images of their body. The patient demography based on gender, race, age, and psoriasis duration are shown as charts in Figure 5.5.

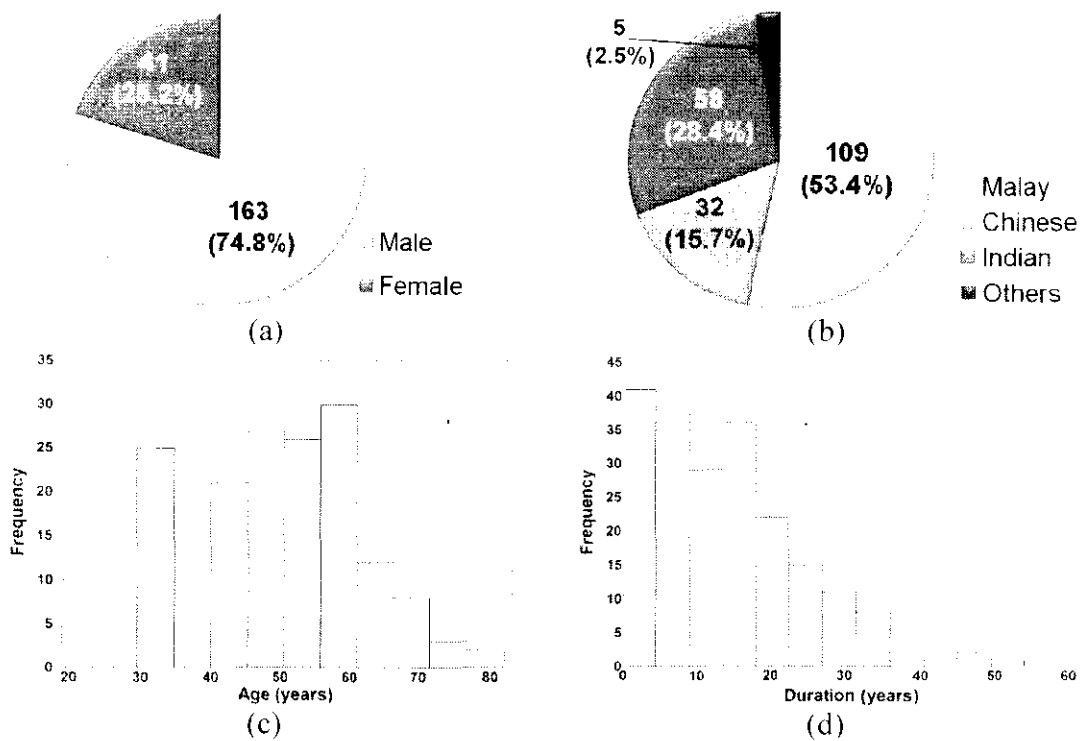


**Figure 5.5** Charts of patient demography based on (a) gender, (b) race, (c) age, and (d) psoriasis duration.

The sample size of roughness measurement is 1,999 psoriasis lesion images collected from 204 psoriasis patients. The images consist of 1,351 images scanned in a single measurement and 648 scanned images in double assessments on 324 lesions.

1,892 psoriasis lesions have been scored 1, 2, 3, or 4 by dermatologists. The score distribution of the lesions is described in Table 5.3.

**Table 5.3** Distribution of PASI Scaliness Score (N=1,892).

PASI Scaliness Score	Number of Lesion	Percentage (%)
1	1,266	66.91
2	409	21.62
3	153	8.09
4	64	3.38
Total	1,892	100.00

Figure 5.6 shows the histogram of the surface roughness of 1,999 psoriasis lesion images. Based on the histogram, the minimum and maximum roughness values are 0.010 mm and 0.187 mm, respectively. A roughness algorithm has been tested at these limit values. The lowest limit of surface roughness has been determined in the measurement of lesion model at flat surface. The value of the lowest limit is 0.0100 mm ( $\bar{x}_{Ref} - 2\sigma_{Ref}$ ).

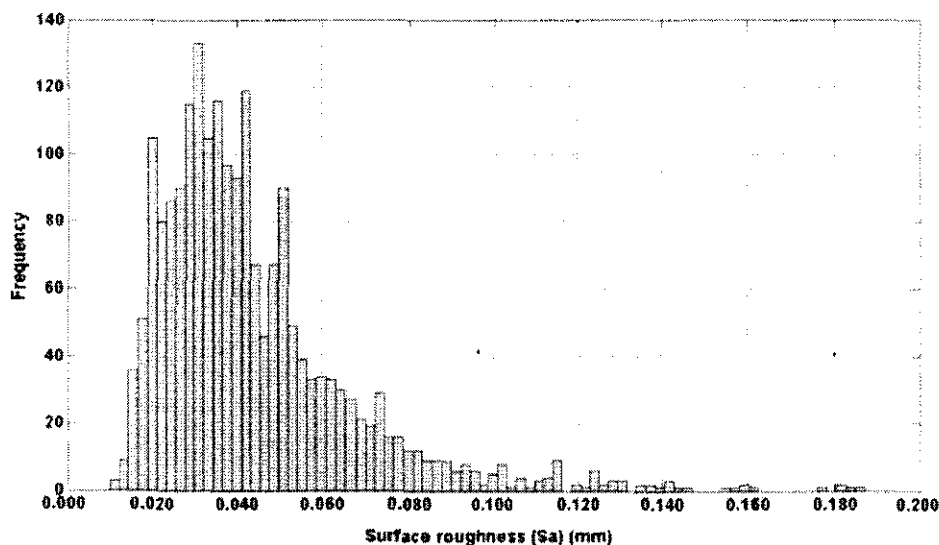


**Figure 5.6** Histogram of surface roughness of collected lesions.

For the highest limit, it can be obtained from validation results of surface roughness algorithm on abrasive papers. The highest surface roughness is found to be 0.3962 mm ( $\bar{S}_a + \sigma$ ). This roughness is found from measurement of the roughest abrasive paper evaluated in the research. Surface roughness values of abrasive paper and lesion model are mentioned in section 4.3.1 and 4.3.2. The histogram is normally distributed but is skewed to the left side with positive skewness of 2.002

to  $T_2$ ). There are only two options for the membership degree - 0 or 1. Figure 5.7 (a) shows that membership degree of  $x_1$  of cluster 2 is 1 whereas the membership degrees of  $x_1$  for the other clusters are 0. In soft clustering (FCM), as shown by Figure 5.7 (b), an input  $x_1$  can be considered as the member of three clusters (cluster 1, 2 and 3). However, it has several different membership degrees. For example, the degree of  $x_1$  belongs to cluster 1, 2, and 3 are 0.8, 0.4, and 0.0, respectively. The classification system decides  $x_1$  as a member of cluster 1. The decision is taken since the membership degree at cluster 1 is the highest one among the clusters.

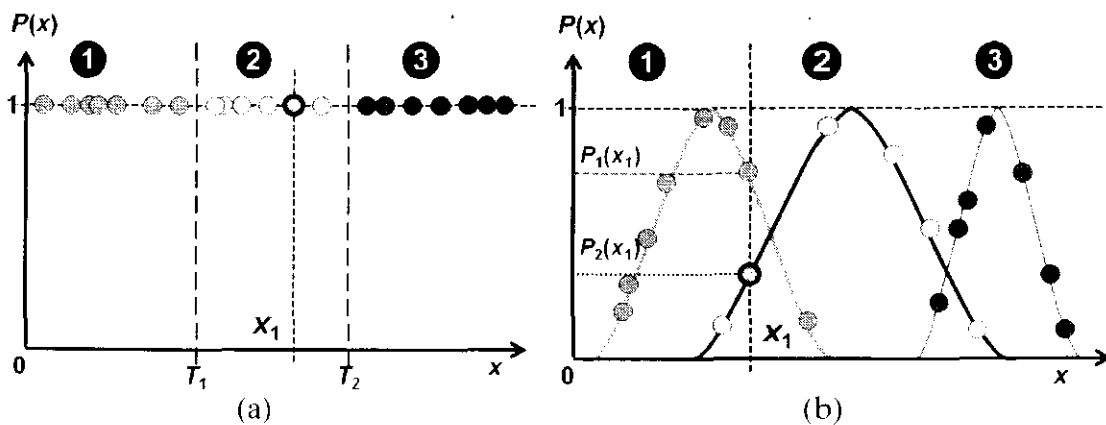


**Figure 5.7** Comparison of classification methods used in (a) hard and (b) soft clustering algorithms.

Both unsupervised clustering algorithms are used in this research. The term of  $k$ -means was proposed by James MacQueen in 1967 based on the idea of a Polish mathematician, Hugo Steinhaus in 1956. The algorithm was then standardised by Stuart Lloyd in 1957 but not published until 1982. At that time, the algorithm was implemented for a pulse-code modulation. Meanwhile, E.W. Forgy proposed a similar clustering method in 1965. For this,  $k$ -means algorithm is also recognised as Lloyd-Forgy method. The  $k$ -means algorithm is simple, efficient, and easy to implement [144].  $K$ -means groups the dataset into a predefined number of clusters. Initial centroids are assigned randomly or by applying certain algorithms to the clusters. Similarities of the dataset and the centroids are examined for every single data point. The data will be considered to belong to a cluster that has the highest similarity. After all of the dataset are completely clustered, some new centroids are recalculated by finding the mean values of the clusters. The process is iterated until the centroids are considered constant. This consistency is indicated by the minimum

changes at all centroids. A certain number of iterations can be also used to define the termination point of the iteration process. A classification system is built based on the final centroids obtained from the clustering process. The system classifies an input data based on the distance between the input data and the cluster centroid. The data will belong to a cluster if it has the highest similarity to the cluster, which is represented by the cluster centroid.

FCM clustering algorithms is also applied in this research to improve scoring performance. Soft decision of FCM is more similar with the fuzziness of human being. Fuzzy  $c$ -means clustering is initially proposed by Bezdek *et al.* in 1984 [147]. The algorithm has been developed based on a fuzzy set proposed by Zadeh [148]. Bezdek introduced this algorithm in order to improve the  $k$ -means algorithm. FCM minimises the limitation of hard clustering algorithm, e.g.  $k$ -means clustering, by associating each data to all existing clusters with a membership degree [149]. The membership degree is represented by a membership matrix  $U = [u_{ik}]$ . The membership degree of a data point in a particular cluster can be considered as a probability of this data point that belongs to the cluster. Subscripts  $i$  and  $k$  are used to index the data point and the cluster, respectively. For instance, if there are a hundred data points ( $i = 1, \dots, 100$ ) and three clusters ( $k = 1, 2, 3$ ), the matrix size of  $U$  will become  $100 \times 3$ . The membership degrees can be any real values but it must be within 0 to 1. A data point will be associated to each cluster and determined by a membership degree. The accumulation of these degrees is always equal to 1. The following equation describes the constraints of the membership degree [150].

$$\sum_{k=1}^K u_{ik} = 1, \quad \forall i = 1, \dots, N; 0 \leq u_{ik} \leq 1 \quad (5-3)$$

The iteration process of FCM algorithm is performed to achieve membership degrees stability. This condition indicates that the data points have been clustered and maximally separated. As applied in  $k$ -means algorithm, the FCM algorithm also has an objective function for the iteration process, as written in (5-4). A new variable, fuzziness coefficient ( $m$ ), is introduced to the equation. The aim of this coefficient is used to symbol the fuzziness of the membership function. This fuzziness represents the softness of the cluster boundaries. As a comparison, the

fuzziness coefficient will be zero in a hard clustering. It denotes firmness of the cluster boundaries for the hard clustering. Variable ( $K$ ) is the number of cluster whereas ( $N$ ) is the number of data point. Centroids initialisation can be executed either randomly or based on prior knowledge.

$$J(C, U, X) = \sum_{k=1}^K \sum_{i=1}^N u_{ik}^m \|x_i - c_k\|^2 \quad (5-4)$$

The iteration process updates the centroids and the membership matrix continuously. The equation for calculating the new centroids is given by

$$c_k = \frac{\sum_{i=1}^N u_{ik}^m x_i}{\sum_{i=1}^N u_{ik}^m} \quad (5-5)$$

The membership matrix is determined by applying the equation below

$$u_{ik} = \frac{1}{\sum_{l=1}^K \left[ \frac{\|x_i - c_k\|}{\|x_i - c_l\|} \right]^{2/(m-1)}} \quad i = 1, 2, \dots, N \quad k = 1, 2, \dots, K \quad (5-6)$$

The objective function is going to be stable when some high membership degrees are assigned near the cluster centroids. While, some low membership degrees are obtained at the data far from the centroids [151]. The iteration process to update matrixes  $U$  and  $M$  is repeated until no changes in the cluster centroids are found. It is indicated by  $\Delta J < \varepsilon$  where  $\varepsilon$  is an acceptable difference to terminate the iteration. The membership degree of a data point in a particular cluster can be considered as a probability of this data point that belongs to the cluster.

**Algorithm 5.1:** The FCM algorithm

- i) Define the number of cluster ( $K$ ), membership matrix ( $u_{i,k}$ ), and fuzziness coefficient ( $m$ ). Use a number of small random numbers to the membership matrix  $u_{i,k}$  and a real value between 1 and 2 for the fuzziness coefficient. Fix the objective function  $J(C)$  equal to 0. The acceptable error ( $\varepsilon$ ) and the maximum number of iteration are also initialised in this step. These values are used to indicate termination point of the iteration.
- ii) Compute new centroids by applying  $u_{i,k}$  and  $x_i$  to equation (5-19).

- iii) Update the new membership matrix based on new centroids at step 2 and equation (5-20).
- iv) Determine the objective function  $J(C)$  by applying the centroids and the membership matrix to equation (5-4).
- v) Determine the difference between the latest to the previous objective function. The difference is denoted as  $\Delta J$ . If the difference is larger than the predefined acceptable error ( $\varepsilon$ ), continue the iteration to step 3. The iteration could be terminated if  $\Delta J < \varepsilon$  or the iteration number is over the maximum value. Here, the value of  $\varepsilon$  is  $10^{-5}$ .

End.

From the clustering result, it is found that the membership degrees are not calculated at every data point values outside the values given in the training stage. Therefore, a membership function is required to determine the membership degrees at any data points. The membership degrees of the cluster are used to create a membership function. In this case, the curve fitting algorithms can be applied to find the best membership function. Gaussian functions might also be used to fit the membership degrees of the clustered data points. The classification of any input data is decided by comparing the membership degrees of the input. The data will be included to a cluster if its membership degree is higher than the membership degrees to the other clusters.

Two unsupervised clustering methods,  $k$ -means and FCM algorithms are investigated.  $K$ -means clustering is used to classify  $n$  observed pattern into  $k$  clusters. Each observation data point is classified into a cluster with the nearest mean. In this research, psoriasis lesions are classified into four score groups by applying  $k$ -means clustering to the surface roughness dataset. The objective of the  $k$ -means algorithm is to divide the dataset into  $k$  clusters to achieve the minimum within-group sum of squares. The basic form of the  $k$ -means algorithm is based on the iteration of two processes. The first process is the assignment of data points into score groups. A data point is assigned to the closest group in term of Euclidean distance. The second process is the calculation of new group means, namely group

centroid, based on the new assignments. The processes will be terminated when there is no any new assignment required. In this stage, the centroids of score groups are maximally separated [144]. A boundary level between two adjacent score groups is then determined by finding a middle point between the centroids of adjacent groups. 1,351 lesions are used in the training. The dataset is selected based on the criteria as mentioned in the previous section. Table 5.4 describes the score group centroids of PASI scaliness scores.

**Table 5.4** Centroid of PASI scaliness scores.

PASI scaliness score	Score Centroid (mm)	$N$	Percentage (%)
1	0.024	486	35.97
2	0.040	523	38.71
3	0.061	285	21.10
4	0.106	57	4.22
Total		1,351	100.00

Furthermore, the  $k$ -means clustering algorithm ability to classify scaliness of psoriasis lesion based on surface roughness is validated by applying the algorithm to divided datasets. Here, the dataset is randomly partitioned into two equal sized datasets (Subset 1 and Subset 2). The scores are properly clustered (maximally separated) if the score centroids for all datasets are consistent. In other words, the score centroids are not influenced by a dataset partition since the sample size of each score is statistically accepted (sample size is greater than 30).  $K$ -means clustering algorithm, thus, requires a large dataset for each score to achieve centroid stability.

Table 5.5 and Table 5.6 depict the stability of the score centroids of partitioned datasets. The centroid differences of each score between Subset 1 and Subset 2 are smaller than 0.004 mm. Meanwhile, to observe centroid consistency on a smaller sample size, the dataset is randomly partitioned into three datasets (Subset 1, Subset 2, and Subset 3). The centroid consistency of subsets can be observed in two and three partitions. The differences of centroid are not more than  $3\sigma_{Total}$  (0.005 mm) except for the centroid difference of score 4 in three partitions (0.008 mm). The centroid difference is greater because the size of clustered dataset is insufficient (<30 samples).

**Table 5.5** Score centroids of subset 1 and 2.

PASI Score	Subset 1 (N=676)		Subset 2 (N=675)		Centroid difference (mm)
	Centroid (mm)	N	Centroid (mm)	N	
1	0.024	226	0.024	227	0.001
2	0.038	247	0.038	264	0.000
3	0.057	169	0.059	155	0.004
4	0.104	34	0.104	29	0.000

**Table 5.6** Score centroids of subset 1, 2, and 3.

PASI Score	Subset 1 (N=451)		Subset 2 (N=450)		Subset 3 (N=450)		Average centroid difference (mm)
	Centroid (mm)	N	Centroid (mm)	N	Centroid (mm)	N	
1	0.024	156	0.023	164	0.025	158	0.001
2	0.040	180	0.038	155	0.039	164	0.001
3	0.061	90	0.058	117	0.058	96	0.002
4	0.102	25	0.109	14	0.097	32	0.008

The boundary levels of surface roughness for PASI Scaliness scores are calculated from Table 5.4 . A boundary level between Score 1 and Score 2 is the midpoint between score centroids. For instance, the boundary level between score 1 and 2 is 0.032 mm. It is obtained from  $(\text{Centroid 1} + \text{Centroid 2}) / 2 = (0.024 + 0.040) / 2 = 0.032$  mm. This method is also applied to determine the next boundary levels. If there is a lesion with surface roughness equal to the boundary level, the lesion will be classified to have a higher score. Finally, the boundary levels of surface roughness for PASI Scaliness score are given as described in Table 5.7

**Table 5.7** Boundary levels of surface roughness for PASI scaliness score.

Score	Boundary Levels (mm)
1	$S_a \leq 0.032$
2	$0.032 < S_a \leq 0.051$
3	$0.051 < S_a \leq 0.084$
4	$S_a > 0.084$

PASI scaliness score is then determined by applying the score rules to the surface roughness of psoriasis lesions. The clustering results on the test dataset is summarised as shown in Figure 5.8. Assessment consistency of first and second assessment is symbolised by coincident markers of both assessments.

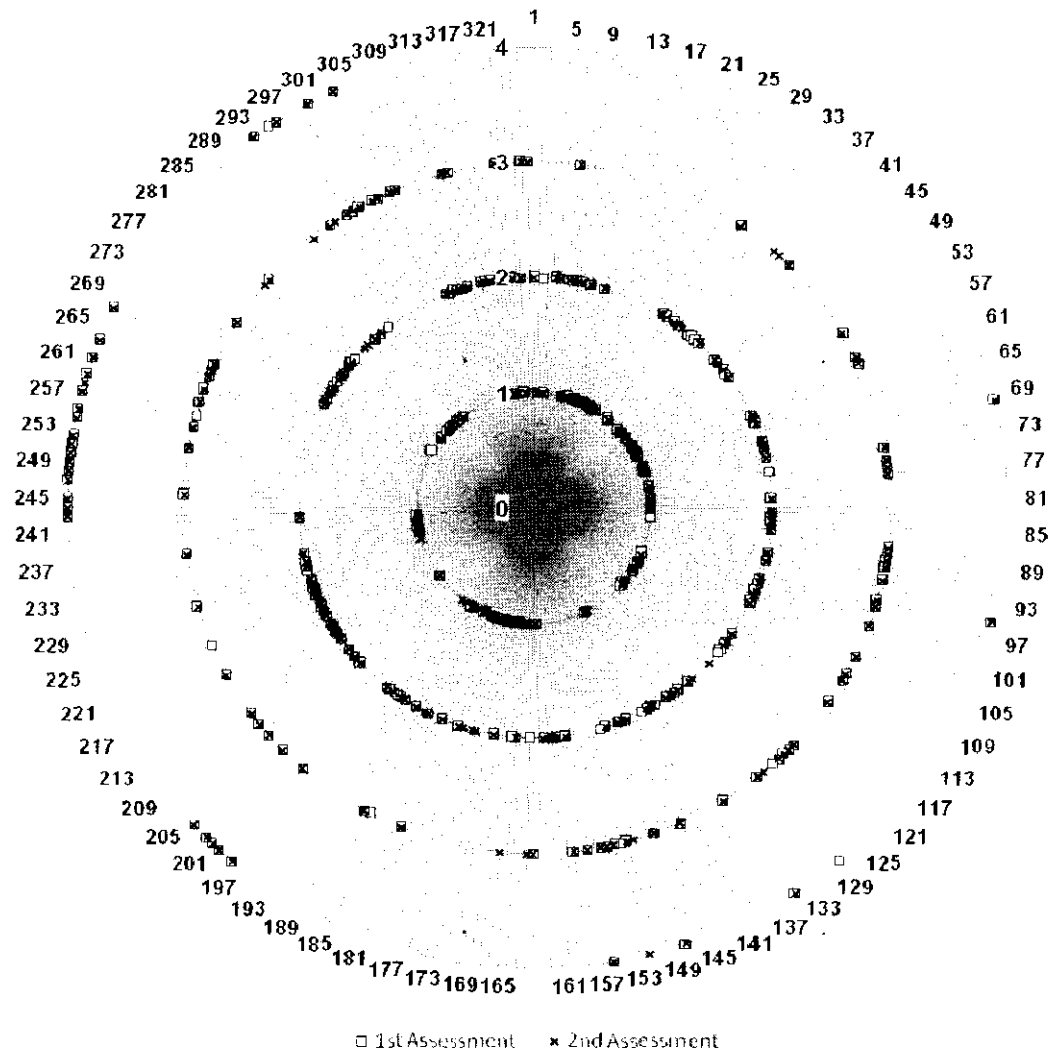


**Figure 5.8** Clustering results of *k*-means algorithm on test dataset.

324 data points are used as test dataset. The detailed clustering result is described in the appendix section. 289 (89.2 %) data points are successfully classified as the same cluster in the first and second assessments. However, 35 (10.8 %) data points of double assessments are classified as different cluster. The misclassifications can be categorised into three types based on location of the occurrences. The first type is misclassification in determining either score 1 or score 2. The score 1 might be found in the first assessment and then followed by score 2 in the second assessment otherwise score 2 precedes the score 1. The second type is the classification uncertainty of score 2 or 3. The last type is the scoring vagueness between score 3 and 4. Two different scores can also be obtained in the second and the third types as exemplified by the first type. These measurement inconsistencies occur when the surface roughness data points are located too close to the score

boundary levels.

As described in Table 5.7, there are three boundary levels can be defined. These boundary levels distinguish a score cluster from the other clusters. The levels are labelled as  $B_1$ ,  $B_2$ , and  $B_3$ .  $B_1$  is used to separate score 1 from score 2. The second boundary is  $B_2$  that divides score 2 from score 3. The last boundary is  $B_3$ . This boundary splits score 3 from score 4. The values of  $B_1$ ,  $B_2$ , and  $B_3$  are 0.032 mm, 0.051 mm, and 0.084 respectively. Closeness of the measured surface roughness to each boundary level is computed by applying Euclidean distance equation. The equation is given by

$$D_{B_i}(S_a) = \sqrt{(S_{a_1} - B_i)^2 + (S_{a_2} - B_i)^2} \quad i = 1,2,3 \quad (5-7)$$

$S_{a_1}$  and  $S_{a_2}$  are measured surface roughness from the first and the second assessments.  $B_i$  is used to represent the boundary level at  $i$ , as mentioned in previous paragraph. The Euclidean distance equation is applied to the test dataset that have been misclassified in the score clustering. All of the misclassification types are found in this work. There are 21 misclassification cases of type 1 (score 1 and 2), 10 cases of type 2 (score 2 and 3), and only 4 cases for the type 3 (score 3 and 4). The closeness of the measured surface roughness to the existing boundary levels are determined by applying equation (5-7). Furthermore, an average of the Euclidean distance is calculated to indicate closeness of the misclassification type with a certain boundary level.

The closeness measurement results are described in Table 5.8. The distances are determined from misclassification cases on test dataset. Misclassification type 1 occurs when the measured surface roughness values are close to the boundary level  $B_1$ . This closeness is shown by the  $\overline{D_{B_1}}$  value (0.003 mm) which is 11% smaller than  $D_{B_2}$  (0.028 mm) and  $D_{B_3}$  (0.075 mm). Misclassification type 2 is indicated by the smallest value of  $D_{B_2}$  (0.003 mm) compared to  $D_{B_1}$  (0.026 mm) and  $D_{B_3}$  (0.048 mm). For the type 3, the trend still follows the previous types. The smallest Euclidean distance is obtained at the  $D_{B_3}$  (0.004 mm) value. The  $D_{B_1}$  (0.072 mm) and  $D_{B_2}$  (0.046) are found much larger than  $D_{B_3}$ . The closeness distances of all

misclassification types are less than 0.005 mm.

**Table 5.8** Average of Euclidean distances of surface roughness and boundary levels of *k*-means classification algorithm.

Misclassification Type	$\overline{D_{B_1}}$ (mm)	$\overline{D_{B_2}}$ (mm)	$\overline{D_{B_3}}$ (mm)	<i>N</i>
Type 1, score 1 and 2	0.003	0.028	0.075	21
Type 2, score 2 and 3	0.026	0.003	0.048	10
Type 3, score 3 and 4	0.072	0.046	0.004	4

A small Euclidean distance at a certain boundary level is only found in the misclassification cases. Small Euclidean distances cannot be found in the data points that correctly classified. All of surface roughness data points are located beyond from the boundary levels. Thus, the misclassification cases can be minimised. The average of Euclidean distance is much higher than 0.005 mm for all score groups, as listed in Table 5.9.

**Table 5.9** Average of Euclidean distances of surface roughness and boundary levels determined from correct classification cases of *k*-means algorithm.

Score Group	$\overline{D_{B_1}}$ (mm)	$\overline{D_{B_2}}$ (mm)	$\overline{D_{B_3}}$ (mm)	<i>N</i>
Score 1	0.012	0.039	0.085	79
Score 2	0.011	0.016	0.063	110
Score 3	0.046	0.019	0.028	70
Score 4	0.120	0.093	0.046	30

To avoid incorrect classification, it is recommended to collect more than a single data point if the surface roughness measured near the boundary levels. The surface roughness input is then determined by averaging the surface roughness values of multiple measurements. The surface roughness ranges that require multiple measurements are defined in Table 5.10.

**Table 5.10** The surface roughness ranges near the boundary levels of *k*-means classification algorithm.

Misclassification Type	Surface Roughness Interval (mm) $S_a - 3\sigma_{Total} \leq B_i \leq S_a + 3\sigma_{Total}$
Type 1, score 1 and 2	$0.027 \leq S_a \leq 0.037$
Type 2, score 2 and 3	$0.046 \leq S_a \leq 0.056$
Type 3, score 3 and 4	$0.079 \leq S_a \leq 0.089$

The second clustering method applied in the research is FCM (fuzzy *c*-means) clustering. This algorithm aims to improve the classification reliability especially at

a border region between two adjacent clusters. Rigidity at the border region in the  $k$ -means clustering is reduced by implementing the fuzziness of FCM clustering.

An example that shows  $k$ -means rigidity is when the results of two consecutive measurements are classified into two different clusters. It can be occurred when the boundary level is located in the middle area of the first and the second assessments. The first measurement is classified belong to the first cluster whereas the second measurement is considered to be the second cluster. Here, the similar dataset that has been applied to  $k$ -means clustering is used by FCM clustering. The size of training dataset is 1,351. The clustering iteration gives the membership degrees of each data point. For this dataset, 67 iteration steps are required to achieve its stability at the objective function  $J(C, U, X)$  equals 0.0503. The function  $J(C, U, X)$  is determined by applying equation (5-4). This objective function determines summation of the cluster member aggregation and the separability among the existing clusters. In perfect condition the value of the final objective function should be nearly zero. This condition is achieved when all of the cluster members are located close to its cluster centroids and there are no intersections among the membership functions, as found in hard clustering.

To reduce the iteration number, the predefined membership degrees are assigned before the iteration process. Four functions are required to determine predefined membership degrees of the score groups. To build the functions, the maximum interval of surface roughness is then divided into four equally score intervals. The cluster centroid is computed from the middle point of the score interval. Figure 5.9 show the score intervals that divide surface roughness interval into four score groups. Each score group is bordered with two boundary levels. For instance, score 1 is bordered by  $L_1$  and  $L_3$ . The centroid of score 1 is then calculated from the middle point of  $L_1$  and  $L_3$ . Here, the centroid is represented by variable  $L_2$ . This similar method is also applied to determine the centroids for cluster 2, 3, and 4.

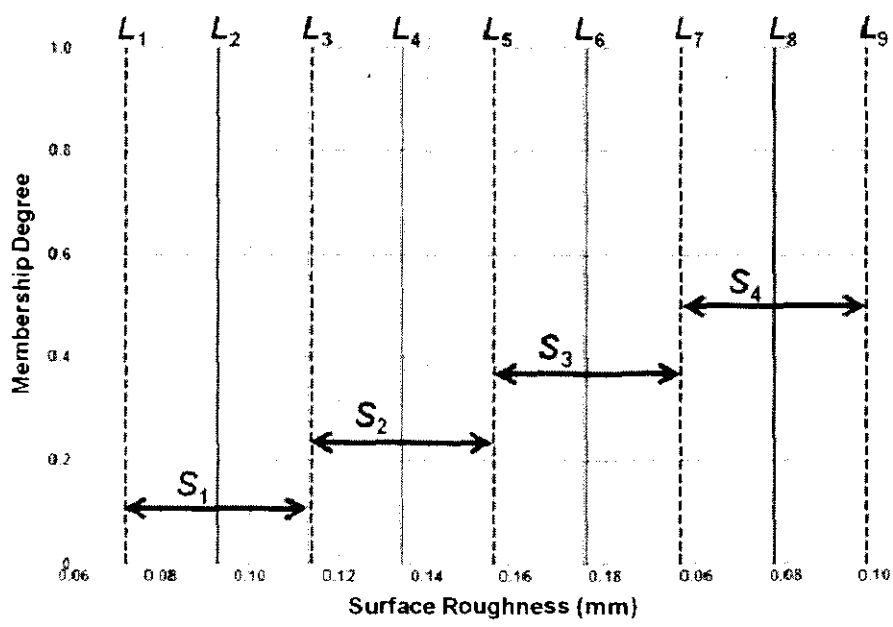


**Figure 5.9** Surface roughness intervals of score groups.

A triangular function is used to calculate the membership degrees of the training dataset. This triangular shape is selected because the shape will have the maximum value only at a data point. By using this shape, the membership degrees of another data points can be also linearly determined. The edges of the triangle legs are fixed at minimum and maximum values of training dataset. Here, the minimum and maximum values of abscissae are 0.0120 mm and 0.1780 mm, respectively. To create triangle shape, the highest membership degree is assigned to the cluster centroid. The predefined membership degrees of score clusters are determined by applying equations (5-8) to (5-15). These predefined membership degrees are used to initiate the clustering iteration. Variables  $c_1, c_2, c_3$ , and  $c_4$  are the cluster centroids that assigned from  $L_2, L_4, L_6$ , and  $L_8$  respectively, as described in Figure 5.9.  $L_1$  and  $L_9$  are the minimum and maximum values of the training dataset.  $S_a$ . The matrix size of of the membership degree is  $N \times 4$ . The  $N$  is the size of training dataset. The details of membership degree equations are formulated as follows:

Membership degrees of Score 1,  $c_1 = L_2$

$$\text{if } S_a(i) < c_1; \quad u_{i,1} = \frac{1}{(c_1 - L_1)} \times (S_a(i) - L_1) \quad (5-8)$$

$$\text{if } S_a(i) \geq c_1; \quad u_{i,1} = \frac{-1}{(L_9 - c_1)} \times (S_a(i) - c_1) + 1 \quad (5-9)$$

Membership degrees of Score 2,  $c_2 = L_4$

$$\text{if } S_a(i) < c_2; \quad u_{i,2} = \frac{1}{(c_2 - L_1)} \times (S_a(i) - L_1) \quad (5-10)$$

$$\text{if } S_a(i) \geq c_2; \quad u_{i,2} = \frac{-1}{(L_9 - c_2)} \times (S_a(i) - c_2) + 1 \quad (5-11)$$

Membership degrees of Score 3,  $c_3 = L_6$

$$\text{if } S_a(i) < c_3; \quad u_{i,3} = \frac{1}{(c_3 - L_1)} \times (S_a(i) - L_1) \quad (5-12)$$

$$\text{if } S_a(i) \geq c_3; \quad u_{i,3} = \frac{-1}{(L_9 - c_3)} \times (S_a(i) - c_3) + 1 \quad (5-13)$$

Membership degrees of Score 4,  $c_4 = L_8$

$$\text{if } S_a(i) < c_2; \quad u_{i,4} = \frac{1}{(c_4 - L_1)} \times (S_a(i) - L_1) \quad (5-14)$$

$$\text{if } S_a(i) \geq c_2; \quad u_{i,4} = \frac{-1}{(L_9 - c_4)} \times (S_a(i) - c_4) + 1 \quad (5-15)$$

The predefined membership degrees of the score groups are plotted to create membership degree distribution. The degrees obtained from interval division are plotted as shown in Figure 5.10.

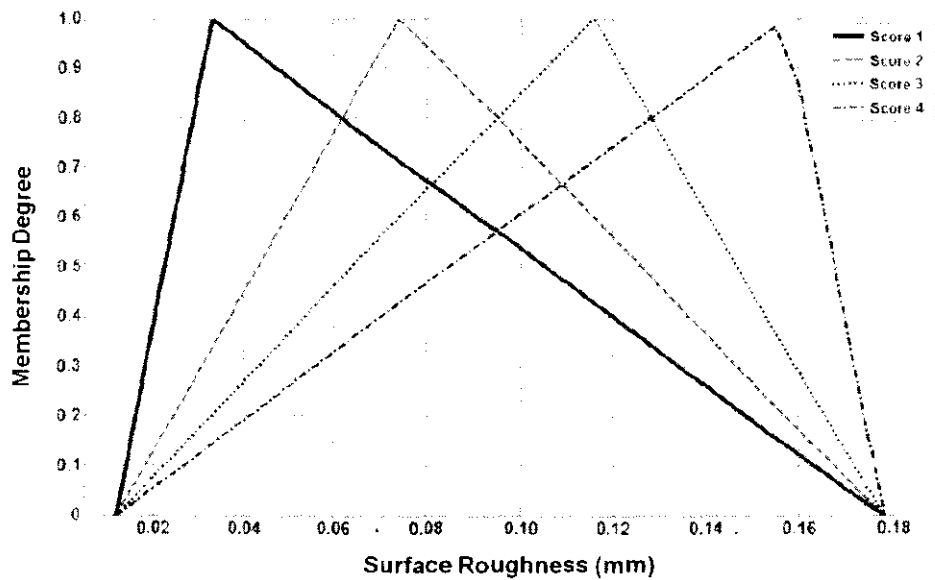


**Figure 5.10** Predefined membership degrees of score groups.

Comparison of iteration process that uses predefined and random membership degrees is shown in Figure 5.11. By applying predefined membership degrees, the iteration number has been reduced from 67 steps to 31 steps.

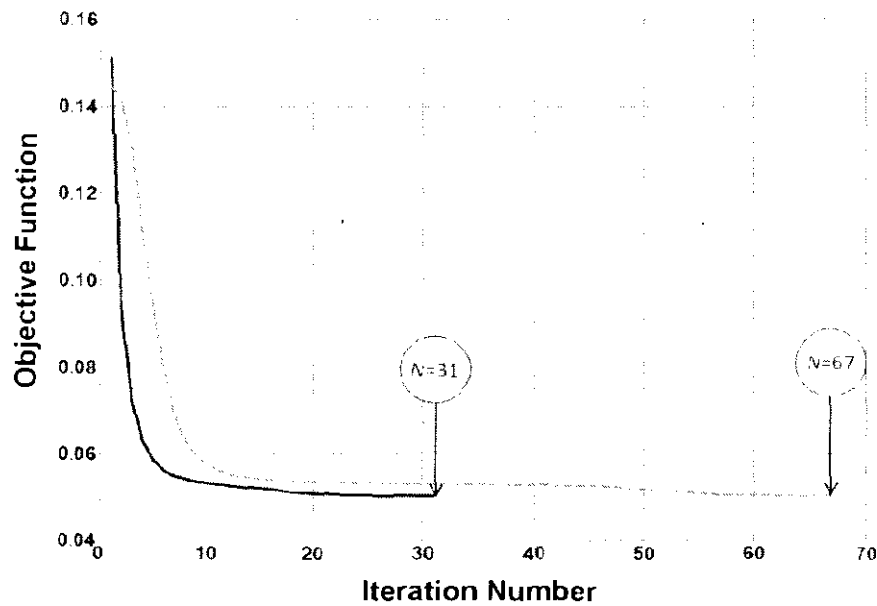


**Figure 5.11** Iteration of FCM clustering with random (dotted line) and predefined (solid line) membership degrees.

Membership degrees of the training dataset are obtained from the iteration of FCM clustering. The degrees are clustered and scattered according to the existing clusters as depicted in Figure 5.12.

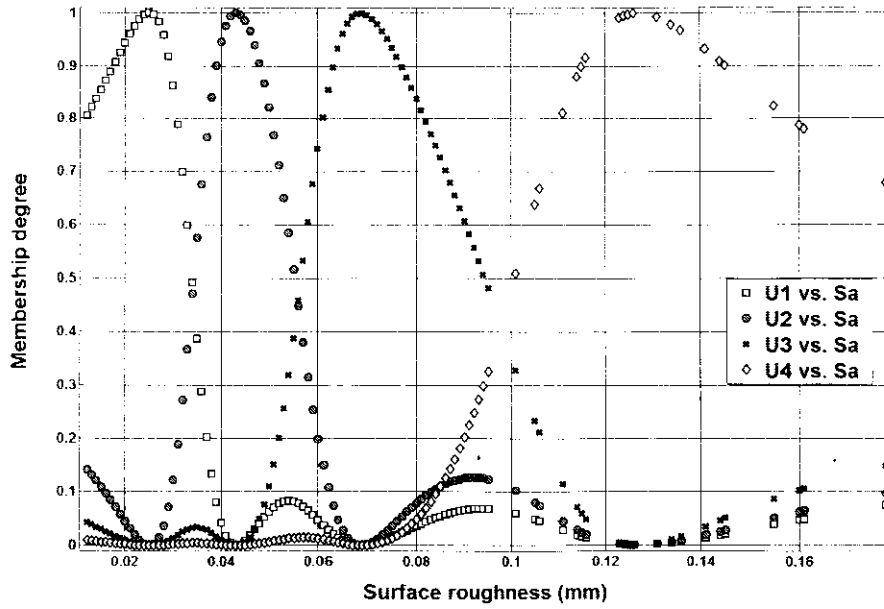


**Figure 5.12** Membership degrees scattering of clustered dataset.

Gaussian fitting function is used to obtain the membership degrees or the probabilities of surface roughness at any input values. The general form of the Gaussian equation for representing the membership function of scaliness score is given by equation (5-16). The coefficients of scaliness score functions are listed in Table 5.11. The membership degrees of clustered data have been fitted to the Gaussian function with  $R^2 \approx 1$ . The membership degree of a certain surface roughness  $S_a$  is calculated by applying all membership functions,  $P_n(S_a)$ , from  $n=1$  to  $n=4$ . The subscript  $n$  on variable  $P_n(S_a)$  represents the group of scaliness score. Equation (5-16) is constructed from the summation of two Gaussian fitting functions, which have different means and standard deviations. For the first Gaussian function, coefficient  $a_1$  is the maximum height of the distribution,  $b_1$  is the mean of Gaussian distribution, and  $c_1$  is the standard deviation. The same meanings are also applied for the second Gaussian function.

$$P_n(S_a) = a_1 \exp\left(-\left(\frac{S_a - b_1}{c_1}\right)^2\right) + a_2 \exp\left(-\left(\frac{S_a - b_2}{c_2}\right)^2\right) \quad (5-16)$$

**Table 5.11** Coefficients of Gaussian functions for the roughness classification of PASI scaliness scores.

Scaliness score	$a_1$	$b_1$	$c_1$	$a_2$	$b_2$	$c_2$	$R^2$
Score 1 (S1)	0.609	0.029	0.007	0.888	0.018	0.011	0.994
Score 2 (S2)	0.514	0.038	0.006	0.858	0.048	0.010	0.992
Score 3 (S3)	0.635	0.064	0.010	0.784	0.081	0.018	0.995
Score 4 (S4)	0.708	0.118	0.023	0.792	0.160	0.039	0.997

The membership functions of PASI scaliness scores are plotted in Figure 5.13. PASI scaliness score is determined by applying the rule of scaliness score as written in (5-17). An input of surface roughness is classified into a particular score if the input gives the highest membership degree or probability among the scaliness scores.

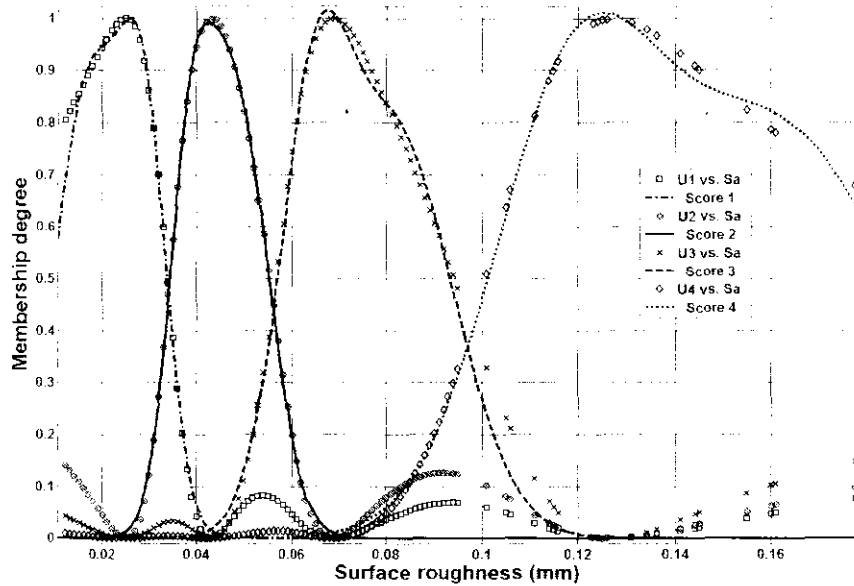


**Figure 5.13** Membership functions of PASI scaliness scores.

$$S(S_a) = \begin{cases} 1, \max(P_1(S_a), P_2(S_a), P_3(S_a), P_4(S_a)) = P_1(S_a) \\ 2, \max(P_1(S_a), P_2(S_a), P_3(S_a), P_4(S_a)) = P_2(S_a) \\ 3, \max(P_1(S_a), P_2(S_a), P_3(S_a), P_4(S_a)) = P_3(S_a) \\ 4, \max(P_1(S_a), P_2(S_a), P_3(S_a), P_4(S_a)) = P_4(S_a) \end{cases} \quad (5-17)$$

Some examples of score calculations are listed in Table 5.12. Sample 1, a lesion with surface roughness 0.039 mm would be classified into a PASI scaliness score. Membership degrees of the sample for score clusters (score 1 to 4) are 0.100, 0.913, 0.005, and 0.000. The highest degree is obtained at second cluster  $P_2(\bar{S}_a) = 0.913$  therefore the sample can be categorised as score 2. This is similarly applied to the

subsequent lesion samples in Table 5.12.

**Table 5.12** Calculations of PASI scaliness scores by applying FCM algorithm

No	$\bar{S}_a$ (mm)	$P_1(\bar{S}_a)$	$P_2(\bar{S}_a)$	$P_3(\bar{S}_a)$	$P_4(\bar{S}_a)$	$P_{max}$	Score
1	0.039	0.100	0.913	0.005	0.000	0.913	2
2	0.017	0.908	0.000	0.000	0.000	0.908	1
3	0.063	0.000	0.085	0.911	0.004	0.911	3
4	0.112	0.000	0.000	0.044	0.837	0.837	4

Figure 5.14 describes the complete scaliness scores that have been classified by applying FCM algorithm. Several lesions that have been scored by FCM are shown in Figure 5.15. The complete results of FCM are listed in appendix section.

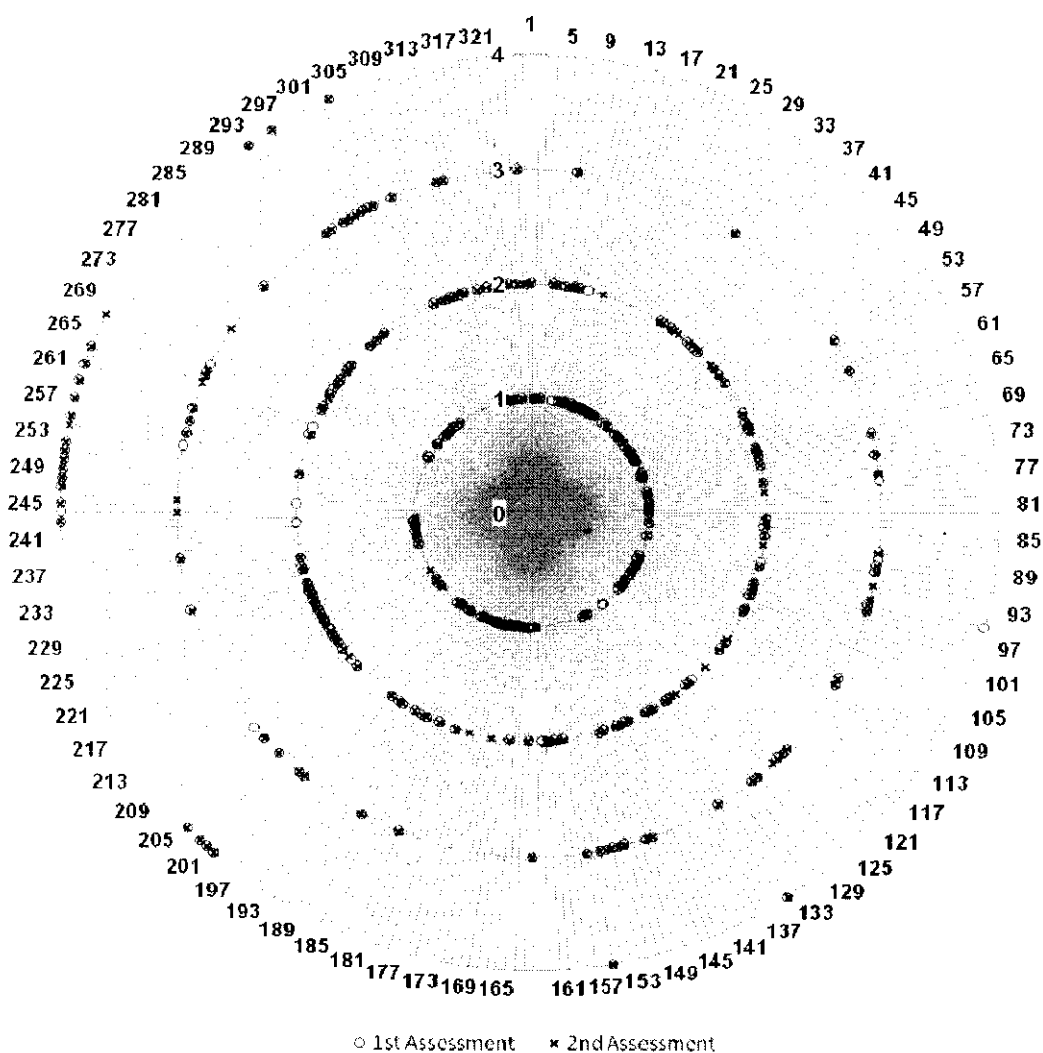


**Figure 5.14** Clustering results of FCM algorithm on test dataset.

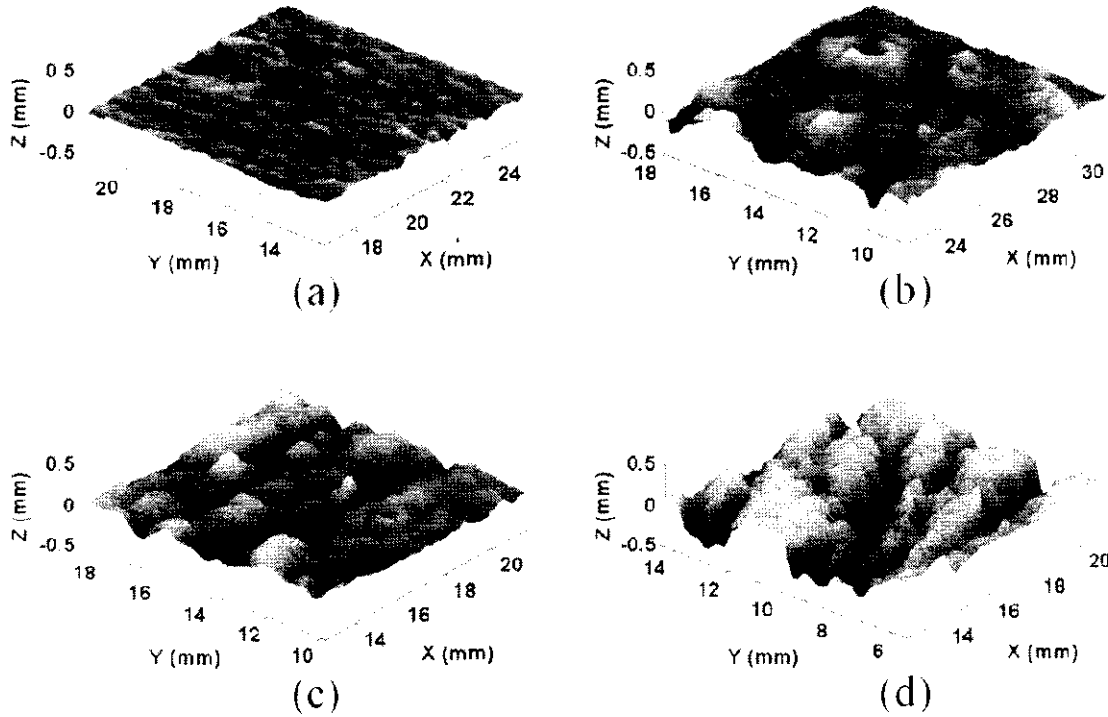


**Figure 5.15** Deviation surfaces of psoriasis lesions: (a) score 1, (b) score 2, (c) score 3, and (d) score 4, determined by the surface roughness algorithm and classified by the FCM algorithm.

The same test dataset is applied to FCM algorithm. From 324 data points tested, a total of 295 (91.0 %) data points are correctly classified in the double assessment sessions. Misclassified data points are found at 29 (9.0 %) data points. As observed in *k*-means algorithm, similar misclassifications also happen in FCM implementation. It occurs in the locations near the boundary levels of the score groups. Here, the boundary levels of FCM algorithm would not be considered in classification process. These boundary levels are determined in order to find the transition boundary from a certain score to another score group.

A boundary level is defined as intersection point of two overlapping membership functions. Figure 5.16 shows an example of boundary level between score 1 and score 2. The boundary level is depicted as a green circle. In this point, both overlapping membership functions (score 1 and score 2) give a same membership degree for a certain surface roughness. This membership degree relation can be expressed by  $P_1(0.034) = P_2(0.034) = 0.4564$ . A misclassification case appears when the measured surface roughness values are located in the left and the right sides

of boundary level, as illustrated in Figure 5.16. The first assessment,  $S_{a1}$ , is classified as score 1 because membership function of score 1 gives the largest membership degree at  $P_1(0.030) = 0.8684$ . Conversely, in the second assessment, the highest membership degree,  $P_2(0.036) = 0.6781$ , is given by membership function of score 2. Thus, the measured surface roughness  $S_{a2}$  is considered as score 2. Finally, all boundary levels of FCM algorithm are obtained from the intersection point of membership functions. The boundary levels of misclassification type 1, 2, and 3 are 0.034 mm, 0.056 mm, and 0.097 mm respectively. These levels are not equal to the boundary levels of  $k$ -means algorithm. In the FCM algorithm, the levels depend on the curve shape of the membership functions. Therefore, the levels are not exactly located in the middle point of two cluster centroids, as found in  $k$ -means algorithm.

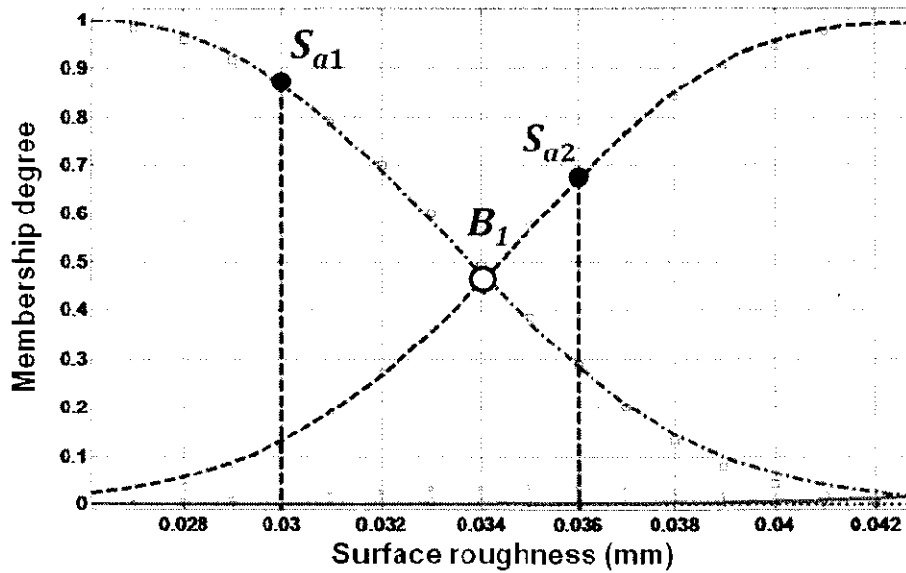


**Figure 5.16** A boundary level (white circle) splits membership functions of score 1 (dot-dashed line) and score 2 (dashed line).

As conducted in previous section, the average of Euclidean distance is computed to find closeness of the measured surface roughness with the boundary levels. Equation (5-7) is applied to compute the Euclidean distance for each misclassified data point. Table 5.13 shows the closeness of measured data to the boundary levels of FCM algorithm. The data is summarised from misclassified data points. Misclassification type 1 exists when the measurement results are located near to the first boundary level,  $B_1$ . The average distance  $\overline{D_{B_1}}$  (0.003 mm) is small and not more

then 10% of  $D_{B_2}$  (0.030 mm) and  $D_{B_3}$  (0.088 mm). Misclassification type 2 and 3 are also indicated by the closeness of the measured surface roughness to the boundary levels. A small value of  $D_{B_2}$  (0.004 mm) shows the closeness of measured surface roughness to the boundary level of misclassification type 2. The occurrence of misclassification type 3 is explained by a small distance value of  $D_{B_3}$  (0.004 mm).

**Table 5.13** Average of Euclidean distances of surface roughness and boundary levels of FCM classification algorithm

Misclassification Type	$\overline{D_{B_1}}$ (mm)	$\overline{D_{B_2}}$ (mm)	$\overline{D_{B_3}}$ (mm)	$N$
Type 1, score 1 and 2	0.003	0.030	0.088	17
Type 2, score 2 and 3	0.033	0.004	0.056	8
Type 3, score 3 and 4	0.091	0.060	0.004	4

These small distances do not occur for the cases with correct classifications. The measured surface roughnesses are located far from the boundary levels. Therefore, misclassification cases could be avoided in these measurements. Here, the averages of Euclidean distances are also found higher than 0.005 mm, as shown in correct classification cases of  $k$ -means algorithm. The distances for all score groups are summarised in Table 5.17.

**Table 5.14** Average of Euclidean distances of surface roughness and boundary levels determined from correct classification cases of FCM algorithm.

Score Group	$\overline{D_{B_1}}$ (mm)	$\overline{D_{B_2}}$ (mm)	$\overline{D_{B_3}}$ (mm)	$N$
Score 1	0.012	0.043	0.101	104
Score 2	0.014	0.018	0.076	114
Score 3	0.053	0.022	0.036	55
Score 4	0.128	0.097	0.039	22

Two methods are recommended to minimise misclassification cases. The first method is performed by acquiring more data points if the surface roughness is lie close to the boundary levels. An average value of this multiple measurement is then applied to score the surface roughness. This first method is also suggested to resolve the boundary problems of  $k$ -means algorithm. Table 5.18 summarises the surface roughness ranges that need to be considered for performing multiple measurements.

**Table 5.15** The surface roughness ranges near the boundary levels of FCM classification algorithm.

Misclassification Type	Surface Roughness Interval (mm) $S_a - 3\sigma_{Total} \leq B_i \leq S_a + 3\sigma_{Total}$
Type 1, score 1 and 2	$0.029 \leq S_a \leq 0.084$
Type 2, score 2 and 3	$0.051 \leq S_a \leq 0.106$
Type 3, score 3 and 4	$0.092 \leq S_a \leq 0.147$

In the second method, the score group is determined by comparing the membership degrees of the decided score groups. As exemplified in Figure 5.16, the final score cannot be determined because there are two different scores from two measurement sessions. The final score can be obtained by comparing the maximum membership degrees of the first ( $P_1(0.030) = 0.8684$ ) and the second ( $P_2(0.036) = 0.6781$ ) assessments. From the comparison, it is known that  $0.8684 > 0.6781$  therefore the final score for this data point is score 1. A mathematical expression is formulated to determine final score  $S(S_a)$  from  $n$ -times measurements. Let  $m_i(S_i, P_{max,i})$  represents  $i$ -th measurement which has final score  $S_i$  at maximum membership degree  $P_{max,i}$ . Then, the equation can be given by

$$S(S_a) = S_k, \max(P_{max,1}, P_{max,2}, \dots, P_{max,k}, \dots, P_{max,n}) = P_{max,k}(S_a) \quad (5-18)$$

### 5.3 The Agreement Analysis of Psoriasis Assessment

The inter-rater variation of two independent observers can be evaluated by using the kappa coefficient analysis. The Kappa coefficient has been proposed by Cohen in 1960 and has been widely used to measure an agreement among clinicians on the scores of a medical assessment. Kappa coefficient is expressed by following equation [152]:

$$\kappa = \frac{p_0 - p_c}{1 - p_c} \quad (5-19)$$

The probability variable,  $p_0$  is the proportion of units in which the observers agreed with and  $p_c$  is the proportion of units for which agreement is expected by chance. Kappa's possible values are limited from -1 up to 1. As an example, suppose there are two observers,  $O_1$  and  $O_2$ . As an example, suppose there are two observers,  $O_1$

and  $O_2$ . The observers are asked to examine and score 20 subjects. They may give a score for the subjects, either score 1 or 2. Scoring results and summary of agreement for this scoring are given by Table 5.16 and Table 5.17, respectively.

**Table 5.16** Scoring results of two observers,  $O_1$  and  $O_2$ .

$O_1$ vs. $O_2$	Number of Assessment Samples																			
	1	2	3	4	5	6	7	8	9	10	11	12	13	14	15	16	17	18	19	20
$O_1$	1	1	1	1	1	1	1	1	1	1	1	2	1	2	2	2	2	2	2	2
$O_2$	1	1	1	1	1	1	1	2	2	1	1	2	1	2	2	2	2	2	2	2

**Table 5.17** Summary of agreement from scoring by two observers.

$O_1$ Assessment vs. $O_2$ Assessment		Scores of $O_2$ Assessment		Total
		1	2	
Scores of $O_1$ Assessment	1	10	2	12
	2	0	8	8
Total		10	10	18

To obtain kappa coefficient as formulated in (5-19), variables  $p_0$  and  $p_c$  need to be determined. Variable  $p_0$  is determined from a ratio of total agreement of both observers to the total of sample. The calculations of  $p_0$  is given as follows:

$$p_0 = \frac{(N_{O_1O_2,Score1} + N_{O_1O_2,Score2})}{N_{Sample}} = \frac{(10 + 8)}{20} = 0.90 \quad (5-20)$$

Variable  $p_c$  is computed by adding between probability both observers give score 1 and probability both observers give score 2. The solution can be found as:

$$p_c = \left( \frac{N_{O_1,Score1}}{N_{Sample}} \times \frac{N_{O_2,Score1}}{N_{Sample}} \right) + \left( \frac{N_{O_1,Score2}}{N_{Sample}} \times \frac{N_{O_2,Score2}}{N_{Sample}} \right) \quad (5-21)$$

$$p_c = \left( \frac{10}{20} \times \frac{12}{20} \right) + \left( \frac{10}{20} \times \frac{8}{20} \right) = (0.5 \times 0.6) + (0.5 \times 0.4) \quad (5-22)$$

$$p_c = 0.3 + 0.2 = 0.50 \quad (5-23)$$

Finally, values of  $p_0$  and  $p_c$  are substituted into (5-19) to calculate the kappa coefficient.

$$\kappa = \frac{0.90 - 0.50}{1 - 0.50} = 0.80 \quad (5-24)$$

The maximum value ( $\kappa=1.0$ ) represents that the observers agree in all of examination samples. Landis interpretation on Kappa coefficient values can be summarised as shown in Table 5.18 [153].

**Table 5.18** Agreement interpretation of Kappa coefficient.

Kappa	Agreement interpretation
< 0	Less than chance agreement
0.01 – 0.20	Slight agreement
0.21 – 0.40	Fair agreement
0.41 – 0.60	Moderate agreement
0.61 – 0.80	Substantial agreement
0.81 – 0.99	Almost perfect agreement

To evaluate an agreement between two dermatologists, the Kappa coefficient value of PASI Scaliness scores of 1,283 lesions are determined. The Kappa coefficient value between Dermatologist 1 and Dermatologist 2 is 0.55 and is categorised as a moderate agreement. The Kappa coefficient of 0.55 indicates that the dermatologists have achieved 55% agreement of total assessment and 45% agreement will be expected by chance. A perfect agreement is achieved if the Kappa coefficient is greater than 0.80. As a result, the dermatologists' scores cannot be considered as a ground truth in evaluating the algorithm performance since the Kappa coefficient among the dermatologists is only 0.55.

To evaluate the performance of PASI Scaliness algorithm, several lesion samples are imaged in two successive scans. PASI scaliness scores of lesion images are then analysed by the same user in separated calculations. The number of samples is 324 lesions (648 images). The number of tested lesions is less than the number of scored lesions by dermatologists because not all lesions are scanned twice. Kappa coefficients between the first assessment and the second assessment that are obtained from *k*-means and FCM algorithms are evaluated. Table 5.19, Table 5.20, and Table 5.21 show the agreement summary of dermatologists, *k*-means clustering, and FCM clustering, respectively. Table 5.22 lists the comparisons on Kappa coefficients obtained from three scoring methods. The Kappa coefficients are computed through the same way as exemplified in the previous section. It can be seen that the FCM

gives better Kappa coefficient agreement than *k*-means clustering.

**Table 5.19** Summary of agreement from scoring by dermatologists.

First Assessment vs. Second Assessment		Scores of Dermatologist 2 Assessment				Total
		1	2	3	4	
Scores of Dermatologist 1 Assessment	1	634	200	4	0	838
	2	37	204	39	0	280
	3	4	24	75	5	108
	4	1	0	16	40	57
Total		676	428	134	45	1,283

**Table 5.20** Summary of agreement from scoring by applying *k*-means algorithm.

First Assessment vs. Second Assessment		Scores of Second Assessment				Total
		1	2	3	4	
Scores of First Assessment	1	79	10	0	0	89
	2	11	110	7	0	128
	3	0	3	70	2	75
	4	0	0	2	30	32
Total		90	123	79	32	289

**Table 5.21** Summary of agreement from scoring by applying FCM algorithm.

First Assessment vs. Second Assessment		Scores of Second Assessment				Total
		1	2	3	4	
Scores of First Assessment	1	104	12	0	0	116
	2	5	108	4	0	117
	3	0	6	59	1	66
	4	0	0	1	24	25
Total		109	126	64	25	295

**Table 5.22** Comparison of Kappa coefficients using *k*-means and FCM.

Clustering algorithm	Kappa coefficient	N
Dermatologist	0.5500	1,283
<i>K</i> -means	0.8473	324
FCM	0.8708	324

Perfect agreement between the first assessment and the second assessment for *k*-means and FCM algorithms are achieved since Kappa coefficients are found to be greater than 0.81. The FCM performance (0.8708) of surface roughness classification is slightly better than *k*-means (0.8473). FCM clustering, as a soft clustering, can better solve the boundary problems compare to *k*-means clustering. Figure 5.17 depicts an example of the double measurement result. These measurements are taken from a lesion at an upper limb region (lesion number: 1600

and 1601). The first and second measurements give  $S_a = 0.030$  mm and 0.033 mm, respectively. In  $k$ -means clustering, the measurement results will be classified as the different score clusters (score 1 and score 2) because the boundary level of score 1 and 2 is located in the middle of measurement results. These measurement results are sharply classified into different scores by  $k$ -means clustering even the images are acquired from the same lesion. FCM however, is able to accommodate this condition by giving the membership degrees or the probabilities of the measured data to cluster 1 and 2. Although the membership degrees of the first and second measurements are changing, the final decision is equal, both of measurements are classified as score 1.

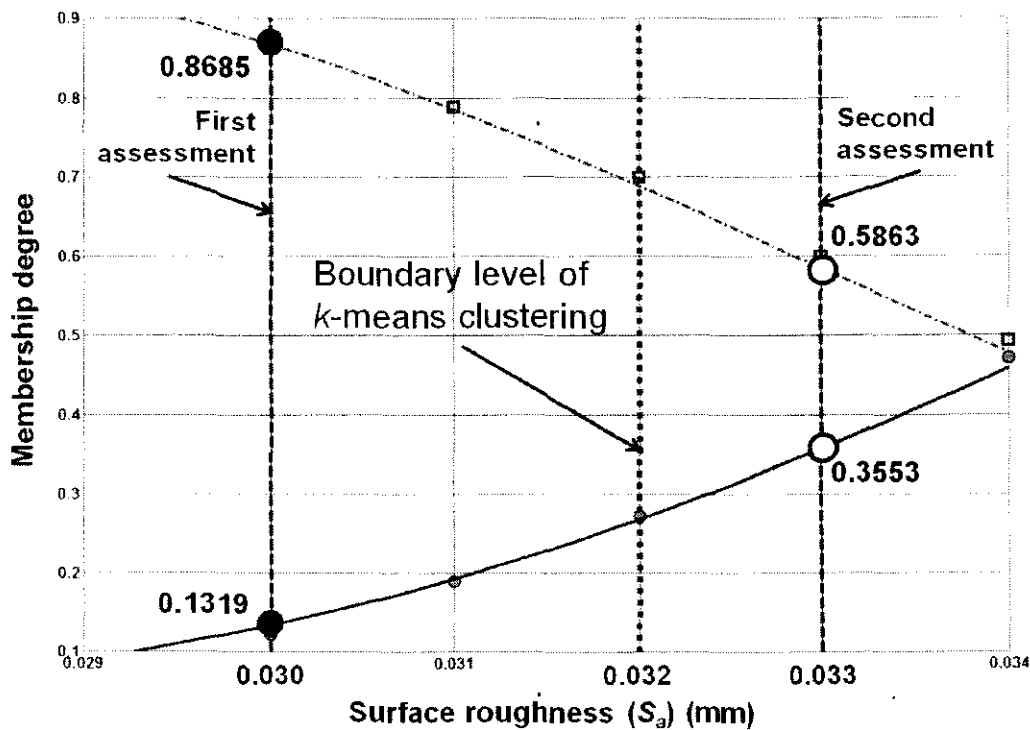


**Figure 5.17** Clustering of the  $k$ -means and FCM at the boundary of two clusters - score 1 and score 2. A boundary level of the  $k$ -means clustering (dotted-line) crosses the membership functions of score 1 (dot-dashed line) and score 2 (solid line).

#### 5.4 Summary

Sampling sizes are determined to ensure that the collected data is statically representative. A margin error equation in this case is rearranged to provide a sample size equation.  $Z$  scores at a certain confidence level, population standard

deviation, and maximum allowable error are used to compute the sample size. To obtain the confidence level 95% and error 10%, the sample size of scaliness scores are differently found among the scores. A minimum required sample size is found to be 25 samples. To cover the data from all scores (four score groups), the total required sample size is 100 samples. A scaliness sample is calculated from surface roughness of a single psoriasis lesion. Based on the sample size calculation, it is found that a total amount of 100 psoriasis lesions are required to achieve the confidence level of 95% for all scaliness scores. The lesion data themselves have been collected from registered psoriasis patients at Department of Dermatology, Hospital Kuala Lumpur.

A total of 204 patients are recruited in this clinical study – consisting of 163 males and 41 females. The study has been approved by the Clinical Research Centre, Ministry of Health, Malaysia and registered at NMRR-09-1098-4863. A total of 1,999 psoriasis lesions are collected in the study. From this total number, 1,892 lesions are assessed by dermatologists to obtain PASI scaliness scores. The percentage of the lesion with score 1, 2, 3, and 4 are 66.91%, 21.62%, 8.09%, and 3.38%, respectively. The proportion of lesions at a mild severity is greater since most of the lesions are still under a continuous treatment.

Two unsupervised clustering methods, *k*-means and fuzzy *c*-means (FCM) algorithms are studied in the research work. These clustering algorithms are widely applied in many medical applications. *K*-means clustering is used to classify *n* observed pattern into *k* clusters. Here, each data point is classified into the cluster with the nearest mean. There are four clusters representing four sets of PASI scaliness score. *K*-means clustering algorithm is validated by applying a clustering algorithm towards the divided dataset. The dataset of lesion roughness is randomly partitioned into two equal sized datasets. The consistency of score centroids for all dataset then shows that the score clusters are maximally separated. Centroid consistency is additionally observed on a smaller sample size and the dataset is randomly partitioned into three datasets. It is found that centroid differences are not more than  $3\sigma_{Total}$  (0.005 mm) - except for one-third partitions of score 4 (0.008 mm). The greater difference is a result of the size of clustered dataset that is less than 30

samples.

In addition, FCM clustering is applied to improve the classification reliability. The improvement is given at a border area between two adjacent clusters. The rigorousness of  $k$ -means clustering is reduced by applying the softness of FCM clustering. The clustering iteration provides the membership degrees of each data point. Gaussian fitting function furthermore is fitted to the clustered dataset in order to obtain the membership degrees of the dataset. Meanwhile, the PASI scaliness score is determined by comparing the membership degrees of an input data to the existing clusters. The input surface roughness is classified into a particular score cluster if it has the highest membership degree among the clusters of scaliness scores.

Kappa coefficient analysis is used to evaluate Inter-rater variation of two independent observers. To evaluate a dermatologist agreement, the assessments of two dermatologists on 1,283 lesions are determined. Kappa coefficient of dermatologist is found to be 0.55 that is less than the required agreement, namely 0.81. Therefore, the dermatologist agreement is not considered as the ground truth for evaluating algorithm performance.

The agreement analysis of PASI scaliness algorithm is performed by comparing two measurements obtained from two successive scans. The number of samples is 324 lesions (648 two successive images). Kappa coefficients between the first assessment and the second assessment obtained from  $k$ -means and FCM clustering algorithms are evaluated. The Kappa coefficients for  $k$ -means and FCM are 0.8473 and 0.8708, respectively. Both of agreements are considered as a perfect agreement since the coefficients are found to be greater than 0.81. In this agreement analysis, FCM classification is better than  $k$ -means.

FCM can solve the boundary problems better than  $k$ -means clustering. In the classification of  $k$ -means clustering, a surface roughness can be classified as different groups since the group separation is very strict. The FCM algorithm determines membership degrees for each measured data point. Therefore, the score classifications are decided based on similarity quantification which is represented by these degrees. In several boundary cases, the  $k$ -means algorithm can give several

different scores for the same lesions that are successively acquired in double measurements. FCM similarly can give several different membership degrees for the lesions. However, the final classification decides that the lesions are still in the same cluster. This decision is taken because the membership degrees are considered maximum in the first and second measurements.

## CHAPTER 6

### CONCLUSION AND RECOMMENDATION

#### 6.1 Conclusion

In this research, the problems of skin roughness measurement for psoriasis assessment are investigated. The investigation aims to provide a practical solution for clinical treatment in daily practice. Psoriasis appears as a red plaque lesion and covers a localised area of the body. In severe stages, the lesion can be widespread all over the body. The disease is caused by the wrong signals of the immune system that accelerates the cycle of skin cells' growth.

Psoriasis patients need periodic medical treatment continuously as the disease cannot be completely cured. The PASI (Psoriasis Area and Severity Index) scoring method is considered as gold standard for the severity assessment. To determine the psoriasis severity, the PASI scoring system defines four parameters, *i.e.* area (ratio of lesion area to total body surface area), erythema (colour of lesion inflammation), lesion thickness and scaliness. These parameters are scored at four body regions, namely head, trunk, upper limbs and lower limbs. In practice, an assessment of dermatologist can be subjective due to intra- and inter-rater variability of human assessment. The subjectivity is influenced either by the perception or by the clinical experience of the dermatologist.

An imaging approach is proposed to provide an objective PASI scaliness assessment based on skin surface roughness measurement. Several imaging solutions have been developed for measuring skin surface roughness. The earlier methods including mechanical surface profilometry, laser profilometry, light scattering, and speckle imaging have been applied in skin surface roughness measurement. However, these methods have some disadvantages, such as limited

resolution of profiler size and time-consuming process that occur in mechanical surface profilometry. The fast scanning also could not be performed by applying laser profilometry though it can provide high scan resolution. Light scattering and speckle imaging methods are able to provide non-contact measurement and fast scanning. However, both methods require sophisticated system arrangement and standardised environment lighting. Moreover, the measured area is limited to a small dimension. Lastly, 3D surface acquired by structured light projection method is applied in the research. This method has advantages more than the aforementioned methods. The method can perform *in vivo* high speed scan at high resolution. Therefore it can overcome the scan problem on constant vibration of skin surface.

To achieve this objective, the PASI scaliness visual descriptors are studied and defined in terms on surface roughness. This feature can be measured by an imaging modality and its values are related to the PASI scaliness scores. An unsupervised clustering algorithm is applied to classify the lesion surface into the PASI scaliness scores. In this research work, the clustering algorithm is built based on the collected data from a clinical study at Department of Dermatology, Hospital Kuala Lumpur.

As stated in the Chapter 1, there are two research objectives of this thesis. The first objective is to develop a 3D imaging algorithm for accurately measuring the surface roughness of skin lesions. This first objective has been achieved in the research in which the algorithm has been validated for all skin lesions that appear at any body parts. A validation study furthermore is conducted on a set of lesion models. A total of 390 lesion models are pasted on a life-size mannequin to simulate a number of psoriasis lesions on human body. The life-size mannequin is suitable to model the human body curvature. The mannequin is commonly used in the research related with the surface determination such as body surface area measurement. The measurement methods are mostly applied in clothes designing and medical applications. Wurong and Bugao used life-size mannequin to validate a 3D reconstruction method for whole body surface imaging [154]. Wang *et al.* conducted a research on measurement of human body volumes. A laser scanner is applied to acquire 3D rigid object of the life-size mannequin. The body volume is computed from the 3D volume of the scanned mannequin. To validate the result, the mannequin is then immersed into a water tank to obtain body volume based on water

displacement [155]. The life-size mannequin is usually constructed based on human body modelling. This model is determined and developed from the real body proportions. As reported in [156], Jin Gu *et al.* have developed a human body model by stacking a set of skin contours. The contours are extracted from the edge images of the real human body.

Douros and Buxton have conducted a research on the construction of curvature maps for 3D human body surfaces. In this research they defined that the body skin surface is constructed by many skin patches. There are four basic shapes of the skin patches. The shapes are flat, elliptic, parabolic, and saddle surfaces. All of these basic shapes can be properly modelled by applying second order polynomial [157]. In this research smaller lesion surface areas are fitted with the second and third order polynomial. Moreover, the lesion area is also divided into four subdivided surfaces to reduce the surface curvedness. By applying this method, the lesion surface can be flattened and its vertical deviations are determined accurately.

From the validation study, it can be found that the developed surface roughness has an error of  $0.0008 \pm 0.0017$  mm ( $Error \pm \sigma_{Total}$ ) and gives accuracy of 94.12%. This accuracy is quite high (>90%) and therefore the developed algorithm can be implemented to measure real lesions. The measurement errors mostly are caused by the limitation of the scanning system. The system could not measure the lesion model surface accurately if a part of the lesion surface is in a deep concave area. In this area, the scanned surface might be located outside the depth of field interval ( $\pm 50$  mm).

There is no previous works on surface roughness measurement of psoriasis lesion. Most of the works were conducted on normal skin surfaces. Tchvialeva *et al.* [109] summarised the skin surface roughness determinations using two different acquisition methods, structured light projection and speckle imaging [116] [158] [159]. The structured light projection method is evaluated for measuring skin replica and the actual skin surfaces. Jacobi *et al.* have conducted a research on skin surface measurement. The samples were taken from several regions such as forearm, back, and forehead with size 18 mm  $\times$  13 mm. A 3D scanner using structured light projection is applied to measure the skin surfaces. From the experiment, the average roughness of skin surfaces at back region is  $0.0368 \pm 0.0094$  mm whereas the surface

roughness of forearm region is  $0.0302 \pm 0.0038$  mm [160]. Table 6.1 summarises the comparison of surface roughness measurements on skin surfaces.

For the arm and hand regions, it can be shown that the surface roughness values are increasing from the structured light projection on skin replica to speckle imaging methods. The printing process of skin replica cannot completely duplicate the skin profile details with high frequencies. Only the skin profiles with lower frequencies and less variance are preserved by skin replica. Therefore its surface roughness is lower than *in vivo* structured light projection and speckle imaging methods. In 2D calculation, the surface roughness is determined higher than the other methods. This result can be caused by incompleteness of measured profiles. Here, the vertical deviations of the surface profile are extracted only from a single axis. The maximum surface roughness measured from psoriasis lesion (0.1870 mm) is higher than all surface roughness values presented in Table 6.1. This value shows that the psoriasis lesions surfaces are rougher than the normal skin surfaces.

**Table 6.1** Comparison of skin surface roughness measurements.

Method	Average roughness of skin surfaces at several body regions (mm)			
	Arm	Hand	Cheek	Back
Structured light projection on skin replica	0.0050 - 0.0078 [116] [158] [159]	0.0122 [116]	0.0110 [121]	
<i>In vivo</i> structured light projection	0.0074 - 0.0184 [116] [158] [159]	0.0134 [116]	0.0430 [121]	
Speckle imaging	$0.0276 \pm 0.0076$ [109]	$0.0386 \pm 0.0056$ [109]	$0.0354 \pm 0.0064$ [109]	$0.0298 \pm 0.0092$ [109]
Structured light projection, 2D calculation	$0.0302 \pm 0.0038$ [160]			$0.0368 \pm 0.0094$ [160]
Developed method on the surfaces of psoriasis lesion	0.0100 - 0.1870			

The second objective is to develop an objective and reliable PASI scaliness scoring. An unsupervised clustering is also applied to score PASI scaliness based on lesion surface roughness. *K*-means and fuzzy *c*-means (FCM) algorithms furthermore are studied in the research work. The implementation of *k*-means clustering algorithm has been validated by applying a clustering algorithm towards the divided dataset. The dataset of lesion roughness is randomly split into two equal

sized datasets. The clustering reliability is shown by the consistency of score centroids for all datasets. It proves that the score clusters are maximally separated. Centroid differences are not more than  $3\sigma_{Total}$  (0.005 mm), except for a clustered data that have size less than 30 samples. Stability of FCM algorithms is shown by fittingness of Gaussian function to the membership functions of scaliness scores. All of the Gaussian function can be fitted with  $R^2 \approx 1$ . The objectives of these clustering algorithms are indicated from the kappa agreement analysis. Since the scoring agreement between the dermatologists (0.55) is less than 0.81, their assessment cannot be considered as a ground truth for evaluating the algorithm. 3D images from two successive scans are used to evaluate the scoring objectivity of the developed algorithm. The objectives of both clustering algorithms have been proven by the kappa coefficients of  $k$ -means and FCM algorithms. The coefficient value of  $k$ -means is 0.8473 whereas the coefficient of FCM is 0.8708. FCM clustering, as the soft clustering, can solve the boundary problems better than  $k$ -means clustering and it therefore can give higher kappa agreement coefficient.

The research works in this thesis show that the developed algorithm enables to provide an objective measurement for PASI scaliness assessment. The developed algorithm resolves the problems of surface roughness determination on curved surfaces of human skin. The algorithm has been validated for accurately measuring the surface roughness of skin lesions at any body parts. These methods have been validated and accepted to be used in a clinical study involving registered 204 psoriasis patients of Hospital Kuala Lumpur. Furthermore, unsupervised clustering algorithm for scoring PASI scaliness has been developed. The algorithm is developed based on surface roughness data of the collected psoriasis lesions. High agreement between the first and the second assessments of psoriasis lesions demonstrates objectivity and reliability of the developed clustering algorithm.

## 6.2 Recommendations for Further Work

Currently, many scoring systems are still manually performed by dermatologist. As explained from this research, the assessment given by dermatologist might be subjective and can result in treatment inefficacy for the patient. Therefore, an objective assessment is still required in a clinical practice. Surface roughness is

known as one of the important parameters on skin analysis and assessment. The developed algorithm is potentially applied to another skin surface analysis that considers skin surface roughness as its parameter. The example of these skin problems, beside psoriasis, might be atopic dermatitis (atopic eczema), wrinkle analysis, and burnt skin. The surface roughness measurement either can subsequently be intended for monitoring on skin disease treatment or for any applications related to the cosmetics purposes.

Polynomial surface fitting has been validated to fit most of body surface areas. From this result, it can be shown that the algorithm is suitable for determining the curvature of human body surfaces. The maximum coverage area of the algorithm is limited by the scanning frame of 3D optical scanner. The size of this frame is  $40 \times 30 \text{ mm}^2$ . Lesions could be widely distributed on the body regions or appear as a single lesion covering a large area. To scan a larger area ( $>40 \times 30 \text{ mm}^2$ ), multiple scans and assessments on adjacent areas are required, as shown in Figure 6.1. The lesions can be represented by several sampled areas. The average surface roughness for the assessed region would then be determined by averaging the surface roughness of the sampled areas.

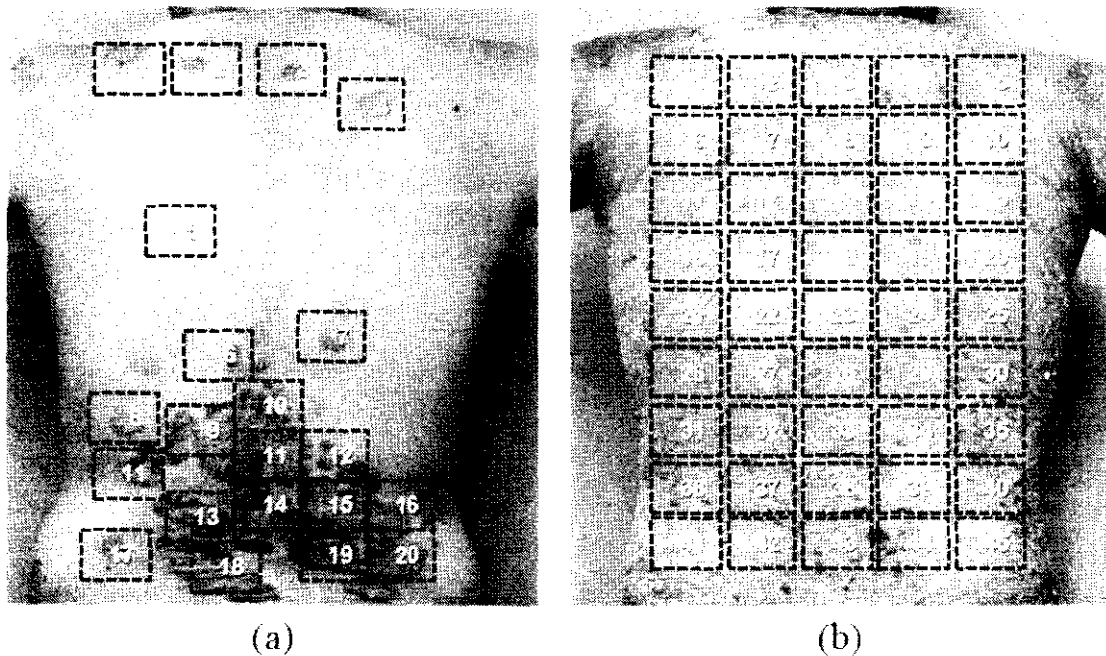


**Figure 6.1** Multiple scans for a single large lesion: (a) Large lesion covering part of the region and (b) Single large lesion covering the whole region.

## REFERENCES

- [1] J. Svrbely, C. M. Puhlmann, and J. E. Harl, "Dermatology," *Medal.org*, 2012. [Online]. Available: <http://www.medal.org/visitor/www/ch21/ch21.aspx>.
- [2] National Psoriasis Foundation, "Statistics," *National Psoriasis Foundation*, 2012. [Online]. Available: [http://www.psoriasis.org/learn\\_statistics](http://www.psoriasis.org/learn_statistics). [Accessed: 19-Jul-2012].
- [3] International Federation of Psoriasis Associations, "Facts About Psoriasis," *International Federation of Psoriasis Associations*, 2012. [Online]. Available: <http://www.worldpsoriasisday.com/web/page.aspx?refid=130>. [Accessed: 19-Jul-2012].
- [4] A. L. Neimann, S. B. Porter, and J. M. Gelfand, "The epidemiology of psoriasis," *Expert Review of Dermatology*, vol. 1, no. 1, pp. 63–76, 2006.
- [5] V. Chandran and S. P. Raychaudhuri, "Geoepidemiology and environmental factors of psoriasis and psoriatic arthritis," *Journal of Autoimmunity*, vol. 34, no. 3, pp. J314–J321, May 2010.
- [6] P. D. Malaysia, "Overview of Psoriasis in Malaysia," vol. 2011, no. 20 February 2011. Persatuan Dermatologi Malaysia., 2011.
- [7] Hospital Kuala Lumpur, "Registered patient in Hospital Kuala Lumpur." Information System of Hospital Kuala Lumpur, Malaysia, Kuala Lumpur.
- [8] Lippincott Williams & Wilkins., *Pathophysiology: a 2-in-1 reference for nurses*. Philadelphia: Lippincott Williams & Wilkins, 2005.
- [9] M. D. Nili N. Alai FAAD, "Psoriasis," 2011. [Online]. Available: [http://www.psoriasis.org/netcommunity/learn\\_statistics](http://www.psoriasis.org/netcommunity/learn_statistics). [Accessed: 07-Feb-2011].
- [10] M. J. Bhosle, A. Kulkarni, F. SR, R. Balkrishnan, and S. R. Feldman, "Quality of life in patients with psoriasis.," *Health and quality of life outcomes*, vol. 4, p. 35, Jan. 2006.
- [11] R. Lewis, *Life*. Boston: McGraw-Hill Higher Education, 2004.
- [12] A. Pivarcsi, I. Nagy, and L. Kemeny, "Innate Immunity in the Skin: How Keratinocytes Fight Against Pathogens," *Current Immunology Reviews*, vol. 1, no. 1, pp. 29–42, 2005.
- [13] A. Faller, M. Schunke, G. Schunke, and E. Taub, *The human body: an introduction to structure and function*. Stuttgart; New York: Georg Thieme, 2004.
- [14] American Association for the Advancement of Science., *The Science Inside Skin*. Washington, D.C.: American Association for the Advancement of Science (AAAS), 2004.
- [15] Society for Dermopharmacy, "The life cycle of a horny cell," *This Skin Care Forum Online publication*, 2011. [Online]. Available: [http://www.scf-online.com/english/35\\_e/frontpage35\\_e.htm](http://www.scf-online.com/english/35_e/frontpage35_e.htm).

- [16] Lutz Slomianka. "Blue Histology - Integumentary System," *The University of Western Australia*. 2009. [Online]. Available: <http://www.lab.anhb.uwa.edu.au/mb140/corepages/integumentary/integum.htm>. [Accessed: 07-May-2012].
- [17] G. T. Overney. "Human Histology for Amateur Microscopists," *Microscopy-UK*, 2002. [Online]. Available: <http://www.microscopy-uk.org.uk/mag/indexmag.html?http://www.microscopy-uk.org.uk/mag/artaug02/gohisto.html>. [Accessed: 07-May-2012].
- [18] J. M. Weinberg. "Psoriasis," in *Sauer's Manual of Skin Diseases*, 10th ed., B. J. Hall and J. C. Hall, Eds. Riverwoods, Illinois: Lippincott Williams & Wilkins. 2010. pp. 160–163.
- [19] S. R. Feldman and G. G. Krueger. "Psoriasis assessment tools in clinical trials." *Annals of the rheumatic diseases*, vol. 64, pp. 65–68, 2005.
- [20] V. Bronsard, C. Paul, S. Pr y, E. Puze at, P.-A. Gourraud, S. Aractingi, F. Aubin, M. Bagot, B. Cribier, P. Joly, D. Jullien, M. Le Maitre, M.-A. Richard-Lallemand, and J.-P. Ortonne. "What are the best outcome measures for assessing plaque psoriasis severity? A systematic review of the literature." *Journal of the European Academy of Dermatology and Venereology JEADV*, vol. 24 Suppl 2, no. December 2009, pp. 17–22, 2010.
- [21] T. Fredriksson and U. Pettersson. "Severe psoriasis--oral therapy with a new retinoid." *Dermatologica*, vol. 157, no. 4, pp. 238–244, 1978.
- [22] P. G. Buettner and C. Garbe. "Agreement between self-assessment of melanocytic nevi by patients and dermatologic examination." *American Journal of Epidemiology*, vol. 151, no. 1, pp. 72–77, 2000.
- [23] M. Masters, M. McMahon, and B. Svens. "Reliability testing of a new scar assessment tool, Matching Assessment of Scars and Photographs (MAPS)." *The Journal of burn care rehabilitation*, vol. 26, no. 3, pp. 273–284, 2005.
- [24] A. M. Kligman. "Personal Perspectives on Bioengineering and the Skin: The Successful Past and the Brilliant Future," in *Handbook of non-invasive methods and the skin*, J. Serup, G. B. E. Jemec, and G. L. Grove, Eds. Taylor & Francis Group, 2005, pp. 3–7.
- [25] N. N. Alai and G. W. Cole. "Rosacea," *MedicineNet.com*, 2009. [Online]. Available: <http://www.medicinenet.com/rosacea/page2.htm>. [Accessed: 12-Jul-2012].
- [26] I. Sadiq and T. Stoudemayer. "Fiber-Optic Microscopy System for Skin Surface Imaging," in *Handbook of non-invasive methods and the skin*, J. Serup, G. B. E. Jemec, and G. L. Grove, Eds. Taylor & Francis Group, 2005, pp. 125–133.
- [27] D. E. Kligman and Y. Zhen. "Intense pulsed light treatment of photoaged facial skin." 2004.
- [28] G. Micali, F. Lacarrubba, D. Massimino, and R. A. Schwartz. "Dermatoscopy: alternative uses in daily clinical practice." *Journal of the American Academy of Dermatology*, vol. 64, no. 6, pp. 1135–1146, 2011.

- [29] Better Medicine. "Skin Symptoms," *Health Grades, Inc.*, 2011. [Online]. Available: <http://www.localhealth.com/article/skin-symptoms>.
- [30] RightDiagnosis. "Causes of Skin lesion," 2012. [Online]. Available: [http://www.rightdiagnosis.com/symptoms/skin\\_lesion/causes.htm](http://www.rightdiagnosis.com/symptoms/skin_lesion/causes.htm). [Accessed: 22-Jun-2012].
- [31] MedicineNet, "Definition of Lesion,," vol. 2011, no. 5/13/2011. MedicineNet, Inc., 2011.
- [32] R. J. MacNeal, "Description of Skin Lesions," *The Merck Manuals Online Medical Library*, vol. 2011, no. 5/13/2011. Merck & Co., Inc., New Jersey, 2009.
- [33] C. C. Chang, H. B. Gangaram, and S. H. Hussein. "Malaysian Psoriasis Registry - Preliminary report of a pilot study using a newly revised registry form." *Med. J. Malays. Medical Journal of Malaysia*, vol. 63, no. SUPPL. C, pp. 68–71, 2008.
- [34] D. B. Light, *Cells, tissues, and skin*. Philadelphia: Chelsea House Publishers, 2004.
- [35] C.-Y. Yu, C.-H. Lin, and Y.-H. Yang, "Human body surface area database and estimation formula," *Burns-Journal of the International Society for Burn Injuries*, vol. 36, no. 5, pp. 616–629, Aug. 2010.
- [36] M. A. Lowes, A. M. Bowcock, and J. G. Krueger, "Pathogenesis and therapy of psoriasis," *Nature*, vol. 445, no. 7130, pp. 866–873, Feb. 2007.
- [37] C. E. M. Griffiths and J. N. W. N. Barker, "Pathogenesis and clinical features of psoriasis," *Lancet*, vol. 370, no. 9583, pp. 263–271, 2007.
- [38] G. A. McCracke and D. Eilers, "Psoriasis," *Medical Update for Psychiatrists*, vol. 2, no. 3, pp. 78–80, May 1997.
- [39] J. Bhalerao and a M. Bowcock, "The genetics of psoriasis: a complex disorder of the skin and immune system," *Human molecular genetics*, vol. 7, no. 10, pp. 1537–1545, Jan. 1998.
- [40] D. Goodless, "Symptoms of Psoriasis," *About.com*, 2008. [Online]. Available: <http://psoriasis.about.com/od/symptomsdiagnosis/tp/symptomsofpsoriasis.htm>. [Accessed: 18-Sep-2012].
- [41] Zygote Media Group, "Solid 3D Male Body Model," *3dscience.com*, 2011. [Online]. Available: [http://www.3dscience.com/3D\\_Models/Human\\_Anatomy/Solid\\_Models/solid-3d-male-model](http://www.3dscience.com/3D_Models/Human_Anatomy/Solid_Models/solid-3d-male-model).
- [42] LEO Pharma, "Where can psoriasis be located?," 2007. [Online]. Available: <http://www.psorinfo.com/Locations.aspx?ID=80>. [Accessed: 20-Sep-2012].
- [43] R. G. B. Langley, G. G. Krueger, and C. E. M. Griffiths, "Psoriasis: epidemiology, clinical features, and quality of life," *Annals of the Rheumatic Diseases*, vol. 64, no. Suppl 2, pp. ii18–i23; discussion ii24–i25, 2005.

- [44] Penn Medicine. "Psoriasis - guttate," 2011. [Online]. Available: [http://www.pennmedicine.org/encyclopedia/em\\_PrintArticle.aspx?gclid=000822&ptid=1](http://www.pennmedicine.org/encyclopedia/em_PrintArticle.aspx?gclid=000822&ptid=1).
- [45] G. W. Cole, Diseasestreatments.com. and Psoriasisiskindisorder.com. "Guttate Psoriasis." *Diseasestreatments.com*, 2012. [Online]. Available: <http://diseasestreatments.com/guttate-psoriasis/>. [Accessed: 21-Aug-2012].
- [46] A. N. Binnick and T. P. Habif, "Psoriasis - Scalp, Ear." [Online]. Available: <http://hardinmd.lib.uiowa.edu/dermnet/psoriasis76.html>.
- [47] DermIs.net, "Generalised Pustular Psoriasis, von Zumbusch Type." 2012. [Online]. Available: <http://www.dermis.net/dermisroot/en/32467/image.htm>.
- [48] Salford Royal Foundation Trust. "Psoriasis: what does it look like?." 2011. [Online]. Available: <http://www.impactpsoriasis.org.uk/About/AboutPsoriasisLookLike.html>.
- [49] The Psoriasis and Psoriatic Alliance. "About Psoriasis." 2013. [Online]. Available: <http://www.papaa.org/resources/about-psoriasis>.
- [50] National Psoriasis Foundation. "Types of Psoriasis." *National Psoriasis Foundation*, 2012. [Online]. Available: <http://www.psoriasis.org/about-psoriasis/types>. [Accessed: 02-Jul-2012].
- [51] PsoriasisTreatment.com, "Erythrodermic Psoriasis Pictures (4)," 2012. [Online]. Available: <http://psortreatment.com/erythrodermic-psoriasis-pictures/erythrodermic-psoriasis-pictures-4/>. [Accessed: 22-Sep-2012].
- [52] M. Esposito, R. Saraceno, C. Schipani, D. Di Marcantonio, L. Bianchi, and S. Chimenti, "Trimethoprim-sulfamethoxazole induced erythrodermic psoriasis." *Journal of Infection*, vol. 57, no. 1, pp. 90–92, Jul. 2008.
- [53] PsoriasisTreatment.com, "Erythrodermic Psoriasis Pictures (12)." 2012. [Online]. Available: <http://psortreatment.com/erythrodermic-psoriasis-pictures/erythrodermic-psoriasis-pictures-12/>. [Accessed: 22-Sep-2012].
- [54] A. Menter and C. E. M. Griffiths, "Current and future management of psoriasis.," *Lancet*, vol. 370, no. 9583, pp. 272–284, 2007.
- [55] C. O. Mendonça and A. D. Burden, "Current concepts in psoriasis and its treatment.," *Pharmacology therapeutics*, vol. 99, no. 2, pp. 133–147, 2003.
- [56] K. O'goshi, "Use of Compact Digital Camera for Snap Photography," in in *Handbook of non-invasive methods and the skin*, 2nd ed., J. Serup, G. B. E. Jemec, and G. L. Grove, Eds. Taylor & Francis Group, 2006, pp. 89–94.
- [57] W. Westerhof, "Dermatoscopy," in in *Handbook of non-invasive methods and the skin*, 2nd ed., J. Serup, G. B. E. Jemec, and G. L. Grove, Eds. Taylor & Francis Group, 2006, pp. 109–122.
- [58] A. Kawada, M. Asai, H. Kameyama, Y. Sangen, Y. Aragane, T. Tezuka, and K. Iwakiri, "Videomicroscopic and histopathological investigation of intense pulsed light therapy for solar lentiginos.," *Journal of Dermatological Science*, vol. 29, no. 2, pp. 91–96, 2002.

- [59] M. C. Pierce, J. Strasswimmer, B. H. Park, B. Cense, and J. F. De Boer. "Advances in optical coherence tomography imaging for dermatology.." 2004.
- [60] S. González, Y. G. Calzada, P. J. Olasold, M. Rajadhyaksha, A. Torres, and A. Halpern. "In Vivo Reflectance Mode Confocal Microscopy in Clinical and Surgical Dermatology," in in *Handbook of non-invasive methods and the skin*. 2nd ed., J. Serup, G. B. E. Jemec, and G. L. Grove, Eds. Taylor & Francis Group, 2006. pp. 268–275.
- [61] J. Gassmueller, A. Kecskés, and P. Jahn, "Stylus Method for Skin Surface Contour Measurement," in in *Handbook of non-invasive methods and the skin*. 2nd ed., J. Serup, G. B. E. Jemec, and G. L. Grove, Eds. Taylor & Francis Group, 2006, pp. 163–168.
- [62] J. Efsen, S. Christiansen, H. N. Hansen, and J. Keiding, "Laser Profilometry," in in *Handbook of non-invasive methods and the skin*, 2nd ed., J. Serup, G. B. E. Jemec, and G. L. Grove, Eds. Taylor & Francis Group, 2006, pp. 169–177.
- [63] H. Zahouani, R. Vargiolu, G. Boyer, C. Pailler-Mattei, L. Laquieze, and A. Mavon. "Friction noise of human skin in vivo," *Wear*, vol. 267, no. 5, p. 1274, 2009.
- [64] J. M. Hanifin, M. Thurston, M. Omoto, R. Cherill, S. J. Tofte, and M. Graeber. "The eczema area and severity index (EASI): assessment of reliability in atopic dermatitis. EASI Evaluator Group.," *Experimental Dermatology*, vol. 10, no. 1, pp. 11–18, 2001.
- [65] I. Schäfer, J. Hacker, S. J. Rustenbach, M. Radtke, N. Franzke, and M. Augustin, "Concordance of the Psoriasis Area and Severity Index (PASI) and patient-reported outcomes in psoriasis treatment.," *European journal of dermatology EJD*, vol. 20, no. 1, pp. 62–67, 2009.
- [66] C. Charman and H. Williams, "Outcome measures of disease severity in atopic eczema.," *Archives of Dermatology*, vol. 136, no. 6, pp. 763–769, 2000.
- [67] Z. L. Bonilla-martinez, J. Albrecht, A. B. Troxel, L. Taylor, J. Okawa, S. Dulay, and V. P. Werth, "The Cutaneous Lupus Erythematosus Disease Area and Severity Index," *Ethics*, vol. 144, no. 2, pp. 173–180, 2008.
- [68] R. G. Langley and C. N. Ellis, "Evaluating psoriasis with Psoriasis Area and Severity Index, Psoriasis Global Assessment, and Lattice System Physician's Global Assessment.," 2004.
- [69] J. Berth-Jones, J. Thompson, and K. Papp, "A study examining inter-rater and intrarater reliability of a novel instrument for assessment of psoriasis: the Copenhagen Psoriasis Severity Index.," *The British journal of dermatology*, vol. 159, no. 2, pp. 407–412, 2008.
- [70] S. Chen, Q. Wang, T. Chu, and M. Zheng, "Inter-observer reliability in assessment of sensation of skin lesion and enlargement of peripheral nerves in leprosy patients.," *Leprosy review*, vol. 77, no. 4, pp. 371–376, 2006.
- [71] L. Forbes-Duchart, S. Marshall, A. Strock, and J. E. Cooper, "Determination of inter-rater reliability in pediatric burn scar assessment using a modified version of the Vancouver Scar Scale.," *Journal of burn care research official*

- publication of the American Burn Association*, vol. 28, no. 3, pp. 460–467, 2007.
- [72] J. Fluhr, “Practical aspects of cosmetic testing how to set up a scientific study in skin physiology.” Springer, Berlin: Heidelberg, 2011.
- [73] R. J. G. Chalmers, “Psoriasis Area & Severity Index,” *The Psoriasis and Psoriatic Alliance*, 2008. [Online]. Available: <http://www.papaa.org/articles/psoriasis-area-severity-index>. [Accessed: 23-Sep-2012].
- [74] R. J. G. Chalmers, “Psoriasis Area & Severity Index,” *The Psoriasis and Psoriatic Alliance*, 2008.
- [75] PASITraining.com, “Scaling Grades,” 2009. [Online]. Available: <http://www.pasitraining.com/eis/index.html>.
- [76] A. B. Fleischer, S. R. Rapp, D. M. Reboussin, J. C. Vanarthos, and S. R. Feldman, “Patient measurement of psoriasis disease severity with a structured instrument,” *The Journal of investigative dermatology*, vol. 102, no. 6, pp. 967–969, 1994.
- [77] B. Dhanasekar, N. K. Mohan, B. Bhaduri, and B. Ramamoorthy, “Evaluation of surface roughness based on monochromatic speckle correlation using image processing,” *Precision engineering*, vol. 32, no. 3, pp. 196–206, 2008.
- [78] D. J. Whitehouse, “Surfaces and their measurement.” HPS, London, 2002.
- [79] H. Ostadi, K. Jiang, and D. W. L. Hukins, “A comparison of surface roughness analysis methods applied to urinary catheters,” *Precision Engineering*, vol. 34, no. 4, pp. 798–801, Oct. 2010.
- [80] D. J. Whitehouse, *Handbook of surface and nanometrology*. Bristol: Institute of Physics Pub., 2003.
- [81] U. Persson, “Measurement of surface roughness using infrared scattering,” *Measurement*, vol. 18, no. 2, pp. 109–116, 1996.
- [82] J. Ohtsubo and T. Asakura, “Measurement of surface roughness properties using speckle patterns with non-Gaussian statistics,” *Optics Communications*, vol. 25, no. 3, pp. 315–319, 1978.
- [83] G. Frankowski, M. Chen, and T. Huth, “Real-time 3D shape measurement with digital stripe projection by Texas Instruments Micro Mirror Devices DMD,” *Proceedings of SPIE*, vol. 3958, pp. 90–105, 2000.
- [84] S. Zhang, “High-resolution 3D profilometry with binary phase-shifting methods,” *Appl. Opt.*, vol. 50, no. 12, pp. 1753–1757, Apr. 2011.
- [85] J. Geng, “Structured-light 3D surface imaging: a tutorial,” *Adv. Opt. Photon.*, vol. 3, no. 2, pp. 128–160, Jun. 2011.
- [86] R. J. Hocken, N. Chakraborty, and C. Brown, “Optical metrology of surfaces,” *CIRP Annals-Manufacturing Technology*, vol. 54, no. 2, pp. 169–183, 2005.
- [87] Y. Hao, Y. Zhao, and D. Li, “Shape measurement of objects with large discontinuities and surface isolations using complementary grating projection,” in *Proc. of SPIE*, 1999, vol. 3898, pp. 338–343.

- [88] L. Blunt and X. Jiang, *Advanced techniques for assessment surface topography: development of a basis for 3D surface texture standards "surfstand."* London; Sterling, VA: Kogan Page Science, 2003, p. 355.
- [89] D. J. Whitehouse. *Handbook of surface metrology*. Bristol; Philadelphia: Institute of Physics Pub.. 1994.
- [90] B. Muralikrishnan and J. Raja, *Computational surface and roundness metrology*, 1st ed. London: Springer, 2009, p. 260.
- [91] J. Raja and V. Radhakrishnan, "Filtering of surface profiles using fast fourier transform," *International Journal of Machine Tool Design and Research*, vol. 19, no. 3, pp. 133–141, 1979.
- [92] Á. Czifra, T. Goda, and E. Garbayo, "Surface characterisation by parameter-based technique, slicing method and PSD analysis," *Measurement*, vol. 44, no. 5, pp. 906–916, Jun. 2011.
- [93] W. P. Dong, E. Mainsah, and K. J. Stout, "Reference planes for the assessment of surface roughness in three dimensions," *International Journal of Machine Tools and Manufacture*, vol. 35, no. 2, pp. 263–271, Feb. 1995.
- [94] K. Stout, *Development of methods for the characterisation of roughness in three dimensions*. London: Penton Press, 2000.
- [95] B. Buxton, L. Dekker, I. Douros, and T. Vassilev, "Reconstruction and interpretation of 3D whole body surface images," *Scanning*, 2000.
- [96] L. Skedung, K. Danerlöv, U. Olofsson, C. Michael Johannesson, M. Aikala, J. Kettle, M. Arvidsson, B. Berglund, and M. W. Rutland, "Tactile perception: Finger friction, surface roughness and perceived coarseness," *Tribology International*, vol. 44, no. 5, pp. 505–512, May 2011.
- [97] P. Corcuff and G. E. Pierard, "Skin Imaging: State of the Art at the Dawn of the Year 2000," *Current problems in dermatology*, vol. 26, p. 1, 1998.
- [98] A. H. M. Sarah Marshall, "Skin Biopsy (continued)," *WebMD Medical Reference*. [Online]. Available: <http://www.webmd.com/cancer/skin-biopsy?page=3>. [Accessed: 07-Aug-2012].
- [99] T. Tsuji, T. Yorifuji, Y. Hayashi, and T. Hamada, "Light and scanning electron microscopic studies on wrinkles in aged persons' skin.," *The British journal of dermatology*, vol. 114, no. 3, pp. 329–335, 1986.
- [100] O. Chilhwan, M. G. Kim, and J. S. Moon, "Stereoimaging for Skin Contour Measurement." in *Bioengineering of The Skin: Skin Imaging and Analysis*, 2nd ed.. Informa Plc, 2006.
- [101] B. Eberlein-König, T. Schäfer, J. Huss-Marp, U. Darsow, M. Möhrensclager, O. Herbert, D. Abeck, U. Krämer, H. Behrendt, and J. Ring, "Skin surface pH, stratum corneum hydration, trans-epidermal water loss and skin roughness related to atopic eczema and skin dryness in a population of primary school children.," *Acta dermato-venereologica*, vol. 80, no. 3, pp. 188–91, May 2000.
- [102] T. G. Mathia, P. Pawlus, and M. Wieczorowski, "Recent trends in surface metrology," *Wear*, vol. In Press,.

- [103] P. Nardin, D. Nita, and J. Mignot, "Automation of a series of cutaneous topography measurements from silicon rubber replicas." *Skin Research and Technology*, vol. 8, no. 2, pp. 112–117, 2002.
- [104] I. Sarkany and R. R. Phillips, "Microtopography of The Skin." *Medical biological illustration*, vol. 15, pp. SUPPL:57–61, 1965.
- [105] D. Battistutta, N. Pandeya, G. M. Strutton, A. Fourtanier, S. Tison, and A. C. Green. "Skin surface topography grading is a valid measure of skin photoaging." *Photodermatology, photoimmunology & photomedicine*, vol. 22, no. 1, pp. 39–45, 2006.
- [106] Bo Forslind, "Skin Replication for Light and Scanning Electron Microscopy." in in *Non-Invasive Methods and the Skin*, 2nd ed., J. Serup, G. B. Jemec, and G. Grove, Eds. Boca Raton, California, USA: CRC Press Taylor & Francis Group, 2006, pp. 147–153.
- [107] J. Gassmueller, A. Kecskés, and P. Jahn. "Stylus Method for Skin Surface Contour Measurement," in in *Non-Invasive Methods and the Skin*, 2nd ed., J. Serup, G. B. Jemec, and G. Grove, Eds. Boca Raton, California, USA: CRC Press Taylor & Francis Group, 2006, pp. 163–168.
- [108] Hommelwerke, "HOMMEL TESTER T500 - The benchmark for portable and precise in-process measurement of surface roughness." Hommelwerke, Schwenningen, 2005.
- [109] L. Tchvialeva, H. Zeng, I. Markhvida, D. I. McLean, H. Lui, and T. K. Lee. "Skin Roughness Assessment," *New Developments in Biomedical Engineering*, pp. 341–358, 2010.
- [110] J. Efsen, S. Christiansen, H. N. Hansen, and J. Keiding, "Laser Profilometry," in in *Non-Invasive Methods and the Skin*, 2nd ed., J. Serup, G. B. Jemec, and G. Grove, Eds. Boca Raton, California, USA: CRC Press Taylor & Francis Group, 2006, pp. 169–177.
- [111] Schut Geometrical Metrology, "3D CNC Coordinate Measuring Machines." Schut Geometrische Meettechniek, Groningen, The Netherlands, p. 2, 2010.
- [112] T. W. Fischer, W. Wigger-Alberti, and P. Elsner, "Direct and non-direct measurement techniques for analysis of skin surface topography.," *Skin Pharmacology and Applied Skin Physiology*, vol. 12, no. 1–2, pp. 1–11, 1999.
- [113] M. Breuer and W. Voss, "Proving for Efficacy: Laser Profilometry," pp. 48155–48155, 1994.
- [114] S. Makki, J. C. Barbenel, and P. Agache, "A quantitative method for the assessment of the microtopography of human skin," *Acta Derm Venereol*, vol. 59, no. 4, pp. 285–291, 1979.
- [115] G. Frankowski and M. Chen, "Optical 3D in vivo Measurement of Human Skin Surfaces with PRIMOS," in *Proc. of Fringe*, 2001.
- [116] C. Hof and H. Hopermann. "Comparison of Replica and In Vivo-Measurement of the Microtopography of Human Skin," *SOFW Journal*, vol. 126, no. Part 9, pp. 40–47, 2000.

- [117] M. Loden, "Atopic dermatitis and other skin diseases." in in *Bioengineering of The Skin: Skin Imaging and Analysis*, K. P. Wilhelm, Ed. New York: Informa Healthcare USA. Inc., 2007.
- [118] H. Fujii and T. Asakura, "Effect of surface roughness on the statistical distribution of image speckle intensity," *Optics Communications*, vol. 11, no. 1, pp. 35–38, May 1974.
- [119] L. RS, T. GY, D. Gledhill, and S. Ward, "Grinding surface roughness measurement based on the co-occurrence matrix of speckle pattern texture.." *Applied optics*, vol. 45, no. 35, pp. 8839–8847, 2006.
- [120] Z. Li, H. Li, and Y. Qiu, "Fractal analysis of laser speckle for measuring roughness [6027-64]." in *Proceedings- SPIE The International Society for Optical Engineering*, 2006, vol. 6027, p. 60271S.
- [121] P. M. Friedman, G. R. Skover, G. Payonk, A. N. B. Kauvar, and R. G. Geronemus, "3D in-vivo optical skin imaging for topographical quantitative assessment of non-ablative laser technology.." *Dermatologic surgery official publication for American Society for Dermatologic Surgery et al*, vol. 28, no. 3, pp. 199–204, 2002.
- [122] C. Edwards, R. Heggie, and R. Marks, "A study of differences in surface roughness between sun-exposed and unexposed skin with age.." *Photodermatology photoimmunology photomedicine*, vol. 19, no. 4, pp. 169–174, 2003.
- [123] P. R. Bargo and N. Kollias, "Measurement of skin texture through polarization imaging.." *The British journal of dermatology*, vol. 162, no. 4, pp. 724–731, 2010.
- [124] W. Manuskiatti, D. A. Schwindt, and H. I. Maibach, "Influence of age, anatomic site and race on skin roughness and scaliness.." *Dermatology Basel Switzerland*, vol. 196, no. 4, pp. 401–407, 1998.
- [125] GFMesstechnik, "User Manual: PRIMOS optical 3D skin measuring device." GFMesstechnik GmbH, 2008.
- [126] J. S. Yoon, C. Ryu, and J. H. Lee, "Developable polynomial surface approximation to smooth surfaces for fabrication parameters of a large curved shell plate by Differential Evolution," *Computer-Aided Design*, vol. 40, no. 9, pp. 905–915, Sep. 2008.
- [127] G. J. Borradaile, *Statistics of earth science data: their distribution in time, space, and orientation*. Berlin; New York: Springer, 2003.
- [128] G. Barbato Carneiro, K., Garnaes, J., Gori, G., Hughes, G., Jensen, C.P., Jørgensen, J.F., Jusko, O., Livi, S., McQuoid, H., Nielsen, L., Picotto, G.B., Wilkening, G, "Scanning Tunnelling Microscopy Methods for Roughness and Micro Hardness Measurements," 1994.
- [129] Y. Lee, S. Lee, I. Ivriissimtzis, and H.-P. Seidel, "Overfitting control for surface reconstruction," in *ACM International Conference Proceeding Series*, 2006, vol. 256, pp. 231–234.

- [130] Sizes.com. "Grades of sandpaper (coated abrasives)." 2000. [Online]. Available: <http://www.sizes.com/tools/sandpaper.htm>.
- [131] GFMesstechnik. "Technical Data of 3D PRIMOS Portable." GFMesstechnik GmbH, Teltow, Germany, p. 2, 2008.
- [132] A. D. McNaught and A. Wilkinson, *IUPAC - Compendium of Chemical Terminology*, 2nd ed. Blackwell Scientific Publications, Oxford, 1997.
- [133] J. . Bland and D. . Altman, "Statistical methods for assessing agreement between two methods of clinical measurement.," *Lancet*, vol. 1. no. 8476, pp. 307–310, 1986.
- [134] K. J. Stout and L. Blunt, "Nanometres to micrometres: three-dimensional surface measurement in bio-engineering," *Surface and Coatings Technology*, vol. 71, no. 2, pp. 69–81, Mar. 1995.
- [135] S. A. Whitehead, A. C. Shearer, D. C. Watts, and N. H. Wilson, "Comparison of two stylus methods for measuring surface texture.," *Dental materials official publication of the Academy of Dental Materials*, vol. 15, no. 2, pp. 79–86, 1999.
- [136] K. Arrell and S. Carver, "Surface Roughness Scaling Trends," in *Geomorphometry 2009 Conference Proceedings*, R. Purves, S. Gruber, R. Straumann, and T. Hengl, Eds. University of Zurich, Zurich, 2009, pp. 120–123.
- [137] A. F. M. Hani, D. Sathyamoorthy, and V. Sagayan Asirvadam, "A method for computation of surface roughness of digital elevation model terrains via multiscale analysis," *Computers & Geosciences*, vol. 37, no. 2, pp. 177–192, Feb. 2011.
- [138] N. Fardin, O. Stephansson, and L. Jing, "The scale dependence of rock joint surface roughness," *International Journal of Rock Mechanics and Mining Sciences*, vol. 38, no. 5, pp. 659–669, 2001.
- [139] L. J. van Ruijven, M. Beek, and T. M. van Eijden, "Fitting parametrized polynomials with scattered surface data.," *Journal of biomechanics*, vol. 32, no. 7, pp. 715–20, Jul. 1999.
- [140] W. G. Cochran, *Sampling techniques*. John Wiley & Sons, 2007.
- [141] H. Nugroho, N.-E. Batool, A. F. M Hani, and PA Venkatachalam, "Surface Analysis of Psoriasis for PASI Scaliness Assessment," in *2007 4th International Conference on Intelligent and Advanced Systems (ICIAS)*, pp. 798–802.
- [142] J. M. Gelfand, R. Weinstein, S. B. Porter, A. L. Neimann, J. A. Berlin, and D. J. Margolis, "Prevalence and treatment of psoriasis in the United Kingdom: a population-based study.," *Archives of Dermatology*, vol. 141, no. 12, pp. 1537–41, 2005.
- [143] A. K. Jain, M. N. Murty, and P. J. Flynn, "Data clustering: a review," *ACM computing surveys (CSUR)*, vol. 31, no. 3, pp. 264–323, 1999.
- [144] A. K. Jain, "Data clustering: 50 years beyond K-means," *Pattern Recognition Letters*, vol. 31, no. 8, pp. 651–666, 2010.

- [145] C. H. Li and P. C. Yuen, "Regularized color clustering in medical image database.," *IEEE Transactions on Medical Imaging*, vol. 19, no. 11, pp. 1150–1155, 2000.
- [146] F. Masulli and A. Schenone. "A fuzzy clustering based segmentation system as support to diagnosis in medical imaging.," *Artificial Intelligence in Medicine*, vol. 16, no. 2, pp. 129–147, 1999.
- [147] J. C. Bezdek, R. Ehrlich, and W. Full, "FCM: The fuzzy c-means clustering algorithm." *Computers & Geosciences*, vol. 10, no. 2–3, pp. 191–203. 1984.
- [148] L. A. Zadeh, "Fuzzy sets," *Information and Control*, vol. 8, no. 3, pp. 338–353, Jun. 1965.
- [149] R. Xu and D. C. Wunsch, "Clustering Algorithms in Biomedical Research: A Review," *IEEE Reviews in Biomedical Engineering*, vol. 3, pp. 120–154. 2010.
- [150] E. A. Zanaty, "Determining the number of clusters for kernelized fuzzy C-means algorithms for automatic medical image segmentation." *Egyptian Informatics Journal*, vol. 13, no. 1, pp. 39–58, Mar. 2012.
- [151] E. A. Zanaty, "Determining the number of clusters for kernelized fuzzy C-means algorithms for automatic medical image segmentation." *Egyptian Informatics Journal*, vol. 13, no. 1, pp. 39–58, Mar. 2012.
- [152] J. Cohen, "A Coefficient of Agreement for Nominal-Scales," *Educational and Psychological Measurement*, vol. 20, no. 1, pp. 37–46, 1960.
- [153] A. J. Viera and J. M. Garrett, "Research Series - Understanding Interobserver Agreement: The Kappa Statistic," *Family medicine.*, vol. 37, no. 5, p. 360. 2005.
- [154] W. Yu and B. Xu, "A portable stereo vision system for whole body surface imaging," *Image and Vision Computing*, vol. 28, no. 4, pp. 605–613, 2009.
- [155] J. Wang, D. Gallagher, J. C. Thornton, W. Yu, M. Horlick, and F. X. Pi-Sunyer, "Validation of a 3-dimensional photonic scanner for the measurement of body volumes, dimensions, and percentage body fat," *The American journal of clinical nutrition*, vol. 83, no. 4, pp. 809–816, 2006.
- [156] J. Gu, T. Chang, I. Mak, S. Gopalsamy, H. Shen, and M. Yuen, "A 3D reconstruction system for human body modeling," *Modelling and Motion Capture Techniques for Virtual Environments*, pp. 229–241, 1998.
- [157] I. Douros and B. Buxton, "Three-dimensional surface curvature estimation using quadric surface patches," *Scanning*, 2002.
- [158] M. Rohr and K. Schrader, "Fast Optical in vivo Topometry of Human Skin ( FOITS ) Comparative Investigations with Laser Profilometry," pp. 52 – 59, 1998.
- [159] B.-G. Rosén, L. Blunt, T. R. Thomas, B.-G. R. et al, and B.-G. R. et Al, "On in-vivo skin topography metrology and replication techniques," *Journal of Physics: Conference Series*, vol. 13, no. 1, p. 325, Jan. 2005.

- [160] U. Jacobi, M. Chen, G. Frankowski, R. Sinkgraven, M. Hund, B. Rzany, W. Sterry, and J. Lademann, "In vivo determination of skin surface topography using an optical 3D device," *Skin Research and Technology*, vol. 10, no. 4, pp. 207–214, 2004.

APPENDIX A: SURFACE ROUGHNESS OF LESION MODEL AT  
FLAT SURFACES

Lesion model	Assessment	Width (mm)	Height (mm)	$S_{a,2}$ (mm)	$R_2^2$	$S_{a,3}$ (mm)	$R_3^2$	$S_{final}$ (mm)	$R_{final}^2$	$\overline{S_{final}}$ (mm)
1	1	12.23	10.44	0.0142	0.997	0.0138	0.997	0.0138	0.997	0.0139
	2	12.23	10.44	0.0146	0.996	0.0142	0.997	0.0142	0.997	
	3	12.23	10.44	0.0140	0.996	0.0137	0.997	0.0137	0.997	
2	1	14.65	10.31	0.0123	0.998	0.0120	0.998	0.0120	0.998	0.0130
	2	14.65	10.31	0.0122	0.998	0.0119	0.998	0.0119	0.998	
	3	14.65	10.31	0.0151	0.997	0.0149	0.997	0.0149	0.997	
3	1	14.65	10.31	0.0124	0.994	0.0122	0.994	0.0122	0.994	0.0122
	2	14.65	10.31	0.0125	0.994	0.0122	0.994	0.0122	0.994	
	3	14.65	10.31	0.0123	0.994	0.0121	0.994	0.0121	0.994	
4	1	13.88	9.80	0.0123	0.994	0.0119	0.994	0.0119	0.994	0.0118
	2	13.88	9.80	0.0122	0.994	0.0118	0.994	0.0118	0.994	
	3	13.88	9.80	0.0123	0.994	0.0118	0.994	0.0118	0.994	
5	1	12.86	9.67	0.0134	0.995	0.0132	0.995	0.0132	0.995	0.0149
	2	12.86	9.67	0.0187	0.992	0.0186	0.992	0.0186	0.992	
	3	12.86	9.67	0.0130	0.996	0.0129	0.996	0.0129	0.996	
6	1	12.10	9.93	0.0146	0.950	0.0139	0.954	0.0139	0.954	0.0132
	2	12.10	9.93	0.0129	0.952	0.0122	0.957	0.0122	0.957	
	3	12.10	9.93	0.0141	0.921	0.0135	0.928	0.0135	0.928	
7	1	11.21	9.67	0.0112	0.997	0.0111	0.997	0.0111	0.997	0.0112
	2	11.21	9.67	0.0115	0.997	0.0114	0.997	0.0114	0.997	
	3	11.21	9.67	0.0112	0.997	0.0112	0.997	0.0112	0.997	
8	1	12.35	9.67	0.0128	0.993	0.0122	0.994	0.0122	0.994	0.0114
	2	12.35	9.67	0.0118	0.994	0.0110	0.995	0.0110	0.995	
	3	12.35	9.67	0.0117	0.994	0.0109	0.995	0.0109	0.995	
9	1	14.14	9.55	0.0125	0.980	0.0122	0.981	0.0122	0.981	0.0122
	2	14.14	9.55	0.0124	0.981	0.0121	0.982	0.0121	0.982	
	3	14.14	9.55	0.0125	0.982	0.0122	0.983	0.0122	0.983	
10	1	13.25	9.29	0.0113	0.993	0.0110	0.994	0.0110	0.994	0.0109
	2	13.25	9.29	0.0109	0.994	0.0105	0.994	0.0105	0.994	
	3	13.25	9.29	0.0116	0.993	0.0112	0.993	0.0112	0.993	
11	1	12.23	9.93	0.0133	0.987	0.0129	0.987	0.0129	0.987	0.0124
	2	12.23	9.93	0.0119	0.990	0.0116	0.990	0.0116	0.990	
	3	12.23	9.93	0.0131	0.988	0.0128	0.989	0.0128	0.989	
12	1	11.59	9.67	0.0119	0.985	0.0115	0.986	0.0115	0.986	0.0118
	2	11.59	9.67	0.0127	0.983	0.0124	0.985	0.0124	0.985	
	3	11.59	9.67	0.0120	0.985	0.0116	0.986	0.0116	0.986	

Lesion model	Assessment	Width (mm)	Height (mm)	$S_{a,2}$ (mm)	$R_2^2$	$S_{a,3}$ (mm)	$R_3^2$	$S_{final}$ (mm)	$R_{final}^2$	$\overline{S_{final}}$ (mm)
13	1	12.99	10.05	0.0113	0.990	0.0109	0.991	0.0109	0.991	0.0108
	2	12.99	10.05	0.0110	0.991	0.0107	0.991	0.0107	0.991	
	3	12.99	10.05	0.0113	0.991	0.0109	0.991	0.0109	0.991	
14	1	10.06	9.93	0.0134	0.972	0.0127	0.975	0.0127	0.975	0.0117
	2	10.06	9.93	0.0117	0.980	0.0109	0.983	0.0109	0.983	
	3	10.06	9.93	0.0122	0.976	0.0115	0.979	0.0115	0.979	
15	1	10.44	9.93	0.0124	0.991	0.0116	0.992	0.0116	0.992	0.0115
	2	10.44	9.93	0.0121	0.992	0.0115	0.993	0.0115	0.993	
	3	10.44	9.93	0.0121	0.992	0.0114	0.992	0.0114	0.992	
16	1	11.59	10.56	0.0114	0.993	0.0111	0.994	0.0111	0.994	0.0110
	2	11.59	10.56	0.0113	0.993	0.0110	0.993	0.0110	0.993	
	3	11.59	10.56	0.0112	0.993	0.0109	0.993	0.0109	0.993	
17	1	11.21	9.93	0.0161	0.988	0.0152	0.989	0.0152	0.989	0.0131
	2	11.21	9.93	0.0130	0.992	0.0119	0.993	0.0119	0.993	
	3	11.21	9.93	0.0135	0.992	0.0123	0.993	0.0123	0.993	
18	1	11.21	10.18	0.0122	0.997	0.0113	0.998	0.0113	0.998	0.0114
	2	11.21	10.18	0.0126	0.997	0.0118	0.997	0.0118	0.997	
	3	11.21	10.18	0.0121	0.997	0.0112	0.998	0.0112	0.998	
19	1	11.59	10.05	0.0169	0.992	0.0166	0.992	0.0166	0.992	0.0137
	2	11.59	10.05	0.0128	0.995	0.0125	0.995	0.0125	0.995	
	3	11.59	10.05	0.0120	0.996	0.0118	0.996	0.0118	0.996	
20	1	12.61	10.56	0.0117	0.998	0.0106	0.998	0.0106	0.998	0.0108
	2	12.61	10.56	0.0123	0.997	0.0111	0.998	0.0111	0.998	
	3	12.61	10.56	0.0116	0.998	0.0106	0.998	0.0106	0.998	
21	1	13.50	10.82	0.0134	0.972	0.0128	0.975	0.0128	0.975	0.0118
	2	13.50	10.82	0.0124	0.977	0.0116	0.979	0.0116	0.979	
	3	13.50	10.82	0.0119	0.975	0.0111	0.979	0.0111	0.979	
22	1	13.76	10.44	0.0127	0.989	0.0123	0.990	0.0123	0.990	0.0124
	2	13.76	10.44	0.0134	0.987	0.0130	0.988	0.0130	0.988	
	3	13.76	10.44	0.0123	0.990	0.0120	0.990	0.0120	0.990	
23	1	11.72	10.56	0.0133	0.971	0.0126	0.974	0.0126	0.974	0.0125
	2	11.72	10.56	0.0128	0.973	0.0123	0.976	0.0123	0.976	
	3	11.72	10.56	0.0133	0.969	0.0126	0.972	0.0126	0.972	
24	1	13.12	10.05	0.0129	0.958	0.0128	0.959	0.0128	0.959	0.0129
	2	13.12	10.05	0.0126	0.966	0.0125	0.966	0.0125	0.966	
	3	13.12	10.05	0.0136	0.962	0.0134	0.963	0.0134	0.963	
25	1	12.48	10.05	0.0122	0.996	0.0113	0.997	0.0113	0.997	0.0109
	2	12.48	10.05	0.0116	0.996	0.0108	0.997	0.0108	0.997	
	3	12.48	10.05	0.0114	0.997	0.0106	0.997	0.0106	0.997	
26	1	12.10	10.44	0.0127	0.990	0.0124	0.991	0.0124	0.991	0.0127
	2	12.10	10.44	0.0131	0.986	0.0126	0.989	0.0126	0.989	
	3	12.10	10.44	0.0136	0.984	0.0131	0.987	0.0131	0.987	

Lesion model	Assessment	Width (mm)	Height (mm)	$S_{a,2}$ (mm)	$R_2^2$	$S_{a,3}$ (mm)	$R_3^2$	$S_{final}$ (mm)	$R_{final}^2$	$\overline{S_{final}}$ (mm)
27	1	12.23	10.18	0.0129	0.997	0.0124	0.997	0.0124	0.997	0.0120
	2	12.23	10.18	0.0123	0.998	0.0118	0.998	0.0118	0.998	
	3	12.23	10.18	0.0124	0.998	0.0119	0.998	0.0119	0.998	
28	1	14.14	10.69	0.0133	0.997	0.0130	0.997	0.0130	0.997	0.0130
	2	14.14	10.69	0.0139	0.996	0.0135	0.997	0.0135	0.997	
	3	14.14	10.69	0.0129	0.997	0.0125	0.997	0.0125	0.997	
29	1	14.65	9.5450	0.0116	0.985	0.0115	0.985	0.0115	0.985	0.0116
	2	15.16	8.7820	0.0119	0.984	0.0116	0.985	0.0116	0.985	
	3	15.92	9.2910	0.0117	0.986	0.0116	0.986	0.0116	0.986	
30	1	14.52	8.5280	0.0113	0.989	0.0109	0.989	0.0109	0.989	0.0109
	2	13.63	8.9090	0.0112	0.988	0.0109	0.988	0.0109	0.988	
	3	14.65	9.1640	0.0112	0.989	0.0108	0.990	0.0108	0.990	
31	1	15.41	8.6550	0.0112	0.986	0.0111	0.986	0.0111	0.986	0.0112
	2	14.65	8.5270	0.0114	0.984	0.0113	0.984	0.0113	0.984	
	3	15.03	8.5270	0.0113	0.985	0.0111	0.985	0.0111	0.985	
32	1	0.0146	0.965	0.0147	0.964	0.0146	0.965	0.0146	0.965	0.0145
	2	0.0117	0.977	0.0119	0.976	0.0117	0.977	0.0117	0.977	
	3	0.0172	0.954	0.0175	0.952	0.0172	0.954	0.0172	0.954	
33	1	0.0096	0.977	0.0095	0.978	0.0095	0.978	0.0095	0.978	0.0121
	2	0.0124	0.965	0.0123	0.965	0.0123	0.965	0.0123	0.965	
	3	0.0147	0.948	0.0146	0.949	0.0146	0.949	0.0146	0.949	

APPENDIX B: SURFACE ROUGHNESS OF LESION MODEL AT  
CURVE SURFACES

No	Lesion ID	Width (mm)	Height (mm)	$S_{a,2}$ (mm)	$R_2^2$	$S_{a,3}$ (mm)	$R_3^2$	$R_{final}^2$	$\overline{S_{final}}$ (mm)
1	H-2	10.05	9.04	0.014	0.996	0.015	0.995	0.996	0.014
2	H-4	11.58	9.42	0.015	0.991	0.015	0.991	0.991	0.015
3	H-5	11.96	7.77	0.015	0.999	0.015	0.999	0.999	0.015
4	H-6	13.49	8.40	0.013	0.996	0.013	0.996	0.996	0.013
5	H-7	9.54	7.64	0.014	0.998	0.014	0.998	0.998	0.014
6	H-10	11.71	6.87	0.014	0.981	0.014	0.982	0.982	0.014
7	U-2	8.53	5.09	0.015	0.987	0.015	0.987	0.987	0.015
8	U-4	9.80	4.84	0.012	0.971	0.013	0.964	0.971	0.012
9	U-5	9.67	16.42	0.012	0.998	0.012	0.998	0.998	0.012
10	U-6	10.18	3.82	0.011	0.996	0.013	0.994	0.996	0.011
11	U-7	8.53	4.07	0.012	0.970	0.012	0.964	0.970	0.012
12	U-8	10.56	4.07	0.012	0.995	0.013	0.994	0.995	0.012
13	U-9	7.51	4.33	0.012	0.995	0.012	0.995	0.995	0.012
14	U-10	8.53	4.20	0.012	0.963	0.012	0.961	0.963	0.012
15	U-11	10.18	16.42	0.013	0.997	0.015	0.997	0.997	0.013
16	U-12	9.54	5.47	0.012	0.994	0.014	0.992	0.994	0.012
17	U-13	9.29	3.95	0.015	0.985	0.015	0.984	0.985	0.015
18	U-14	9.54	4.33	0.011	0.991	0.013	0.988	0.991	0.011
19	U-15	9.03	4.58	0.012	0.960	0.012	0.961	0.961	0.012
20	U-16	8.91	3.69	0.012	0.998	0.015	0.998	0.998	0.012
21	U-17	9.80	15.78	0.011	0.988	0.013	0.989	0.989	0.013
22	U-18	10.43	16.42	0.012	0.996	0.016	0.993	0.996	0.012
23	U-19	8.91	4.46	0.013	0.993	0.016	0.988	0.993	0.013
24	U-20	15.27	7.26	0.014	0.989	0.014	0.990	0.990	0.014
25	U-23	9.67	11.08	0.013	0.986	0.014	0.982	0.986	0.013
26	U-24	9.67	5.35	0.011	0.994	0.012	0.993	0.994	0.011
27	U-25	7.76	5.35	0.012	0.991	0.013	0.989	0.991	0.012
28	U-26	9.54	5.09	0.011	0.992	0.011	0.991	0.992	0.011
29	U-27	9.93	16.93	0.011	0.990	0.013	0.988	0.990	0.011
30	U-28	10.05	4.84	0.012	0.993	0.012	0.992	0.993	0.012
31	U-30	8.40	15.40	0.015	0.996	0.011	0.998	0.998	0.011
32	U-31	10.05	4.58	0.012	0.989	0.012	0.989	0.989	0.012
33	U-32	9.92	15.66	0.014	0.998	0.020	0.996	0.998	0.014
34	U-33	9.54	4.20	0.013	0.984	0.013	0.985	0.985	0.013
35	U-34	9.92	16.55	0.012	0.994	0.012	0.994	0.994	0.012
36	U-35	9.67	15.78	0.011	0.989	0.013	0.985	0.989	0.011
37	U-36	9.16	5.22	0.012	0.956	0.012	0.956	0.956	0.012

No	Lesion ID	Width (mm)	Height (mm)	$S_{a,2}$ (mm)	$R_2^2$	$S_{a,3}$ (mm)	$R_3^2$	$R_{final}^2$	$\overline{S}_{final}$ (mm)
38	U-38	9.67	14.51	0.012	0.998	0.014	0.997	0.998	0.012
39	U-39	9.16	5.73	0.011	0.991	0.010	0.991	0.991	0.011
40	U-40	9.54	15.40	0.012	0.996	0.013	0.995	0.996	0.012
41	U-41	9.67	3.95	0.011	0.973	0.012	0.967	0.973	0.011
42	U-42	9.42	15.66	0.011	0.993	0.013	0.990	0.993	0.011
43	U-43	10.05	5.35	0.012	0.984	0.012	0.984	0.984	0.012
44	U-44	6.87	4.58	0.014	0.975	0.013	0.978	0.978	0.013
45	U-45	9.42	3.69	0.011	0.995	0.011	0.996	0.996	0.011
46	U-46	9.54	4.33	0.010	0.928	0.011	0.945	0.945	0.011
47	U-47	10.56	5.73	0.011	0.992	0.011	0.992	0.992	0.011
48	U-48	10.82	15.15	0.011	0.993	0.012	0.993	0.993	0.011
49	U-49	10.56	4.58	0.012	0.980	0.013	0.979	0.980	0.012
50	U-50	9.03	4.71	0.013	0.948	0.013	0.948	0.948	0.013
51	U-52	8.53	4.07	0.015	0.968	0.017	0.961	0.968	0.015
52	U-53	9.03	3.95	0.011	0.974	0.012	0.973	0.974	0.011
53	U-54	9.67	5.86	0.012	0.969	0.013	0.962	0.969	0.012
54	U-55	10.18	4.97	0.014	0.983	0.014	0.983	0.983	0.014
55	U-56	9.03	6.11	0.011	0.984	0.011	0.982	0.984	0.011
56	U-57	9.16	4.84	0.011	0.910	0.012	0.920	0.920	0.012
57	U-58	9.92	5.35	0.011	0.963	0.012	0.956	0.963	0.011
58	U-59	9.93	4.71	0.015	0.984	0.014	0.986	0.986	0.014
59	U-60	9.16	3.57	0.013	0.936	0.013	0.934	0.936	0.013
60	U-62	9.80	4.46	0.011	0.997	0.012	0.997	0.997	0.011
61	U-63	9.29	5.09	0.011	0.986	0.012	0.983	0.986	0.011
62	U-64	9.16	4.71	0.011	0.926	0.011	0.939	0.939	0.011
63	U-65	9.29	5.09	0.011	0.984	0.011	0.983	0.984	0.011
64	U-66	10.56	17.69	0.011	0.990	0.013	0.988	0.990	0.011
65	U-67	9.42	5.22	0.014	0.958	0.014	0.954	0.958	0.014
66	U-68	9.03	4.71	0.014	0.991	0.015	0.991	0.991	0.014
67	U-69	9.03	3.31	0.012	0.996	0.012	0.996	0.996	0.012
68	U-70	10.18	4.20	0.012	0.972	0.012	0.969	0.972	0.012
69	U-71	10.82	17.06	0.015	0.996	0.013	0.996	0.996	0.015
70	U-72	9.67	4.71	0.013	0.985	0.013	0.985	0.985	0.013
71	U-73	10.05	4.58	0.015	0.992	0.015	0.992	0.992	0.015
72	U-75	9.54	5.73	0.012	0.991	0.012	0.990	0.991	0.012
73	U-76	8.27	5.86	0.014	0.984	0.014	0.983	0.984	0.014
74	U-77	9.54	16.04	0.012	0.999	0.015	0.998	0.999	0.012
75	U-78	10.69	14.77	0.011	0.997	0.011	0.997	0.997	0.011
76	U-79	10.56	16.42	0.012	0.997	0.011	0.997	0.997	0.012
77	U-80	9.93	15.79	0.011	0.996	0.012	0.995	0.996	0.011
78	U-81	10.43	17.44	0.011	0.995	0.011	0.995	0.995	0.011
79	U-82	10.69	5.09	0.012	0.984	0.013	0.983	0.984	0.012
80	U-83	10.05	16.04	0.013	0.994	0.014	0.994	0.994	0.013

No	Lesion ID	Width (mm)	Height (mm)	$S_{a,2}$ (mm)	$R_2^2$	$S_{a,3}$ (mm)	$R_3^2$	$R_{final}^2$	$\overline{S}_{final}$ (mm)
81	U-84	10.43	5.09	0.012	0.997	0.014	0.996	0.997	0.012
82	U-87	10.31	5.98	0.012	0.998	0.012	0.998	0.998	0.012
83	U-88	10.05	6.24	0.014	0.978	0.014	0.980	0.980	0.014
84	U-89	10.69	5.47	0.011	0.992	0.011	0.992	0.992	0.011
85	U-90	9.93	5.22	0.013	0.997	0.014	0.997	0.997	0.013
86	U-91	10.43	4.71	0.012	0.993	0.013	0.993	0.993	0.012
87	U-92	8.02	17.31	0.012	0.988	0.012	0.987	0.988	0.012
88	U-93	10.18	4.84	0.011	0.987	0.012	0.984	0.987	0.011
89	U-94	8.40	17.70	0.013	0.991	0.014	0.990	0.991	0.013
90	U-95	10.18	5.22	0.012	0.930	0.014	0.914	0.930	0.012
91	U-96	10.82	5.09	0.011	0.993	0.011	0.993	0.993	0.011
92	U-97	9.80	5.35	0.013	0.969	0.013	0.968	0.969	0.013
93	U-98	10.18	16.55	0.012	0.988	0.014	0.986	0.988	0.012
94	T-1	14.12	8.02	0.018	0.977	0.011	0.992	0.992	0.011
95	T-2	13.23	7.00	0.011	0.949	0.012	0.940	0.949	0.011
96	T-3	15.01	7.77	0.012	0.944	0.015	0.905	0.944	0.012
97	T-4	9.93	6.49	0.013	0.992	0.013	0.992	0.992	0.013
98	T-5	12.34	7.13	0.014	0.990	0.014	0.990	0.990	0.014
99	T-6	11.71	6.24	0.015	0.999	0.018	0.999	0.999	0.015
100	T-7	10.82	7.26	0.011	0.988	0.012	0.985	0.988	0.011
101	T-8	12.22	7.51	0.012	0.977	0.016	0.962	0.977	0.012
102	T-9	12.85	6.49	0.013	0.988	0.013	0.989	0.989	0.013
103	T-10	12.98	10.18	0.016	0.989	0.017	0.988	0.989	0.016
104	T-11	11.20	6.62	0.012	0.968	0.011	0.971	0.971	0.011
105	T-12	13.23	8.40	0.012	0.986	0.013	0.985	0.986	0.012
106	T-13	11.83	7.51	0.012	0.989	0.014	0.974	0.989	0.012
107	T-14	11.20	9.55	0.014	0.988	0.013	0.988	0.988	0.014
108	T-16	10.56	8.02	0.013	0.983	0.014	0.977	0.983	0.013
109	T-17	9.67	8.40	0.015	0.983	0.015	0.983	0.983	0.015
110	T-18	10.31	7.77	0.014	0.996	0.016	0.995	0.996	0.014
111	T-19	13.11	7.89	0.012	0.962	0.012	0.981	0.981	0.012
112	T-20	9.42	8.28	0.014	0.997	0.014	0.997	0.997	0.014
113	T-21	10.43	7.26	0.012	0.993	0.013	0.993	0.993	0.012
114	T-22	13.11	9.80	0.011	0.991	0.011	0.991	0.991	0.011
115	T-23	12.72	8.15	0.011	0.974	0.011	0.975	0.975	0.011
116	T-24	17.56	8.40	0.012	0.933	0.012	0.933	0.933	0.012
117	T-25	12.09	7.77	0.012	0.963	0.012	0.964	0.964	0.012
118	T-26	12.72	7.26	0.012	0.995	0.012	0.995	0.995	0.012
119	T-28	12.72	9.42	0.014	0.963	0.014	0.964	0.964	0.014
120	T-29	13.49	7.13	0.013	0.946	0.014	0.958	0.958	0.014
121	T-30	12.34	7.26	0.011	0.950	0.012	0.942	0.950	0.011
122	T-31	11.83	7.89	0.014	0.924	0.014	0.930	0.930	0.014
123	T-32	15.01	9.29	0.013	0.979	0.017	0.964	0.979	0.013

No	Lesion ID	Width (mm)	Height (mm)	$S_{a,2}$ (mm)	$R_2^2$	$S_{a,3}$ (mm)	$R_3^2$	$R_{final}^2$	$\overline{S_{final}}$ (mm)
124	T-33	10.56	7.13	0.014	0.998	0.014	0.998	0.998	0.014
125	T-34	12.60	9.04	0.013	0.985	0.015	0.978	0.985	0.013
126	T-35	12.22	7.51	0.012	0.985	0.013	0.984	0.985	0.012
127	T-36	15.01	7.26	0.013	0.980	0.013	0.981	0.981	0.013
128	T-37	10.56	7.89	0.013	0.943	0.012	0.950	0.950	0.012
129	T-38	13.23	8.91	0.013	0.996	0.014	0.995	0.996	0.013
130	T-39	14.38	9.93	0.013	0.996	0.015	0.995	0.996	0.013
131	T-40	15.65	8.78	0.011	0.993	0.012	0.992	0.993	0.011
132	T-41	13.23	9.55	0.013	0.997	0.013	0.997	0.997	0.013
133	T-42	14.51	7.13	0.013	0.991	0.012	0.992	0.992	0.012
134	T-43	13.11	8.02	0.013	0.990	0.012	0.990	0.990	0.013
135	T-45	14.12	9.80	0.013	0.988	0.013	0.986	0.988	0.013
136	T-46	16.80	9.29	0.014	0.983	0.017	0.976	0.983	0.014
137	T-47	11.96	8.66	0.014	0.957	0.014	0.948	0.957	0.014
138	T-48	13.23	9.80	0.013	0.982	0.013	0.960	0.982	0.013
139	T-49	15.40	10.57	0.016	0.975	0.020	0.954	0.975	0.016
140	T-50	11.45	7.26	0.012	0.979	0.012	0.980	0.980	0.012
141	T-51	13.36	8.40	0.013	0.977	0.013	0.978	0.978	0.013
142	T-52	11.45	8.66	0.012	0.924	0.011	0.929	0.929	0.011
143	T-53	12.60	8.15	0.011	0.981	0.012	0.975	0.981	0.011
144	T-58	9.29	14.51	0.014	0.999	0.017	0.998	0.999	0.014
145	T-60	17.56	9.29	0.015	0.932	0.015	0.933	0.933	0.015
146	T-61	9.93	8.91	0.011	0.980	0.012	0.978	0.980	0.011
147	T-62	12.85	8.53	0.014	0.972	0.015	0.968	0.972	0.014
148	T-63	15.27	8.15	0.015	0.973	0.018	0.961	0.973	0.015
149	T-64	15.65	8.91	0.012	0.997	0.026	0.984	0.997	0.012
150	T-65	14.51	8.53	0.012	0.991	0.014	0.987	0.991	0.012
151	T-67	16.54	10.44	0.015	0.991	0.015	0.992	0.992	0.015
152	T-68	11.58	7.77	0.013	0.953	0.012	0.975	0.975	0.012
153	T-69	13.11	8.91	0.013	0.989	0.013	0.988	0.989	0.013
154	T-72	11.83	7.13	0.012	0.991	0.012	0.992	0.992	0.012
155	T-73	15.40	10.31	0.011	0.958	0.011	0.960	0.960	0.011
156	T-78	14.25	9.67	0.015	0.990	0.015	0.990	0.990	0.015
157	T-79	11.96	8.02	0.014	0.999	0.015	0.998	0.999	0.014
158	T-80	13.36	5.98	0.011	0.997	0.011	0.997	0.997	0.011
159	T-81	14.25	7.89	0.013	0.977	0.013	0.974	0.977	0.013
160	T-82	13.74	7.26	0.013	0.974	0.014	0.963	0.974	0.013
161	T-83	13.87	9.17	0.013	0.985	0.013	0.982	0.985	0.013
162	T-85	12.09	8.53	0.012	0.971	0.011	0.974	0.974	0.011
163	T-86	14.00	8.40	0.012	0.993	0.011	0.993	0.993	0.012
164	T-88	15.14	9.29	0.013	0.993	0.013	0.993	0.993	0.013
165	T-89	12.72	8.15	0.012	0.965	0.013	0.960	0.965	0.012
166	T-90	13.62	7.26	0.012	0.997	0.011	0.998	0.998	0.011

No	Lesion ID	Width (mm)	Height (mm)	$S_{a,2}$ (mm)	$R_2^2$	$S_{a,3}$ (mm)	$R_3^2$	$R_{final}^2$	$\overline{S}_{final}$ (mm)
167	T-91	15.01	9.04	0.012	0.996	0.013	0.996	0.996	0.012
168	T-92	15.14	8.27	0.013	0.995	0.014	0.995	0.995	0.013
169	T-93	14.38	9.80	0.014	0.977	0.014	0.977	0.977	0.014
170	T-94	14.38	8.53	0.013	0.955	0.013	0.953	0.955	0.013
171	T-95	10.82	7.89	0.015	0.988	0.014	0.989	0.989	0.014
172	T-96	12.22	7.64	0.012	0.947	0.013	0.954	0.954	0.013
173	T-98	11.83	7.89	0.013	0.998	0.018	0.997	0.998	0.013
174	T-99	9.42	7.26	0.014	0.984	0.013	0.986	0.986	0.013
175	T-101	9.03	5.47	0.011	0.991	0.012	0.991	0.991	0.011
176	T-102	11.45	8.27	0.014	0.996	0.014	0.996	0.996	0.014
177	T-104	13.23	8.91	0.012	0.988	0.013	0.987	0.988	0.012
178	T-105	11.32	7.38	0.015	0.975	0.016	0.970	0.975	0.015
179	T-107	10.05	6.24	0.015	0.966	0.016	0.959	0.966	0.015
180	T-108	14.38	7.13	0.014	0.970	0.014	0.967	0.970	0.014
181	T-109	12.34	6.62	0.013	0.993	0.014	0.992	0.993	0.013
182	T-110	16.80	7.38	0.015	0.996	0.016	0.996	0.996	0.015
183	T-111	10.82	5.22	0.015	0.994	0.016	0.994	0.994	0.015
184	T-114	13.23	7.38	0.014	0.962	0.015	0.955	0.962	0.014
185	T-118	13.49	8.53	0.014	0.982	0.016	0.975	0.982	0.014
186	T-124	9.03	4.58	0.014	0.999	0.016	0.999	0.999	0.014
187	T-127	9.54	6.36	0.014	0.992	0.014	0.992	0.992	0.014
188	T-128	6.74	8.02	0.014	0.998	0.014	0.998	0.998	0.014
189	T-131	12.34	5.98	0.015	0.998	0.015	0.998	0.998	0.015
190	T-132	15.14	8.40	0.015	0.969	0.014	0.984	0.984	0.014
191	T-133	10.43	8.02	0.016	0.967	0.016	0.967	0.967	0.016
192	T-134	11.07	7.13	0.014	0.995	0.014	0.995	0.995	0.014
193	T-135	7.00	8.40	0.015	0.981	0.015	0.980	0.981	0.015
194	T-136	13.36	6.87	0.013	0.993	0.013	0.993	0.993	0.013
195	T-137	13.11	7.38	0.014	0.999	0.014	0.999	0.999	0.014
196	T-138	13.36	8.53	0.015	0.998	0.015	0.998	0.998	0.015
197	T-139	11.32	7.13	0.015	0.998	0.016	0.998	0.998	0.015
198	T-143	10.05	6.75	0.013	0.995	0.013	0.995	0.995	0.013
199	T-146	9.29	9.29	0.015	0.993	0.015	0.993	0.993	0.015
200	T-147	12.85	6.49	0.013	0.993	0.014	0.991	0.993	0.013
201	T-150	10.18	5.22	0.013	0.990	0.014	0.990	0.990	0.013
202	T-151	9.80	5.73	0.015	0.976	0.015	0.974	0.976	0.015
203	T-156	7.89	4.07	0.014	0.992	0.014	0.992	0.992	0.014
204	T-158	8.78	3.95	0.014	0.974	0.014	0.973	0.974	0.014
205	T-159	10.05	4.33	0.011	0.936	0.012	0.923	0.936	0.011
206	T-160	9.67	4.96	0.013	0.964	0.013	0.962	0.964	0.013
207	T-161	9.03	4.71	0.014	0.924	0.014	0.927	0.927	0.014
208	T-163	10.18	4.97	0.012	0.976	0.014	0.970	0.976	0.012
209	T-165	10.69	5.98	0.015	0.985	0.015	0.985	0.985	0.015

No	Lesion ID	Width (mm)	Height (mm)	$S_{a,2}$ (mm)	$R_2^2$	$S_{a,3}$ (mm)	$R_3^2$	$R_{final}^2$	$\overline{S}_{final}$ (mm)
210	T-166	8.27	3.82	0.013	0.994	0.013	0.994	0.994	0.013
211	T-170	8.53	5.09	0.011	0.994	0.011	0.994	0.994	0.011
212	T-171	8.40	5.98	0.012	0.997	0.017	0.994	0.997	0.012
213	T-172	8.53	4.07	0.012	0.995	0.012	0.995	0.995	0.012
214	T-173	9.42	4.33	0.011	0.968	0.011	0.967	0.968	0.011
215	T-174	7.64	12.48	0.015	0.993	0.015	0.993	0.993	0.015
216	T-175	7.25	4.07	0.011	0.971	0.012	0.967	0.971	0.011
217	T-176	8.65	3.95	0.012	0.939	0.013	0.932	0.939	0.012
218	T-178	10.05	4.97	0.012	0.942	0.014	0.918	0.942	0.012
219	T-182	8.65	4.71	0.013	0.961	0.013	0.957	0.961	0.013
220	T-183	9.16	8.40	0.013	0.987	0.015	0.983	0.987	0.013
221	T-185	8.14	3.82	0.014	0.984	0.014	0.983	0.984	0.014
222	T-187	8.14	3.95	0.013	0.997	0.017	0.995	0.997	0.013
223	T-188	7.51	4.07	0.013	0.993	0.016	0.990	0.993	0.013
224	T-189	7.51	4.96	0.011	0.968	0.012	0.964	0.968	0.011
225	T-190	11.45	6.62	0.013	0.990	0.013	0.990	0.990	0.013
226	T-191	8.53	5.09	0.014	0.933	0.014	0.926	0.933	0.014
227	T-193	10.69	3.69	0.013	0.953	0.013	0.951	0.953	0.013
228	T-197	10.31	4.46	0.014	0.993	0.014	0.993	0.993	0.014
229	T-199	15.40	6.49	0.013	0.999	0.014	0.998	0.999	0.013
230	T-200	17.18	6.49	0.014	0.998	0.013	0.998	0.998	0.014
231	T-201	13.49	7.13	0.013	0.995	0.015	0.994	0.995	0.013
232	T-202	12.60	6.37	0.011	0.997	0.013	0.996	0.997	0.011
233	T-203	13.23	6.24	0.011	0.998	0.013	0.997	0.998	0.011
234	T-204	15.14	6.11	0.014	0.998	0.014	0.998	0.998	0.014
235	T-205	16.16	7.00	0.014	0.991	0.014	0.990	0.991	0.014
236	T-207	14.89	7.00	0.013	0.998	0.013	0.998	0.998	0.013
237	T-208	12.72	6.24	0.014	0.996	0.013	0.997	0.997	0.013
238	T-209	14.00	6.87	0.013	0.994	0.014	0.993	0.994	0.013
239	T-210	13.74	6.62	0.012	0.950	0.012	0.951	0.951	0.012
240	T-211	11.45	5.60	0.012	0.993	0.012	0.993	0.993	0.012
241	T-212	13.36	7.13	0.015	0.989	0.014	0.990	0.990	0.014
242	T-213	12.72	6.87	0.014	0.998	0.014	0.998	0.998	0.014
243	T-214	11.07	10.31	0.014	0.997	0.013	0.997	0.997	0.014
244	T-215	14.12	7.51	0.015	0.997	0.014	0.997	0.997	0.015
245	T-216	12.85	6.62	0.013	0.995	0.013	0.995	0.995	0.013
246	T-218	10.56	3.82	0.013	0.922	0.012	0.928	0.928	0.012
247	T-219	9.80	4.20	0.013	0.990	0.013	0.990	0.990	0.013
248	T-220	5.47	5.98	0.014	0.968	0.014	0.968	0.968	0.014
249	T-221	10.69	5.86	0.014	0.987	0.015	0.985	0.987	0.014
250	T-222	10.05	5.86	0.014	0.994	0.014	0.994	0.994	0.014
251	T-223	5.85	6.11	0.014	0.992	0.014	0.992	0.992	0.014
252	T-224	10.18	5.47	0.013	0.998	0.013	0.998	0.998	0.013

No	Lesion ID	Width (mm)	Height (mm)	$S_{a,2}$ (mm)	$R_2^2$	$S_{a,3}$ (mm)	$R_3^2$	$R_{final}^2$	$\overline{S}_{final}$ (mm)
253	L-2	9.29	12.48	0.012	0.982	0.014	0.984	0.984	0.014
254	L-3	9.54	4.46	0.014	0.967	0.015	0.959	0.967	0.014
255	L-4	9.42	9.42	0.016	0.970	0.018	0.965	0.970	0.016
256	L-7	10.18	5.73	0.013	0.959	0.014	0.950	0.959	0.013
257	L-8	9.67	14.51	0.011	0.970	0.011	0.975	0.975	0.011
258	L-10	9.42	4.07	0.013	0.960	0.014	0.956	0.960	0.013
259	L-11	9.42	4.46	0.014	0.949	0.015	0.942	0.949	0.014
260	L-13	9.54	5.60	0.014	0.986	0.014	0.986	0.986	0.014
261	L-14	9.67	5.35	0.015	0.918	0.015	0.913	0.918	0.015
262	L-18	8.40	15.53	0.015	0.983	0.020	0.970	0.983	0.015
263	L-19	10.05	5.73	0.012	0.952	0.013	0.954	0.954	0.013
264	L-20	9.16	5.35	0.012	0.920	0.012	0.913	0.920	0.012
265	L-21	9.54	4.96	0.014	0.954	0.016	0.946	0.954	0.014
266	L-22	8.40	4.97	0.013	0.978	0.015	0.970	0.978	0.013
267	L-23	9.92	4.33	0.012	0.963	0.014	0.966	0.966	0.014
268	L-24	8.91	5.22	0.011	0.988	0.014	0.980	0.988	0.011
269	L-25	8.91	4.96	0.012	0.987	0.013	0.983	0.987	0.012
270	L-28	9.54	16.80	0.016	0.954	0.019	0.934	0.954	0.016
271	L-29	9.93	16.68	0.016	0.971	0.016	0.971	0.971	0.016
272	L-30	9.42	5.60	0.014	0.955	0.019	0.913	0.955	0.014
273	L-31	9.42	14.13	0.015	0.965	0.015	0.973	0.973	0.015
274	L-32	10.05	5.09	0.014	0.958	0.015	0.947	0.958	0.014
275	L-36	9.03	4.46	0.015	0.953	0.016	0.943	0.953	0.015
276	L-37	9.29	4.33	0.015	0.965	0.017	0.952	0.965	0.015
277	L-38	9.67	4.33	0.011	0.994	0.015	0.987	0.994	0.011
278	L-39	9.80	4.96	0.013	0.978	0.014	0.974	0.978	0.013
279	L-41	10.05	5.22	0.015	0.944	0.017	0.932	0.944	0.015
280	L-42	10.43	4.07	0.013	0.962	0.013	0.961	0.962	0.013
281	L-43	9.29	5.09	0.013	0.943	0.013	0.937	0.943	0.013
282	L-44	10.05	5.47	0.012	0.960	0.014	0.945	0.960	0.012
283	L-45	10.18	4.84	0.013	0.941	0.015	0.938	0.941	0.013
284	L-46	8.53	4.46	0.014	0.976	0.014	0.975	0.976	0.014
285	L-51	9.80	5.22	0.011	0.974	0.012	0.970	0.974	0.011
286	L-52	9.42	5.22	0.015	0.942	0.017	0.929	0.942	0.015
287	L-53	9.16	5.22	0.012	0.944	0.012	0.950	0.950	0.012
288	L-58	9.03	5.22	0.014	0.921	0.014	0.923	0.923	0.014
289	L-59	8.40	5.35	0.015	0.934	0.016	0.928	0.934	0.015
290	L-69	9.16	5.98	0.012	0.918	0.012	0.917	0.918	0.012
291	L-70	10.18	6.11	0.015	0.935	0.015	0.930	0.935	0.015
292	L-73	8.65	4.58	0.012	0.939	0.012	0.944	0.944	0.012
293	L-74	8.91	4.71	0.012	0.989	0.012	0.990	0.990	0.012
294	L-75	9.03	4.58	0.012	0.996	0.012	0.996	0.996	0.012
295	L-76	9.03	5.47	0.013	0.918	0.014	0.903	0.918	0.013

No	Lesion ID	Width (mm)	Height (mm)	$S_{a,2}$ (mm)	$R_2^2$	$S_{a,3}$ (mm)	$R_3^2$	$R_{final}^2$	$S_{final}$ (mm)
296	L-78	8.02	4.46	0.013	0.974	0.014	0.969	0.974	0.013
297	L-80	8.65	5.86	0.015	0.930	0.016	0.919	0.930	0.015
298	L-85	8.91	4.46	0.014	0.936	0.015	0.958	0.958	0.015
299	L-88	9.29	4.58	0.013	0.983	0.015	0.977	0.983	0.013
300	L-89	11.83	5.60	0.013	0.982	0.013	0.982	0.982	0.013
301	L-90	11.58	5.73	0.014	0.995	0.014	0.995	0.995	0.014
302	L-92	10.69	4.97	0.014	0.978	0.014	0.977	0.978	0.014
303	L-93	9.93	4.33	0.013	0.988	0.013	0.987	0.988	0.013
304	L-94	8.65	4.84	0.012	0.972	0.013	0.964	0.972	0.012
305	L-95	10.05	4.97	0.013	0.966	0.013	0.966	0.966	0.013
306	L-96	8.40	4.84	0.015	0.932	0.015	0.932	0.932	0.015
307	L-97	8.53	5.22	0.012	0.947	0.012	0.961	0.961	0.012
308	L-98	9.16	5.22	0.014	0.981	0.014	0.981	0.981	0.014
309	L-99	9.42	4.46	0.012	0.963	0.012	0.963	0.963	0.012
310	L-100	10.56	6.11	0.015	0.903	0.014	0.910	0.910	0.014
311	L-101	8.40	5.47	0.016	0.945	0.016	0.946	0.946	0.016
312	L-103	6.49	4.07	0.011	0.968	0.011	0.968	0.968	0.011
313	L-104	8.65	5.98	0.013	0.962	0.013	0.962	0.962	0.013
314	L-105	8.27	5.22	0.013	0.986	0.013	0.987	0.987	0.013
315	L-106	9.03	12.86	0.013	0.958	0.013	0.959	0.959	0.013
316	L-107	10.05	5.60	0.013	0.935	0.014	0.917	0.935	0.013
317	L-108	9.16	6.11	0.011	0.944	0.011	0.946	0.946	0.011
318	L-109	9.93	6.37	0.012	0.924	0.012	0.926	0.926	0.012
319	L-111	9.16	5.47	0.012	0.929	0.013	0.924	0.929	0.012
320	L-117	9.54	6.37	0.014	0.996	0.014	0.996	0.996	0.014
321	L-118	9.29	6.75	0.014	0.983	0.015	0.982	0.983	0.014
322	L-123	10.05	5.47	0.014	0.987	0.013	0.988	0.988	0.013
323	L-125	8.91	6.24	0.015	0.989	0.015	0.988	0.989	0.015
324	L-127	9.29	4.96	0.012	0.971	0.011	0.972	0.972	0.011
325	L-128	9.80	5.86	0.014	0.998	0.015	0.998	0.998	0.014
326	L-130	9.54	6.24	0.012	0.983	0.013	0.977	0.983	0.012
327	L-131	9.67	5.86	0.013	0.934	0.015	0.924	0.934	0.013
328	L-135	10.43	5.09	0.014	0.946	0.013	0.966	0.966	0.013
329	L-137	6.62	2.80	0.012	0.990	0.012	0.990	0.990	0.012
330	L-139	9.80	4.46	0.013	0.993	0.013	0.993	0.993	0.013
331	L-140	9.80	4.84	0.012	0.990	0.012	0.989	0.990	0.012
332	L-143	9.67	6.36	0.015	0.928	0.015	0.915	0.928	0.015
333	L-144	10.18	16.04	0.016	0.996	0.023	0.991	0.996	0.016
334	L-145	10.18	5.22	0.014	0.948	0.015	0.941	0.948	0.014
335	L-147	10.56	5.09	0.013	0.953	0.013	0.963	0.963	0.013
336	L-151	9.80	5.60	0.013	0.965	0.016	0.946	0.965	0.013
337	L-152	8.65	6.62	0.014	0.982	0.016	0.978	0.982	0.014
338	L-153	9.16	6.24	0.012	0.975	0.015	0.963	0.975	0.012

No	Lesion ID	Width (mm)	Height (mm)	$S_{a,2}$ (mm)	$R_2^2$	$S_{a,3}$ (mm)	$R_3^2$	$R_{final}^2$	$\bar{S}_{final}$ (mm)
339	L-156	9.42	5.98	0.014	0.942	0.016	0.929	0.942	0.014
340	L-158	8.91	4.33	0.013	0.988	0.017	0.982	0.988	0.013
341	L-160	10.82	5.60	0.015	0.996	0.015	0.996	0.996	0.015
342	L-162	10.43	4.96	0.013	0.992	0.015	0.989	0.992	0.013
343	L-164	10.05	5.22	0.012	0.971	0.015	0.958	0.971	0.012
344	L-165	9.54	4.71	0.015	0.954	0.016	0.948	0.954	0.015
345	L-166	9.67	5.86	0.012	0.982	0.014	0.975	0.982	0.012
346	L-172	8.91	5.73	0.011	0.986	0.011	0.986	0.986	0.011
347	L-173	10.56	5.86	0.013	0.957	0.013	0.957	0.957	0.013
348	L-174	11.71	17.31	0.015	0.987	0.015	0.988	0.988	0.015
349	L-175	16.29	6.87	0.012	0.985	0.019	0.963	0.985	0.012
350	L-176	11.07	5.35	0.014	0.948	0.014	0.951	0.951	0.014
351	L-180	9.54	5.60	0.015	0.994	0.015	0.994	0.994	0.015
352	L-181	9.03	5.47	0.014	0.992	0.014	0.991	0.992	0.014
353	L-183	9.29	5.35	0.013	0.974	0.015	0.963	0.974	0.013
354	L-184	9.93	5.98	0.014	0.974	0.016	0.964	0.974	0.014
355	L-186	9.54	5.47	0.013	0.981	0.014	0.977	0.981	0.013
356	L-187	9.80	16.80	0.014	0.987	0.018	0.970	0.987	0.014
357	L-188	10.05	5.73	0.012	0.977	0.011	0.978	0.978	0.011
358	L-190	9.42	5.73	0.011	0.984	0.012	0.979	0.984	0.011
359	L-191	9.42	4.71	0.012	0.987	0.013	0.984	0.987	0.012
360	L-192	8.02	6.62	0.013	0.937	0.014	0.945	0.945	0.014
361	L-193	10.05	5.98	0.013	0.969	0.014	0.964	0.969	0.013
362	L-194	10.18	16.55	0.012	0.987	0.016	0.980	0.987	0.012
363	L-195	9.67	5.09	0.014	0.926	0.014	0.926	0.926	0.014
364	L-196	9.54	4.33	0.015	0.927	0.014	0.930	0.930	0.014
365	L-197	9.93	4.97	0.012	0.979	0.014	0.971	0.979	0.012
366	L-198	8.78	4.96	0.011	0.959	0.011	0.961	0.961	0.011
367	L-199	9.93	4.96	0.011	0.992	0.015	0.981	0.992	0.011
368	L-201	7.89	3.69	0.015	0.906	0.015	0.905	0.906	0.015
369	L-202	9.42	14.38	0.015	0.969	0.015	0.965	0.969	0.015
370	L-203	8.14	4.96	0.012	0.918	0.012	0.916	0.918	0.012
371	L-204	8.53	5.73	0.013	0.952	0.013	0.952	0.952	0.013
372	L-205	9.93	5.98	0.015	0.961	0.015	0.960	0.961	0.015
373	L-211	7.76	3.44	0.013	0.998	0.014	0.998	0.998	0.013
374	L-213	8.91	5.09	0.015	0.974	0.016	0.969	0.974	0.015
375	L-215	9.16	6.24	0.011	0.903	0.011	0.903	0.903	0.011
376	L-217	9.42	14.51	0.011	0.940	0.012	0.944	0.944	0.012
377	L-218	10.56	5.09	0.013	0.959	0.013	0.959	0.959	0.013
378	L-219	8.78	4.20	0.014	0.941	0.015	0.936	0.941	0.014
379	L-221	10.82	4.71	0.012	0.942	0.013	0.931	0.942	0.012
380	L-222	10.56	4.20	0.011	0.956	0.011	0.957	0.957	0.011
381	L-223	8.91	4.71	0.013	0.965	0.013	0.963	0.965	0.013

No	Lesion ID	Width (mm)	Height (mm)	$S_{a,2}$ (mm)	$R_2^2$	$S_{a,3}$ (mm)	$R_3^2$	$R_{final}^2$	$\overline{S_{final}}$ (mm)
382	L-224	10.56	4.58	0.015	0.979	0.015	0.979	0.979	0.015
383	L-226	9.29	3.82	0.013	0.998	0.017	0.996	0.998	0.013
384	L-227	9.93	4.07	0.013	0.987	0.012	0.989	0.989	0.012
385	L-228	8.02	3.95	0.012	0.998	0.012	0.998	0.998	0.012
386	L-229	8.53	4.58	0.014	0.996	0.014	0.996	0.996	0.014
387	L-231	9.54	5.22	0.012	0.991	0.012	0.991	0.991	0.012
388	L-233	10.94	7.64	0.014	0.998	0.014	0.998	0.998	0.014
389	L-236	11.32	3.69	0.014	0.992	0.015	0.989	0.992	0.014
390	L-237	14.51	6.87	0.014	0.996	0.014	0.996	0.996	0.014

## APPENDIX C: TRAINING DATASET OF PSORIASIS LESION

No	Patient	Age	Gender	Region	Width (mm)	Height (mm)	$S_{a,2}$ (mm)	$R_2^2$	$S_{a,3}$ (mm)	$R_3^2$	$R_{final}^2$	$S_{final}$ (mm)
1	P-4-MOH	36	M	H1	12.86	17.69	0.031	0.967	0.033	0.967	0.967	0.033
2	P-4-MOH	36	M	T1	16.43	19.22	0.036	0.939	0.038	0.930	0.939	0.036
3	P-4-MOH	36	M	T2	9.17	10.44	0.041	0.960	0.041	0.961	0.961	0.041
4	P-4-MOH	36	M	U2	6.50	10.05	0.018	0.997	0.016	0.998	0.998	0.016
5	P-5-IBR	69	M	U3	6.75	7.13	0.026	0.926	0.028	0.918	0.926	0.026
6	P-6-AZI	32	M	H1	9.30	7.38	0.049	0.978	0.049	0.978	0.978	0.049
7	P-6-AZI	32	M	L1	12.86	12.09	0.052	0.964	0.052	0.963	0.964	0.052
8	P-6-AZI	32	M	T1	13.88	7.51	0.058	0.950	0.052	0.941	0.950	0.058
9	P-6-AZI	32	M	U1	11.72	7.76	0.035	0.977	0.037	0.975	0.977	0.035
10	P-6-AZI	32	M	U2	13.50	12.60	0.054	0.779	0.043	0.915	0.915	0.043
11	P-6-AZI	32	M	U3	8.79	7.51	0.046	0.954	0.045	0.954	0.954	0.045
12	P-7-SIV	40	M	L2	10.44	10.31	0.030	0.904	0.027	0.920	0.920	0.027
13	P-7-SIV	40	M	L3	6.37	6.75	0.036	0.916	0.037	0.914	0.916	0.036
14	P-7-SIV	40	M	T1	6.62	6.87	0.029	0.969	0.029	0.968	0.969	0.029
15	P-7-SIV	40	M	T2	7.39	7.89	0.044	0.901	0.046	0.857	0.901	0.044
16	P-7-SIV	40	M	T3	6.88	7.13	0.024	0.964	0.020	0.976	0.976	0.020
17	P-8-SUN	62	M	H1	4.97	5.85	0.020	0.924	0.020	0.924	0.924	0.020
18	P-8-SUN	62	M	L2	7.52	7.25	0.025	0.964	0.027	0.954	0.964	0.025
19	P-8-SUN	62	M	L3	6.88	4.96	0.025	0.928	0.025	0.928	0.928	0.025
20	P-8-SUN	62	M	T1	14.14	13.11	0.035	0.984	0.036	0.984	0.984	0.036
21	P-8-SUN	62	M	T3	5.73	4.71	0.020	0.949	0.020	0.949	0.949	0.020
22	P-8-SUN	62	M	U1	2.93	3.44	0.020	0.908	0.022	0.911	0.911	0.022
23	P-8-SUN	62	M	U3	3.95	3.69	0.019	0.932	0.019	0.932	0.932	0.019
24	P-9-MOH	60	M	L12	12.74	14.25	0.065	0.955	0.061	0.961	0.961	0.061
25	P-9-MOH	60	M	L2	16.05	17.05	0.041	0.985	0.038	0.987	0.987	0.038
26	P-9-MOH	60	M	T1	16.56	15.53	0.045	0.976	0.045	0.975	0.976	0.045
27	P-9-MOH	60	M	T2	12.23	12.34	0.040	0.967	0.042	0.951	0.967	0.040
28	P-9-MOH	60	M	T3	16.17	14.38	0.096	0.945	0.092	0.950	0.950	0.092
29	P-9-MOH	60	M	U1	7.26	13.87	0.032	0.969	0.029	0.955	0.969	0.032
30	P-9-MOH	60	M	U2	7.90	13.75	0.038	0.980	0.039	0.978	0.980	0.038
31	P-9-MOH	60	M	U3	11.85	11.45	0.042	0.983	0.040	0.985	0.985	0.040
32	P-10-MUH	28	M	H1	9.55	9.29	0.038	0.950	0.037	0.948	0.950	0.038
33	P-10-MUH	28	M	L12	6.24	11.96	0.072	0.969	0.069	0.972	0.972	0.069
34	P-10-MUH	28	M	L3	9.55	12.85	0.051	0.976	0.051	0.975	0.976	0.051
35	P-10-MUH	28	M	T2	5.48	4.20	0.037	0.908	0.037	0.907	0.908	0.037
36	P-10-MUH	28	M	T4	16.05	15.40	0.077	0.967	0.070	0.972	0.972	0.070
37	P-10-MUH	28	M	U2	4.71	8.53	0.026	0.920	0.025	0.928	0.928	0.025
38	P-11-THA	43	F	H	10.32	13.24	0.023	0.977	0.024	0.975	0.977	0.023
39	P-11-THA	43	F	L1	4.20	5.60	0.016	0.933	0.016	0.936	0.936	0.016
40	P-11-THA	43	F	L3	4.84	5.50	0.024	0.959	0.024	0.959	0.959	0.024

No	Patient	Age	Gender	Region	Width (mm)	Height (mm)	$S_{a,2}$ (mm)	$R_2^2$	$S_{a,3}$ (mm)	$R_3^2$	$R_{final}^2$	$\overline{S_{final}}$ (mm)
41	P-11-THA	43	F	T1	11.08	8.66	0.058	0.912	0.052	0.907	0.912	0.058
42	P-11-THA	43	F	T2	7.51	5.09	0.026	0.965	0.025	0.966	0.966	0.025
43	P-11-THA	43	F	T3	6.62	10.05	0.026	0.950	0.024	0.956	0.956	0.024
44	P-11-THA	43	F	U1	8.28	9.93	0.030	0.958	0.029	0.960	0.960	0.029
45	P-11-THA	43	F	U2	5.09	5.47	0.028	0.974	0.026	0.977	0.977	0.026
46	P-11-THA	43	F	U3	7.90	11.58	0.029	0.986	0.030	0.986	0.986	0.030
47	P-12-YEE	57	M	L2	10.95	7.26	0.043	0.952	0.042	0.953	0.953	0.042
48	P-12-YEE	57	M	L3	7.39	11.96	0.035	0.956	0.033	0.962	0.962	0.033
49	P-12-YEE	57	M	T2	9.17	6.62	0.026	0.978	0.027	0.976	0.978	0.026
50	P-12-YEE	57	M	T3	7.64	5.60	0.035	0.909	0.046	0.786	0.909	0.035
51	P-12-YEE	57	M	U3	5.09	5.09	0.016	0.981	0.015	0.982	0.982	0.015
52	P-13-ABD	60	M	T1	6.24	8.27	0.039	0.938	0.039	0.938	0.938	0.039
53	P-13-ABD	60	M	T2	5.60	6.11	0.015	0.943	0.015	0.943	0.943	0.015
54	P-13-ABD	60	M	T4	21.14	26.98	0.059	0.970	0.065	0.962	0.970	0.059
55	P-13-ABD	60	M	U3	8.15	5.34	0.041	0.850	0.034	0.921	0.921	0.034
56	P-14-FAT	60	F	H2	5.73	5.98	0.028	0.933	0.028	0.934	0.934	0.028
57	P-14-FAT	60	F	L2	7.00	4.33	0.027	0.959	0.026	0.961	0.961	0.026
58	P-14-FAT	60	F	T2	5.35	5.09	0.028	0.930	0.027	0.933	0.933	0.027
59	P-14-FAT	60	F	U1	3.82	4.46	0.019	0.947	0.018	0.952	0.952	0.018
60	P-14-FAT	60	F	U2	4.97	4.45	0.021	0.964	0.021	0.964	0.964	0.021
61	P-14-FAT	60	F	U3	4.97	4.20	0.020	0.960	0.018	0.966	0.966	0.018
62	P-15-AIZ	37	M	L1	6.37	10.05	0.029	0.926	0.029	0.923	0.926	0.029
63	P-15-AIZ	37	M	T1	5.48	12.60	0.032	0.983	0.031	0.984	0.984	0.031
64	P-15-AIZ	37	M	T2	11.21	7.64	0.035	0.944	0.035	0.943	0.944	0.035
65	P-15-AIZ	37	M	U2	4.59	5.22	0.019	0.912	0.018	0.915	0.915	0.018
66	P-15-AIZ	37	M	U3	5.09	5.85	0.030	0.906	0.030	0.903	0.906	0.030
67	P-16-AZH	47	M	U2	5.22	6.87	0.048	0.906	0.049	0.904	0.906	0.048
68	P-16-AZH	47	M	T1	4.46	6.24	0.017	0.945	0.017	0.945	0.945	0.017
69	P-16-AZH	47	M	L1	5.86	8.40	0.032	0.926	0.034	0.933	0.933	0.034
70	P-16-AZH	47	M	L2	4.46	5.85	0.019	0.973	0.020	0.973	0.973	0.020
71	P-17-MUH	22	M	U1	11.84	12.86	0.028	0.981	0.028	0.981	0.981	0.028
72	P-17-MUH	22	M	U2	12.48	14.25	0.022	0.958	0.021	0.960	0.960	0.021
73	P-17-MUH	22	M	U3	10.44	10.05	0.036	0.969	0.037	0.968	0.969	0.036
74	P-17-MUH	22	M	T3	8.41	8.53	0.031	0.925	0.030	0.930	0.930	0.030
75	P-17-MUH	22	M	L1	10.19	16.80	0.034	0.987	0.034	0.984	0.987	0.034
76	P-17-MUH	22	M	L2	15.03	13.75	0.080	0.960	0.078	0.961	0.961	0.078
77	P-17-MUH	22	M	L3	11.84	16.55	0.035	0.988	0.035	0.988	0.988	0.035
78	P-17-MUH	22	M	L4	29.55	22.91	0.040	0.977	0.042	0.991	0.991	0.042
79	P-17-MUH	22	M	L5	18.98	21.38	0.038	0.987	0.038	0.987	0.987	0.038
80	P-18-SID	41	M	U2	5.22	5.85	0.028	0.951	0.028	0.952	0.952	0.028
81	P-18-SID	41	M	U3	6.62	6.87	0.031	0.921	0.031	0.918	0.921	0.031
82	P-18-SID	41	M	T3	5.73	7.89	0.034	0.934	0.033	0.936	0.936	0.033
83	P-18-SID	41	M	L1	11.59	10.06	0.025	0.967	0.025	0.968	0.968	0.025
84	P-18-SID	41	M	L2	8.66	11.20	0.029	0.969	0.028	0.970	0.970	0.028

No	Patient	Age	Gender	Region	Width (mm)	Height (mm)	$S_{a,2}$ (mm)	$R_2^2$	$S_{a,3}$ (mm)	$R_3^2$	$R_{final}^2$	$\overline{S}_{final}$ (mm)
85	P-19-NUR	19	F	H1	6.88	12.35	0.027	0.953	0.029	0.947	0.953	0.027
86	P-19-NUR	19	F	U1	7.77	10.82	0.039	0.946	0.043	0.937	0.946	0.039
87	P-19-NUR	19	F	U2	8.79	11.96	0.040	0.949	0.039	0.951	0.951	0.039
88	P-19-NUR	19	F	U3	11.85	15.40	0.057	0.951	0.059	0.947	0.951	0.057
89	P-19-NUR	19	F	T1	11.84	10.82	0.041	0.980	0.041	0.980	0.980	0.041
90	P-19-NUR	19	F	T2	11.08	9.42	0.040	0.981	0.040	0.981	0.981	0.040
91	P-19-NUR	19	F	T3	8.79	8.02	0.042	0.950	0.041	0.954	0.954	0.041
92	P-19-NUR	19	F	L1	9.30	13.11	0.036	0.993	0.036	0.993	0.993	0.036
93	P-19-NUR	19	F	L2	8.79	11.20	0.035	0.956	0.034	0.958	0.958	0.034
94	P-19-NUR	19	F	L3	6.88	8.65	0.022	0.970	0.022	0.973	0.973	0.022
95	P-20-MOH	34	M	U3	34.64	13.75	0.079	0.961	0.078	0.962	0.962	0.078
96	P-20-MOH	34	M	T1	20.89	16.80	0.078	0.948	0.076	0.950	0.950	0.076
97	P-20-MOH	34	M	T3	13.12	10.82	0.051	0.967	0.048	0.970	0.970	0.048
98	P-20-MOH	34	M	T5	23.94	21.00	0.115	0.967	0.120	0.964	0.967	0.115
99	P-20-MOH	34	M	T6	37.95	28.38	0.136	0.964	0.148	0.954	0.964	0.136
100	P-20-MOH	34	M	T7	9.93	7.25	0.076	0.958	0.063	0.953	0.958	0.076
101	P-20-MOH	34	M	L1	19.10	16.04	0.131	0.931	0.131	0.933	0.933	0.131
102	P-20-MOH	34	M	L2	37.19	13.24	0.125	0.941	0.116	0.923	0.941	0.125
103	P-20-MOH	34	M	L3	7.00	8.78	0.030	0.980	0.027	0.966	0.980	0.030
104	P-21-ZAI	62	M	U1	13.25	11.58	0.049	0.941	0.044	0.956	0.956	0.044
105	P-21-ZAI	62	M	U3	6.11	6.74	0.029	0.948	0.030	0.947	0.948	0.029
106	P-21-ZAI	62	M	T1	25.47	21.89	0.036	0.996	0.032	0.997	0.997	0.032
107	P-21-ZAI	62	M	T2	13.25	12.85	0.038	0.960	0.035	0.963	0.963	0.035
108	P-21-ZAI	62	M	T3	25.35	7.51	0.067	0.962	0.070	0.960	0.962	0.067
109	P-21-ZAI	62	M	L1	6.62	11.20	0.028	0.985	0.028	0.985	0.985	0.028
110	P-21-ZAI	62	M	L2	20.38	17.82	0.041	0.990	0.042	0.990	0.990	0.042
111	P-21-ZAI	62	M	L3	15.67	19.22	0.029	0.963	0.027	0.968	0.968	0.027
112	P-22-MOH	38	M	U1	20.76	17.44	0.050	0.968	0.051	0.968	0.968	0.051
113	P-22-MOH	38	M	L4	34.26	27.74	0.045	0.975	0.050	0.972	0.975	0.045
114	P-22-MOH	38	M	L5	30.44	27.49	0.032	0.976	0.046	0.987	0.987	0.046
115	P-22-MOH	38	M	L6	31.08	26.35	0.032	0.982	0.042	0.990	0.990	0.042
116	P-24-KAM	60	M	U1	8.28	12.22	0.036	0.965	0.036	0.965	0.965	0.036
117	P-24-KAM	60	M	T1	9.43	10.56	0.026	0.965	0.026	0.963	0.965	0.026
118	P-24-KAM	60	M	T2	9.17	12.98	0.026	0.978	0.025	0.979	0.979	0.025
119	P-24-KAM	60	M	T3	17.83	13.75	0.035	0.971	0.034	0.973	0.973	0.034
120	P-25-RAB	74	F	U1	8.66	5.98	0.019	0.985	0.019	0.985	0.985	0.019
121	P-25-RAB	74	F	T4	35.79	28.25	0.051	0.913	0.056	0.736	0.913	0.051
122	P-25-RAB	74	F	T2	18.09	11.58	0.026	0.991	0.025	0.992	0.992	0.025
123	P-25-RAB	74	F	L2	10.06	5.73	0.031	0.924	0.030	0.928	0.928	0.030
124	P-25-RAB	74	F	L3	12.35	12.34	0.071	0.917	0.071	0.917	0.917	0.071
125	P-26-SAM	44	M	U1	4.33	3.95	0.033	0.953	0.032	0.954	0.954	0.032
126	P-26-SAM	44	M	U2	2.29	2.93	0.018	0.923	0.018	0.923	0.923	0.018
127	P-26-SAM	44	M	U3	4.33	4.45	0.015	0.925	0.015	0.928	0.928	0.015
128	P-26-SAM	44	M	T2	5.22	5.73	0.025	0.917	0.027	0.931	0.931	0.027

No	Patient	Age	Gender	Region	Width (mm)	Height (mm)	$S_{a,2}$ (mm)	$R_2^2$	$S_{a,3}$ (mm)	$R_3^2$	$R_{final}^2$	$\overline{S}_{final}$ (mm)
129	P-26-SAM	44	M	L2	23.05	24.18	0.051	0.976	0.055	0.985	0.985	0.055
130	P-26-SAM	44	M	L3	7.26	8.15	0.023	0.941	0.023	0.942	0.942	0.023
131	P-27-ROH	27	F	H1	6.88	9.29	0.025	0.984	0.024	0.985	0.985	0.024
132	P-27-ROH	27	F	U1	4.84	5.73	0.033	0.964	0.034	0.963	0.964	0.033
133	P-27-ROH	27	F	U2	3.06	3.56	0.024	0.920	0.023	0.926	0.926	0.023
134	P-27-ROH	27	F	U3	4.58	5.47	0.026	0.946	0.026	0.946	0.946	0.026
135	P-27-ROH	27	F	T1	3.44	3.95	0.026	0.952	0.026	0.933	0.952	0.026
136	P-27-ROH	27	F	L1	8.02	8.65	0.025	0.960	0.023	0.965	0.965	0.023
137	P-27-ROH	27	F	L2	3.44	3.82	0.016	0.951	0.015	0.956	0.956	0.015
138	P-27-ROH	27	F	L3	6.62	2.93	0.031	0.937	0.031	0.937	0.937	0.031
139	P-28-MAR	52	M	U2	12.86	13.24	0.068	0.921	0.068	0.921	0.921	0.068
140	P-28-MAR	52	M	T1	9.93	9.42	0.047	0.911	0.047	0.913	0.913	0.047
141	P-28-MAR	52	M	T2	3.69	4.84	0.025	0.924	0.025	0.925	0.925	0.025
142	P-28-MAR	52	M	L2	20.63	16.67	0.036	0.978	0.033	0.979	0.979	0.033
143	P-28-MAR	52	M	L3	18.60	18.84	0.049	0.965	0.051	0.961	0.965	0.049
144	P-28-MAR	52	M	L5	24.84	27.87	0.044	0.989	0.046	0.986	0.989	0.044
145	P-29-BAK	39	M	U3	10.44	10.05	0.031	0.955	0.030	0.955	0.955	0.030
146	P-29-BAK	39	M	L1	9.93	9.29	0.044	0.938	0.044	0.939	0.939	0.044
147	P-29-BAK	39	M	L2	17.96	8.02	0.040	0.950	0.042	0.935	0.950	0.040
148	P-29-BAK	39	M	L4	11.72	14.89	0.032	0.960	0.032	0.960	0.960	0.032
149	P-30-CHE	27	M	H1	4.97	6.24	0.023	0.984	0.023	0.984	0.984	0.023
150	P-30-CHE	27	M	U1	14.65	8.15	0.052	0.939	0.045	0.920	0.939	0.052
151	P-30-CHE	27	M	T1	18.21	13.87	0.054	0.975	0.053	0.975	0.975	0.053
152	P-30-CHE	27	M	T2	17.96	11.84	0.037	0.936	0.033	0.948	0.948	0.033
153	P-30-CHE	27	M	T3	25.22	15.27	0.077	0.923	0.077	0.924	0.924	0.077
154	P-30-CHE	27	M	T4	14.14	26.22	0.048	0.910	0.049	0.906	0.910	0.048
155	P-30-CHE	27	M	T5	24.07	13.24	0.059	0.950	0.059	0.951	0.951	0.059
156	P-30-CHE	27	M	L1	22.42	23.80	0.040	0.986	0.042	0.984	0.986	0.040
157	P-30-CHE	27	M	L32	16.30	26.73	0.051	0.960	0.050	0.961	0.961	0.050
158	P-31-CHE	32	F	H1	11.08	10.18	0.061	0.920	0.061	0.921	0.921	0.061
159	P-31-CHE	32	F	U2	17.19	17.95	0.057	0.940	0.053	0.946	0.946	0.053
160	P-31-CHE	32	F	U3	20.76	12.22	0.060	0.917	0.059	0.918	0.918	0.059
161	P-31-CHE	32	F	T1	16.17	21.38	0.055	0.942	0.053	0.948	0.948	0.053
162	P-31-CHE	32	F	T4	12.10	9.93	0.055	0.934	0.054	0.935	0.935	0.054
163	P-31-CHE	32	F	L1	13.37	9.54	0.044	0.953	0.043	0.943	0.953	0.044
164	P-31-CHE	32	F	L3	18.98	16.04	0.029	0.966	0.029	0.966	0.966	0.029
165	P-31-CHE	32	F	L4	16.30	15.65	0.042	0.978	0.042	0.978	0.978	0.042
166	P-31-CHE	32	F	L5	8.79	10.05	0.034	0.949	0.033	0.951	0.951	0.033
167	P-32-LEA	48	F	U3	14.52	14.26	0.040	0.967	0.040	0.967	0.967	0.040
168	P-32-LEA	48	F	T1	15.41	14.00	0.033	0.951	0.033	0.952	0.952	0.033
169	P-32-LEA	48	F	T2	11.46	14.13	0.031	0.948	0.030	0.950	0.950	0.030
170	P-32-LEA	48	F	T3	16.05	11.33	0.049	0.970	0.048	0.971	0.971	0.048
171	P-32-LEA	48	F	L3	16.17	11.58	0.089	0.950	0.089	0.951	0.951	0.089
172	P-33-LAW	59	M	H1	8.92	9.04	0.038	0.940	0.038	0.941	0.941	0.038

No	Patient	Age	Gender	Region	Width (mm)	Height (mm)	$S_{a,2}$ (mm)	$R_2^2$	$S_{a,3}$ (mm)	$R_3^2$	$R_{fmat}^2$	$\overline{S}_{ymat}$ (mm)
173	P-33-LAW	59	M	U1	11.59	12.98	0.034	0.980	0.034	0.980	0.980	0.034
174	P-33-LAW	59	M	U3	10.70	10.82	0.034	0.951	0.033	0.954	0.954	0.033
175	P-33-LAW	59	M	T1	21.27	16.29	0.069	0.967	0.073	0.963	0.967	0.069
176	P-33-LAW	59	M	T2	25.73	14.00	0.058	0.970	0.056	0.972	0.972	0.056
177	P-33-LAW	59	M	T3	18.34	13.36	0.066	0.959	0.064	0.960	0.960	0.064
178	P-33-LAW	59	M	T4	34.26	27.36	0.065	0.953	0.072	0.952	0.953	0.065
179	P-33-LAW	59	M	T5	19.23	12.47	0.053	0.967	0.051	0.968	0.968	0.051
180	P-33-LAW	59	M	L1	8.28	10.82	0.031	0.945	0.030	0.947	0.947	0.030
181	P-33-LAW	59	M	L3	8.79	10.94	0.046	0.963	0.046	0.964	0.964	0.046
182	P-34-RIZ	23	F	H1	5.48	8.27	0.021	0.989	0.020	0.990	0.990	0.020
183	P-34-RIZ	23	F	U1	10.83	24.82	0.040	0.984	0.039	0.984	0.984	0.039
184	P-34-RIZ	23	F	T1	20.00	13.36	0.038	0.951	0.040	0.942	0.951	0.038
185	P-34-RIZ	23	F	T2	12.99	7.38	0.047	0.901	0.044	0.911	0.911	0.044
186	P-34-RIZ	23	F	T3	12.10	10.44	0.041	0.964	0.041	0.964	0.964	0.041
187	P-34-RIZ	23	F	L1	18.34	10.95	0.031	0.960	0.031	0.958	0.960	0.031
188	P-34-RIZ	23	F	L2	8.53	16.16	0.035	0.970	0.034	0.971	0.971	0.034
189	P-34-RIZ	23	F	L3	13.63	8.15	0.041	0.959	0.041	0.940	0.959	0.041
190	P-34-RIZ	23	F	L4	10.06	7.64	0.031	0.955	0.029	0.962	0.962	0.029
191	P-34-RIZ	23	F	L5	29.04	15.65	0.068	0.960	0.069	0.957	0.960	0.068
192	P-35-RAJ	67	M	H1	11.08	12.60	0.029	0.908	0.029	0.910	0.910	0.029
193	P-35-RAJ	67	M	U1	20.00	12.22	0.044	0.950	0.043	0.953	0.953	0.043
194	P-35-RAJ	67	M	U2	13.88	10.82	0.022	0.978	0.021	0.979	0.979	0.021
195	P-35-RAJ	67	M	U3	10.06	8.78	0.037	0.925	0.035	0.921	0.925	0.037
196	P-35-RAJ	67	M	T1	9.93	14.13	0.046	0.843	0.040	0.907	0.907	0.040
197	P-35-RAJ	67	M	T2	21.01	17.95	0.044	0.972	0.045	0.968	0.972	0.044
198	P-35-RAJ	67	M	T4	5.60	5.22	0.045	0.914	0.045	0.914	0.914	0.045
199	P-35-RAJ	67	M	L1	7.64	15.40	0.037	0.985	0.035	0.986	0.986	0.035
200	P-35-RAJ	67	M	L2	8.15	15.91	0.027	0.996	0.025	0.996	0.996	0.025
201	P-36-NUR	21	F	H1	14.77	16.93	0.065	0.948	0.063	0.952	0.952	0.063
202	P-36-NUR	21	F	U3	31.97	8.91	0.042	0.988	0.036	0.991	0.991	0.036
203	P-36-NUR	21	F	T3	26.75	15.53	0.053	0.941	0.052	0.944	0.944	0.052
204	P-36-NUR	21	F	L2	14.27	13.75	0.036	0.990	0.038	0.989	0.990	0.036
205	P-36-NUR	21	F	L3	16.30	21.38	0.040	0.991	0.043	0.990	0.991	0.040
206	P-36-NUR	21	F	L4	31.46	26.47	0.057	0.990	0.063	0.987	0.990	0.057
207	P-37-VAD	37	F	H12	4.59	4.07	0.032	0.951	0.031	0.955	0.955	0.031
208	P-37-VAD	37	F	U1	2.55	3.06	0.016	0.959	0.016	0.959	0.959	0.016
209	P-37-VAD	37	F	U2	2.55	3.18	0.016	0.953	0.016	0.954	0.954	0.016
210	P-37-VAD	37	F	T1	11.08	11.33	0.022	0.973	0.021	0.975	0.975	0.021
211	P-37-VAD	37	F	T2	5.10	6.11	0.019	0.973	0.019	0.973	0.973	0.019
212	P-37-VAD	37	F	T3	4.33	6.11	0.048	0.936	0.047	0.939	0.939	0.047
213	P-38-ROM	43	F	H1	3.31	4.07	0.028	0.904	0.034	0.692	0.904	0.028
214	P-38-ROM	43	F	U1	10.19	12.22	0.022	0.952	0.019	0.947	0.952	0.022
215	P-38-ROM	43	F	U2	4.20	5.85	0.017	0.957	0.017	0.957	0.957	0.017
216	P-38-ROM	43	F	U3	3.44	4.71	0.016	0.943	0.017	0.943	0.943	0.017

No	Patient	Age	Gender	Region	Width (mm)	Height (mm)	$S_{a,2}$ (mm)	$R_2^2$	$S_{a,3}$ (mm)	$R_3^2$	$R_{final}^2$	$\bar{S}_{final}$ (mm)
217	P-38-ROM	43	F	T2	8.53	7.76	0.016	0.938	0.016	0.936	0.938	0.016
218	P-38-ROM	43	F	T3	8.02	6.62	0.022	0.977	0.022	0.977	0.977	0.022
219	P-38-ROM	43	F	L1	5.09	7.89	0.018	0.936	0.018	0.938	0.938	0.018
220	P-38-ROM	43	F	L2	9.04	7.00	0.018	0.963	0.017	0.964	0.964	0.017
221	P-38-ROM	43	F	L3	3.06	3.69	0.016	0.957	0.016	0.959	0.959	0.016
222	P-39-MOH	44	M	U1	7.13	9.80	0.048	0.949	0.048	0.949	0.949	0.048
223	P-39-MOH	44	M	U2	2.55	4.46	0.023	0.914	0.023	0.913	0.914	0.023
224	P-39-MOH	44	M	U3	5.35	10.18	0.022	0.985	0.020	0.988	0.988	0.020
225	P-39-MOH	44	M	T1	11.08	7.76	0.030	0.964	0.028	0.970	0.970	0.028
226	P-39-MOH	44	M	T2	10.83	14.00	0.023	0.933	0.022	0.937	0.937	0.022
227	P-39-MOH	44	M	T3	18.85	6.75	0.033	0.981	0.032	0.982	0.982	0.032
228	P-39-MOH	44	M	L1	8.41	10.69	0.054	0.940	0.052	0.946	0.946	0.052
229	P-39-MOH	44	M	L3	8.79	7.51	0.069	0.925	0.068	0.927	0.927	0.068
230	P-40-MOH	46	M	H1	5.60	9.67	0.018	0.970	0.017	0.971	0.971	0.017
231	P-40-MOH	46	M	U1	9.42	10.44	0.044	0.940	0.041	0.946	0.946	0.041
232	P-40-MOH	46	M	U3	7.26	9.42	0.030	0.949	0.030	0.949	0.949	0.030
233	P-40-MOH	46	M	L1	14.90	15.65	0.053	0.968	0.058	0.961	0.968	0.053
234	P-40-MOH	46	M	L2	7.77	8.91	0.034	0.952	0.034	0.954	0.954	0.034
235	P-41-SHA	59	M	H1	11.97	15.91	0.059	0.919	0.059	0.921	0.921	0.059
236	P-41-SHA	59	M	U1	4.59	9.16	0.024	0.952	0.023	0.955	0.955	0.023
237	P-41-SHA	59	M	U2	3.69	4.07	0.016	0.915	0.016	0.927	0.927	0.016
238	P-41-SHA	59	M	U3	4.46	4.58	0.015	0.926	0.015	0.926	0.926	0.015
239	P-41-SHA	59	M	T1	4.33	4.33	0.023	0.939	0.024	0.938	0.939	0.023
240	P-41-SHA	59	M	T2	4.71	6.49	0.018	0.968	0.018	0.969	0.969	0.018
241	P-41-SHA	59	M	T3	3.57	6.11	0.022	0.929	0.021	0.936	0.936	0.021
242	P-41-SHA	59	M	L2	14.39	28.00	0.069	0.957	0.066	0.964	0.964	0.066
243	P-41-SHA	59	M	L3	5.60	6.11	0.027	0.909	0.021	0.907	0.909	0.027
244	P-42-SEL	34	M	H1	4.20	3.69	0.020	0.952	0.018	0.963	0.963	0.018
245	P-42-SEL	34	M	U1	6.37	5.47	0.021	0.987	0.021	0.985	0.987	0.021
246	P-42-SEL	34	M	U2	3.31	4.58	0.023	0.946	0.022	0.946	0.946	0.022
247	P-42-SEL	34	M	T1	7.00	4.96	0.032	0.964	0.032	0.964	0.964	0.032
248	P-42-SEL	34	M	T3	3.44	3.31	0.032	0.944	0.033	0.943	0.944	0.032
249	P-42-SEL	34	M	L1	2.55	3.18	0.016	0.962	0.016	0.962	0.962	0.016
250	P-42-SEL	34	M	L2	5.48	4.46	0.031	0.906	0.031	0.906	0.906	0.031
251	P-42-SEL	34	M	L3	8.53	9.55	0.040	0.904	0.037	0.918	0.918	0.037
252	P-43-MUK	56	M	H1	9.04	9.54	0.035	0.975	0.037	0.973	0.975	0.035
253	P-43-MUK	56	M	U1	9.17	8.02	0.032	0.980	0.033	0.979	0.980	0.032
254	P-43-MUK	56	M	U2	5.22	6.36	0.021	0.987	0.021	0.987	0.987	0.021
255	P-43-MUK	56	M	U3	4.71	7.51	0.072	0.906	0.072	0.908	0.908	0.072
256	P-43-MUK	56	M	T2	6.62	4.96	0.019	0.975	0.019	0.976	0.976	0.019
257	P-43-MUK	56	M	T3	5.60	4.84	0.034	0.959	0.034	0.959	0.959	0.034
258	P-43-MUK	56	M	L1	6.11	7.00	0.020	0.958	0.021	0.947	0.958	0.020
259	P-43-MUK	56	M	L2	3.82	5.09	0.028	0.938	0.027	0.925	0.938	0.028
260	P-43-MUK	56	M	L3	4.58	5.73	0.014	0.984	0.014	0.984	0.984	0.014

No	Patient	Age	Gender	Region	Width (mm)	Height (mm)	$S_{a,2}$ (mm)	$R_2^2$	$S_{a,3}$ (mm)	$R_3^2$	$R_{final}^2$	$\overline{S_{final}}$ (mm)
261	P-44-RAM	38	M	H1	14.14	10.95	0.037	0.976	0.041	0.972	0.976	0.637
262	P-44-RAM	38	M	U1	8.40	8.53	0.043	0.906	0.043	0.906	0.906	0.043
263	P-44-RAM	38	M	U2	5.99	8.02	0.042	0.962	0.042	0.961	0.962	0.042
264	P-44-RAM	38	M	T2	10.44	9.54	0.016	0.984	0.015	0.985	0.985	0.015
265	P-44-RAM	38	M	T3	6.11	10.05	0.028	0.963	0.026	0.968	0.968	0.026
266	P-44-RAM	38	M	L1	7.77	8.78	0.026	0.983	0.028	0.981	0.983	0.026
267	P-44-RAM	38	M	L2	7.64	6.49	0.020	0.952	0.020	0.950	0.952	0.020
268	P-44-RAM	38	M	L3	13.50	11.07	0.036	0.950	0.036	0.950	0.950	0.036
269	P-45-CHA	67	M	U3	4.08	6.11	0.035	0.930	0.035	0.931	0.931	0.035
270	P-45-CHA	67	M	T1	17.07	18.07	0.043	0.950	0.040	0.957	0.957	0.040
271	P-45-CHA	67	M	T2	7.13	8.15	0.038	0.944	0.039	0.942	0.944	0.038
272	P-45-CHA	67	M	T3	25.22	20.49	0.036	0.988	0.045	0.969	0.988	0.036
273	P-45-CHA	67	M	L1	19.10	13.75	0.048	0.954	0.048	0.954	0.954	0.048
274	P-45-CHA	67	M	L2	18.21	12.73	0.036	0.981	0.035	0.982	0.982	0.035
275	P-45-CHA	67	M	L3	18.98	14.38	0.035	0.971	0.034	0.972	0.972	0.034
276	P-46-SUB	61	M	T1	5.48	4.33	0.027	0.920	0.027	0.918	0.920	0.027
277	P-46-SUB	61	M	T2	2.42	1.78	0.012	0.971	0.012	0.971	0.971	0.012
278	P-46-SUB	61	M	T3	2.80	4.20	0.021	0.961	0.020	0.961	0.961	0.020
279	P-46-SUB	61	M	L1	28.02	9.29	0.023	0.983	0.021	0.985	0.985	0.021
280	P-46-SUB	61	M	L2	9.68	10.44	0.019	0.967	0.019	0.968	0.968	0.019
281	P-46-SUB	61	M	L3	7.26	9.04	0.017	0.931	0.017	0.932	0.932	0.017
282	P-47-MUH	34	M	U1	17.32	10.06	0.039	0.950	0.039	0.931	0.950	0.039
283	P-47-MUH	34	M	U2	6.24	7.26	0.017	0.979	0.017	0.979	0.979	0.017
284	P-47-MUH	34	M	U3	6.37	7.13	0.016	0.987	0.016	0.988	0.988	0.016
285	P-47-MUH	34	M	T1	8.53	8.15	0.033	0.976	0.032	0.978	0.978	0.032
286	P-47-MUH	34	M	T2	5.60	7.00	0.019	0.956	0.017	0.941	0.956	0.019
287	P-47-MUH	34	M	L1	15.28	16.42	0.057	0.991	0.056	0.991	0.991	0.056
288	P-47-MUH	34	M	L2	12.86	17.56	0.038	0.952	0.039	0.950	0.952	0.038
289	P-48-WON	49	M	U1	8.66	10.18	0.028	0.968	0.028	0.969	0.969	0.028
290	P-48-WON	49	M	U2	6.88	8.02	0.038	0.967	0.038	0.967	0.967	0.038
291	P-48-WON	49	M	T1	10.06	12.60	0.041	0.968	0.041	0.967	0.968	0.041
292	P-48-WON	49	M	T2	8.28	14.25	0.037	0.964	0.040	0.959	0.964	0.037
293	P-48-WON	49	M	L1	24.07	15.02	0.040	0.991	0.034	0.993	0.993	0.034
294	P-48-WON	49	M	L2	5.86	6.24	0.024	0.957	0.024	0.954	0.957	0.024
295	P-48-WON	49	M	L3	2.80	3.31	0.017	0.961	0.017	0.961	0.961	0.017
296	P-49-MUN	47	M	H1	16.30	12.35	0.052	0.987	0.048	0.990	0.990	0.048
297	P-49-MUN	47	M	U1	6.50	7.51	0.038	0.952	0.036	0.952	0.952	0.036
298	P-49-MUN	47	M	U2	5.60	6.62	0.020	0.976	0.019	0.978	0.978	0.019
299	P-49-MUN	47	M	T1	10.44	8.65	0.046	0.973	0.045	0.973	0.973	0.045
300	P-49-MUN	47	M	T3	7.01	6.24	0.042	0.929	0.040	0.934	0.934	0.040
301	P-49-MUN	47	M	L1	6.75	12.60	0.031	0.904	0.030	0.914	0.914	0.030
302	P-49-MUN	47	M	L3B	9.42	10.44	0.039	0.920	0.040	0.919	0.920	0.039
303	P-50-LIM	57	M	H1	10.06	9.42	0.039	0.993	0.037	0.994	0.994	0.037
304	P-50-LIM	57	M	U3	4.84	7.26	0.029	0.952	0.028	0.952	0.952	0.028

No	Patient	Age	Gender	Region	Width (mm)	Height (mm)	$S_{a,2}$ (mm)	$R_2^2$	$S_{a,3}$ (mm)	$R_3^2$	$R_{final}^2$	$S_{final}$ (mm)
305	P-50-LIM	57	M	T1	9.81	6.75	0.030	0.947	0.029	0.949	0.949	0.029
306	P-50-LIM	57	M	T2	11.46	5.60	0.027	0.911	0.026	0.914	0.914	0.026
307	P-50-LIM	57	M	T3	6.24	12.09	0.067	0.924	0.074	0.921	0.924	0.067
308	P-50-LIM	57	M	T4	36.43	25.58	0.076	0.974	0.080	0.992	0.992	0.080
309	P-50-LIM	57	M	L1	7.64	7.76	0.020	0.972	0.020	0.972	0.972	0.020
310	P-50-LIM	57	M	L3	5.99	7.76	0.032	0.960	0.032	0.961	0.961	0.032
311	P-51-TEN	32	M	U1	14.77	17.31	0.027	0.989	0.027	0.990	0.990	0.027
312	P-51-TEN	32	M	U3	6.11	5.85	0.033	0.939	0.033	0.938	0.939	0.033
313	P-51-TEN	32	M	T1	7.51	7.38	0.035	0.901	0.030	0.918	0.918	0.030
314	P-51-TEN	32	M	T2	7.51	10.95	0.029	0.918	0.026	0.933	0.933	0.026
315	P-51-TEN	32	M	T3	9.55	11.96	0.027	0.956	0.028	0.953	0.956	0.027
316	P-51-TEN	32	M	L1	11.08	14.51	0.034	0.992	0.034	0.992	0.992	0.034
317	P-51-TEN	32	M	L2	20.00	14.13	0.054	0.955	0.052	0.957	0.957	0.052
318	P-51-TEN	32	M	L3	17.45	21.38	0.033	0.993	0.036	0.992	0.993	0.033
319	P-52-VIJ	35	M	H1	5.86	7.89	0.026	0.914	0.026	0.917	0.917	0.026
320	P-52-VIJ	35	M	U1	25.47	20.11	0.072	0.981	0.071	0.982	0.982	0.071
321	P-52-VIJ	35	M	U2	14.39	19.98	0.038	0.982	0.039	0.981	0.982	0.038
322	P-52-VIJ	35	M	U3	16.81	23.67	0.055	0.985	0.053	0.985	0.985	0.053
323	P-52-VIJ	35	M	T1	18.98	23.80	0.052	0.925	0.048	0.940	0.940	0.048
324	P-52-VIJ	35	M	T2	12.99	10.44	0.039	0.921	0.042	0.941	0.941	0.042
325	P-52-VIJ	35	M	T3	10.06	10.18	0.039	0.984	0.039	0.984	0.984	0.039
326	P-52-VIJ	35	M	T5	18.34	25.33	0.082	0.970	0.081	0.971	0.971	0.081
327	P-52-VIJ	35	M	L1	18.60	9.29	0.026	0.979	0.025	0.981	0.981	0.025
328	P-52-VIJ	35	M	L2	27.51	23.80	0.073	0.977	0.081	0.969	0.977	0.073
329	P-52-VIJ	35	M	L3	13.63	11.46	0.030	0.988	0.029	0.988	0.988	0.029
330	P-53-KAM	63	M	U1	4.84	6.36	0.017	0.968	0.018	0.967	0.968	0.017
331	P-53-KAM	63	M	U2	4.46	6.24	0.029	0.961	0.031	0.948	0.961	0.029
332	P-53-KAM	63	M	T1	5.86	12.22	0.031	0.953	0.030	0.946	0.953	0.031
333	P-53-KAM	63	M	T2	6.24	7.38	0.017	0.946	0.017	0.947	0.947	0.017
334	P-53-KAM	63	M	T3	20.63	19.85	0.067	0.953	0.066	0.954	0.954	0.066
335	P-53-KAM	63	M	T4	3.44	3.44	0.038	0.919	0.038	0.919	0.919	0.038
336	P-53-KAM	63	M	L1	6.49	5.73	0.023	0.933	0.022	0.936	0.936	0.022
337	P-53-KAM	63	M	L3	9.68	7.76	0.025	0.945	0.028	0.930	0.945	0.025
338	P-54-LIE	52	M	U1	5.73	5.86	0.045	0.938	0.045	0.939	0.939	0.045
339	P-54-LIE	52	M	U2	5.48	4.96	0.031	0.976	0.031	0.976	0.976	0.031
340	P-54-LIE	52	M	U3	5.60	5.86	0.030	0.906	0.029	0.907	0.907	0.029
341	P-54-LIE	52	M	T1	15.28	11.84	0.042	0.962	0.041	0.964	0.964	0.041
342	P-54-LIE	52	M	T5	12.35	8.27	0.025	0.947	0.024	0.949	0.949	0.024
343	P-54-LIE	52	M	L1	4.46	5.73	0.027	0.962	0.028	0.961	0.962	0.027
344	P-54-LIE	52	M	L3	4.97	8.27	0.039	0.923	0.037	0.931	0.931	0.037
345	P-55-NED	42	M	H1	8.28	5.85	0.018	0.991	0.016	0.993	0.993	0.016
346	P-55-NED	42	M	U1	11.59	10.82	0.043	0.975	0.041	0.978	0.978	0.041
347	P-55-NED	42	M	U3	16.17	14.51	0.086	0.981	0.086	0.981	0.981	0.086
348	P-55-NED	42	M	T1	13.12	14.51	0.054	0.982	0.055	0.981	0.982	0.054

No	Patient	Age	Gender	Region	Width (mm)	Height (mm)	$S_{a,2}$ (mm)	$R_2^2$	$S_{a,3}$ (mm)	$R_3^2$	$R_{fmat}^2$	$\bar{S}_{fmat}$ (mm)
349	P-55-NED	42	M	T2	11.34	11.84	0.035	0.923	0.034	0.928	0.928	0.034
350	P-55-NED	42	M	T3	3.95	6.87	0.019	0.968	0.017	0.976	0.976	0.017
351	P-55-NED	42	M	L1	32.60	10.18	0.057	0.962	0.056	0.967	0.967	0.056
352	P-55-NED	42	M	L2	7.64	6.62	0.027	0.965	0.027	0.963	0.965	0.027
353	P-55-NED	42	M	L3	9.93	14.38	0.027	0.954	0.031	0.945	0.954	0.027
354	P-55-NED	42	M	L4	32.22	27.11	0.084	0.971	0.103	0.946	0.971	0.084
355	P-56-ROS	53	M	U1	13.63	11.45	0.044	0.983	0.042	0.985	0.985	0.042
356	P-56-ROS	53	M	U2	8.79	11.07	0.052	0.919	0.052	0.914	0.919	0.052
357	P-56-ROS	53	M	U3	9.04	9.29	0.041	0.903	0.042	0.901	0.903	0.041
358	P-56-ROS	53	M	T12	12.99	17.82	0.074	0.929	0.066	0.947	0.947	0.066
359	P-56-ROS	53	M	T2	5.99	4.96	0.023	0.928	0.021	0.941	0.941	0.021
360	P-56-ROS	53	M	L1	8.92	7.38	0.020	0.938	0.022	0.929	0.938	0.020
361	P-56-ROS	53	M	L2	13.76	18.96	0.095	0.946	0.093	0.949	0.949	0.093
362	P-56-ROS	53	M	L3	13.63	12.09	0.034	0.931	0.034	0.932	0.932	0.034
363	P-56-ROS	53	M	L4	30.18	22.15	0.098	0.951	0.106	0.952	0.952	0.106
364	P-56-ROS	53	M	L5	27.89	25.33	0.071	0.944	0.072	0.949	0.949	0.072
365	P-56-ROS	53	M	L6	12.48	10.94	0.090	0.914	0.089	0.908	0.914	0.090
366	P-57-RAM	56	F	H1	5.99	7.89	0.026	0.980	0.025	0.982	0.982	0.025
367	P-57-RAM	56	F	U1	4.58	5.86	0.023	0.967	0.023	0.966	0.967	0.023
368	P-57-RAM	56	F	U2	9.68	13.24	0.042	0.981	0.042	0.981	0.981	0.042
369	P-57-RAM	56	F	U3	3.95	5.35	0.024	0.956	0.022	0.961	0.961	0.022
370	P-57-RAM	56	F	T1	13.37	20.49	0.041	0.908	0.039	0.911	0.911	0.039
371	P-57-RAM	56	F	T2	10.06	10.44	0.041	0.914	0.041	0.914	0.914	0.041
372	P-57-RAM	56	F	T3	7.77	8.78	0.022	0.932	0.022	0.934	0.934	0.022
373	P-57-RAM	56	F	L1	7.51	9.67	0.037	0.941	0.036	0.944	0.944	0.036
374	P-57-RAM	56	F	L2	6.50	9.42	0.029	0.970	0.027	0.974	0.974	0.027
375	P-58-MOH	31	M	H1	7.00	5.73	0.022	0.969	0.022	0.970	0.970	0.022
376	P-58-MOH	31	M	U1	3.06	3.06	0.034	0.917	0.034	0.917	0.917	0.034
377	P-58-MOH	31	M	U2	2.42	3.31	0.023	0.968	0.023	0.967	0.968	0.023
378	P-58-MOH	31	M	U3	7.51	9.55	0.044	0.919	0.044	0.920	0.920	0.044
379	P-58-MOH	31	M	T2	2.29	2.93	0.014	0.917	0.015	0.915	0.917	0.014
380	P-58-MOH	31	M	L3	11.84	12.47	0.030	0.987	0.030	0.988	0.988	0.030
381	P-59-TAM	47	M	U2	12.86	22.53	0.028	0.978	0.026	0.969	0.978	0.028
382	P-59-TAM	47	M	T1	17.58	18.84	0.026	0.995	0.031	0.993	0.995	0.026
383	P-59-TAM	47	M	L11	12.99	21.13	0.028	0.957	0.028	0.958	0.958	0.028
384	P-60-JAM	59	M	H1	12.99	15.27	0.040	0.988	0.039	0.989	0.989	0.039
385	P-60-JAM	59	M	L12	36.43	28.25	0.053	0.989	0.058	0.987	0.989	0.053
386	P-61-DUR	28	M	H1	5.60	6.49	0.051	0.939	0.051	0.938	0.939	0.051
387	P-61-DUR	28	M	U1	4.58	5.09	0.015	0.964	0.015	0.965	0.965	0.015
388	P-61-DUR	28	M	U3	2.80	3.44	0.015	0.938	0.015	0.938	0.938	0.015
389	P-61-DUR	28	M	T1	2.80	4.20	0.015	0.933	0.015	0.932	0.933	0.015
390	P-61-DUR	28	M	T2	4.07	4.20	0.019	0.921	0.019	0.918	0.921	0.019
391	P-61-DUR	28	M	T3	5.99	6.87	0.015	0.970	0.014	0.971	0.971	0.014
392	P-61-DUR	28	M	L1	5.98	7.64	0.020	0.957	0.019	0.958	0.958	0.019

No	Patient	Age	Gender	Region	Width (mm)	Height (mm)	$S_{a,2}$ (mm)	$R_2^2$	$S_{a,3}$ (mm)	$R_3^2$	$R_{final}^2$	$\bar{S}_{final}$ (mm)
393	P-61-DUR	28	M	L2	5.60	5.22	0.022	0.945	0.023	0.945	0.945	0.023
394	P-61-DUR	28	M	L3	3.44	4.20	0.038	0.930	0.038	0.930	0.930	0.038
395	P-62-VEE	50	M	H1	11.08	16.42	0.101	0.926	0.084	0.946	0.946	0.084
396	P-62-VEE	50	M	U1	3.95	3.31	0.026	0.945	0.026	0.946	0.946	0.026
397	P-62-VEE	50	M	U2	13.88	14.26	0.052	0.909	0.052	0.911	0.911	0.052
398	P-62-VEE	50	M	U3	22.16	11.20	0.053	0.968	0.053	0.968	0.968	0.053
399	P-62-VEE	50	M	T2	8.92	10.69	0.036	0.961	0.037	0.946	0.961	0.036
400	P-62-VEE	50	M	T3	11.34	11.07	0.040	0.954	0.035	0.962	0.962	0.035
401	P-62-VEE	50	M	T4	37.19	29.02	0.052	0.978	0.052	0.976	0.978	0.052
402	P-62-VEE	50	M	T5	36.93	28.76	0.089	0.931	0.094	0.926	0.931	0.089
403	P-62-VEE	50	M	L1	15.67	14.89	0.038	0.982	0.037	0.983	0.983	0.037
404	P-62-VEE	50	M	L2	18.09	16.42	0.028	0.981	0.030	0.980	0.981	0.028
405	P-62-VEE	50	M	L3	16.56	14.13	0.047	0.933	0.045	0.939	0.939	0.045
406	P-63-MUN	32	M	H1	7.90	14.38	0.048	0.929	0.046	0.934	0.934	0.046
407	P-63-MUN	32	M	U3	5.48	5.98	0.038	0.924	0.036	0.930	0.930	0.036
408	P-63-MUN	32	M	T2	10.32	9.55	0.035	0.936	0.035	0.937	0.937	0.035
409	P-63-MUN	32	M	T3	13.63	14.89	0.066	0.947	0.064	0.947	0.947	0.064
410	P-63-MUN	32	M	L1	7.00	7.89	0.030	0.975	0.030	0.975	0.975	0.030
411	P-63-MUN	32	M	L2	7.00	8.65	0.026	0.969	0.026	0.969	0.969	0.026
412	P-64-PAL	55	M	H1	7.39	9.80	0.044	0.925	0.044	0.926	0.926	0.044
413	P-64-PAL	55	M	U1	12.35	14.76	0.030	0.986	0.028	0.988	0.988	0.028
414	P-64-PAL	55	M	U2	6.37	8.27	0.025	0.951	0.024	0.953	0.953	0.024
415	P-64-PAL	55	M	U3	11.84	13.36	0.038	0.968	0.036	0.952	0.968	0.038
416	P-64-PAL	55	M	T1	11.08	13.49	0.048	0.934	0.048	0.933	0.934	0.048
417	P-64-PAL	55	M	T2	10.83	9.55	0.042	0.972	0.041	0.973	0.973	0.041
418	P-64-PAL	55	M	T3	9.81	10.31	0.040	0.959	0.038	0.963	0.963	0.038
419	P-64-PAL	55	M	L1	14.90	17.82	0.046	0.975	0.043	0.978	0.978	0.043
420	P-64-PAL	55	M	L2	23.43	15.02	0.046	0.992	0.041	0.993	0.993	0.041
421	P-64-PAL	55	M	L3	12.10	10.82	0.052	0.946	0.052	0.947	0.947	0.052
422	P-65-ONG	56	M	H1	10.57	7.76	0.033	0.973	0.028	0.980	0.980	0.028
423	P-65-ONG	56	M	U3	3.44	4.71	0.037	0.929	0.037	0.929	0.929	0.037
424	P-65-ONG	56	M	T1	34.01	10.31	0.052	0.987	0.054	0.983	0.987	0.052
425	P-65-ONG	56	M	T2	14.65	13.11	0.024	0.959	0.029	0.944	0.959	0.024
426	P-65-ONG	56	M	T3	11.84	8.91	0.018	0.952	0.018	0.953	0.953	0.018
427	P-65-ONG	56	M	T4	9.42	8.02	0.029	0.931	0.029	0.931	0.931	0.029
428	P-65-ONG	56	M	L1	6.50	7.64	0.035	0.944	0.033	0.950	0.950	0.033
429	P-65-ONG	56	M	L2	8.53	7.13	0.053	0.941	0.053	0.942	0.942	0.053
430	P-65-ONG	56	M	L3	8.41	10.95	0.058	0.906	0.056	0.907	0.907	0.056
431	P-66-AZR	49	M	H1	4.71	6.49	0.035	0.965	0.034	0.966	0.966	0.034
432	P-66-AZR	49	M	U1	3.57	4.46	0.029	0.759	0.027	0.907	0.907	0.027
433	P-66-AZR	49	M	U2	3.82	4.58	0.027	0.955	0.026	0.959	0.959	0.026
434	P-66-AZR	49	M	U3	2.93	3.18	0.027	0.939	0.025	0.950	0.950	0.025
435	P-66-AZR	49	M	T1	18.72	13.75	0.050	0.952	0.049	0.953	0.953	0.049
436	P-66-AZR	49	M	T2	8.41	14.13	0.045	0.929	0.045	0.933	0.933	0.045

No	Patient	Age	Gender	Region	Width (mm)	Height (mm)	$S_{a,2}$ (mm)	$R_2^2$	$S_{a,3}$ (mm)	$R_3^2$	$R_{fmat}^2$	$S_{fmat}$ (mm)
437	P-66-AZR	49	M	T3	17.32	9.16	0.057	0.937	0.059	0.934	0.937	0.057
438	P-66-AZR	49	M	L1	24.84	16.16	0.047	0.971	0.048	0.969	0.971	0.047
439	P-66-AZR	49	M	L2	9.95	21.51	0.049	0.945	0.059	0.930	0.945	0.049
440	P-66-AZR	49	M	L3	9.93	11.71	0.038	0.984	0.039	0.984	0.984	0.039
441	P-67-CHE	60	M	U1	6.11	7.38	0.021	0.965	0.020	0.969	0.969	0.020
442	P-67-CHE	60	M	U2	5.99	9.04	0.024	0.937	0.022	0.946	0.946	0.022
443	P-67-CHE	60	M	U3	9.81	5.85	0.028	0.951	0.028	0.951	0.951	0.028
444	P-67-CHE	60	M	T1	15.03	12.09	0.036	0.955	0.035	0.955	0.955	0.035
445	P-67-CHE	60	M	L1	21.27	9.42	0.033	0.994	0.035	0.994	0.994	0.035
446	P-67-CHE	60	M	L2	19.10	15.78	0.035	0.965	0.036	0.965	0.965	0.036
447	P-67-CHE	60	M	L3	17.45	12.35	0.035	0.984	0.036	0.983	0.984	0.035
448	P-68-CHO	61	M	U1	6.24	5.98	0.032	0.978	0.033	0.975	0.978	0.032
449	P-68-CHO	61	M	U2	5.60	5.85	0.058	0.911	0.058	0.910	0.911	0.058
450	P-68-CHO	61	M	U3	17.32	13.11	0.036	0.961	0.038	0.958	0.961	0.036
451	P-68-CHO	61	M	T1	5.86	4.46	0.030	0.945	0.030	0.945	0.945	0.030
452	P-68-CHO	61	M	T2	8.02	4.46	0.020	0.939	0.020	0.936	0.939	0.020
453	P-68-CHO	61	M	T3	4.07	4.07	0.027	0.955	0.027	0.955	0.955	0.027
454	P-68-CHO	61	M	L1	5.86	5.98	0.027	0.945	0.027	0.949	0.949	0.027
455	P-68-CHO	61	M	L3	34.90	12.85	0.035	0.979	0.034	0.981	0.981	0.034
456	P-69-MAL	32	M	H1	2.80	4.07	0.037	0.916	0.038	0.915	0.916	0.037
457	P-69-MAL	32	M	U1	9.42	5.09	0.039	0.978	0.040	0.978	0.978	0.040
458	P-69-MAL	32	M	U2	8.15	5.85	0.023	0.936	0.023	0.940	0.940	0.023
459	P-69-MAL	32	M	U3	4.71	3.18	0.022	0.943	0.022	0.944	0.944	0.022
460	P-69-MAL	32	M	T12	3.57	3.69	0.026	0.931	0.027	0.930	0.931	0.026
461	P-69-MAL	32	M	T2	3.31	2.93	0.017	0.909	0.017	0.908	0.909	0.017
462	P-69-MAL	32	M	T3	3.57	3.31	0.026	0.941	0.026	0.942	0.942	0.026
463	P-69-MAL	32	M	I2	15.67	27.36	0.050	0.975	0.046	0.979	0.979	0.046
464	P-69-MAL	32	M	L3	27.77	13.62	0.030	0.976	0.039	0.974	0.976	0.030
465	P-70-GAN	51	M	H1	27.38	26.73	0.081	0.973	0.080	0.973	0.973	0.080
466	P-70-GAN	51	M	U1	25.98	10.82	0.065	0.964	0.060	0.968	0.968	0.060
467	P-70-GAN	51	M	U2	35.53	9.55	0.070	0.966	0.064	0.967	0.967	0.064
468	P-70-GAN	51	M	T1	10.19	11.96	0.059	0.909	0.058	0.910	0.910	0.058
469	P-70-GAN	51	M	T4	36.94	28.13	0.094	0.984	0.116	0.972	0.984	0.094
470	P-70-GAN	51	M	T7	37.95	28.13	0.125	0.942	0.131	0.940	0.942	0.125
471	P-70-GAN	51	M	L1	19.10	26.35	0.074	0.955	0.071	0.956	0.956	0.071
472	P-70-GAN	51	M	L2	19.49	16.80	0.090	0.972	0.082	0.977	0.977	0.082
473	P-70-GAN	51	M	L3	31.97	9.67	0.051	0.985	0.049	0.987	0.987	0.049
474	P-71-BUR	34	M	H1	15.41	15.27	0.088	0.928	0.078	0.944	0.944	0.078
475	P-71-BUR	34	M	U1	16.81	18.58	0.044	0.988	0.044	0.988	0.988	0.044
476	P-71-BUR	34	M	U3	16.81	11.71	0.029	0.981	0.028	0.983	0.983	0.028
477	P-71-BUR	34	M	T1	16.05	13.49	0.043	0.964	0.045	0.963	0.964	0.043
478	P-71-BUR	34	M	T3	12.10	15.65	0.050	0.956	0.050	0.956	0.956	0.050
479	P-71-BUR	34	M	T4	17.07	20.49	0.044	0.932	0.043	0.936	0.936	0.043
480	P-71-BUR	34	M	T5	10.70	11.58	0.036	0.929	0.035	0.931	0.931	0.035

No	Patient	Age	Gender	Region	Width (mm)	Height (mm)	$S_{a,2}$ (mm)	$R_2^2$	$S_{a,3}$ (mm)	$R_3^2$	$R_{final}^2$	$\bar{S}_{final}$ (mm)
481	P-71-BUR	34	M	T7	7.90	11.20	0.023	0.968	0.024	0.943	0.968	0.023
482	P-71-BUR	34	M	L1	16.17	13.11	0.035	0.966	0.032	0.969	0.969	0.032
483	P-71-BUR	34	M	L2	15.54	15.02	0.035	0.990	0.033	0.991	0.991	0.033
484	P-72-CHE	47	M	H1	3.57	5.98	0.025	0.923	0.025	0.922	0.923	0.025
485	P-72-CHE	47	M	U1	12.99	17.82	0.051	0.954	0.048	0.959	0.959	0.048
486	P-72-CHE	47	M	U2	11.59	15.40	0.033	0.945	0.031	0.953	0.953	0.031
487	P-72-CHE	47	M	U3	20.76	15.27	0.064	0.982	0.071	0.980	0.982	0.064
488	P-72-CHE	47	M	T1	20.38	7.25	0.087	0.982	0.088	0.981	0.982	0.087
489	P-72-CHE	47	M	T2	18.34	16.55	0.053	0.953	0.051	0.957	0.957	0.051
490	P-72-CHE	47	M	T3	19.36	29.53	0.084	0.933	0.083	0.933	0.933	0.083
491	P-72-CHE	47	M	T4	19.36	18.20	0.052	0.932	0.055	0.919	0.932	0.052
492	P-72-CHE	47	M	T6	37.83	28.89	0.077	0.985	0.091	0.976	0.985	0.077
493	P-72-CHE	47	M	L1	18.34	16.55	0.028	0.957	0.028	0.963	0.963	0.028
494	P-72-CHE	47	M	L2	11.84	12.98	0.022	0.963	0.021	0.988	0.988	0.021
495	P-72-CHE	47	M	L3	23.05	17.82	0.049	0.968	0.045	0.973	0.973	0.045
496	P-72-CHE	47	M	L4	12.23	10.05	0.055	0.930	0.060	0.920	0.930	0.055
497	P-73-NUR	26	F	U1	5.48	4.71	0.032	0.962	0.031	0.964	0.964	0.031
498	P-73-NUR	26	F	U2	7.01	6.11	0.034	0.920	0.033	0.924	0.924	0.033
499	P-73-NUR	26	F	U3	8.02	16.42	0.039	0.978	0.041	0.977	0.978	0.039
500	P-73-NUR	26	F	T1	11.21	11.33	0.043	0.962	0.041	0.964	0.964	0.041
501	P-73-NUR	26	F	T2	9.68	9.29	0.040	0.959	0.041	0.952	0.959	0.040
502	P-73-NUR	26	F	T3	6.62	9.67	0.042	0.953	0.041	0.955	0.955	0.041
503	P-73-NUR	26	F	L1	6.62	5.98	0.037	0.928	0.037	0.926	0.928	0.037
504	P-73-NUR	26	F	L2	5.35	5.09	0.036	0.930	0.036	0.930	0.930	0.036
505	P-95-MOH	53	M	H1	5.22	10.18	0.051	0.917	0.052	0.917	0.917	0.052
506	P-95-MOH	53	M	U1	23.82	13.49	0.051	0.968	0.051	0.966	0.968	0.051
507	P-95-MOH	53	M	U2	11.33	8.65	0.025	0.954	0.025	0.954	0.954	0.025
508	P-95-MOH	53	M	U3	9.81	13.11	0.048	0.950	0.048	0.949	0.950	0.048
509	P-95-MOH	53	M	T1	18.72	21.38	0.036	0.972	0.039	0.966	0.972	0.036
510	P-95-MOH	53	M	T2	30.06	20.24	0.038	0.983	0.050	0.969	0.983	0.038
511	P-96-ZAI	62	M	H1	7.00	10.82	0.028	0.966	0.029	0.963	0.966	0.028
512	P-96-ZAI	62	M	U1	17.07	23.80	0.067	0.950	0.064	0.951	0.951	0.064
513	P-96-ZAI	62	M	U2	14.14	13.87	0.049	0.971	0.050	0.957	0.971	0.049
514	P-96-ZAI	62	M	T2	6.11	8.27	0.032	0.936	0.031	0.937	0.937	0.031
515	P-96-ZAI	62	M	T3	15.41	10.82	0.054	0.946	0.040	0.970	0.970	0.040
516	P-96-ZAI	62	M	T4	30.18	26.34	0.155	0.932	0.141	0.921	0.932	0.155
517	P-96-ZAI	62	M	T5	35.02	28.64	0.123	0.973	0.139	0.964	0.973	0.123
518	P-96-ZAI	62	M	T6	39.61	24.31	0.186	0.941	0.178	0.943	0.943	0.178
519	P-96-ZAI	62	M	L1	32.48	6.49	0.069	0.964	0.064	0.969	0.969	0.064
520	P-96-ZAI	62	M	L2	8.53	21.51	0.063	0.968	0.060	0.971	0.971	0.060
521	P-96-ZAI	62	M	L4	5.60	14.64	0.044	0.984	0.044	0.983	0.984	0.044
522	P-96-ZAI	62	M	L5	11.84	17.31	0.070	0.952	0.071	0.951	0.952	0.070
523	P-97-SAT	54	M	U1	8.53	11.45	0.022	0.970	0.021	0.974	0.974	0.021
524	P-97-SAT	54	M	U2	16.81	23.67	0.034	0.984	0.041	0.978	0.984	0.034

No	Patient	Age	Gender	Region	Width (mm)	Height (mm)	$S_{a,2}$ (mm)	$R_2^2$	$S_{a,3}$ (mm)	$R_3^2$	$R_{final}^2$	$\bar{S}_{fmat}$ (mm)
525	P-97-SAT	54	M	U3	8.02	14.25	0.023	0.984	0.024	0.983	0.984	0.023
526	P-97-SAT	54	M	T1	6.62	13.49	0.021	0.950	0.023	0.941	0.950	0.021
527	P-97-SAT	54	M	T2	7.51	6.24	0.027	0.940	0.027	0.940	0.940	0.027
528	P-97-SAT	54	M	L1	16.18	23.04	0.050	0.933	0.049	0.935	0.935	0.049
529	P-97-SAT	54	M	L2	14.90	12.73	0.032	0.961	0.031	0.962	0.962	0.031
530	P-98-MOH	35	M	H1	7.39	7.76	0.044	0.963	0.044	0.963	0.963	0.044
531	P-98-MOH	35	M	U1	7.13	7.00	0.031	0.974	0.031	0.974	0.974	0.031
532	P-98-MOH	35	M	U2	8.15	10.56	0.039	0.931	0.037	0.937	0.937	0.037
533	P-98-MOH	35	M	U3	7.13	5.85	0.060	0.982	0.060	0.981	0.982	0.060
534	P-98-MOH	35	M	T1	3.82	4.58	0.022	0.946	0.023	0.944	0.946	0.022
535	P-98-MOH	35	M	T2	3.18	4.07	0.019	0.938	0.019	0.938	0.938	0.019
536	P-98-MOH	35	M	T3	3.06	3.44	0.018	0.917	0.018	0.915	0.917	0.018
537	P-98-MOH	35	M	L1	2.93	2.80	0.023	0.953	0.022	0.958	0.958	0.022
538	P-99-ROH	39	M	H1	8.28	8.53	0.024	0.964	0.026	0.958	0.964	0.024
539	P-99-ROH	39	M	U1	15.54	13.11	0.036	0.980	0.035	0.982	0.982	0.035
540	P-99-ROH	39	M	U2	9.17	7.13	0.036	0.988	0.037	0.988	0.988	0.037
541	P-99-ROH	39	M	U3	11.72	11.84	0.022	0.989	0.022	0.989	0.989	0.022
542	P-99-ROH	39	M	T3	6.75	4.07	0.024	0.949	0.025	0.944	0.949	0.024
543	P-99-ROH	39	M	L2	11.34	8.53	0.032	0.955	0.031	0.956	0.956	0.031
544	P-99-ROH	39	M	L3	7.77	8.15	0.028	0.962	0.028	0.962	0.962	0.028
545	P-100-MAT	55	M	H1	10.19	8.40	0.048	0.939	0.048	0.940	0.940	0.048
546	P-100-MAT	55	M	U1	16.56	25.07	0.079	0.965	0.075	0.969	0.969	0.075
547	P-100-MAT	55	M	U3	11.59	18.33	0.035	0.986	0.036	0.986	0.986	0.036
548	P-100-MAT	55	M	T1	31.33	7.76	0.058	0.927	0.056	0.932	0.932	0.056
549	P-100-MAT	55	M	T2	27.51	11.71	0.057	0.963	0.065	0.952	0.963	0.057
550	P-100-MAT	55	M	T4	36.68	28.13	0.105	0.964	0.125	0.950	0.964	0.105
551	P-100-MAT	55	M	T5	9.43	11.20	0.037	0.952	0.033	0.961	0.961	0.033
552	P-100-MAT	55	M	L1	13.88	27.24	0.073	0.971	0.069	0.973	0.973	0.069
553	P-100-MAT	55	M	L2	24.45	16.42	0.026	0.987	0.034	0.977	0.987	0.026
554	P-100-MAT	55	M	L3	11.72	27.87	0.037	0.970	0.037	0.970	0.970	0.037
555	P-101-NAN	31	M	H1	11.33	9.67	0.042	0.950	0.040	0.956	0.956	0.040
556	P-101-NAN	31	M	U1	25.98	11.33	0.059	0.945	0.057	0.948	0.948	0.057
557	P-101-NAN	31	M	U3	15.54	14.00	0.038	0.974	0.038	0.975	0.975	0.038
558	P-101-NAN	31	M	T2	16.43	21.13	0.043	0.939	0.043	0.941	0.941	0.043
559	P-101-NAN	31	M	T3	27.51	11.58	0.054	0.990	0.054	0.990	0.990	0.054
560	P-101-NAN	31	M	L1	25.22	13.49	0.047	0.988	0.047	0.988	0.988	0.047
561	P-101-NAN	31	M	L2	15.67	20.11	0.057	0.983	0.056	0.984	0.984	0.056
562	P-102-MUH	56	M	U1	13.88	13.75	0.042	0.970	0.039	0.975	0.975	0.039
563	P-102-MUH	56	M	U2	15.79	8.78	0.053	0.927	0.051	0.927	0.927	0.051
564	P-102-MUH	56	M	U3	11.46	7.64	0.028	0.984	0.029	0.984	0.984	0.029
565	P-102-MUH	56	M	T1	12.35	13.75	0.043	0.930	0.042	0.930	0.930	0.042
566	P-102-MUH	56	M	9T2	10.06	8.53	0.048	0.981	0.048	0.982	0.982	0.048
567	P-102-MUH	56	M	T3	15.54	18.07	0.083	0.964	0.083	0.966	0.966	0.083
568	P-102-MUH	56	M	T4	36.17	28.76	0.037	0.994	0.044	0.990	0.994	0.037

No	Patient	Age	Gender	Region	Width (mm)	Height (mm)	$S_{a,2}$ (mm)	$R_2^2$	$S_{a,3}$ (mm)	$R_3^2$	$R_{final}^2$	$\bar{S}_{final}$ (mm)
569	P-102-MUH	56	M	L1A	15.54	15.53	0.049	0.988	0.053	0.985	0.988	0.049
570	P-102-MUH	56	M	L2	13.76	8.27	0.038	0.962	0.036	0.967	0.967	0.036
571	P-102-MUH	56	M	L3	9.30	7.13	0.032	0.951	0.031	0.955	0.955	0.031
572	P-103-TAN	56	M	H1	7.90	7.51	0.040	0.936	0.040	0.936	0.936	0.040
573	P-103-TAN	56	M	U2	7.39	8.53	0.036	0.954	0.036	0.955	0.955	0.036
574	P-103-TAN	56	M	U3	17.70	26.09	0.053	0.968	0.048	0.954	0.968	0.053
575	P-103-TAN	56	M	T1	12.48	16.80	0.037	0.845	0.038	0.906	0.906	0.038
576	P-103-TAN	56	M	T2	25.09	19.47	0.043	0.957	0.054	0.954	0.957	0.043
577	P-103-TAN	56	M	L1	14.26	16.55	0.033	0.982	0.038	0.978	0.982	0.033
578	P-103-TAN	56	M	L3	13.12	12.98	0.034	0.962	0.035	0.962	0.962	0.035
579	P-104-AHM	21	M	H1	5.86	5.98	0.021	0.979	0.021	0.978	0.979	0.021
580	P-104-AHM	21	M	U1	3.31	5.09	0.030	0.943	0.029	0.946	0.946	0.029
581	P-104-AHM	21	M	U2	3.69	4.71	0.025	0.938	0.024	0.941	0.941	0.024
582	P-104-AHM	21	M	U3	2.17	2.42	0.015	0.928	0.015	0.927	0.928	0.015
583	P-104-AHM	21	M	T1	10.95	9.93	0.044	0.973	0.046	0.972	0.973	0.044
584	P-104-AHM	21	M	T2	7.77	8.65	0.030	0.935	0.029	0.937	0.937	0.029
585	P-104-AHM	21	M	T3	9.68	5.60	0.063	0.945	0.064	0.941	0.945	0.063
586	P-104-AHM	21	M	L1	5.10	5.60	0.025	0.945	0.025	0.945	0.945	0.025
587	P-104-AHM	21	M	L2	3.82	3.44	0.034	0.920	0.034	0.921	0.921	0.034
588	P-105-SHA	30	M	T1	34.39	10.82	0.065	0.955	0.066	0.953	0.955	0.065
589	P-105-SHA	30	M	T2	22.67	13.36	0.050	0.957	0.049	0.958	0.958	0.049
590	P-105-SHA	30	M	T3	12.86	8.78	0.034	0.926	0.034	0.928	0.928	0.034
591	P-105-SHA	30	M	L1	31.33	21.00	0.053	0.992	0.058	0.990	0.992	0.053
592	P-105-SHA	30	M	L1B	23.94	15.65	0.045	0.985	0.046	0.985	0.985	0.046
593	P-105-SHA	30	M	L2	11.46	17.31	0.060	0.956	0.061	0.956	0.956	0.061
594	P-105-SHA	30	M	L3	11.84	7.64	0.054	0.917	0.052	0.922	0.922	0.052
595	P-106-HUS	38	M	H1	3.82	4.58	0.026	0.976	0.026	0.976	0.976	0.026
596	P-106-HUS	38	M	U1	6.62	11.45	0.038	0.958	0.033	0.968	0.968	0.033
597	P-106-HUS	38	M	U2	3.57	3.56	0.016	0.944	0.016	0.944	0.944	0.016
598	P-106-HUS	38	M	U3	5.99	7.64	0.021	0.993	0.019	0.967	0.993	0.021
599	P-106-HUS	38	M	T1	6.88	8.27	0.016	0.991	0.016	0.991	0.991	0.016
600	P-106-HUS	38	M	T2	7.13	10.56	0.022	0.955	0.019	0.967	0.967	0.019
601	P-106-HUS	38	M	T3	9.17	4.45	0.019	0.976	0.019	0.976	0.976	0.019
602	P-106-HUS	38	M	T4	4.71	4.20	0.021	0.989	0.021	0.989	0.989	0.021
603	P-106-HUS	38	M	T5	3.31	5.09	0.016	0.943	0.016	0.943	0.943	0.016
604	P-106-HUS	38	M	L1	7.90	13.75	0.024	0.938	0.021	0.945	0.945	0.021
605	P-106-HUS	38	M	L2	8.92	12.47	0.030	0.983	0.030	0.984	0.984	0.030
606	P-106-HUS	38	M	L3	6.75	10.94	0.022	0.972	0.020	0.976	0.976	0.020
607	P-107-ABD	54	M	U1	8.15	8.78	0.040	0.962	0.040	0.961	0.962	0.040
608	P-107-ABD	54	M	U2	13.25	9.93	0.028	0.960	0.028	0.959	0.960	0.028
609	P-107-ABD	54	M	T1	10.19	7.89	0.038	0.918	0.038	0.919	0.919	0.038
610	P-107-ABD	54	M	T2	3.57	4.71	0.029	0.936	0.028	0.937	0.937	0.028
611	P-107-ABD	54	M	T3	5.99	6.24	0.032	0.945	0.032	0.945	0.945	0.032
612	P-107-ABD	54	M	L1	8.41	9.93	0.043	0.934	0.043	0.933	0.934	0.043

No	Patient	Age	Gender	Region	Width (mm)	Height (mm)	$S_{a,2}$ (mm)	$R_2^2$	$S_{a,3}$ (mm)	$R_3^2$	$R_{fmat}^2$	$\overline{S}_{fmat}$ (mm)
613	P-108-RAH	56	M	H1	9.30	11.58	0.067	0.938	0.063	0.942	0.942	0.063
614	P-108-RAH	56	M	U1	13.88	10.82	0.041	0.942	0.038	0.928	0.942	0.041
615	P-108-RAH	56	M	U2	8.02	8.91	0.043	0.916	0.042	0.931	0.931	0.042
616	P-108-RAH	56	M	U3	5.22	5.85	0.020	0.943	0.020	0.943	0.943	0.020
617	P-108-RAH	56	M	T1	24.45	19.60	0.050	0.973	0.049	0.973	0.973	0.049
618	P-108-RAH	56	M	T2	25.34	15.40	0.074	0.978	0.074	0.978	0.978	0.074
619	P-108-RAH	56	M	L1	18.98	23.29	0.059	0.983	0.059	0.983	0.983	0.059
620	P-108-RAH	56	M	L2	23.69	26.60	0.039	0.996	0.038	0.996	0.996	0.038
621	P-108-RAH	56	M	L3	29.55	24.95	0.046	0.996	0.046	0.996	0.996	0.046
622	P-109-BAF	60	M	H1	7.77	8.66	0.051	0.946	0.051	0.946	0.946	0.051
623	P-109-BAF	60	M	U3	18.98	28.51	0.043	0.974	0.063	0.952	0.974	0.043
624	P-109-BAF	60	M	T1	27.00	16.80	0.052	0.949	0.074	0.928	0.949	0.052
625	P-109-BAF	60	M	T2	24.33	8.78	0.047	0.955	0.045	0.959	0.959	0.045
626	P-109-BAF	60	M	T3	8.41	11.96	0.038	0.956	0.038	0.956	0.956	0.038
627	P-109-BAF	60	M	T4	25.73	13.75	0.064	0.961	0.058	0.967	0.967	0.058
628	P-109-BAF	60	M	L1	18.47	20.62	0.063	0.969	0.066	0.968	0.969	0.063
629	P-109-BAF	60	M	L2	23.94	12.35	0.045	0.951	0.035	0.968	0.968	0.035
630	P-109-BAF	60	M	L3	7.90	6.87	0.026	0.962	0.025	0.962	0.962	0.025
631	P-110-TAN	38	M	U1	16.05	14.00	0.046	0.977	0.041	0.980	0.980	0.041
632	P-110-TAN	38	M	U3	12.23	11.96	0.047	0.966	0.046	0.967	0.967	0.046
633	P-110-TAN	38	M	T2	9.55	16.16	0.038	0.959	0.038	0.959	0.959	0.038
634	P-110-TAN	38	M	T3	19.61	19.60	0.091	0.954	0.089	0.957	0.957	0.089
635	P-110-TAN	38	M	T5	36.94	28.76	0.124	0.957	0.156	0.930	0.957	0.124
636	P-110-TAN	38	M	L1	24.07	17.56	0.082	0.946	0.068	0.948	0.948	0.068
637	P-110-TAN	38	M	L2	15.16	29.02	0.077	0.978	0.072	0.982	0.982	0.072
638	P-110-TAN	38	M	L3	24.58	26.73	0.067	0.961	0.061	0.963	0.963	0.061
639	P-110-TAN	38	M	L4	38.34	29.02	0.101	0.962	0.126	0.990	0.990	0.126
640	P-110-TAN	38	M	L5	38.72	28.25	0.095	0.971	0.089	0.973	0.973	0.089
641	P-111-ONG	64	M	H1	10.95	10.56	0.035	0.936	0.032	0.943	0.943	0.032
642	P-111-ONG	64	M	U1	7.39	10.18	0.045	0.962	0.044	0.963	0.963	0.044
643	P-111-ONG	64	M	U2	6.49	7.76	0.035	0.971	0.033	0.973	0.973	0.033
644	P-111-ONG	64	M	U3	7.13	7.13	0.049	0.932	0.048	0.932	0.932	0.048
645	P-111-ONG	64	M	T3	5.60	7.38	0.031	0.962	0.030	0.963	0.963	0.030
646	P-111-ONG	64	M	L1	30.06	16.16	0.067	0.941	0.064	0.943	0.943	0.064
647	P-111-ONG	64	M	L1B	20.63	18.71	0.037	0.983	0.035	0.985	0.985	0.035
648	P-111-ONG	64	M	L2	17.19	17.82	0.053	0.979	0.051	0.976	0.979	0.053
649	P-111-ONG	64	M	L3	22.03	19.09	0.044	0.967	0.039	0.974	0.974	0.039
650	P-112-SEL	42	M	U3	16.68	17.44	0.067	0.969	0.068	0.968	0.969	0.067
651	P-112-SEL	42	M	T1	10.70	20.74	0.039	0.988	0.034	0.967	0.988	0.039
652	P-112-SEL	42	M	T2	20.50	13.62	0.049	0.940	0.046	0.953	0.953	0.046
653	P-112-SEL	42	M	T3	29.55	23.04	0.037	0.992	0.043	0.981	0.992	0.037
654	P-112-SEL	42	M	L1	23.82	28.64	0.049	0.981	0.070	0.962	0.981	0.049
655	P-112-SEL	42	M	L2	20.89	16.93	0.062	0.985	0.064	0.984	0.985	0.062
656	P-112-SEL	42	M	L3	30.57	13.24	0.059	0.968	0.051	0.982	0.982	0.051

No	Patient	Age	Gender	Region	Width (mm)	Height (mm)	$S_{a,2}$ (mm)	$R_2^2$	$S_{a,3}$ (mm)	$R_3^2$	$R_{final}^2$	$\overline{S_{final}}$ (mm)
657	P-113-NOR	21	F	H1	5.22	5.85	0.037	0.929	0.037	0.930	0.930	0.037
658	P-113-NOR	21	F	U1	8.41	6.24	0.030	0.940	0.032	0.931	0.940	0.030
659	P-113-NOR	21	F	U2	3.44	3.31	0.025	0.924	0.025	0.924	0.924	0.025
660	P-113-NOR	21	F	U3	3.18	2.55	0.023	0.915	0.022	0.916	0.916	0.022
661	P-113-NOR	21	F	T3	7.00	7.00	0.032	0.919	0.032	0.918	0.919	0.032
662	P-113-NOR	21	F	L1	11.59	8.40	0.034	0.952	0.029	0.962	0.962	0.029
663	P-113-NOR	21	F	L2	3.95	3.69	0.018	0.929	0.021	0.916	0.929	0.018
664	P-113-NOR	21	F	L3	5.09	4.58	0.022	0.930	0.021	0.937	0.937	0.021
665	P-114-MOH	29	M	H1	5.48	6.24	0.038	0.927	0.037	0.929	0.929	0.037
666	P-114-MOH	29	M	U1	5.99	11.71	0.037	0.942	0.030	0.946	0.946	0.030
667	P-114-MOH	29	M	U2	7.39	7.76	0.031	0.971	0.028	0.974	0.974	0.028
668	P-114-MOH	29	M	T1	31.08	15.02	0.064	0.907	0.062	0.911	0.911	0.062
669	P-114-MOH	29	M	T2	29.17	17.18	0.075	0.970	0.065	0.960	0.970	0.075
670	P-114-MOH	29	M	T3	25.35	12.86	0.086	0.969	0.081	0.973	0.973	0.081
671	P-114-MOH	29	M	T4	38.21	28.89	0.088	0.978	0.126	0.950	0.978	0.088
672	P-114-MOH	29	M	L1	13.37	17.56	0.046	0.973	0.045	0.955	0.973	0.046
673	P-114-MOH	29	M	L2	30.31	12.60	0.061	0.973	0.054	0.977	0.977	0.054
674	P-114-MOH	29	M	L3	9.55	9.93	0.042	0.948	0.041	0.949	0.949	0.041
675	P-114-MOH	29	M	L4	9.04	11.20	0.098	0.929	0.093	0.937	0.937	0.093
676	P-114-MOH	29	M	L5	38.34	28.76	0.088	0.948	0.088	0.949	0.949	0.088
677	P-115-RAJ	32	M	U1	37.57	13.36	0.090	0.923	0.067	0.931	0.931	0.067
678	P-115-RAJ	32	M	U2	39.61	10.56	0.070	0.951	0.070	0.950	0.951	0.070
679	P-115-RAJ	32	M	U3	22.29	22.15	0.054	0.971	0.053	0.972	0.972	0.053
680	P-115-RAJ	32	M	T1	19.87	18.20	0.078	0.966	0.078	0.967	0.967	0.078
681	P-115-RAJ	32	M	T2	28.02	14.76	0.064	0.964	0.067	0.961	0.964	0.064
682	P-115-RAJ	32	M	T3	27.13	19.73	0.068	0.955	0.066	0.958	0.958	0.066
683	P-115-RAJ	32	M	T4	36.17	26.73	0.051	0.932	0.051	0.932	0.932	0.051
684	P-115-RAJ	32	M	L1	17.19	18.33	0.047	0.951	0.045	0.954	0.954	0.045
685	P-115-RAJ	32	M	L2	22.67	24.56	0.051	0.970	0.050	0.971	0.971	0.050
686	P-115-RAJ	32	M	L3	15.54	28.38	0.052	0.987	0.051	0.988	0.988	0.051
687	P-116-SUP	54	M	H1	21.91	26.09	0.045	0.993	0.044	0.993	0.993	0.044
688	P-116-SUP	54	M	U1	6.37	6.49	0.032	0.960	0.031	0.961	0.961	0.031
689	P-116-SUP	54	M	U3	4.97	5.35	0.020	0.953	0.020	0.953	0.953	0.020
690	P-116-SUP	54	M	T1	4.07	5.09	0.025	0.944	0.026	0.943	0.944	0.025
691	P-116-SUP	54	M	T2	4.07	2.93	0.024	0.914	0.023	0.917	0.917	0.023
692	P-116-SUP	54	M	T3	5.35	6.24	0.034	0.928	0.034	0.928	0.928	0.034
693	P-116-SUP	54	M	L1	28.91	16.29	0.029	0.989	0.028	0.989	0.989	0.028
694	P-116-SUP	54	M	L2	33.11	15.53	0.035	0.993	0.037	0.992	0.993	0.035
695	P-117-ROS	45	M	U1	4.46	4.45	0.022	0.935	0.022	0.935	0.935	0.022
696	P-117-ROS	45	M	T1	12.74	15.27	0.050	0.921	0.040	0.947	0.947	0.040
697	P-117-ROS	45	M	T2	10.06	10.82	0.053	0.916	0.053	0.918	0.918	0.053
698	P-117-ROS	45	M	L1	19.87	12.35	0.050	0.974	0.048	0.975	0.975	0.048
699	P-117-ROS	45	M	L2	4.97	5.60	0.031	0.952	0.031	0.952	0.952	0.031
700	P-117-ROS	45	M	L3	13.88	11.71	0.066	0.930	0.065	0.931	0.931	0.065

No	Patient	Age	Gender	Region	Width (mm)	Height (mm)	$S_{a,2}$ (mm)	$R_2^2$	$S_{a,3}$ (mm)	$R_3^2$	$R_{fmat}^2$	$\bar{S}_{fmat}$ (mm)
701	P-118-RAJ	47	M	U1	8.92	15.91	0.046	0.915	0.043	0.926	0.926	0.043
702	P-118-RAJ	47	M	U3	6.75	7.38	0.033	0.943	0.033	0.945	0.945	0.033
703	P-118-RAJ	47	M	T3	7.90	8.65	0.060	0.941	0.062	0.953	0.953	0.062
704	P-118-RAJ	47	M	L1B	33.88	12.85	0.052	0.972	0.049	0.973	0.973	0.049
705	P-118-RAJ	47	M	L2C	15.67	27.49	0.054	0.972	0.051	0.973	0.973	0.051
706	P-118-RAJ	47	M	L3a	8.02	10.56	0.054	0.956	0.056	0.953	0.956	0.054
707	P-119-RAT	45	M	H1	7.13	6.62	0.021	0.987	0.021	0.987	0.987	0.021
708	P-119-RAT	45	M	U1	20.00	16.42	0.035	0.990	0.034	0.991	0.991	0.034
709	P-119-RAT	45	M	U2	13.63	15.53	0.040	0.971	0.041	0.971	0.971	0.041
710	P-119-RAT	45	M	U4	39.74	22.91	0.045	0.980	0.048	0.978	0.980	0.045
711	P-119-RAT	45	M	T1	25.47	16.42	0.040	0.960	0.044	0.976	0.976	0.044
712	P-119-RAT	45	M	T2	27.77	16.67	0.045	0.929	0.043	0.937	0.937	0.043
713	P-119-RAT	45	M	T3	15.79	16.54	0.048	0.951	0.048	0.953	0.953	0.048
714	P-119-RAT	45	M	L1	38.72	19.22	0.032	0.991	0.050	0.981	0.991	0.032
715	P-119-RAT	45	M	L2	13.75	16.04	0.033	0.992	0.033	0.992	0.992	0.033
716	P-120-ROS	40	M	U1	7.26	6.11	0.034	0.942	0.034	0.943	0.943	0.034
717	P-120-ROS	40	M	U2	5.22	5.60	0.029	0.949	0.028	0.950	0.950	0.028
718	P-120-ROS	40	M	U3	2.68	3.05	0.018	0.959	0.018	0.958	0.959	0.018
719	P-120-ROS	40	M	T1	9.30	11.07	0.029	0.954	0.029	0.956	0.956	0.029
720	P-120-ROS	40	M	T2	7.64	4.20	0.026	0.964	0.024	0.969	0.969	0.024
721	P-120-ROS	40	M	L1	6.11	9.93	0.028	0.953	0.028	0.953	0.953	0.028
722	P-120-ROS	40	M	L2	6.37	9.55	0.029	0.957	0.029	0.957	0.957	0.029
723	P-121-PAR	52	M	U1	16.43	17.31	0.065	0.933	0.063	0.936	0.936	0.063
724	P-121-PAR	52	M	U2	20.38	19.09	0.046	0.985	0.044	0.986	0.986	0.044
725	P-121-PAR	52	M	U3	15.67	19.22	0.037	0.939	0.037	0.940	0.940	0.037
726	P-121-PAR	52	M	T1	12.74	11.07	0.029	0.965	0.028	0.968	0.968	0.028
727	P-121-PAR	52	M	T2	10.70	16.16	0.035	0.944	0.033	0.948	0.948	0.033
728	P-121-PAR	52	M	T3	12.23	15.40	0.022	0.958	0.024	0.954	0.958	0.022
729	P-121-PAR	52	M	L2	19.36	18.71	0.028	0.947	0.030	0.946	0.947	0.028
730	P-121-PAR	52	M	L3	17.58	15.53	0.061	0.953	0.058	0.958	0.958	0.058
731	P-121-PAR	52	M	L4	25.35	24.56	0.026	0.965	0.032	0.992	0.992	0.032
732	P-122-RIZ	38	M	H1	12.86	12.98	0.027	0.996	0.026	0.996	0.996	0.026
733	P-122-RIZ	38	M	U1	10.19	8.78	0.024	0.980	0.024	0.981	0.981	0.024
734	P-122-RIZ	38	M	U2	9.81	8.91	0.054	0.947	0.053	0.948	0.948	0.053
735	P-122-RIZ	38	M	U3	5.99	8.15	0.033	0.966	0.032	0.968	0.968	0.032
736	P-122-RIZ	38	M	T1	20.76	14.89	0.049	0.968	0.049	0.967	0.968	0.049
737	P-122-RIZ	38	M	T2	18.60	10.95	0.039	0.914	0.046	0.905	0.914	0.039
738	P-122-RIZ	38	M	T3	8.92	12.09	0.042	0.947	0.042	0.933	0.947	0.042
739	P-122-RIZ	38	M	L1	15.28	25.33	0.043	0.964	0.042	0.964	0.964	0.042
740	P-122-RIZ	38	M	L2	16.94	15.02	0.034	0.980	0.033	0.981	0.981	0.033
741	P-122-RIZ	38	M	L5	8.28	11.45	0.030	0.964	0.030	0.963	0.964	0.030
742	P-123-NUR	23	F	U1	17.58	12.85	0.022	0.988	0.022	0.988	0.988	0.022
743	P-123-NUR	23	F	U2B	7.13	8.91	0.051	0.970	0.050	0.971	0.971	0.050
744	P-123-NUR	23	F	T2	8.79	7.13	0.027	0.943	0.025	0.947	0.947	0.025

No	Patient	Age	Gender	Region	Width (mm)	Height (mm)	$S_{a,2}$ (mm)	$R_2^2$	$S_{a,3}$ (mm)	$R_3^2$	$R_{final}^2$	$\bar{S}_{final}$ (mm)
745	P-123-NUR	23	F	T3	6.37	5.22	0.028	0.924	0.026	0.933	0.933	0.026
746	P-123-NUR	23	F	L1	28.78	19.98	0.030	0.990	0.035	0.988	0.990	0.030
747	P-123-NUR	23	F	L2	20.25	19.47	0.023	0.959	0.022	0.964	0.964	0.022
748	P-123-NUR	23	F	L3B	10.06	8.02	0.050	0.919	0.050	0.918	0.919	0.050
749	P-124-SAN	38	M	H1	32.73	13.11	0.054	0.989	0.051	0.990	0.990	0.051
750	P-124-SAN	38	M	U1	10.83	12.47	0.028	0.970	0.027	0.972	0.972	0.027
751	P-124-SAN	38	M	U2	15.28	27.87	0.047	0.987	0.046	0.987	0.987	0.046
752	P-124-SAN	38	M	U3	13.75	13.36	0.034	0.968	0.033	0.968	0.968	0.033
753	P-124-SAN	38	M	T1	17.07	25.07	0.058	0.959	0.057	0.958	0.959	0.058
754	P-124-SAN	38	M	T3	21.14	12.34	0.083	0.934	0.082	0.936	0.936	0.082
755	P-124-SAN	38	M	L2	17.83	17.82	0.021	0.994	0.020	0.994	0.994	0.020
756	P-124-SAN	38	M	L4	33.37	26.60	0.032	0.996	0.044	0.990	0.996	0.032
757	P-125-LIM	71	M	U2	16.94	14.13	0.034	0.962	0.035	0.962	0.962	0.035
758	P-125-LIM	71	M	U3	12.61	15.53	0.049	0.917	0.048	0.918	0.918	0.048
759	P-125-LIM	71	M	T1	23.69	14.76	0.055	0.941	0.054	0.942	0.942	0.054
760	P-125-LIM	71	M	T2	16.94	23.16	0.056	0.977	0.052	0.980	0.980	0.052
761	P-125-LIM	71	M	T3	14.01	20.11	0.033	0.964	0.033	0.964	0.964	0.033
762	P-125-LIM	71	M	L1B	22.54	22.78	0.054	0.988	0.051	0.988	0.988	0.051
763	P-125-LIM	71	M	L2	13.88	12.22	0.045	0.983	0.044	0.983	0.983	0.044
764	P-125-LIM	71	M	L3	24.20	13.49	0.064	0.973	0.058	0.977	0.977	0.058
765	P-126-WAN	23	M	H1	5.35	7.64	0.025	0.967	0.025	0.967	0.967	0.025
766	P-126-WAN	23	M	U1	4.46	4.96	0.020	0.970	0.020	0.971	0.971	0.020
767	P-126-WAN	23	M	U2	3.82	4.96	0.025	0.932	0.025	0.935	0.935	0.025
768	P-126-WAN	23	M	U3	3.18	2.80	0.020	0.948	0.020	0.948	0.948	0.020
769	P-126-WAN	23	M	T1	5.99	9.04	0.014	0.979	0.015	0.962	0.979	0.014
770	P-126-WAN	23	M	T2	3.18	4.84	0.014	0.988	0.014	0.988	0.988	0.014
771	P-126-WAN	23	M	T3	3.82	3.69	0.018	0.936	0.018	0.936	0.936	0.018
772	P-126-WAN	23	M	L1	11.46	19.09	0.040	0.986	0.037	0.988	0.988	0.037
773	P-126-WAN	23	M	L2	13.50	16.04	0.039	0.977	0.038	0.979	0.979	0.038
774	P-126-WAN	23	M	L3B	7.51	6.11	0.020	0.932	0.020	0.929	0.932	0.020
775	P-127-EMA	60	F	T1	9.81	5.47	0.023	0.955	0.022	0.958	0.958	0.022
776	P-127-EMA	60	F	T2	12.10	11.71	0.055	0.948	0.052	0.952	0.952	0.052
777	P-127-EMA	60	F	T3	4.84	8.15	0.032	0.960	0.031	0.963	0.963	0.031
778	P-127-EMA	60	F	L1	12.74	17.95	0.048	0.967	0.047	0.969	0.969	0.047
779	P-127-EMA	60	F	L2B	4.20	4.84	0.020	0.934	0.020	0.934	0.934	0.020
780	P-127-EMA	60	F	L3	5.35	12.98	0.049	0.971	0.049	0.970	0.971	0.049
781	P-128-SHA	41	M	H1	9.93	10.82	0.026	0.986	0.024	0.988	0.988	0.024
782	P-128-SHA	41	M	U1	10.83	15.15	0.033	0.982	0.036	0.981	0.982	0.033
783	P-128-SHA	41	M	U3	20.76	12.22	0.047	0.971	0.045	0.973	0.973	0.045
784	P-128-SHA	41	M	T2	7.51	7.64	0.028	0.977	0.026	0.978	0.978	0.026
785	P-128-SHA	41	M	T3	10.32	9.67	0.051	0.946	0.052	0.944	0.946	0.051
786	P-128-SHA	41	M	T4	37.44	28.76	0.103	0.971	0.111	0.986	0.986	0.111
787	P-128-SHA	41	M	L1	20.50	16.93	0.038	0.992	0.039	0.992	0.992	0.039
788	P-128-SHA	41	M	L2	18.60	13.62	0.059	0.987	0.047	0.992	0.992	0.047

No	Patient	Age	Gender	Region	Width (mm)	Height (mm)	$S_{a,2}$ (mm)	$R_2^2$	$S_{a,3}$ (mm)	$R_3^2$	$R_{final}^2$	$\overline{S}_{final}$ (mm)
789	P-128-SHA	41	M	L3	14.14	11.07	0.027	0.979	0.027	0.979	0.979	0.027
790	P-128-SHA	41	M	L4	36.68	29.15	0.042	0.994	0.077	0.972	0.994	0.042
791	P-74-LAT	50	M	H1	4.075	3.691	0.021	0.936	0.021	0.935	0.936	0.021
792	P-74-LAT	50	M	U1	12.864	20.491	0.095	0.958	0.101	0.955	0.958	0.095
793	P-74-LAT	50	M	U2	3.311	3.437	0.028	0.931	0.028	0.931	0.931	0.028
794	P-74-LAT	50	M	U3	9.552	12.345	0.045	0.948	0.041	0.955	0.955	0.041
795	P-74-LAT	50	M	T1	4.203	4.963	0.035	0.929	0.035	0.928	0.929	0.035
796	P-74-LAT	50	M	T2	4.203	5.855	0.027	0.912	0.026	0.917	0.917	0.026
797	P-74-LAT	50	M	T3	11.717	11.582	0.044	0.962	0.042	0.965	0.965	0.042
798	P-74-LAT	50	M	L1	12.226	15.654	0.063	0.950	0.057	0.957	0.957	0.057
799	P-74-LAT	50	M	L2	16.811	14.890	0.057	0.967	0.057	0.966	0.967	0.057
800	P-74-LAT	50	M	L3	15.156	16.672	0.069	0.953	0.066	0.956	0.956	0.066
801	P-75-PON	51	M	H1	3.821	3.309	0.016	0.947	0.019	0.924	0.947	0.016
802	P-75-PON	51	M	U1	7.259	5.981	0.037	0.945	0.037	0.945	0.945	0.037
803	P-75-PON	51	M	U2	10.189	11.327	0.056	0.979	0.054	0.980	0.980	0.054
804	P-75-PON	51	M	U3	9.170	6.109	0.045	0.962	0.047	0.958	0.962	0.045
805	P-75-PON	51	M	T2	11.462	16.036	0.036	0.977	0.034	0.979	0.979	0.034
806	P-75-PON	51	M	T1	11.080	13.490	0.039	0.947	0.040	0.946	0.947	0.039
807	P-75-PON	51	M	L1	21.142	12.599	0.023	0.976	0.028	0.984	0.984	0.028
808	P-75-PON	51	M	L2	16.684	16.163	0.087	0.917	0.091	0.911	0.917	0.087
809	P-75-PON	51	M	L3	12.354	11.200	0.029	0.984	0.029	0.985	0.985	0.029
810	P-76-MOH	47	M	H1	6.113	7.509	0.018	0.985	0.018	0.986	0.986	0.018
811	P-76-MOH	47	M	U1	17.194	15.654	0.032	0.963	0.033	0.962	0.963	0.032
812	P-76-MOH	47	M	U2	15.028	12.091	0.029	0.972	0.030	0.971	0.972	0.029
813	P-76-MOH	47	M	U3	7.259	11.454	0.028	0.980	0.027	0.981	0.981	0.027
814	P-76-MOH	47	M	T1	21.524	19.599	0.033	0.975	0.030	0.978	0.978	0.030
815	P-76-MOH	47	M	T2	19.359	17.181	0.062	0.945	0.061	0.948	0.948	0.061
816	P-76-MOH	47	M	T3	11.844	9.163	0.025	0.961	0.026	0.957	0.961	0.025
817	P-76-MOH	47	M	T4	11.081	8.654	0.049	0.975	0.048	0.975	0.975	0.048
818	P-76-MOH	47	M	L1	10.316	7.382	0.031	0.987	0.031	0.986	0.987	0.031
819	P-76-MOH	47	M	L2	4.202	7.509	0.030	0.967	0.029	0.969	0.969	0.029
820	P-76-MOH	47	M	L3	9.552	9.036	0.035	0.989	0.035	0.990	0.990	0.035
821	P-77-AZI	46	M	H1	14.647	13.745	0.022	0.979	0.022	0.979	0.979	0.022
822	P-77-AZI	46	M	T1	21.269	28.254	0.040	0.937	0.045	0.928	0.937	0.040
823	P-77-AZI	46	M	T4	20.123	18.327	0.037	0.994	0.036	0.994	0.994	0.036
824	P-77-AZI	46	M	L2	14.646	13.363	0.051	0.977	0.052	0.978	0.978	0.052
825	P-77-AZI	46	M	L3	9.551	9.927	0.053	0.983	0.053	0.983	0.983	0.053
826	P-78-NUR	25	F	H1	30.948	10.055	0.039	0.984	0.038	0.987	0.987	0.038
827	P-78-NUR	25	F	U1	19.996	20.108	0.058	0.984	0.059	0.983	0.984	0.058
828	P-78-NUR	25	F	U2	19.358	28.890	0.055	0.958	0.057	0.952	0.958	0.055
829	P-78-NUR	25	F	U3	16.684	15.273	0.036	0.996	0.035	0.996	0.996	0.035
830	P-78-NUR	25	F	T1	18.085	10.563	0.076	0.980	0.075	0.980	0.980	0.075
831	P-78-NUR	25	F	T2	16.557	29.272	0.050	0.932	0.049	0.933	0.933	0.049
832	P-78-NUR	25	F	T3	14.137	21.891	0.073	0.925	0.073	0.925	0.925	0.073

No	Patient	Age	Gender	Region	Width (mm)	Height (mm)	$S_{a,2}$ (mm)	$R_2^2$	$S_{a,3}$ (mm)	$R_3^2$	$R_{final}^2$	$\overline{S}_{final}$ (mm)
833	P-78-NUR	25	F	L2	17.958	20.490	0.055	0.965	0.062	0.957	0.965	0.055
834	P-78-NUR	25	F	L3	12.481	11.327	0.066	0.967	0.064	0.969	0.969	0.064
835	P-79-AZM	27	M	H1	4.967	4.964	0.036	0.945	0.036	0.944	0.945	0.036
836	P-79-AZM	27	M	U1	20.887	20.999	0.041	0.971	0.044	0.978	0.978	0.044
837	P-79-AZM	27	M	U2	10.953	14.254	0.048	0.928	0.047	0.933	0.933	0.047
838	P-79-AZM	27	M	U3	11.462	11.072	0.034	0.979	0.033	0.980	0.980	0.033
839	P-79-AZM	27	M	T1	11.972	11.581	0.047	0.950	0.046	0.951	0.951	0.046
840	P-79-AZM	27	M	T2	13.245	17.436	0.057	0.930	0.057	0.928	0.930	0.057
841	P-79-AZM	27	M	T3	13.119	11.327	0.049	0.967	0.047	0.969	0.969	0.047
842	P-79-AZM	27	M	L1	9.170	9.927	0.027	0.965	0.027	0.968	0.968	0.027
843	P-79-AZM	27	M	L2	7.514	9.800	0.036	0.944	0.035	0.964	0.964	0.035
844	P-79-AZM	27	M	L3	19.613	9.291	0.045	0.966	0.046	0.964	0.966	0.045
845	P-80-SIN	78	M	U1	14.392	12.855	0.064	0.952	0.071	0.949	0.952	0.064
846	P-80-SIN	78	M	T1	22.670	22.018	0.057	0.974	0.059	0.972	0.974	0.057
847	P-80-SIN	78	M	T4	24.580	22.908	0.054	0.970	0.062	0.957	0.970	0.054
848	P-81-SEL	57	M	H1	8.151	7.127	0.032	0.941	0.031	0.944	0.944	0.031
849	P-81-SEL	57	M	U1	10.953	13.872	0.048	0.954	0.048	0.948	0.954	0.048
850	P-81-SEL	57	M	U3	5.477	5.855	0.028	0.934	0.028	0.933	0.934	0.028
851	P-81-SEL	57	M	T1	10.826	7.891	0.046	0.950	0.044	0.955	0.955	0.044
852	P-81-SEL	57	M	T2	26.745	8.909	0.051	0.988	0.050	0.988	0.988	0.050
853	P-81-SEL	57	M	T3	13.755	14.000	0.040	0.964	0.041	0.951	0.964	0.040
854	P-81-SEL	57	M	L1	22.161	17.182	0.057	0.979	0.055	0.980	0.980	0.055
855	P-81-SEL	57	M	L2	28.783	16.927	0.066	0.961	0.072	0.953	0.961	0.066
856	P-81-SEL	57	M	L3	20.377	28.508	0.059	0.987	0.063	0.986	0.987	0.059
857	P-82-MAH	51	M	U1	6.495	8.145	0.036	0.940	0.036	0.940	0.940	0.036
858	P-82-MAH	51	M	U2	8.533	13.872	0.038	0.966	0.038	0.967	0.967	0.038
859	P-82-MAH	51	M	U3	6.750	3.054	0.023	0.947	0.023	0.947	0.947	0.023
860	P-82-MAH	51	M	T1	12.609	12.091	0.050	0.961	0.050	0.960	0.961	0.050
861	P-82-MAH	51	M	T2	6.878	8.527	0.036	0.956	0.036	0.956	0.956	0.036
862	P-82-MAH	51	M	T3	16.939	13.363	0.032	0.975	0.039	0.966	0.975	0.032
863	P-82-MAH	51	M	L1	12.226	11.582	0.025	0.995	0.027	0.993	0.995	0.025
864	P-82-MAH	51	M	L2	4.967	5.345	0.021	0.911	0.021	0.911	0.911	0.021
865	P-82-MAH	51	M	L3	5.732	7.000	0.040	0.937	0.039	0.943	0.943	0.039
866	P-83-SHA	34	M	H1	4.967	4.073	0.031	0.966	0.031	0.966	0.966	0.031
867	P-83-SHA	34	M	U1	17.067	7.891	0.039	0.971	0.043	0.966	0.971	0.039
868	P-83-SHA	34	M	U2	11.335	22.908	0.052	0.965	0.049	0.957	0.965	0.052
869	P-83-SHA	34	M	U3	7.896	8.654	0.057	0.912	0.065	0.905	0.912	0.057
870	P-83-SHA	34	M	T1	14.647	26.090	0.051	0.978	0.056	0.973	0.978	0.051
871	P-83-SHA	34	M	T2	33.114	16.799	0.073	0.978	0.072	0.979	0.979	0.072
872	P-83-SHA	34	M	T3	29.038	13.745	0.070	0.956	0.069	0.958	0.958	0.069
873	P-83-SHA	34	M	L1	14.902	25.072	0.059	0.966	0.061	0.964	0.966	0.059
874	P-83-SHA	34	M	L2	30.948	17.181	0.064	0.990	0.066	0.988	0.990	0.064
875	P-83-SHA	34	M	L3	16.684	24.690	0.085	0.938	0.085	0.941	0.941	0.085
876	P-84-NOO	49	F	H1	18.977	15.527	0.040	0.962	0.042	0.958	0.962	0.040

No	Patient	Age	Gender	Region	Width (mm)	Height (mm)	$S_{a,2}$ (mm)	$R_2^2$	$S_{a,3}$ (mm)	$R_3^2$	$R_{final}^2$	$S_{final}$ (mm)
877	P-84-NOO	49	F	U1	8.915	20.745	0.056	0.942	0.055	0.941	0.942	0.056
878	P-84-NOO	49	F	U2	15.283	20.491	0.088	0.982	0.087	0.982	0.982	0.087
879	P-84-NOO	49	F	T1	10.316	18.454	0.061	0.905	0.058	0.913	0.913	0.058
880	P-84-NOO	49	F	T3	24.071	14.126	0.072	0.921	0.075	0.913	0.921	0.072
881	P-84-NOO	49	F	L1	14.519	19.981	0.032	0.988	0.037	0.986	0.988	0.032
882	P-84-NOO	49	F	L2	17.449	17.817	0.061	0.913	0.059	0.916	0.916	0.059
883	P-84-NOO	49	F	L3	23.689	16.672	0.058	0.979	0.072	0.972	0.979	0.058
884	P-85-CHE	61	M	U1	11.335	7.127	0.026	0.970	0.026	0.968	0.970	0.026
885	P-85-CHE	61	M	U2	7.514	12.218	0.048	0.926	0.049	0.922	0.926	0.048
886	P-85-CHE	61	M	U3	13.245	17.054	0.071	0.945	0.067	0.949	0.949	0.067
887	P-85-CHE	61	M	T1	10.699	13.236	0.043	0.960	0.043	0.960	0.960	0.043
888	P-85-CHE	61	M	T2	14.774	12.981	0.040	0.924	0.041	0.923	0.924	0.040
889	P-85-CHE	61	M	T3	16.684	15.527	0.068	0.933	0.068	0.958	0.958	0.068
890	P-85-CHE	61	M	T4	30.439	27.999	0.093	0.931	0.091	0.933	0.933	0.091
891	P-85-CHE	61	M	L1	16.684	13.618	0.038	0.957	0.038	0.958	0.958	0.038
892	P-85-CHE	61	M	L2	9.552	23.672	0.060	0.979	0.060	0.979	0.979	0.060
893	P-86-AKI	47	F	U2	2.674	3.818	0.022	0.972	0.022	0.972	0.972	0.022
894	P-86-AKI	47	F	U3	4.585	7.000	0.023	0.925	0.023	0.924	0.925	0.023
895	P-86-AKI	47	F	T1	5.349	7.636	0.037	0.934	0.036	0.967	0.967	0.036
896	P-86-AKI	47	F	T2	5.604	5.982	0.020	0.957	0.020	0.958	0.958	0.020
897	P-86-AKI	47	F	T3	4.840	5.091	0.043	0.957	0.042	0.958	0.958	0.042
898	P-86-AKI	47	F	L1	5.477	4.454	0.026	0.964	0.027	0.963	0.964	0.026
899	P-86-AKI	47	F	L2	5.604	5.982	0.046	0.931	0.046	0.933	0.933	0.046
900	P-86-AKI	47	F	L3	5.986	7.763	0.026	0.924	0.026	0.920	0.924	0.026
901	P-87-NOR	33	F	H1	8.024	6.363	0.029	0.932	0.030	0.920	0.932	0.029
902	P-87-NOR	33	F	U1	18.340	14.508	0.050	0.953	0.049	0.954	0.954	0.049
903	P-87-NOR	33	F	U2	11.972	12.091	0.054	0.995	0.054	0.996	0.996	0.054
904	P-87-NOR	33	F	T1	19.359	16.418	0.054	0.933	0.053	0.935	0.935	0.053
905	P-87-NOR	33	F	L1	16.303	14.636	0.036	0.972	0.035	0.973	0.973	0.035
906	P-87-NOR	33	F	L3	11.972	9.163	0.045	0.948	0.034	0.937	0.948	0.045
907	P-88-SAW	57	M	H1	12.227	13.364	0.040	0.962	0.036	0.958	0.962	0.040
908	P-88-SAW	57	M	U1	9.552	5.727	0.024	0.971	0.023	0.973	0.973	0.023
909	P-88-SAW	57	M	U2	6.622	5.091	0.028	0.976	0.028	0.976	0.976	0.028
910	P-88-SAW	57	M	T1	9.042	13.872	0.041	0.923	0.041	0.925	0.925	0.041
911	P-88-SAW	57	M	T2	11.972	5.346	0.042	0.929	0.040	0.934	0.934	0.040
912	P-88-SAW	57	M	T3	10.316	7.891	0.046	0.935	0.043	0.943	0.943	0.043
913	P-88-SAW	57	M	T4	11.717	12.600	0.054	0.936	0.057	0.924	0.936	0.054
914	P-88-SAW	57	M	L1	10.062	10.309	0.035	0.960	0.034	0.962	0.962	0.034
915	P-88-SAW	57	M	L2	7.387	8.018	0.042	0.945	0.039	0.950	0.950	0.039
916	P-89-BAK	48	M	H1	3.439	4.072	0.020	0.966	0.020	0.966	0.966	0.020
917	P-89-BAK	48	M	U1	13.500	10.945	0.070	0.950	0.066	0.956	0.956	0.066
918	P-89-BAK	48	M	U2	10.953	12.981	0.060	0.957	0.060	0.957	0.957	0.060
919	P-89-BAK	48	M	U3	26.491	14.764	0.086	0.944	0.075	0.954	0.954	0.075
920	P-89-BAK	48	M	T2	21.524	11.455	0.080	0.964	0.084	0.960	0.964	0.080

No	Patient	Age	Gender	Region	Width (mm)	Height (mm)	$S_{a,2}$ (mm)	$R_2^2$	$S_{a,3}$ (mm)	$R_3^2$	$R_{final}^2$	$\overline{S}_{final}$ (mm)
921	P-89-BAK	48	M	T3	9.424	20.108	0.048	0.973	0.048	0.974	0.974	0.048
922	P-89-BAK	48	M	T4	6.877	9.545	0.046	0.946	0.041	0.956	0.956	0.041
923	P-89-BAK	48	M	T6	31.840	26.090	0.070	0.948	0.073	0.942	0.948	0.070
924	P-89-BAK	48	M	L1	16.175	16.036	0.042	0.981	0.037	0.985	0.985	0.037
925	P-89-BAK	48	M	L2	21.906	17.436	0.063	0.964	0.062	0.965	0.965	0.062
926	P-89-BAK	48	M	L3	9.934	9.036	0.037	0.946	0.035	0.950	0.950	0.035
927	P-90-MOH	51	M	U1	8.405	5.473	0.026	0.920	0.026	0.920	0.920	0.026
928	P-90-MOH	51	M	U3	4.712	4.709	0.021	0.948	0.020	0.954	0.954	0.020
929	P-90-MOH	51	M	T1	4.968	5.473	0.038	0.926	0.025	0.955	0.955	0.025
930	P-90-MOH	51	M	T2	6.496	7.127	0.025	0.960	0.025	0.932	0.960	0.025
931	P-90-MOH	51	M	T3	2.929	3.436	0.020	0.935	0.021	0.935	0.935	0.021
932	P-90-MOH	51	M	T4	11.844	15.527	0.032	0.940	0.031	0.941	0.941	0.031
933	P-90-MOH	51	M	L2	4.076	4.582	0.031	0.939	0.029	0.947	0.947	0.029
934	P-91-MOH	28	M	H1	8.915	10.309	0.024	0.951	0.025	0.946	0.951	0.024
935	P-91-MOH	28	M	U1	12.481	13.363	0.042	0.966	0.041	0.966	0.966	0.041
936	P-91-MOH	28	M	U2	23.944	18.073	0.068	0.962	0.067	0.962	0.962	0.067
937	P-91-MOH	28	M	U3	9.807	9.927	0.042	0.956	0.041	0.958	0.958	0.041
938	P-91-MOH	28	M	T1	26.618	10.945	0.072	0.970	0.068	0.973	0.973	0.068
939	P-91-MOH	28	M	T2	23.052	13.108	0.071	0.930	0.071	0.932	0.932	0.071
940	P-91-MOH	28	M	T3	17.066	12.854	0.066	0.920	0.065	0.921	0.921	0.065
941	P-91-MOH	28	M	T4	9.170	7.764	0.028	0.939	0.028	0.939	0.939	0.028
942	P-91-MOH	28	M	T5	28.656	26.090	0.116	0.909	0.132	0.789	0.909	0.116
943	P-91-MOH	28	M	T6	25.727	25.326	0.085	0.933	0.076	0.931	0.933	0.085
944	P-91-MOH	28	M	L1	18.468	18.454	0.071	0.978	0.069	0.980	0.980	0.069
945	P-91-MOH	28	M	L2	17.321	18.072	0.059	0.956	0.059	0.957	0.957	0.059
946	P-91-MOH	28	M	L3	23.307	13.363	0.056	0.951	0.054	0.956	0.956	0.054
947	P-92-ASO	55	M	H1	9.043	12.854	0.029	0.927	0.030	0.926	0.927	0.029
948	P-92-ASO	55	M	U1	17.703	11.199	0.049	0.983	0.049	0.982	0.983	0.049
949	P-92-ASO	55	M	U2	11.335	7.382	0.026	0.953	0.025	0.955	0.955	0.025
950	P-92-ASO	55	M	U3	7.133	8.655	0.028	0.959	0.029	0.956	0.959	0.028
951	P-92-ASO	55	M	T1	6.750	13.873	0.046	0.962	0.041	0.967	0.967	0.041
952	P-92-ASO	55	M	T2	4.585	5.473	0.024	0.929	0.024	0.930	0.930	0.024
953	P-92-ASO	55	M	L1	12.609	12.855	0.050	0.977	0.048	0.977	0.977	0.048
954	P-92-ASO	55	M	L2	9.934	13.872	0.032	0.982	0.030	0.983	0.983	0.030
955	P-92-ASO	55	M	L3	19.995	14.127	0.057	0.959	0.055	0.962	0.962	0.055
956	P-93-CHE	40	M	H1	17.321	18.708	0.080	0.939	0.085	0.947	0.947	0.085
957	P-93-CHE	40	M	U1	10.062	11.327	0.036	0.949	0.035	0.938	0.949	0.036
958	P-93-CHE	40	M	U2	8.916	8.781	0.037	0.981	0.033	0.986	0.986	0.033
959	P-93-CHE	40	M	U3	12.991	11.200	0.028	0.967	0.029	0.966	0.967	0.028
960	P-93-CHE	40	M	T1	23.052	14.000	0.063	0.969	0.063	0.970	0.970	0.063
961	P-93-CHE	40	M	T2	17.958	9.673	0.040	0.928	0.037	0.925	0.928	0.040
962	P-93-CHE	40	M	T3	20.632	9.927	0.060	0.917	0.059	0.919	0.919	0.059
963	P-93-CHE	40	M	T4	21.524	18.581	0.055	0.967	0.054	0.969	0.969	0.054
964	P-93-CHE	40	M	T5	32.222	25.199	0.051	0.969	0.058	0.970	0.970	0.058

No	Patient	Age	Gender	Region	Width (mm)	Height (mm)	$S_{a,2}$ (mm)	$R_2^2$	$S_{a,3}$ (mm)	$R_3^2$	$R_{final}^2$	$\overline{S_{final}}$ (mm)
965	P-93-CHE	40	M	L1	15.028	17.308	0.033	0.986	0.032	0.986	0.986	0.032
966	P-93-CHE	40	M	L3	16.812	11.964	0.062	0.949	0.060	0.951	0.951	0.060
967	P-94-UVA	22	M	U1	5.477	5.345	0.013	0.965	0.013	0.965	0.965	0.013
968	P-94-UVA	22	M	U2	5.349	6.873	0.024	0.928	0.023	0.930	0.930	0.023
969	P-94-UVA	22	M	U3	8.279	5.600	0.019	0.971	0.019	0.973	0.973	0.019
970	P-94-UVA	22	M	T1	6.750	5.218	0.025	0.907	0.021	0.930	0.930	0.021
971	P-94-UVA	22	M	T2	3.184	2.927	0.027	0.919	0.027	0.919	0.919	0.027
972	P-94-UVA	22	M	T3	6.113	4.709	0.021	0.945	0.021	0.946	0.946	0.021
973	P-94-UVA	22	M	T4	7.005	4.327	0.015	0.968	0.016	0.966	0.968	0.015
974	P-94-UVA	22	M	L2	4.330	3.946	0.017	0.948	0.017	0.948	0.948	0.017
975	P-94-UVA	22	M	L3	4.330	4.454	0.021	0.985	0.022	0.984	0.985	0.021
976	P-129-JEL	43	F	U11	12.482	12.345	0.031	0.969	0.029	0.973	0.973	0.029
977	P-129-JEL	43	F	U12	12.736	12.218	0.026	0.952	0.027	0.951	0.952	0.026
978	P-129-JEL	43	F	U3	13.373	12.855	0.061	0.926	0.062	0.923	0.926	0.061
979	P-129-JEL	43	F	L1	11.844	11.073	0.035	0.973	0.040	0.938	0.973	0.035
980	P-129-JEL	43	F	L2	11.590	16.163	0.048	0.929	0.049	0.915	0.929	0.048
981	P-129-JEL	43	F	L3	9.425	11.327	0.041	0.879	0.038	0.905	0.905	0.038
982	P-129-JEL	43	F	L32	9.934	10.308	0.041	0.964	0.041	0.964	0.964	0.041
983	P-129-JEL	43	F	L33	9.297	11.581	0.051	0.964	0.051	0.963	0.964	0.051
984	P-130-VIV	67	F	U1	3.311	3.818	0.051	0.920	0.051	0.919	0.920	0.051
985	P-130-VIV	67	F	U2	1.656	2.545	0.020	0.935	0.019	0.936	0.936	0.019
986	P-130-VIV	67	F	U3	2.802	2.546	0.019	0.932	0.020	0.934	0.934	0.020
987	P-130-VIV	67	F	T2	12.736	10.945	0.054	0.766	0.042	0.900	0.900	0.042
988	P-130-VIV	67	F	T3	21.651	12.982	0.070	0.931	0.068	0.936	0.936	0.068
989	P-130-VIV	67	F	L1A	5.476	4.709	0.029	0.922	0.029	0.922	0.922	0.029
990	P-130-VIV	67	F	L2	3.821	4.073	0.017	0.916	0.017	0.915	0.916	0.017
991	P-130-VIV	67	F	L3	3.948	5.218	0.028	0.964	0.027	0.965	0.965	0.027
992	P-131-SIT	58	F	H	8.278	12.218	0.042	0.950	0.041	0.952	0.952	0.041
993	P-131-SIT	58	F	U1	8.024	12.854	0.043	0.962	0.043	0.963	0.963	0.043
994	P-131-SIT	58	F	U2	15.920	23.544	0.041	0.966	0.040	0.969	0.969	0.040
995	P-131-SIT	58	F	U3	8.406	10.436	0.027	0.926	0.028	0.924	0.926	0.027
996	P-131-SIT	58	F	T1	11.717	10.054	0.041	0.939	0.039	0.945	0.945	0.039
997	P-131-SIT	58	F	T2	12.481	13.745	0.036	0.944	0.034	0.948	0.948	0.034
998	P-131-SIT	58	F	T3	10.188	12.218	0.037	0.922	0.049	0.913	0.922	0.037
999	P-131-SIT	58	F	L1	14.646	16.036	0.041	0.921	0.041	0.921	0.921	0.041
1000	P-131-SIT	58	F	L2	8.915	12.345	0.046	0.910	0.046	0.911	0.911	0.046
1001	P-131-SIT	58	F	L3	9.679	10.436	0.042	0.960	0.042	0.960	0.960	0.042
1002	P-132-ONG	50	M	U2	4.458	7.254	0.025	0.928	0.025	0.930	0.930	0.025
1003	P-132-ONG	50	M	U3	5.221	5.472	0.028	0.947	0.028	0.947	0.947	0.028
1004	P-132-ONG	50	M	T1	6.495	9.036	0.036	0.954	0.035	0.955	0.955	0.035
1005	P-132-ONG	50	M	T2	6.114	5.727	0.032	0.934	0.032	0.947	0.947	0.032
1006	P-132-ONG	50	M	T3	6.241	5.346	0.030	0.937	0.029	0.938	0.938	0.029
1007	P-132-ONG	50	M	L2	5.222	4.963	0.023	0.926	0.023	0.927	0.927	0.023
1008	P-132-ONG	50	M	L3	5.731	6.237	0.019	0.958	0.019	0.959	0.959	0.019

No	Patient	Age	Gender	Region	Width (mm)	Height (mm)	$S_{a,2}$ (mm)	$R_2^2$	$S_{a,3}$ (mm)	$R_3^2$	$R_{fmat}^2$	$\overline{S}_{fmat}$ (mm)
1009	P-133-SUB	49	M	U1	14.391	21.763	0.043	0.990	0.049	0.988	0.990	0.043
1010	P-133-SUB	49	M	U2	21.906	9.164	0.080	0.994	0.085	0.993	0.994	0.080
1011	P-133-SUB	49	M	U3	16.047	15.017	0.073	0.959	0.075	0.958	0.959	0.073
1012	P-133-SUB	49	M	U4	34.515	27.745	0.167	0.955	0.160	0.958	0.958	0.160
1013	P-133-SUB	49	M	T1	20.251	25.199	0.079	0.949	0.083	0.940	0.949	0.079
1014	P-133-SUB	49	M	T2	27.510	11.327	0.053	0.990	0.055	0.989	0.990	0.053
1015	P-133-SUB	49	M	T3	15.283	11.200	0.034	0.950	0.034	0.946	0.950	0.034
1016	P-133-SUB	49	M	L1	30.949	15.018	0.128	0.943	0.111	0.956	0.956	0.111
1017	P-133-SUB	49	M	L2	21.523	14.382	0.045	0.921	0.046	0.917	0.921	0.045
1018	P-133-SUB	49	M	L3	19.358	13.363	0.050	0.911	0.064	0.855	0.911	0.050
1019	P-134-JOH	62	M	U1	11.717	22.526	0.052	0.986	0.045	0.989	0.989	0.045
1020	P-134-JOH	62	M	U2	13.118	16.036	0.044	0.968	0.042	0.970	0.970	0.042
1021	P-134-JOH	62	M	U3	13.755	16.799	0.048	0.976	0.046	0.977	0.977	0.046
1022	P-134-JOH	62	M	T1	12.100	14.381	0.036	0.925	0.036	0.922	0.925	0.036
1023	P-134-JOH	62	M	T2	5.858	5.855	0.025	0.910	0.025	0.911	0.911	0.025
1024	P-134-JOH	62	M	T3	4.839	6.109	0.029	0.928	0.029	0.929	0.929	0.029
1025	P-134-JOH	62	M	L1	19.868	18.073	0.122	0.952	0.114	0.958	0.958	0.114
1026	P-134-JOH	62	M	L2	11.335	14.127	0.029	0.988	0.031	0.986	0.988	0.029
1027	P-134-JOH	62	M	L3	20.505	16.672	0.032	0.994	0.031	0.994	0.994	0.031
1028	P-135-RUS	44	M	H	11.081	7.000	0.024	0.973	0.022	0.976	0.976	0.022
1029	P-135-RUS	44	M	J2	5.604	5.982	0.022	0.923	0.022	0.924	0.924	0.022
1030	P-135-RUS	44	M	U3	6.877	9.291	0.033	0.967	0.033	0.967	0.967	0.033
1031	P-135-RUS	44	M	T2	9.042	10.563	0.038	0.945	0.038	0.947	0.947	0.038
1032	P-135-RUS	44	M	T3	12.226	12.982	0.044	0.925	0.040	0.933	0.933	0.040
1033	P-135-RUS	44	M	L3	7.132	5.855	0.055	0.920	0.055	0.920	0.920	0.055
1034	P-136-SAI	51	M	U1	11.335	13.109	0.063	0.708	0.044	0.911	0.911	0.044
1035	P-136-SAI	51	M	U3	13.500	18.582	0.073	0.934	0.071	0.940	0.940	0.071
1036	P-136-SAI	51	M	T1	21.015	6.109	0.154	0.916	0.134	0.932	0.932	0.134
1037	P-136-SAI	51	M	T12	25.090	10.818	0.146	0.939	0.145	0.939	0.939	0.145
1038	P-136-SAI	51	M	T2	10.953	16.036	0.036	0.972	0.032	0.978	0.978	0.032
1039	P-136-SAI	51	M	T3	29.038	17.182	0.078	0.981	0.074	0.983	0.983	0.074
1040	P-136-SAI	51	M	L2	16.939	27.872	0.168	0.955	0.161	0.957	0.957	0.161
1041	P-136-SAI	51	M	L3	12.099	15.400	0.112	0.904	0.094	0.930	0.930	0.094
1042	P-137-KRI	57	M	U1	8.915	10.436	0.036	0.948	0.036	0.949	0.949	0.036
1043	P-137-KRI	57	M	U2	17.321	9.672	0.057	0.928	0.061	0.923	0.928	0.057
1044	P-137-KRI	57	M	U3	19.996	18.327	0.058	0.984	0.064	0.979	0.984	0.058
1045	P-137-KRI	57	M	T1	9.425	23.800	0.042	0.977	0.040	0.979	0.979	0.040
1046	P-137-KRI	57	M	T3	15.410	11.963	0.076	0.932	0.071	0.928	0.932	0.076
1047	P-137-KRI	57	M	L1	26.236	14.635	0.036	0.993	0.043	0.991	0.993	0.036
1048	P-137-KRI	57	M	L2	25.472	9.418	0.027	0.994	0.033	0.992	0.994	0.027
1049	P-137-KRI	57	M	L3	17.958	18.454	0.046	0.992	0.049	0.990	0.992	0.046
1050	P-138-BAH	44	M	U1	18.722	14.891	0.060	0.957	0.063	0.955	0.957	0.060
1051	P-138-BAH	44	M	U2	20.377	15.654	0.072	0.980	0.076	0.978	0.980	0.072
1052	P-138-BAH	44	M	U3	15.920	13.872	0.072	0.959	0.065	0.969	0.969	0.065

No	Patient	Age	Gender	Region	Width (mm)	Height (mm)	$S_{a,2}$ (mm)	$R_2^2$	$S_{a,3}$ (mm)	$R_3^2$	$R_{fmat}^2$	$\bar{S}_{fmat}$ (mm)
1053	P-138-BAH	44	M	T1	37.189	12.727	0.078	0.960	0.075	0.963	0.963	0.075
1054	P-138-BAH	44	M	T2	10.444	13.491	0.056	0.924	0.053	0.933	0.933	0.053
1055	P-138-BAH	44	M	T3	15.793	28.126	0.066	0.973	0.066	0.972	0.973	0.066
1056	P-138-BAH	44	M	L1	14.391	29.272	0.070	0.989	0.078	0.986	0.989	0.070
1057	P-138-BAH	44	M	L2	14.901	14.127	0.086	0.934	0.085	0.937	0.937	0.085
1058	P-138-BAH	44	M	L3	14.010	16.800	0.071	0.976	0.069	0.978	0.978	0.069
1059	P-139-SAR	27	F	U1	14.264	11.454	0.031	0.987	0.031	0.987	0.987	0.031
1060	P-139-SAR	27	F	U2	7.133	8.528	0.025	0.987	0.025	0.986	0.987	0.025
1061	P-139-SAR	27	F	U3	21.397	12.345	0.051	0.994	0.051	0.995	0.995	0.051
1062	P-139-SAR	27	F	U32	12.863	10.182	0.049	0.989	0.049	0.988	0.989	0.049
1063	P-139-SAR	27	F	T1	11.972	11.708	0.024	0.947	0.023	0.953	0.953	0.023
1064	P-139-SAR	27	F	T3	5.477	5.345	0.017	0.981	0.017	0.981	0.981	0.017
1065	P-139-SAR	27	F	L1	14.264	10.436	0.022	0.958	0.021	0.959	0.959	0.021
1066	P-139-SAR	27	F	L2	18.722	16.673	0.052	0.962	0.050	0.963	0.963	0.050
1067	P-139-SAR	27	F	L3	5.476	7.254	0.022	0.926	0.022	0.929	0.929	0.022
1068	P-140-MUR	25	M	U1	14.137	13.236	0.039	0.951	0.037	0.955	0.955	0.037
1069	P-140-MUR	25	M	U2	20.887	15.145	0.051	0.959	0.048	0.963	0.963	0.048
1070	P-140-MUR	25	M	U3	10.189	23.800	0.068	0.974	0.065	0.977	0.977	0.065
1071	P-140-MUR	25	M	T1	10.443	10.818	0.019	0.944	0.021	0.931	0.944	0.019
1072	P-140-MUR	25	M	T2	9.170	11.072	0.045	0.970	0.042	0.973	0.973	0.042
1073	P-140-MUR	25	M	T22	7.768	10.436	0.044	0.917	0.043	0.921	0.921	0.043
1074	P-140-MUR	25	M	T3	6.622	6.746	0.021	0.967	0.022	0.966	0.967	0.021
1075	P-140-MUR	25	M	L1	11.845	7.636	0.067	0.967	0.067	0.967	0.967	0.067
1076	P-140-MUR	25	M	L2	35.916	10.054	0.062	0.933	0.051	0.955	0.955	0.051
1077	P-140-MUR	25	M	L3	13.882	12.472	0.055	0.924	0.049	0.930	0.930	0.049
1078	P-141-AHA	46	M	H	13.373	7.000	0.026	0.977	0.025	0.978	0.978	0.025
1079	P-141-AHA	46	M	H2	6.368	5.473	0.020	0.971	0.020	0.971	0.971	0.020
1080	P-141-AHA	46	M	U1	7.387	18.326	0.079	0.931	0.073	0.938	0.938	0.073
1081	P-141-AHA	46	M	U2	10.316	11.072	0.048	0.960	0.047	0.961	0.961	0.047
1082	P-141-AHA	46	M	U3	5.986	8.400	0.043	0.917	0.044	0.912	0.917	0.043
1083	P-141-AHA	46	M	T1	17.066	24.818	0.046	0.962	0.059	0.965	0.965	0.059
1084	P-141-AHA	46	M	T2	21.524	16.418	0.051	0.954	0.051	0.953	0.954	0.051
1085	P-141-AHA	46	M	T3	13.373	20.363	0.043	0.946	0.043	0.946	0.946	0.043
1086	P-141-AHA	46	M	T4	36.679	28.381	0.058	0.989	0.063	0.986	0.989	0.058
1087	P-141-AHA	46	M	L1	11.081	24.054	0.047	0.973	0.047	0.977	0.977	0.047
1088	P-141-AHA	46	M	L2	9.934	11.836	0.038	0.954	0.038	0.954	0.954	0.038
1089	P-141-AHA	46	M	L3	23.434	12.600	0.063	0.969	0.063	0.969	0.969	0.063
1090	P-142-MAR	55	F	U2	4.967	8.399	0.052	0.904	0.085	0.745	0.904	0.052
1091	P-142-MAR	55	F	U3	5.222	4.327	0.035	0.976	0.036	0.975	0.976	0.035
1092	P-142-MAR	55	F	L1	17.448	13.363	0.030	0.962	0.031	0.963	0.963	0.031
1093	P-142-MAR	55	F	L2	6.114	6.236	0.020	0.988	0.020	0.988	0.988	0.020
1094	P-142-MAR	55	F	L3	7.642	16.545	0.082	0.950	0.071	0.958	0.958	0.071
1095	P-143-RAJ	46	M	U1	9.806	9.418	0.024	0.962	0.025	0.960	0.962	0.024
1096	P-143-RAJ	46	M	U2	5.986	8.655	0.031	0.937	0.031	0.938	0.938	0.031

No	Patient	Age	Gender	Region	Width (mm)	Height (mm)	$S_{a,2}$ (mm)	$R_2^2$	$S_{a,3}$ (mm)	$R_3^2$	$R_{final}^2$	$S_{final}$ (mm)
1097	P-143-RAJ	46	M	U3	5.476	6.364	0.040	0.967	0.040	0.966	0.967	0.040
1098	P-143-RAJ	46	M	T1	14.901	12.982	0.028	0.977	0.029	0.975	0.977	0.028
1099	P-143-RAJ	46	M	T2	9.552	11.200	0.031	0.962	0.030	0.964	0.964	0.030
1100	P-143-RAJ	46	M	T3	34.769	14.763	0.046	0.970	0.046	0.970	0.970	0.046
1101	P-143-RAJ	46	M	L1	6.368	9.037	0.034	0.913	0.034	0.912	0.913	0.034
1102	P-143-RAJ	46	M	L3	4.712	5.218	0.021	0.909	0.021	0.910	0.910	0.021
1103	P-144-ESM	63	F	U1	10.571	15.909	0.059	0.972	0.057	0.949	0.972	0.059
1104	P-144-ESM	63	F	U2	7.387	17.182	0.040	0.984	0.039	0.985	0.985	0.039
1105	P-144-ESM	63	F	U3	9.807	7.255	0.084	0.954	0.078	0.960	0.960	0.078
1106	P-144-ESM	63	F	L1	17.576	13.745	0.047	0.914	0.047	0.918	0.918	0.047
1107	P-144-ESM	63	F	L2	32.094	12.345	0.034	0.950	0.033	0.954	0.954	0.033
1108	P-144-ESM	63	F	L4	33.369	27.490	0.101	0.962	0.103	0.955	0.962	0.101
1109	P-145-MUH	26	M	H	7.387	7.891	0.030	0.928	0.029	0.930	0.930	0.029
1110	P-145-MUH	26	M	U1	4.331	4.327	0.030	0.931	0.030	0.931	0.931	0.030
1111	P-145-MUH	26	M	U2	4.967	4.327	0.036	0.947	0.037	0.946	0.947	0.036
1112	P-145-MUH	26	M	U3	5.222	5.218	0.039	0.941	0.039	0.942	0.942	0.039
1113	P-145-MUH	26	M	T1	10.062	8.400	0.057	0.941	0.054	0.950	0.950	0.054
1114	P-145-MUH	26	M	T2	8.915	7.890	0.053	0.958	0.052	0.959	0.959	0.052
1115	P-145-MUH	26	M	T3	12.100	8.782	0.069	0.954	0.067	0.956	0.956	0.067
1116	P-145-MUH	26	M	L1	5.094	5.472	0.042	0.937	0.040	0.944	0.944	0.040
1117	P-145-MUH	26	M	L3	5.221	3.182	0.034	0.973	0.033	0.974	0.974	0.033
1118	P-146-SAK	48	M	U1	12.991	12.854	0.038	0.956	0.037	0.956	0.956	0.037
1119	P-146-SAK	48	M	U2	20.504	21.254	0.064	0.980	0.068	0.976	0.980	0.064
1120	P-146-SAK	48	M	U3	20.505	17.944	0.090	0.947	0.091	0.945	0.947	0.090
1121	P-146-SAK	48	M	T1	7.515	6.618	0.033	0.929	0.033	0.929	0.929	0.033
1122	P-146-SAK	48	M	T2	19.486	25.708	0.054	0.960	0.053	0.963	0.963	0.053
1123	P-146-SAK	48	M	T3	22.925	10.436	0.039	0.956	0.038	0.959	0.959	0.038
1124	P-146-SAK	48	M	L1	16.939	21.890	0.051	0.971	0.049	0.973	0.973	0.049
1125	P-147-THE	50	M	U2	15.538	11.709	0.052	0.955	0.053	0.954	0.955	0.052
1126	P-147-THE	50	M	T1	13.118	8.018	0.026	0.991	0.026	0.991	0.991	0.026
1127	P-147-THE	50	M	T2	14.519	8.399	0.029	0.991	0.028	0.992	0.992	0.028
1128	P-147-THE	50	M	T3	17.194	10.436	0.055	0.985	0.056	0.984	0.985	0.055
1129	P-147-THE	50	M	T32	18.849	10.309	0.058	0.971	0.057	0.973	0.973	0.057
1130	P-147-THE	50	M	L1	14.647	17.945	0.049	0.984	0.044	0.986	0.986	0.044
1131	P-147-THE	50	M	L2	11.335	18.964	0.056	0.963	0.057	0.960	0.963	0.056
1132	P-147-THE	50	M	L3	18.467	17.436	0.053	0.954	0.053	0.955	0.955	0.053
1133	P-148-AHM	33	M	H	8.279	11.836	0.028	0.937	0.027	0.940	0.940	0.027
1134	P-148-AHM	33	M	U1	14.010	25.708	0.055	0.976	0.056	0.975	0.976	0.055
1135	P-148-AHM	33	M	U2	17.193	10.690	0.057	0.944	0.057	0.943	0.944	0.057
1136	P-148-AHM	33	M	U3	25.090	15.273	0.075	0.991	0.074	0.991	0.991	0.074
1137	P-148-AHM	33	M	T1	36.425	10.691	0.049	0.985	0.051	0.984	0.985	0.049
1138	P-148-AHM	33	M	T2	22.415	16.672	0.078	0.954	0.079	0.953	0.954	0.078
1139	P-148-AHM	33	M	T3	39.099	11.582	0.071	0.921	0.072	0.919	0.921	0.071
1140	P-148-AHM	33	M	L1	15.028	27.490	0.097	0.961	0.090	0.966	0.966	0.090

No	Patient	Age	Gender	Region	Width (mm)	Height (mm)	$S_{a,2}$ (mm)	$R_2^2$	$S_{a,3}$ (mm)	$R_3^2$	$R_{final}^2$	$S_{final}$ (mm)
1141	P-148-AHM	33	M	L2	29.929	21.636	0.095	0.989	0.097	0.988	0.989	0.095
1142	P-148-AHM	33	M	L3	13.501	27.490	0.091	0.951	0.089	0.954	0.954	0.089
1143	P-149-HAS	28	M	H	15.028	10.945	0.028	0.973	0.027	0.973	0.973	0.027
1144	P-149-HAS	28	M	U2	3.948	5.600	0.024	0.928	0.025	0.924	0.928	0.024
1145	P-149-HAS	28	M	U3	3.439	3.691	0.019	0.962	0.018	0.962	0.962	0.018
1146	P-149-HAS	28	M	T1	6.496	5.091	0.039	0.929	0.038	0.930	0.930	0.038
1147	P-149-HAS	28	M	T2	4.457	4.836	0.031	0.926	0.031	0.927	0.927	0.031
1148	P-149-HAS	28	M	L1	9.170	9.799	0.031	0.926	0.032	0.927	0.927	0.032
1149	P-149-HAS	28	M	L2	3.821	3.436	0.021	0.940	0.021	0.941	0.941	0.021
1150	P-149-HAS	28	M	L3	4.203	5.345	0.026	0.973	0.027	0.972	0.973	0.026
1151	P-150-MOH	51	M	U1	4.840	5.981	0.019	0.937	0.019	0.936	0.937	0.019
1152	P-150-MOH	51	M	U2	6.750	6.236	0.015	0.907	0.015	0.909	0.909	0.015
1153	P-150-MOH	51	M	U3	2.802	2.673	0.019	0.950	0.019	0.949	0.950	0.019
1154	P-150-MOH	51	M	T1	24.071	14.508	0.046	0.973	0.046	0.973	0.973	0.046
1155	P-150-MOH	51	M	T2	11.335	17.691	0.038	0.956	0.038	0.957	0.957	0.038
1156	P-150-MOH	51	M	T3	11.717	19.218	0.046	0.954	0.047	0.952	0.954	0.046
1157	P-150-MOH	51	M	L1	24.963	10.945	0.041	0.976	0.039	0.978	0.978	0.039
1158	P-150-MOH	51	M	L2	16.302	16.418	0.023	0.993	0.022	0.993	0.993	0.022
1159	P-150-MOH	51	M	L3	20.887	8.145	0.024	0.993	0.023	0.994	0.994	0.023
1160	P-151-ROS	51	F	H	4.457	3.818	0.022	0.947	0.022	0.947	0.947	0.022
1161	P-151-ROS	51	F	H2	4.203	3.945	0.029	0.857	0.021	0.901	0.901	0.021
1162	P-151-ROS	51	F	U1	12.481	13.109	0.047	0.959	0.048	0.959	0.959	0.048
1163	P-151-ROS	51	F	U3	16.302	13.618	0.056	0.930	0.055	0.933	0.933	0.055
1164	P-151-ROS	51	F	U4	15.538	12.090	0.047	0.965	0.045	0.968	0.968	0.045
1165	P-151-ROS	51	F	U5	11.589	13.109	0.031	0.963	0.032	0.958	0.963	0.031
1166	P-151-ROS	51	F	U6	15.156	16.163	0.028	0.987	0.028	0.986	0.987	0.028
1167	P-151-ROS	51	F	T1	12.736	9.545	0.033	0.987	0.032	0.988	0.988	0.032
1168	P-151-ROS	51	F	T2	6.623	11.327	0.019	0.981	0.019	0.981	0.981	0.019
1169	P-151-ROS	51	F	T3	14.519	15.527	0.066	0.911	0.064	0.916	0.916	0.064
1170	P-151-ROS	51	F	T4	11.462	17.563	0.041	0.983	0.042	0.982	0.983	0.041
1171	P-151-ROS	51	F	T5	9.425	11.964	0.038	0.950	0.035	0.957	0.957	0.035
1172	P-151-ROS	51	F	T6	21.906	12.727	0.049	0.959	0.049	0.945	0.959	0.049
1173	P-151-ROS	51	F	L1	13.882	21.000	0.056	0.976	0.057	0.959	0.976	0.056
1174	P-151-ROS	51	F	L2	9.680	12.472	0.060	0.940	0.056	0.946	0.946	0.056
1175	P-151-ROS	51	F	L3	11.717	14.382	0.037	0.984	0.040	0.981	0.984	0.037
1176	P-152-SIT	59	F	H	9.680	5.982	0.037	0.956	0.037	0.956	0.956	0.037
1177	P-152-SIT	59	F	U1	14.901	16.163	0.037	0.967	0.036	0.969	0.969	0.036
1178	P-152-SIT	59	F	U2	12.227	7.763	0.049	0.942	0.049	0.942	0.942	0.049
1179	P-152-SIT	59	F	U3	23.434	12.472	0.072	0.922	0.070	0.923	0.923	0.070
1180	P-152-SIT	59	F	T1	6.113	10.436	0.043	0.947	0.040	0.956	0.956	0.040
1181	P-152-SIT	59	F	T2	33.623	10.564	0.050	0.932	0.056	0.914	0.932	0.050
1182	P-152-SIT	59	F	T3	19.613	28.127	0.046	0.951	0.046	0.953	0.953	0.046
1183	P-152-SIT	59	F	L1	11.081	16.290	0.034	0.960	0.033	0.961	0.961	0.033
1184	P-152-SIT	59	F	L12	12.609	13.490	0.036	0.973	0.040	0.964	0.973	0.036

No	Patient	Age	Gender	Region	Width (mm)	Height (mm)	$S_{a,2}$ (mm)	$R_2^2$	$S_{a,3}$ (mm)	$R_3^2$	$R_{final}^2$	$S_{final}$ (mm)
1185	P-152-SIT	59	F	L2	9.043	8.400	0.042	0.956	0.042	0.956	0.956	0.042
1186	P-152-SIT	59	F	L3	11.972	10.690	0.062	0.959	0.062	0.959	0.959	0.062
1187	P-153-ZUR	31	F	U1	4.203	4.454	0.029	0.929	0.030	0.926	0.929	0.029
1188	P-153-ZUR	31	F	U2	4.967	8.909	0.026	0.951	0.025	0.953	0.953	0.025
1189	P-153-ZUR	31	F	L1	7.005	10.563	0.017	0.995	0.017	0.995	0.995	0.017
1190	P-153-ZUR	31	F	L2	6.241	5.345	0.023	0.970	0.023	0.969	0.970	0.023
1191	P-153-ZUR	31	F	L3	4.458	5.090	0.022	0.958	0.022	0.957	0.958	0.022
1192	P-154-GUN	34	M	H1	6.878	7.508	0.016	0.909	0.016	0.915	0.915	0.016
1193	P-154-GUN	34	M	U1	7.514	9.290	0.022	0.961	0.020	0.964	0.964	0.020
1194	P-154-GUN	34	M	U2	6.750	10.054	0.051	0.970	0.051	0.969	0.970	0.051
1195	P-154-GUN	34	M	U3	5.603	4.836	0.036	0.912	0.036	0.911	0.912	0.036
1196	P-154-GUN	34	M	T1	23.944	14.000	0.066	0.944	0.067	0.942	0.944	0.066
1197	P-154-GUN	34	M	T2	21.014	12.472	0.055	0.933	0.055	0.933	0.933	0.055
1198	P-154-GUN	34	M	T2C	30.439	12.346	0.052	0.993	0.053	0.992	0.993	0.052
1199	P-154-GUN	34	M	T2D	18.849	19.599	0.045	0.939	0.047	0.935	0.939	0.045
1200	P-154-GUN	34	M	T2E	17.321	21.127	0.040	0.953	0.042	0.946	0.953	0.040
1201	P-154-GUN	34	M	T3	5.604	6.490	0.024	0.960	0.024	0.960	0.960	0.024
1202	P-154-GUN	34	M	L1	22.543	8.781	0.030	0.984	0.030	0.985	0.985	0.030
1203	P-154-GUN	34	M	L1B	21.778	14.636	0.029	0.980	0.031	0.978	0.980	0.029
1204	P-154-GUN	34	M	L3	11.972	19.218	0.046	0.950	0.043	0.960	0.960	0.043
1205	P-155-NOR	41	M	U1	9.425	14.508	0.023	0.986	0.023	0.987	0.987	0.023
1206	P-155-NOR	41	M	U2	11.208	9.672	0.051	0.939	0.052	0.938	0.939	0.051
1207	P-155-NOR	41	M	U3	8.660	7.255	0.029	0.954	0.028	0.945	0.954	0.029
1208	P-155-NOR	41	M	U4	15.410	12.218	0.037	0.970	0.037	0.969	0.970	0.037
1209	P-155-NOR	41	M	T1	14.265	9.164	0.050	0.933	0.049	0.935	0.935	0.049
1210	P-155-NOR	41	M	T3	11.081	5.981	0.042	0.948	0.044	0.933	0.948	0.042
1211	P-155-NOR	41	M	L4	31.076	27.363	0.061	0.964	0.085	0.969	0.969	0.085
1212	P-155-NOR	41	M	L5	35.024	26.981	0.035	0.995	0.074	0.976	0.995	0.035
1213	P-156-HAB	38	F	U1	6.241	6.237	0.019	0.987	0.019	0.987	0.987	0.019
1214	P-156-HAB	38	F	U2	5.732	8.527	0.025	0.946	0.025	0.947	0.947	0.025
1215	P-156-HAB	38	F	U3	11.971	17.182	0.017	0.995	0.017	0.994	0.995	0.017
1216	P-156-HAB	38	F	L1	7.768	10.691	0.034	0.953	0.033	0.955	0.955	0.033
1217	P-156-HAB	38	F	L2	9.424	11.200	0.022	0.980	0.021	0.982	0.982	0.021
1218	P-156-HAB	38	F	L3	5.222	6.745	0.014	0.913	0.011	0.908	0.913	0.014
1219	P-157-SET	62	M	U1	17.194	16.291	0.038	0.959	0.039	0.955	0.959	0.038
1220	P-157-SET	62	M	U2	6.240	8.146	0.031	0.982	0.029	0.983	0.983	0.029
1221	P-157-SET	62	M	U3	4.203	6.618	0.035	0.962	0.035	0.961	0.962	0.035
1222	P-157-SET	62	M	T1	7.005	9.418	0.026	0.904	0.026	0.905	0.905	0.026
1223	P-157-SET	62	M	T2	6.878	7.891	0.023	0.945	0.023	0.948	0.948	0.023
1224	P-157-SET	62	M	L1	8.915	10.436	0.026	0.957	0.025	0.959	0.959	0.025
1225	P-157-SET	62	M	L2	13.628	16.927	0.046	0.955	0.046	0.957	0.957	0.046
1226	P-157-SET	62	M	L3	16.048	25.326	0.055	0.977	0.053	0.980	0.980	0.053
1227	P-157-SET	62	M	L3B	18.849	20.744	0.062	0.982	0.058	0.985	0.985	0.058
1228	P-158-SEL	46	M	H	15.920	10.818	0.041	0.929	0.045	0.917	0.929	0.041

No	Patient	Age	Gender	Region	Width (mm)	Height (mm)	$S_{a,2}$ (mm)	$R_2^2$	$S_{a,3}$ (mm)	$R_3^2$	$R_{final}^2$	$\overline{S_{final}}$ (mm)
1229	P-158-SEL	46	M	U1	17.448	15.654	0.041	0.963	0.038	0.965	0.965	0.038
1230	P-158-SEL	46	M	U2	16.684	14.636	0.029	0.981	0.029	0.981	0.981	0.029
1231	P-158-SEL	46	M	U3	24.580	14.509	0.040	0.967	0.039	0.969	0.969	0.039
1232	P-158-SEL	46	M	T2	11.335	8.145	0.034	0.962	0.032	0.969	0.969	0.032
1233	P-158-SEL	46	M	L1	9.934	8.909	0.030	0.963	0.028	0.980	0.980	0.028
1234	P-158-SEL	46	M	L3	7.387	8.782	0.023	0.974	0.022	0.975	0.975	0.022
1235	P-159-RAJ	51	M	H	7.387	8.273	0.016	0.984	0.017	0.984	0.984	0.017
1236	P-159-RAJ	51	M	U1	21.269	6.873	0.044	0.968	0.038	0.974	0.974	0.038
1237	P-159-RAJ	51	M	U2	10.316	18.709	0.039	0.965	0.036	0.967	0.967	0.036
1238	P-159-RAJ	51	M	U3	9.552	13.236	0.025	0.994	0.028	0.992	0.994	0.025
1239	P-159-RAJ	51	M	L1	16.811	15.527	0.046	0.974	0.039	0.983	0.983	0.039
1240	P-159-RAJ	51	M	L2	26.618	11.964	0.075	0.969	0.070	0.971	0.971	0.070
1241	P-159-RAJ	51	M	L3	13.755	16.290	0.053	0.969	0.052	0.968	0.969	0.053
1242	P-160-SAN	35	F	H	11.717	9.163	0.045	0.955	0.044	0.957	0.957	0.044
1243	P-160-SAN	35	F	U1	13.627	23.545	0.033	0.984	0.031	0.986	0.986	0.031
1244	P-160-SAN	35	F	U2	10.443	10.182	0.049	0.977	0.049	0.977	0.977	0.049
1245	P-160-SAN	35	F	U3	21.014	7.255	0.037	0.972	0.035	0.975	0.975	0.035
1246	P-160-SAN	35	F	U4	24.198	26.726	0.050	0.979	0.052	0.980	0.980	0.052
1247	P-160-SAN	35	F	T1	16.047	25.962	0.051	0.946	0.052	0.945	0.946	0.051
1248	P-160-SAN	35	F	T3	4.839	3.946	0.015	0.957	0.020	0.940	0.957	0.015
1249	P-160-SAN	35	F	L1	12.482	19.090	0.035	0.980	0.034	0.980	0.980	0.034
1250	P-160-SAN	35	F	L2	21.906	18.708	0.042	0.993	0.042	0.993	0.993	0.042
1251	P-160-SAN	35	F	L2B	18.468	18.199	0.037	0.989	0.040	0.987	0.989	0.037
1252	P-160-SAN	35	F	L3	6.368	15.272	0.041	0.929	0.040	0.931	0.931	0.040
1253	P-160-SAN	35	F	L4	26.363	18.582	0.051	0.978	0.052	0.977	0.978	0.051
1254	P-161-RAM	56	M	H	6.113	8.655	0.026	0.965	0.026	0.964	0.965	0.026
1255	P-161-RAM	56	M	U1	11.717	12.345	0.039	0.985	0.038	0.986	0.986	0.038
1256	P-161-RAM	56	M	U2	5.349	8.527	0.023	0.927	0.022	0.928	0.928	0.022
1257	P-161-RAM	56	M	U3	5.222	5.981	0.030	0.940	0.031	0.940	0.940	0.031
1258	P-161-RAM	56	M	T1	8.024	8.018	0.034	0.922	0.035	0.919	0.922	0.034
1259	P-161-RAM	56	M	L1	7.005	7.254	0.017	0.971	0.018	0.971	0.971	0.018
1260	P-161-RAM	56	M	L2	25.599	11.582	0.064	0.975	0.059	0.979	0.979	0.059
1261	P-161-RAM	56	M	L4	31.330	27.618	0.058	0.947	0.068	0.948	0.948	0.068
1262	P-162-BAL	41	M	L22	12.226	14.763	0.075	0.979	0.061	0.985	0.985	0.061
1263	P-163-NOR	29	F	H3	10.316	10.563	0.049	0.968	0.049	0.966	0.968	0.049
1264	P-163-NOR	29	F	U22	4.840	6.490	0.028	0.961	0.028	0.961	0.961	0.028
1265	P-163-NOR	29	F	U51	7.387	8.654	0.037	0.939	0.032	0.924	0.939	0.037
1266	P-164-Low	68	M	T21	11.972	16.036	0.030	0.920	0.031	0.918	0.920	0.030
1267	P-165-BAL	48	M	H2	9.043	4.964	0.050	0.699	0.035	0.911	0.911	0.035
1268	P-165-BAL	48	M	T32	16.175	16.036	0.049	0.948	0.051	0.943	0.948	0.049
1269	P-165-BAL	48	M	L11	19.613	20.491	0.050	0.963	0.053	0.959	0.963	0.050
1270	P-166-TEO	58	M	U31	3.439	3.054	0.016	0.940	0.016	0.939	0.940	0.016
1271	P-167-SAN	33	M	H1	5.477	5.345	0.028	0.937	0.027	0.937	0.937	0.027
1272	P-168-NAG	43	M	T42	8.279	9.418	0.026	0.940	0.027	0.936	0.940	0.026

No	Patient	Age	Gender	Region	Width (mm)	Height (mm)	$S_{a,2}$ (mm)	$R_2^2$	$S_{a,3}$ (mm)	$R_3^2$	$R_{final}^2$	$S_{final}$ (mm)
1273	P-168-NAG	43	M	T52	14.773	11.709	0.028	0.948	0.029	0.945	0.948	0.028
1274	P-170-SIE	56	M	H1	6.496	6.745	0.040	0.937	0.038	0.942	0.942	0.038
1275	P-171-NGS	64	M	T11	3.439	4.073	0.022	0.912	0.023	0.912	0.912	0.023
1276	P-172-SUK	35	M	L52	38.080	24.181	0.087	0.911	0.118	0.508	0.911	0.087
1277	P-173-WON	82	M	U12	6.368	4.582	0.030	0.927	0.031	0.918	0.927	0.030
1278	P-173-WON	82	M	T22	6.878	13.872	0.045	0.926	0.040	0.943	0.943	0.040
1279	P-173-WON	82	M	L22	5.222	5.473	0.036	0.973	0.036	0.973	0.973	0.036
1280	P-173-WON	82	M	L31	5.477	6.491	0.034	0.925	0.034	0.924	0.925	0.034
1281	P-176-ADH	34	M	T11	5.604	7.636	0.042	0.811	0.032	0.911	0.911	0.032
1282	P-176-ADH	34	M	T21	5.349	7.127	0.033	0.928	0.033	0.921	0.928	0.033
1283	P-176-ADH	34	M	L12	7.769	7.381	0.033	0.957	0.031	0.961	0.961	0.031
1284	P-177-MAH	45	M	L31	19.996	9.418	0.092	0.921	0.093	0.921	0.921	0.093
1285	P-179-AAL	31	F	U12	17.448	11.836	0.090	0.939	0.090	0.938	0.939	0.090
1286	P-181-NAK	55	M	L12	11.463	15.654	0.034	0.964	0.034	0.964	0.964	0.034
1287	P-182-WON	68	M	U32	3.820	3.818	0.022	0.918	0.022	0.918	0.918	0.022
1288	P-183-NFR	64	M	T21	13.882	14.254	0.052	0.938	0.052	0.939	0.939	0.052
1289	P-185-LOO	71	M	U32	7.005	6.618	0.045	0.936	0.042	0.945	0.945	0.042
1290	P-184-RAT	28	F	U22	14.774	11.327	0.076	0.902	0.077	0.903	0.903	0.077
1291	P-184-RAT	28	F	T32	14.519	15.145	0.058	0.904	0.058	0.905	0.905	0.058
1292	P-187-TAN	31	F	T11	11.845	8.909	0.077	0.918	0.074	0.921	0.921	0.074
1293	P-187-TAN	31	F	T32	16.047	11.709	0.045	0.942	0.043	0.945	0.945	0.043
1294	P-187-TAN	31	F	T51	7.896	8.400	0.056	0.905	0.054	0.905	0.905	0.054
1295	P-187-TAN	31	F	L22	11.589	10.054	0.039	0.930	0.038	0.933	0.933	0.038
1296	P-187-TAN	31	F	L51	5.731	6.237	0.039	0.757	0.033	0.903	0.903	0.033
1297	P-188-MOH	28	M	U11	8.533	9.927	0.039	0.945	0.038	0.949	0.949	0.038
1298	P-188-MOH	28	M	U21	2.675	3.436	0.017	0.957	0.017	0.955	0.957	0.017
1299	P-188-MOH	28	M	L11	8.915	7.509	0.047	0.963	0.049	0.960	0.963	0.047
1300	P-188-MOH	28	M	L31	8.661	10.181	0.034	0.908	0.041	0.904	0.908	0.034
1301	P-189-MOH	74	M	T62	10.316	4.836	0.022	0.940	0.022	0.940	0.940	0.022
1302	P-189-MOH	74	M	T72	7.260	7.000	0.024	0.928	0.024	0.928	0.928	0.024
1303	P-190-OMA	28	M	U21	11.335	14.127	0.039	0.945	0.037	0.951	0.951	0.037
1304	P-190-OMA	28	M	U43	40.119	29.145	0.141	0.975	0.146	0.956	0.975	0.141
1305	P-190-OMA	28	M	T161	39.609	29.527	0.122	0.821	0.126	0.905	0.905	0.126
1306	P-190-OMA	28	M	T21	18.467	14.254	0.082	0.922	0.083	0.921	0.922	0.082
1307	P-190-OMA	28	M	L121	36.043	28.254	0.156	0.918	0.144	0.931	0.931	0.144
1308	P-190-OMA	28	M	L162	19.231	10.182	0.070	0.935	0.069	0.933	0.935	0.070
1309	P-190-OMA	28	M	L172	17.703	12.727	0.079	0.774	0.094	0.928	0.928	0.094
1310	P-191-ALI	56	M	U32	10.061	3.564	0.041	0.906	0.041	0.912	0.912	0.041
1311	P-191-ALI	56	M	T41	10.061	10.181	0.040	0.924	0.040	0.925	0.925	0.040
1312	P-193-UMI	50	F	U22	5.349	6.491	0.025	0.972	0.026	0.971	0.972	0.025
1313	P-193-UMI	50	F	T41	8.660	8.399	0.049	0.905	0.040	0.907	0.907	0.040
1314	P-195-DEV	42	F	T81	23.943	28.381	0.054	0.924	0.055	0.917	0.924	0.054
1315	P-162-BAL	41	M	U31	7.769	7.128	0.035	0.948	0.033	0.955	0.955	0.033
1316	P-167-SAN	33	M	U11	4.203	4.836	0.041	0.913	0.040	0.917	0.917	0.040

No	Patient	Age	Gender	Region	Width (mm)	Height (mm)	$S_{a,2}$ (mm)	$R_2^2$	$S_{a,3}$ (mm)	$R_3^2$	$R_{final}^2$	$\overline{S}_{final}$ (mm)
1317	P-168-NAG	43	M	T21	11.208	5.981	0.033	0.964	0.032	0.966	0.966	0.032
1318	P-168-NAG	43	M	L11	9.679	7.763	0.024	0.973	0.023	0.975	0.975	0.023
1319	P-169-DUW	51	M	U21	5.604	11.709	0.037	0.961	0.036	0.963	0.963	0.036
1320	P-169-DUW	51	M	T11	16.939	13.490	0.024	0.970	0.025	0.970	0.970	0.025
1321	P-169-DUW	51	M	T21	17.321	14.636	0.021	0.926	0.025	0.901	0.926	0.021
1322	P-169-DUW	51	M	L31	16.811	16.800	0.026	0.991	0.024	0.992	0.992	0.024
1323	P-170-SIE	56	M	U11	4.840	6.873	0.039	0.969	0.037	0.971	0.971	0.037
1324	P-170-SIE	56	M	U21	6.368	8.527	0.027	0.967	0.029	0.963	0.967	0.027
1325	P-170-SIE	56	M	U31	5.095	4.709	0.026	0.973	0.026	0.974	0.974	0.026
1326	P-170-SIE	56	M	L21	8.024	9.672	0.033	0.923	0.032	0.926	0.926	0.032
1327	P-170-SIE	56	M	L31	11.717	18.199	0.031	0.954	0.030	0.947	0.954	0.031
1328	P-171-NG	64	M	U21	2.675	3.182	0.037	0.958	0.036	0.959	0.959	0.036
1329	P-172-SUK	35	M	U21	8.151	7.254	0.031	0.951	0.032	0.940	0.951	0.031
1330	P-173-WON	82	M	U31	4.713	6.364	0.029	0.936	0.027	0.942	0.942	0.027
1331	P-173-WON	82	M	T11	6.368	10.690	0.040	0.930	0.038	0.939	0.939	0.038
1332	P-173-WON	82	M	T31	6.495	6.873	0.051	0.927	0.050	0.928	0.928	0.050
1333	P-173-WON	82	M	L11	6.368	7.127	0.032	0.980	0.033	0.979	0.980	0.032
1334	P-174-MAG	33	F	L21	15.283	14.636	0.040	0.995	0.043	0.994	0.995	0.040
1335	P-175-DEN	62	M	U21	7.387	8.654	0.035	0.927	0.036	0.924	0.927	0.035
1336	P-176-ADH	34	M	H1	7.132	5.218	0.038	0.943	0.039	0.942	0.943	0.038
1337	P-176-ADH	34	M	U31	7.387	11.709	0.035	0.962	0.033	0.968	0.968	0.033
1338	P-177-MAH	45	M	H1	9.807	10.563	0.030	0.926	0.030	0.929	0.929	0.030
1339	P-178-YUR	29	F	L61	9.934	11.581	0.035	0.933	0.034	0.937	0.937	0.034
1340	P-180-SEL	65	M	U11	22.161	16.799	0.045	0.994	0.046	0.994	0.994	0.046
1341	P-181-NAK	55	M	L31	8.151	12.981	0.026	0.973	0.025	0.976	0.976	0.025
1342	P-181-NAK	55	M	L41	8.788	15.399	0.035	0.956	0.031	0.957	0.957	0.031
1343	P-182-WON	68	M	U21	4.967	5.727	0.029	0.971	0.029	0.970	0.971	0.029
1344	P-185-LOO	71	M	T31	27.510	17.563	0.033	0.987	0.038	0.978	0.987	0.033
1345	P-185-LOO	71	M	L21	9.170	15.909	0.035	0.942	0.033	0.955	0.955	0.033
1346	P-188-MOH	28	M	U31	9.552	15.782	0.034	0.980	0.032	0.982	0.982	0.032
1347	P-192-MUH	52	M	T61	10.953	5.600	0.037	0.922	0.027	0.929	0.929	0.027
1348	P-192-MUH	52	M	L41	8.660	9.163	0.044	0.939	0.029	0.982	0.982	0.029
1349	P-192-MUH	52	M	L51	6.240	8.145	0.029	0.985	0.029	0.985	0.985	0.029
1350	P-193-UMI	50	F	L51	4.712	5.854	0.021	0.968	0.021	0.968	0.968	0.021
1351	P-195-DEV	42	F	H1	6.750	12.218	0.022	0.934	0.020	0.947	0.947	0.020

APPENDIX D: SCORING RESULTS BY APPLYING CLUSTERING  
ALGORITHM ON TESTING DATASET

No	Patient	Age	Gender	Region	$S_a$ (mm) 1st Asm	$S_a$ (mm) 2nd Asm	k-Means 1st Asm	k-Means 2nd Asm	FCM 1st Asm	FCM 2nd Asm
1	P-162-BLM	40	M	U1	0.039	0.044	2	2	2	2
2	P-162-BLM	40	M	U2	0.017	0.016	1	1	1	1
3	P-162-BLM	40	M	U3	0.033	0.030	2	1	1	1
4	P-162-BLM	40	M	T1	0.022	0.024	1	1	1	1
5	P-162-BLM	40	M	T2	0.026	0.020	1	1	1	1
6	P-162-BLM	40	M	T3	0.035	0.040	2	2	2	2
7	P-162-BLM	40	M	L1	0.043	0.048	2	2	2	2
8	P-162-BLM	40	M	L2	0.063	0.064	3	3	3	3
9	P-163-NAS	28	F	III	0.045	0.045	2	2	2	2
10	P-163-NAS	28	F	U1	0.034	0.041	2	2	1	2
11	P-163-NAS	28	F	U4	0.041	0.038	2	2	2	2
12	P-163-NAS	28	F	T1	0.041	0.043	2	2	2	2
13	P-163-NAS	28	F	T2	0.021	0.022	1	1	1	1
14	P-163-NAS	28	F	T3	0.036	0.033	2	2	2	1
15	P-163-NAS	28	F	L1	0.023	0.022	1	1	1	1
16	P-163-NAS	28	F	L2	0.019	0.017	1	1	1	1
17	P-163-NAS	28	F	L3	0.034	0.037	2	2	1	2
18	P-163-NAS	28	F	L4	0.017	0.018	1	1	1	1
19	P-163-NAS	28	F	L5	0.024	0.022	1	1	1	1
20	P-163-NAS	28	F	L6	0.026	0.020	1	1	1	1
21	P-163-NAS	28	F	L7	0.028	0.026	1	1	1	1
22	P-164-LAT	67	M	H1	0.029	0.026	1	1	1	1
23	P-164-LAT	67	M	U2	0.014	0.014	1	1	1	1
24	P-164-LAT	67	M	T3	0.027	0.031	1	1	1	1
25	P-164-LAT	67	M	T4	0.017	0.015	1	1	1	1
26	P-164-LAT	67	M	T6	0.018	0.019	1	1	1	1
27	P-164-LAT	67	M	L1	0.020	0.020	1	1	1	1
28	P-164-LAT	67	M	L2	0.029	0.029	1	1	1	1
29	P-164-LAT	67	M	L3	0.010	0.010	1	1	1	1
30	P-165-BLK	47	M	U1	0.025	0.026	1	1	1	1
31	P-165-BLK	47	M	U3	0.044	0.044	2	2	2	2
32	P-165-BLK	47	M	T1	0.037	0.035	2	2	2	2
33	P-165-BLK	47	M	T4	0.061	0.060	3	3	3	3
34	P-165-BLK	47	M	L1	0.043	0.042	2	2	2	2
35	P-165-BLK	47	M	L2	0.034	0.035	2	2	1	2

No	Patient	Age	Gender	Region	$S_a$ (mm) 1st Asm	$S_a$ (mm) 2nd Asm	$k$ -Means 1st Asm	$k$ -Means 2nd Asm	FCM 1st Asm	FCM 2nd Asm
36	P-165-BLK	47	M	L3	0.031	0.037	1	2	1	2
37	P-165-BLK	47	M	L4	0.026	0.024	1	1	1	1
38	P-166-TTL	57	M	U2	0.033	0.029	2	1	1	1
39	P-166-TTL	57	M	T1	0.049	0.051	2	3	2	2
40	P-166-TTL	57	M	T2	0.050	0.051	2	3	2	2
41	P-166-TTL	57	M	T3	0.042	0.041	2	2	2	2
42	P-166-TTL	57	M	T4	0.052	0.055	3	3	2	2
43	P-166-TTL	57	M	L1	0.031	0.028	1	1	1	1
44	P-166-TTL	57	M	L2	0.021	0.020	1	1	1	1
45	P-166-TTL	57	M	L3	0.026	0.026	1	1	1	1
46	P-166-TTL	57	M	L4	0.032	0.035	2	2	1	2
47	P-167-SNR	32	M	U2	0.035	0.038	2	2	2	2
48	P-167-SNR	32	M	L1	0.027	0.023	1	1	1	1
49	P-167-SNR	32	M	L2	0.038	0.038	2	2	2	2
50	P-167-SNR	32	M	L3	0.033	0.026	2	1	1	1
51	P-167-SNR	32	M	L4	0.035	0.042	2	2	2	2
52	P-168-NGJ	42	M	U1	0.019	0.021	1	1	1	1
53	P-168-NGJ	42	M	U2	0.022	0.019	1	1	1	1
54	P-168-NGJ	42	M	U3	0.017	0.019	1	1	1	1
55	P-168-NGJ	42	M	U4	0.076	0.078	3	3	3	3
56	P-168-NGJ	42	M	T1	0.024	0.025	1	1	1	1
57	P-168-NGJ	42	M	T3	0.020	0.022	1	1	1	1
58	P-169-DWA	50	M	H1	0.031	0.029	1	1	1	1
59	P-169-DWA	50	M	U1	0.051	0.055	3	3	2	2
60	P-169-DWA	50	M	T3	0.060	0.059	3	3	3	3
61	P-169-DWA	50	M	T5	0.038	0.042	2	2	2	2
62	P-169-DWA	50	M	T6	0.043	0.038	2	2	2	2
63	P-169-DWA	50	M	L5	0.036	0.035	2	2	2	2
64	P-170-SSG	55	M	T1	0.022	0.022	1	1	1	1
65	P-170-SSG	55	M	T1	0.016	0.015	1	1	1	1
66	P-170-SSG	55	M	T2	0.022	0.024	1	1	1	1
67	P-170-SSG	55	M	T3	0.040	0.042	2	2	2	2
68	P-170-SSG	55	M	T4	0.041	0.045	2	2	2	2
69	P-170-SSG	55	M	T5	0.048	0.044	2	2	2	2
70	P-170-SSG	55	M	T7	0.096	0.096	4	4	3	3
71	P-170-SSG	55	M	L1	0.045	0.040	2	2	2	2
72	P-170-SSG	55	M	L1	0.029	0.030	1	1	1	1
73	P-170-SSG	55	M	L1	0.065	0.068	3	3	3	3
74	P-170-SSG	55	M	L2	0.032	0.028	2	1	1	1
75	P-170-SSG	55	M	L6	0.052	0.051	3	3	2	2

No	Patient	Age	Gender	Region	$S_a$ (mm) 1st Asm	$S_a$ (mm) 2nd Asm	$k$ -Means 1st Asm	$k$ -Means 2nd Asm	FCM 1st Asm	FCM 2nd Asm
76	P-170-SSG	55	M	L7	0.067	0.068	3	3	3	3
77	P-170-SSG	55	M	L8	0.058	0.055	3	3	3	2
78	P-171-NSH	63	M	U1	0.024	0.026	1	1	1	1
79	P-171-NSH	63	M	U3	0.018	0.016	1	1	1	1
80	P-171-NSH	63	M	L1	0.032	0.033	2	2	1	1
81	P-171-NSH	63	M	L3	0.026	0.023	1	1	1	1
82	P-171-NSH	63	M	L4	0.021	0.024	1	1	1	1
83	P-171-NSH	63	M	L5	0.038	0.040	2	2	2	2
84	P-172-SKM	34	M	H1	0.049	0.048	2	2	2	2
85	P-172-SKM	34	M	U1	0.037	0.044	2	2	2	2
86	P-172-SKM	34	M	U2	0.031	0.034	1	2	1	1
87	P-172-SKM	34	M	U3	0.036	0.035	2	2	2	2
88	P-172-SKM	34	M	U4	0.079	0.079	3	3	3	3
89	P-172-SKM	34	M	U5	0.061	0.055	3	3	3	2
90	P-172-SKM	34	M	U6	0.073	0.074	3	3	3	3
91	P-172-SKM	34	M	U8	0.077	0.073	3	3	3	3
92	P-172-SKM	34	M	T1	0.033	0.033	2	2	1	1
93	P-172-SKM	34	M	T2	0.053	0.060	3	3	2	3
94	P-172-SKM	34	M	T3	0.035	0.041	2	2	2	2
95	P-172-SKM	34	M	T4	0.102	0.097	4	4	4	3
96	P-172-SKM	34	M	T5	0.078	0.075	3	3	3	3
97	P-172-SKM	34	M	L1	0.075	0.077	3	3	3	3
98	P-172-SKM	34	M	L2	0.039	0.035	2	2	2	2
99	P-172-SKM	34	M	L3	0.048	0.048	2	2	2	2
100	P-172-SKM	34	M	L6	0.054	0.054	3	3	2	2
101	P-172-SKM	34	M	L7	0.041	0.040	2	2	2	2
102	P-173-WKW	81	M	U3	0.027	0.033	1	2	1	1
103	P-173-WKW	81	M	L1	0.032	0.030	2	1	1	1
104	P-174-MGH	32	F	U1	0.042	0.041	2	2	2	2
105	P-174-MGH	32	F	U2	0.051	0.051	3	3	2	2
106	P-174-MGH	32	F	U3	0.025	0.027	1	1	1	1
107	P-174-MGH	32	F	T2	0.027	0.031	1	1	1	1
108	P-174-MGH	32	F	L1	0.059	0.059	3	3	3	3
109	P-174-MGH	32	F	L3	0.062	0.060	3	3	3	3
110	P-175-DNH	61	M	H1	0.031	0.026	1	1	1	1
111	P-175-DNH	61	M	U1	0.030	0.025	1	1	1	1
112	P-175-DNH	61	M	U3	0.032	0.036	2	2	1	2
113	P-175-DNH	61	M	T2	0.054	0.053	3	3	2	2
114	P-175-DNH	61	M	L1	0.034	0.034	2	2	1	1
115	P-175-DNH	61	M	L2	0.050	0.046	2	2	2	2

No	Patient	Age	Gender	Region	$S_u$ (mm) 1st Asm	$S_u$ (mm) 2nd Asm	k-Means 1st Asm	k-Means 2nd Asm	FCM 1st Asm	FCM 2nd Asm
116	P-176-MDA	33	M	U3	0.033	0.029	2	1	1	1
117	P-176-MDA	33	M	U4	0.033	0.029	2	1	1	1
118	P-176-MDA	33	M	L2	0.022	0.016	1	1	1	1
119	P-176-MDA	33	M	L3	0.031	0.030	1	1	1	1
120	P-177-MHD	44	M	H1	0.030	0.036	1	2	1	2
121	P-177-MHD	44	M	U2	0.061	0.063	3	3	3	3
122	P-177-MHD	44	M	U3	0.067	0.062	3	3	3	3
123	P-177-MHD	44	M	T5	0.062	0.065	3	3	3	3
124	P-177-MHD	44	M	L1	0.056	0.061	3	3	2	3
125	P-177-MHD	44	M	L2	0.053	0.048	3	2	2	2
126	P-177-MHD	44	M	L4	0.041	0.040	2	2	2	2
127	P-177-MHD	44	M	L6	0.086	0.080	4	3	3	3
128	P-177-MHD	44	M	L7	0.066	0.070	3	3	3	3
129	P-178-YRL	28	F	H1	0.032	0.036	2	2	1	2
130	P-178-YRL	28	F	U1	0.034	0.039	2	2	1	2
131	P-178-YRL	28	F	U2	0.049	0.044	2	2	2	2
132	P-178-YRL	28	F	U3	0.036	0.041	2	2	2	2
133	P-178-YRL	28	F	T1	0.112	0.114	4	4	4	4
134	P-178-YRL	28	F	T3	0.082	0.081	3	3	3	3
135	P-178-YRL	28	F	L1	0.039	0.042	2	2	2	2
136	P-178-YRL	28	F	L2	0.035	0.037	2	2	2	2
137	P-178-YRL	28	F	L3	0.037	0.039	2	2	2	2
138	P-178-YRL	28	F	L6	0.034	0.029	2	1	1	1
139	P-179-AMI	30	F	H1	0.024	0.031	1	1	1	1
140	P-179-AMI	30	F	U2	0.028	0.025	1	1	1	1
141	P-179-AMI	30	F	U3	0.056	0.052	3	3	2	2
142	P-179-AMI	30	F	T2	0.041	0.036	2	2	2	2
143	P-179-AMI	30	F	L1	0.039	0.036	2	2	2	2
144	P-179-AMI	30	F	L2	0.044	0.046	2	2	2	2
145	P-180-SLV	64	M	U2	0.077	0.073	3	3	3	3
146	P-180-SLV	64	M	U4	0.094	0.090	4	4	3	3
147	P-180-SLV	64	M	U5	0.047	0.048	2	2	2	2
148	P-180-SLV	64	M	T1	0.050	0.051	2	3	2	2
149	P-180-SLV	64	M	T1	0.071	0.065	3	3	3	3
150	P-180-SLV	64	M	T1	0.080	0.085	3	4	3	3
151	P-180-SLV	64	M	T2	0.061	0.066	3	3	3	3
152	P-180-SLV	64	M	T3	0.071	0.075	3	3	3	3
153	P-180-SLV	64	M	T4	0.074	0.075	3	3	3	3
154	P-180-SLV	64	M	T5	0.112	0.106	4	4	4	4
155	P-180-SLV	64	M	T6	0.069	0.076	3	3	3	3

No	Patient	Age	Gender	Region	$S_a$ (mm) 1st Asm	$S_a$ (mm) 2nd Asm	$k$ -Means 1st Asm	$k$ -Means 2nd Asm	FCM 1st Asm	FCM 2nd Asm
156	P-180-SLV	64	M	T7	0.050	0.047	2	2	2	2
157	P-180-SLV	64	M	T8	0.056	0.051	3	3	2	2
158	P-180-SLV	64	M	L1	0.043	0.042	2	2	2	2
159	P-180-SLV	64	M	L1	0.038	0.041	2	2	2	2
160	P-180-SLV	64	M	L1	0.036	0.040	2	2	2	2
161	P-180-SLV	64	M	L2	0.039	0.032	2	2	2	1
162	P-180-SLV	64	M	L3	0.030	0.030	1	1	1	1
163	P-180-SLV	64	M	L5	0.076	0.079	3	3	3	3
164	P-180-SLV	64	M	L6	0.050	0.054	2	3	2	2
165	P-181-NKR	55	M	H1	0.020	0.023	1	1	1	1
166	P-181-NKR	55	M	U2	0.018	0.020	1	1	1	1
167	P-181-NKR	55	M	T1	0.033	0.034	2	2	1	1
168	P-181-NKR	55	M	T2	0.048	0.051	2	3	2	2
169	P-181-NKR	55	M	T3	0.019	0.022	1	1	1	1
170	P-181-NKR	55	M	T4	0.031	0.031	1	1	1	1
171	P-181-NKR	55	M	T5	0.018	0.017	1	1	1	1
172	P-181-NKR	55	M	T6	0.032	0.037	2	2	1	2
173	P-181-NKR	55	M	T7	0.029	0.029	1	1	1	1
174	P-181-NKR	55	M	L1	0.026	0.025	1	1	1	1
175	P-181-NKR	55	M	L2	0.022	0.015	1	1	1	1
176	P-181-NKR	55	M	L3	0.025	0.032	1	2	1	1
177	P-181-NKR	55	M	L4	0.031	0.035	1	2	1	2
178	P-182-WSS	68	M	U1	0.025	0.025	1	1	1	1
179	P-182-WSS	68	M	U2	0.029	0.033	1	2	1	1
180	P-182-WSS	68	M	T1	0.050	0.045	2	2	2	2
181	P-182-WSS	68	M	T3	0.017	0.021	1	1	1	1
182	P-182-WSS	68	M	T4	0.022	0.025	1	1	1	1
183	P-182-WSS	68	M	T5	0.060	0.060	3	3	3	3
184	P-182-WSS	68	M	T6	0.041	0.040	2	2	2	2
185	P-182-WSS	68	M	L1	0.029	0.030	1	1	1	1
186	P-182-WSS	68	M	L2	0.028	0.027	1	1	1	1
187	P-183-NRM	64	M	T1	0.040	0.036	2	2	2	2
188	P-183-NRM	64	M	T4	0.052	0.050	3	2	2	2
189	P-183-NRM	64	M	L1	0.060	0.059	3	3	3	3
190	P-183-NRM	64	M	L2	0.038	0.036	2	2	2	2
191	P-183-NRM	64	M	L3	0.028	0.029	1	1	1	1
192	P-185-LHM	71	M	H1	0.025	0.027	1	1	1	1
193	P-185-LHM	71	M	U2	0.046	0.044	2	2	2	2
194	P-185-LHM	71	M	T2	0.036	0.035	2	2	2	2
195	P-185-LHM	71	M	T3	0.033	0.028	2	1	1	1

No	Patient	Age	Gender	Region	$S_a$ (mm) 1st Asm	$S_a$ (mm) 2nd Asm	k-Means 1st Asm	k-Means 2nd Asm	FCM 1st Asm	FCM 2nd Asm
196	P-185-LHM	71	M	L1	0.049	0.046	2	2	2	2
197	P-185-LHM	71	M	L2	0.033	0.031	2	1	1	1
198	P-185-LHM	71	M	L3	0.032	0.034	2	2	1	1
199	P-184-RTV	28	F	H1	0.087	0.084	4	4	3	3
200	P-184-RTV	28	F	U3	0.065	0.071	3	3	3	3
201	P-184-RTV	28	F	T1	0.124	0.129	4	4	4	4
202	P-184-RTV	28	F	T4	0.111	0.114	4	4	4	4
203	P-184-RTV	28	F	T5	0.158	0.160	4	4	4	4
204	P-184-RTV	28	F	T8	0.068	0.074	3	3	3	3
205	P-184-RTV	28	F	T9	0.182	0.184	4	4	4	4
206	P-184-RTV	28	F	L2	0.037	0.038	2	2	2	2
207	P-184-RTV	28	F	L4	0.072	0.069	3	3	3	3
208	P-184-RTV	28	F	L5	0.035	0.034	2	2	2	1
209	P-184-RTV	28	F	L6	0.057	0.056	3	3	3	2
210	P-184-RTV	28	F	L7	0.033	0.033	2	2	1	1
211	P-184-RTV	28	F	L9	0.056	0.054	3	3	2	2
212	P-186-HSM	52	M	H1	0.027	0.021	1	1	1	1
213	P-186-HSM	52	M	U1	0.044	0.044	2	2	2	2
214	P-186-HSM	52	M	U3	0.035	0.035	2	2	2	2
215	P-186-HSM	52	M	T1	0.039	0.036	2	2	2	2
216	P-186-HSM	52	M	T2	0.037	0.035	2	2	2	2
217	P-186-HSM	52	M	T3	0.035	0.034	2	2	2	1
218	P-186-HSM	52	M	L1	0.056	0.053	3	3	2	2
219	P-186-HSM	52	M	L2	0.036	0.039	2	2	2	2
220	P-186-HSM	52	M	L3	0.043	0.045	2	2	2	2
221	P-186-HSM	52	M	U2	0.041	0.036	2	2	2	2
222	P-186-HSM	52	M	U3	0.037	0.035	2	2	2	2
223	P-187-TLC	31	F	U4	0.052	0.046	3	2	2	2
224	P-187-TLC	31	F	T4	0.048	0.048	2	2	2	2
225	P-187-TLC	31	F	L1	0.040	0.039	2	2	2	2
226	P-187-TLC	31	F	L3	0.047	0.042	2	2	2	2
227	P-187-TLC	31	F	L4	0.035	0.040	2	2	2	2
228	P-187-TLC	31	F	L6	0.041	0.043	2	2	2	2
229	P-187-TLC	31	F	L7	0.079	0.073	3	3	3	3
230	P-188-MNJ	28	M	U3	0.032	0.031	2	1	1	1
231	P-188-MNJ	28	M	T1	0.040	0.041	2	2	2	2
232	P-188-MNJ	28	M	T3	0.039	0.043	2	2	2	2
233	P-188-MNJ	28	M	T4	0.026	0.031	1	1	1	1
234	P-188-MNJ	28	M	T5	0.039	0.038	2	2	2	2
235	P-188-MNJ	28	M	L2	0.021	0.023	1	1	1	1

No	Patient	Age	Gender	Region	$S_a$ (mm) 1st Asm	$S_a$ (mm) 2nd Asm	k-Means 1st Asm	k-Means 2nd Asm	FCM 1st Asm	FCM 2nd Asm
236	P-189-MYM	74	M	T1	0.020	0.021	1	1	1	1
237	P-189-MYM	74	M	T3	0.073	0.075	3	3	3	3
238	P-189-MYM	74	M	T4	0.021	0.021	1	1	1	1
239	P-189-MYM	74	M	T5	0.017	0.017	1	1	1	1
240	P-189-MYM	74	M	T8	0.019	0.017	1	1	1	1
241	P-189-MYM	74	M	T9	0.022	0.025	1	1	1	1
242	P-190-OMR	28	M	H1	0.038	0.033	2	2	2	1
243	P-190-OMR	28	M	U1	0.130	0.129	4	4	4	4
244	P-190-OMR	28	M	U1	0.101	0.096	4	4	4	3
245	P-190-OMR	28	M	U4	0.141	0.138	4	4	4	4
246	P-190-OMR	28	M	U5	0.054	0.060	3	3	2	3
247	P-190-OMR	28	M	T1	0.113	0.115	4	4	4	4
248	P-190-OMR	28	M	T1	0.119	0.120	4	4	4	4
249	P-190-OMR	28	M	T2	0.100	0.101	4	4	4	4
250	P-190-OMR	28	M	T2	0.182	0.187	4	4	4	4
251	P-190-OMR	28	M	T2	0.139	0.142	4	4	4	4
252	P-190-OMR	28	M	T2	0.137	0.131	4	4	4	4
253	P-190-OMR	28	M	T3	0.055	0.055	3	3	2	2
254	P-190-OMR	28	M	T6	0.097	0.101	4	4	3	4
255	P-190-OMR	28	M	T7	0.116	0.121	4	4	4	4
256	P-190-OMR	28	M	T8	0.081	0.081	3	3	3	3
257	P-190-OMR	28	M	L1	0.100	0.106	4	4	4	4
258	P-190-OMR	28	M	L1	0.079	0.086	3	4	3	3
259	P-190-OMR	28	M	L1	0.112	0.116	4	4	4	4
260	P-190-OMR	28	M	L1	0.065	0.058	3	3	3	3
261	P-190-OMR	28	M	L1	0.101	0.099	4	4	4	4
262	P-190-OMR	28	M	L2	0.056	0.056	3	3	2	2
263	P-190-OMR	28	M	L2	0.100	0.106	4	4	4	4
264	P-190-OMR	28	M	L3	0.056	0.063	3	3	2	3
265	P-190-OMR	28	M	L5	0.069	0.073	3	3	3	3
266	P-190-OMR	28	M	L6	0.072	0.078	3	3	3	3
267	P-190-OMR	28	M	L9	0.096	0.099	4	4	3	4
268	P-191-ALD	56	M	H1	0.035	0.039	2	2	2	2
269	P-191-ALD	56	M	T1	0.039	0.037	2	2	2	2
270	P-191-ALD	56	M	T2	0.031	0.033	1	2	1	1
271	P-191-ALD	56	M	T3	0.033	0.036	2	2	1	2
272	P-191-ALD	56	M	L1	0.045	0.050	2	2	2	2
273	P-191-ALD	56	M	L4	0.055	0.058	3	3	2	3
274	P-192-MTA	52	M	H1	0.039	0.043	2	2	2	2
275	P-192-MTA	52	M	U1	0.045	0.041	2	2	2	2

No	Patient	Age	Gender	Region	$S_a$ (mm) 1st Asm	$S_a$ (mm) 2nd Asm	$k$ -Means 1st Asm	$k$ -Means 2nd Asm	FCM 1st Asm	FCM 2nd Asm
276	P-192-MTA	52	M	U3	0.050	0.044	2	2	2	2
277	P-192-MTA	52	M	T2	0.026	0.025	1	1	1	1
278	P-192-MTA	52	M	T3	0.047	0.050	2	2	2	2
279	P-192-MTA	52	M	T4	0.044	0.042	2	2	2	2
280	P-192-MTA	52	M	T5	0.045	0.052	2	3	2	2
281	P-192-MTA	52	M	L1	0.065	0.066	3	3	3	3
282	P-192-MTA	52	M	L2	0.028	0.029	1	1	1	1
283	P-192-MTA	52	M	L4	0.029	0.033	1	2	1	1
284	P-192-MTA	52	M	L5	0.029	0.033	1	2	1	1
285	P-193-UKY	50	F	H1	0.028	0.025	1	1	1	1
286	P-193-UKY	50	F	U2	0.042	0.037	2	2	2	2
287	P-193-UKY	50	F	T1	0.031	0.028	1	1	1	1
288	P-193-UKY	50	F	T2	0.042	0.037	2	2	2	2
289	P-193-UKY	50	F	L2	0.027	0.031	1	1	1	1
290	P-193-UKY	50	F	L3	0.047	0.054	2	3	2	2
291	P-193-UKY	50	F	L6	0.029	0.024	1	1	1	1
292	P-194-ZHN	34	M	U1	0.114	0.109	4	4	4	4
293	P-194-ZHN	34	M	U1	0.063	0.065	3	3	3	3
294	P-194-ZHN	34	M	U3	0.086	0.083	4	3	3	3
295	P-194-ZHN	34	M	U7	0.128	0.125	4	4	4	4
296	P-194-ZHN	34	M	U9	0.078	0.074	3	3	3	3
297	P-194-ZHN	34	M	T1	0.064	0.066	3	3	3	3
298	P-194-ZHN	34	M	T3	0.062	0.061	3	3	3	3
299	P-194-ZHN	34	M	T4	0.089	0.089	4	4	3	3
300	P-194-ZHN	34	M	T5	0.068	0.073	3	3	3	3
301	P-194-ZHN	34	M	T6	0.067	0.066	3	3	3	3
302	P-194-ZHN	34	M	T7	0.101	0.102	4	4	4	4
303	P-194-ZHN	34	M	L1	0.052	0.055	3	3	2	2
304	P-194-ZHN	34	M	L5	0.065	0.066	3	3	3	3
305	P-195-DVM	42	F	U1	0.044	0.042	2	2	2	2
306	P-195-DVM	42	F	U2	0.039	0.038	2	2	2	2
307	P-195-DVM	42	F	U4	0.035	0.036	2	2	2	2
308	P-195-DVM	42	F	U5	0.043	0.039	2	2	2	2
309	P-195-DVM	42	F	U6	0.043	0.036	2	2	2	2
310	P-195-DVM	42	F	U7	0.038	0.037	2	2	2	2
311	P-195-DVM	42	F	T1	0.067	0.065	3	3	3	3
312	P-195-DVM	42	F	T2	0.060	0.060	3	3	3	3
313	P-195-DVM	42	F	T3	0.044	0.047	2	2	2	2
314	P-195-DVM	42	F	T5	0.032	0.033	2	2	1	1
315	P-195-DVM	42	F	T6	0.039	0.039	2	2	2	2

No	Patient	Age	Gender	Region	$S_a$ (mm) 1st Asm	$S_a$ (mm) 2nd Asm	$k$ -Means 1st Asm	$k$ -Means 2nd Asm	FCM 1st Asm	FCM 2nd Asm
316	P-195-DVM	42	F	T9	0.029	0.030	1	1	1	1
317	P-195-DVM	42	F	L1	0.047	0.043	2	2	2	2
318	P-195-DVM	42	F	L1	0.029	0.025	1	1	1	1
319	P-195-DVM	42	F	L1	0.053	0.056	3	3	2	2
320	P-195-DVM	42	F	L2	0.035	0.042	2	2	2	2
321	P-195-DVM	42	F	L5	0.023	0.017	1	1	1	1
322	P-195-DVM	42	F	L6	0.046	0.049	2	2	2	2
323	P-195-DVM	42	F	L7	0.072	0.072	3	3	3	3
324	P-195-DVM	42	F	L9	0.052	0.052	3	3	2	2

**APPENDIX E: APPROVAL OF OBSERVATIONAL CLINICAL  
STUDY (NMRR-09-1098-4863)**

**NATIONAL INSTITUTES OF HEALTH APPROVAL FOR CONDUCTING RESEARCH  
IN THE MINISTRY OF HEALTH MALAYSIA  
PENGESAHAN INSTITUSI PENYELIDIKAN NEGARA UNTUK MENJALANKAN  
PENYELIDIKAN DI KEMENTERIAN KESIHATAN**

This is an auto computer-generated document. It is issued by one of the research institute under the National Institutes of Health (NIH). These are the Institute for Medical Research (IMR), Clinical Research Centre (CRC), Institute of Public Health (IPH), Institute for Health Management (IHM), Institute for Health Systems Research (IHSR), and Institute for Health Behavioural Research (IHBR).

Dokumen ini adalah cetakan berkomputer. Borang ini dikeluarkan oleh salah satu institusi di bawah National Institutes of Health (NIH) iaitu Institut Penyelidikan Perubatan (IMR), Pusat Penyelidikan Klinikal (CRC), Institut Kesihatan Umum (IKU), Institut Pengurusan Kesihatan (IPK), Institut Pengurusan Sistem Kesihatan (IPSK), Institut Penyelidikan Tingkah laku Kesihatan (IPTK).

Unique NMRR Registration ID (Nombor Pendaftaran)	NMRR-09-1098-4863
Research Title (Tajuk)	OBJECTIVE EVALUATION OF PSORIASIS SEVERITY USING A NEW COMPUTERISED PAS SCORING SYSTEM (Afa-PAS)
Protocol Number if available (Nombor Protokol jika ada)	

No	Investigator Name (Nama Penyelidik)	Institution Name (Nama Institusi)
1	Amjad Fadzil M Haniff	Universiti Teknologi PETRONAS (UTP)
2	Azura Norid Alfand	Kuala Lumpur Hospital
3	Chong Yew Tiong	Kuala Lumpur Hospital
4	Suraya Haniff Hussain	Damansara Specialist Hospital

I have reviewed the above titled research and approve of its design and conduct.

Saya telah menyemak kajian yang bertajuk seperti di atas dan meluluskan reka bentuk dan pelaksanaannya.

Name of Director (Nama Pengerusi)	Dr Lim Teck Onn
NIH Institute (IMR, CRC, IPH, IHM, IHSR and IHBR) (Nama institusi di bawah NIH)	Clinical Research Centre (CRC)
Signature & Official stamp (Tandatangan dan Cap Rasmi)	This is computer generated document therefore no signature is required
Date (Tarikh)	07-04-2010

Note: This is a computer generated document. It may not carry any signature.

## APPENDIX F: SOURCE CODE OF SURFACE ROUGHNESS DETERMINATION (MATLAB CODE)

```

=====
1 ===== FILTER AND OPEN A 3D SURFACE FILE
=====
close all; clear all; clc;
folderToBeOpened = 'C:\...\3D Lesion for scaliness\10';

% read a surface file
cd(folderToBeOpened);
[txtFileNm, folderToBeOpened] = uigetfile('*.txt','Select the M-file');

% read 2D jpg file
N = length(txtFileNm);
imgFileNm = txtFileNm;
imgFileNm(N-2)='j';
imgFileNm(N-1)='p';
imgFileNm(N)='g';
=====
2 ===== End of FILTER AND OPEN A 3D SURFACE FILE
=====

3 ===== READ 2D IMAGE AND SEGMENT THE LESION AREA
=====
I2d = imread([folderToBeOpened, imgFileNm]);
[m2D, n2D] = size(I2d);
n2D = n2D/3;

% Normalise I 2D
for iii=1:m2D
    for jjj=1:n2D
        id = m2D - iii + 1;
        I2dT(id, jjj, :) = I2d(iii, jjj, :);
    end;
end;
I2d = I2dT;
clear I2dT;

figNameStr = ['File Name ', imgFileNm];
figure('Name', figNameStr);

imshow(I2d);
[FW, x, y] = roipoly;
close(figNameStr);

minX = round(min(min(x)));
maxX = round(max(max(x)));

minY = round(min(min(y)));
maxY = round(max(max(y)));

figure, imshow(I2d(minY:maxY, minX:maxX, :));
4 ===== End of READ 2D IMAGE AND SEGMENT THE LESION AREA
=====

```

```

% ===== READ TXT FILE AND CONVERT IT INTO A SURFACE MATRIX =====
% Function hdrload() is created by Jeff Daniels (Dec 20, 2002).
% The file is obtained from
% http://www.mathworks.com/matlabcentral/fileexchange/2973-mhdrload-m

[hdr, A] = hdrload(txtFileNm);

initX = A(1,1);
newX = 1e10;
N = 1;
while initX ~= newX
    N = N + 1;
    newX = A(N,1);
end;
N = N - 1;
lengthA = length(A);
M = lengthA/N;

% Create X matrix
xArr = A(1:N,1);
for i=1:M
    I.X(i,:) = xArr;
end;

% Create Y matrix
for i=1:M
    idx = 1 + (i-1)*N;
    yArr(i) = A(idx,2);
end;
for j=1:N
    I.Y(:,j) = yArr;
end;

% Create Z matrix
idxA = 0;
for i=1:M
    for j=1:N
        idxA = idxA + 1;
        I.Z(i,j) = A(idxA,3);
    end;
end;

% ===== End of READ TXT FILE AND CONVERT IT INTO A SURFACE MATRIX =====

% ===== SAMPLE THE LESION AREA FROM 3D SURFACE DATA =====
k = 1; % for the highest resolution, image size 480 x 640 pixels
minXSc = round(k*minX);
maxXSc = round(k*maxX);

minYSc = round(k*minY);
maxYSc = round(k*maxY);

Xcr=I.X(minYSc:maxYSc, minXSc:maxXSc);
Ycr=I.Y(minYSc:maxYSc, minXSc:maxXSc);
Zcr=I.Z(minYSc:maxYSc, minXSc:maxXSc);

I2.X = Xcr;
I2.Y = Ycr;

```

```

I2.Z = Zcr;

figure
subplot(1,2,1), imshow(I2d);
subplot(1,2,2), imshow(I.Z, []);
figure,
subplot(1,2,1), imshow(I2d(minY:maxY,minX:maxX,:));
subplot(1,2,2), imshow(I2.Z, []);
% =====
% ===== End of SAMPLE THE LESION AREA FROM 3D SURFACE DATA =====
% =====

% =====
% ===== DIVIDE THE SAMPLE INTO 4 SUB-DIVIDED SURFACES =====
% =====

noDiv = 2;
[M,N] = size(I2.Z);

mD = floor(M/noDiv);
nD = floor(N/noDiv);

for i=1:(noDiv)
    cI(i) = 1 + (i-1)*mD;
    cJ(i) = 1 + (i-1)*nD;
end;

idxSd = 0;
for i=1:(noDiv)
    for j=1:(noDiv)
        idxSd = idxSd + 1;
        I2sDiv(idxSd).X = I2.X(cI(i):(cI(i)+mD-1),cJ(j):(cJ(j)+nD-1));
        I2sDiv(idxSd).Y = I2.Y(cI(i):(cI(i)+mD-1),cJ(j):(cJ(j)+nD-1));
        I2sDiv(idxSd).Z = I2.Z(cI(i):(cI(i)+mD-1),cJ(j):(cJ(j)+nD-1));
    end;
end;

figure,
subplot(2,2*noDiv,1), imshow(I2sDiv(1).Z, []);
subplot(2,2*noDiv,2), imshow(I2sDiv(2).Z, []);
subplot(2,2*noDiv,5), imshow(I2sDiv(3).Z, []);
subplot(2,2*noDiv,6), imshow(I2sDiv(4).Z, []);

subplot(2,2*noDiv,3), surf(I2sDiv(1).X,I2sDiv(1).Y,I2sDiv(1).Z);
idx=1;
miX = min(min(I2sDiv(idx).X));
mxX = max(max(I2sDiv(idx).X));
miY = min(min(I2sDiv(idx).Y));
mxY = max(max(I2sDiv(idx).Y));
miZ = min(min(I2sDiv(idx).Z));
mxZ = max(max(I2sDiv(idx).Z));
axis([miX mxX miY mxY miZ mxZ])

subplot(2,2*noDiv,4), surf(I2sDiv(2).X,I2sDiv(2).Y,I2sDiv(2).Z);
idx=2;
miX = min(min(I2sDiv(idx).X));
mxX = max(max(I2sDiv(idx).X));
miY = min(min(I2sDiv(idx).Y));
mxY = max(max(I2sDiv(idx).Y));
miZ = min(min(I2sDiv(idx).Z));
mxZ = max(max(I2sDiv(idx).Z));
axis([miX mxX miY mxY miZ mxZ])

subplot(2,2*noDiv,7), surf(I2sDiv(3).X,I2sDiv(3).Y,I2sDiv(3).Z);
idx=3;
miX = min(min(I2sDiv(idx).X));

```

```

mxX = max(max(I2sDiv(idx).X));
miY = min(min(I2sDiv(idx).Y));
mxY = max(max(I2sDiv(idx).Y));
miZ = min(min(I2sDiv(idx).Z));
mxZ = max(max(I2sDiv(idx).Z));
axis([miX mxX miY mxY miZ mxZ]);

subplot(2,2*noDiv,8), surf(I2sDiv(4).X,I2sDiv(4).Y,I2sDiv(4).Z);
idx=4;
miX = min(min(I2sDiv(idx).X));
mxX = max(max(I2sDiv(idx).X));
miY = min(min(I2sDiv(idx).Y));
mxY = max(max(I2sDiv(idx).Y));
miZ = min(min(I2sDiv(idx).Z));
mxZ = max(max(I2sDiv(idx).Z));
axis([miX mxX miY mxY miZ mxZ])
1 =====
2 ===== End of DIVIDE THE SAMPLE INTO 4 SUB-DIVIDED SURFACES =====
3 =====

-----
4 ===== APPLY 2nd ORDER SURFACE FITTING TO EXTRACT ROUGHNESS =====
-----

noOfAcceptedFitting = 0;
RaAcc = 0;
RsqAcc = 0;
for iSd=1:(noDiv^2)
    [M,N] = size(I2sDiv(iSd).Z);

    X = I2sDiv(iSd).X(1:M,1:N);
    Y = I2sDiv(iSd).Y(1:M,1:N);
    Z = I2sDiv(iSd).Z(1:M,1:N);

    %%%%%%%%%%% Give A Real Surface %%%%%%%%%%%
    rowIdx = 0;
    for i=1:M %noDivSp
        for j=1:N %noDivSp
            rowIdx = rowIdx + 1;
            Xv = X(i,j);
            Yv = Y(i,j);
            Zv = Z(i,j);

            nYv = 2;
            V(rowIdx,1) = (Xv^2)*(Yv^nYv);
            V(rowIdx,2) = (Xv^1)*(Yv^nYv);
            V(rowIdx,3) = (Xv^0)*(Yv^nYv);

            nYv = 1;
            V(rowIdx,4) = (Xv^2)*(Yv^nYv);
            V(rowIdx,5) = (Xv^1)*(Yv^nYv);
            V(rowIdx,6) = (Xv^0)*(Yv^nYv);

            nYv = 0;
            V(rowIdx,7) = (Xv^2)*(Yv^nYv);
            V(rowIdx,8) = (Xv^1)*(Yv^nYv);
            V(rowIdx,9) = (Xv^0)*(Yv^nYv);

            Q(rowIdx,1) = Zv;
        end;
    end;

    VtV= V'*V;
    cf = pinv(VtV)*V'*Q;

    % % % % % Reconstruct

```

```

Zcc = 0;
nYv = 2;
Zcc = Zcc + cf(1)*(X.^2).*(Y.^nYv);
Zcc = Zcc + cf(2)*(X.^1).*(Y.^nYv);
Zcc = Zcc + cf(3)*(X.^0).*(Y.^nYv);

nYv = 1;
Zcc = Zcc + cf(4)*(X.^2).*(Y.^nYv);
Zcc = Zcc + cf(5)*(X.^1).*(Y.^nYv);
Zcc = Zcc + cf(6)*(X.^0).*(Y.^nYv);

nYv = 0;
Zcc = Zcc + cf(7)*(X.^2).*(Y.^nYv);
Zcc = Zcc + cf(8)*(X.^1).*(Y.^nYv);
Zcc = Zcc + cf(9)*(X.^0).*(Y.^nYv);

Zr = Zcc;
err = abs(Z-Zr);

Ra = mean(mean(err));
meanZ = mean(mean(Z));
SStot = sum(sum((Z-meanZ).^2));
SSerr = sum(sum((Z-Zr).^2));
Rsq = 1 - (SSerr/SStot);

Ra_2nd(iSd) = Ra;
Rsq_2nd(iSd) = Rsq;

if and(Rsq_2nd(iSd)>=0.90,Rsq_2nd(iSd)<=1.0)
    noOfAcceptedFitting = noOfAcceptedFitting + 1;
    RaAcc = RaAcc + Ra_2nd(iSd);
    RsqAcc = RsqAcc + Rsq_2nd(iSd);
end;
end;

Ra_2nd_Final = NaN;
Rsq_2nd_Final = NaN;

if noOfAcceptedFitting>0
    Ra_2nd_Final = RaAcc/noOfAcceptedFitting;
    Rsq_2nd_Final = RsqAcc/noOfAcceptedFitting;
end;

ResMat(1,1) = Ra_2nd_Final;
ResMat(1,2) = Rsq_2nd_Final;
% =====
% ===== End of APPLY 2nd ORDER SURFACE FITTING TO EXTRACT ROUGHNESS =====
% =====

% =====
% ===== APPLY 3rd ORDER SURFACE FITTING TO EXTRACT ROUGHNESS =====
% =====

noOfAcceptedFitting = 0;
RaAcc = 0;
RsqAcc = 0;
for iSd=1:(noDiv^2)
    [M,N] = size(I2sDiv(iSd).Z);

    X = I2sDiv(iSd).X(1:M,1:N);
    Y = I2sDiv(iSd).Y(1:M,1:N);
    Z = I2sDiv(iSd).Z(1:M,1:N);

    %%%%%%%%%% Give A Real Surface %%%%%%%%%%
    rowIdx = 0;
    for i=1:M %noDivSp

```

```

for j=1:N %noDivSp
    rowIdx = rowIdx + 1;
    Xv = X(i,j);
    Yv = Y(i,j);
    Zv = Z(i,j);

    nYv = 3;
    V(rowIdx,1) = (Xv^3)*(Yv^nYv);
    V(rowIdx,2) = (Xv^2)*(Yv^nYv);
    V(rowIdx,3) = (Xv^1)*(Yv^nYv);
    V(rowIdx,4) = (Xv^0)*(Yv^nYv);

    nYv = 2;
    V(rowIdx,5) = (Xv^3)*(Yv^nYv);
    V(rowIdx,6) = (Xv^2)*(Yv^nYv);
    V(rowIdx,7) = (Xv^1)*(Yv^nYv);
    V(rowIdx,8) = (Xv^0)*(Yv^nYv);

    nYv = 1;
    V(rowIdx,9) = (Xv^3)*(Yv^nYv);
    V(rowIdx,10) = (Xv^2)*(Yv^nYv);
    V(rowIdx,11) = (Xv^1)*(Yv^nYv);
    V(rowIdx,12) = (Xv^0)*(Yv^nYv);

    nYv = 0;
    V(rowIdx,13) = (Xv^3)*(Yv^nYv);
    V(rowIdx,14) = (Xv^2)*(Yv^nYv);
    V(rowIdx,15) = (Xv^1)*(Yv^nYv);
    V(rowIdx,16) = (Xv^0)*(Yv^nYv);

    Q(rowIdx,1) = Zv;
end;
end;

VtV= V'*V;
cf = pinv(VtV)*V'*Q;

% 3 3 3 3 % Reconstruct
Zcc = 0;
nYv = 3;
Zcc = Zcc + cf(1)*(X.^3).*(Y.^nYv);
Zcc = Zcc + cf(2)*(X.^2).*(Y.^nYv);
Zcc = Zcc + cf(3)*(X.^1).*(Y.^nYv);
Zcc = Zcc + cf(4)*(X.^0).*(Y.^nYv);

nYv = 2;
Zcc = Zcc + cf(5)*(X.^3).*(Y.^nYv);
Zcc = Zcc + cf(6)*(X.^2).*(Y.^nYv);
Zcc = Zcc + cf(7)*(X.^1).*(Y.^nYv);
Zcc = Zcc + cf(8)*(X.^0).*(Y.^nYv);

nYv = 1;
Zcc = Zcc + cf(9)*(X.^3).*(Y.^nYv);
Zcc = Zcc + cf(10)*(X.^2).*(Y.^nYv);
Zcc = Zcc + cf(11)*(X.^1).*(Y.^nYv);
Zcc = Zcc + cf(12)*(X.^0).*(Y.^nYv);

nYv = 0;
Zcc = Zcc + cf(13)*(X.^3).*(Y.^nYv);
Zcc = Zcc + cf(14)*(X.^2).*(Y.^nYv);
Zcc = Zcc + cf(15)*(X.^1).*(Y.^nYv);
Zcc = Zcc + cf(16)*(X.^0).*(Y.^nYv);

Zr = Zcc;
err = abs(Z-Zr);

```

```

Ra = mean(mean(err));
meanZ = mean(mean(Z));
SStot = sum(sum((Z-meanZ).^2));
SSerr = sum(sum((Z-Zr).^2));
Rsqr = 1 - (SSerr/SStot);

Ra_3rd(iSd) = Ra;
Rsqr_3rd(iSd) = Rsqr;

if and(Rsqr_3rd(iSd)>=0.90, Rsqr_3rd(iSd)<=1.0)
    noOfAcceptedFitting = noOfAcceptedFitting + 1;
    RaAcc = RaAcc + Ra_3rd(iSd);
    RsqrAcc = RsqrAcc + Rsqr_3rd(iSd);
end;
end;

Ra_3rd_Final = NaN;
Rsqr_3rd_Final = NaN;

if noOfAcceptedFitting>0
    Ra_3rd_Final = RaAcc/noOfAcceptedFitting;
    Rsqr_3rd_Final = RsqrAcc/noOfAcceptedFitting;
end;

ResMat(2,1) = Ra_3rd_Final;
ResMat(2,2) = Rsqr_3rd_Final;
% ===== End of APPLY 3rd ORDER SURFACE FITTING TO EXTRACT ROUGHNESS =====
% =====

% ===== SELECT THE BEST Ra BASED ON ITS Rsqr =====
% =====

RsqrMax = max(ResMat(:,2));
idxRa = find(ResMat(:,2)==RsqrMax);
RaFinal = ResMat(idxRa(1),1);
disp(['Average roughness is ', num2str(RaFinal), ' mm']);

```

APPENDIX G: SOURCE CODE OF CLUSTERING (FCM)  
IMPLEMENTATION FOR SCORING SCALINESS (MATLAB CODE)

```

close all;
clear all;
clc;

% =====
% Load training dataset to build clustering system based on FCM algorithm.
% FCM is applied to cluster this combined dataset.
% =====
load('C:\...\xData.mat');
x=sort(x);

% =====
% ===== Membership degrees initialisation based on training dataset =====
% =====
L = x;
P = linspace(min(L),max(L),9);

sL = sort(L);
cPMi = P(1);
cPMx = P(9);

for i = 1:length(sL);

    Lv = sL(i);

    % score 1
    cPt = P(2);
    if Lv<cPt
        mD1(i,1) = (1/(cPt-cPMi))*(Lv-cPMi);
    end;
    if Lv==cPt
        mD1(i,1) = 1;
    end;
    if Lv>cPt
        mD1(i,1) = (-1/(cPMx-cPt))*(Lv-cPt) + 1;
    end;

    % score 2
    cPt = P(4);
    if Lv<cPt
        mD2(i,1) = (1/(cPt-cPMi))*(Lv-cPMi);
    end;
    if Lv==cPt
        mD2(i,1) = 1;
    end;
    if Lv>cPt
        mD2(i,1) = (-1/(cPMx-cPt))*(Lv-cPt) + 1;
    end;

    % score 3

```

```

cPt = P(6);
if Lv<cPt
    mD3(i,1) = (1/(cPt-cPMi))*(Lv-cPMi);
end;
if Lv==cPt
    mD3(i,1) = 1;
end;
if Lv>cPt
    mD3(i,1) = (-1/(cPMx-cPt))*(Lv-cPt) + 1;
end;

% score 4
cPt = P(8);
if Lv<cPt
    mD4(i,1) = (1/(cPt-cPMi))*(Lv-cPMi);
end;
if Lv==cPt
    mD4(i,1) = 1;
end;
if Lv>cPt
    mD4(i,1) = (-1/(cPMx-cPt))*(Lv-cPt) + 1;
end;
end;

figure,
plot(sL,mD1, sL,mD2,sL,mD3, sL,mD4);

u={mD1 mD2 mD3 mD4};

% =====
% == END of Membership degrees initialisation based on training dataset ==
% =====

% =====
% ===== SET THE NUMBER OF CLUSTER =====
% =====
k = 4; % number of cluster
N = length(x);

% Fuzziness coefficient is assigned. The best values are between 1.4 and
% 2.8 as mentioned in http://fuzziness.org/fcm
m = 2;

% Initialisation on objective function (OldJm), objective function changes
% during the iteration (deltaJm), and number of interation (noI)
OldJm = 1e9;
deltaJm = 1e9;
noI = 0;

% =====
% ===== DETERMINE MEMBERSHIP DEGREES OF CLUSTERED DATASET =====
% =====
while deltaJm > 1e-5
    noI = noI + 1;

    % Centroids determination
    for j=1:k
        A = 0;
        B = 0;
        for i=1:N
            A = A + (u(i,j)^m*x(i));
            B = B + u(i,j)^m;
        end
    end
end

```

```

        end;
        C(j) = A/B;
    end;

    % Membership degrees determination
    pw = 2/(m-1);
    for j=1:k
        for i=1:N
            A= 0;
            for l=1:k
                A0 = abs(x(i)-C(j));
                B0 = abs(x(i) - C(l));
                A = A + (A0/B0)^pw;
            end;
            u(i,j) = 1/A;
        end;
    end;

    % Objective function determination
    Jm = 0;
    for i=1:N
        for j=1:k
            Jm = Jm + (u(i,j)^m)*(x(i)-C(j))^2;
        end;
    end;

    % update on objective function
    deltaJm = abs(Jm - OldJm);
    OldJm = Jm;

    % showing the outputs in the command window
    JmA(noI) = Jm;
    disp([num2str(noI), ' : ', num2str(Jm)])

    % to prepare some coloums containing cluster centroids
    for i=1:k
        c(i).data = ones(N,1)*C(i);
    end;

    finalMat is used to show the dataset, membership degrees, centroids,
    and objective function
    JmFinalMat = ones(N,1)*Jm;
    finalMat = [];
    finalMat = [x u];
    for i=1:k
        finalMat = [finalMat c(i).data];
    end;
    finalMat = [finalMat JmFinalMat];

    finalMatStruct(noI).data = finalMat;
    disp('-----')
    disp(noI);
    disp(finalMat);
    disp(' ')
end;

% =====
% ===== End of MEMBERSHIP DEGREES DETERMINATION =====
% =====

% =====
% ===== CONSTRUCT MEMBERSHIP FUNCTIONS OF CLUSTERED DATASET =====
% =====

% arrange the columns of membership degrees according to the centroid
% ascending order
noMaxI = length(finalMatStruct);

```

```

finalMatData = finalMatStruct(noMaxI).data;

finalMatData = sortrows(finalMatData,1);
xData = finalMatData(:,1);

for i=1:k
    idxMat(i,1) = i+1;
    idxMat(i,2) = idxMat(i,1)+k;
    idxMat(i,3) = finalMatData(1, (k+1+i));
end;

idxMat2 = sortrows(idxMat,3);

for i=1:k
    idxMatInt = floor(idxMat2(i));
    mFunc(i).d = finalMatData(:,idxMatInt);
end;
centroids = sort(C);

x = xData;
miX = min(xData);
mxX = max(xData);

% Fit the membership degrees of clustered dataset into a gaussian function
% Matlab provides following Gaussian functions
-----
% MODELNAME          EQUATION
% gauss1             Y = a1*exp(-((x-b1)/c1)^2)
% gauss2             Y = a1*exp(-((x-b1)/c1)^2)+a2*exp(-((x-b2)/c2)^2)
% gauss3             Y = a1*exp(-((x-b1)/c1)^2)+...+a3*exp(-((x-
b3)/c3)^2)
% ...
% gauss6             Y = a1*exp(-((x-b1)/c1)^2)+...+a8*exp(-((x-
b8)/c8)^2)
-----

% Fit the membership degrees of clustered dataset to obtain k (number of
% cluster) gaussian
% functions. The function coefficients and the fitting performance
% parameters are stored
% in cfunCls(i).data and rsquareCls(i).data respectively.
for i=1:k
    y = mFunc(i).d;
    [cfun, rsquare] = fit(x,y,'gauss2');
    cfunCls(i).data = cfun;
    rsquareCls(i).data = rsquare;
end;
% =====
% ===== End of CONSTRUCTION ON MEMBERSHIP FUNCTIONS =====
% =====

% =====
% ===== SHOW THE CLUSTERED DATASET AND ITS MEMBERSHIP FUNCTIONS IN THE PLOT =====
% =====

figure,
subplot(211);
for i=1:k
    plot(xData, mFunc(i).d)
    hold all
end;
grid on
axis([miX mxX 0 1.2]);
labelFontSize = 12;
xlabel('Scaliness (mm)', 'FontSize', labelFontSize, 'fontweight', 'b')
ylabel('Membership degree', 'FontSize', labelFontSize, 'fontweight', 'b')

```

```

title('Membership degree of clustered
dataset','FontSize',labelFontSize,'fontweight','b')

subplot(212);
xC = linspace(miX,mxX,100);
for i=1:k

    fitR_sq = rsquareCls(i).data.rsquare;

    if fitR_sq >= 0.9
        a1 = cfunCls(i).data.a1;
        b1 = cfunCls(i).data.b1;
        c1 = cfunCls(i).data.c1;

        a2 = cfunCls(i).data.a2;
        b2 = cfunCls(i).data.b2;
        c2 = cfunCls(i).data.c2;

        fittedMemFunc = a1*exp(-((xC-b1)/c1).^2) + a2*exp(-((xC-b2)/c2).^2);
    end;

    plot(xC,fittedMemFunc), hold all
end;

% preparing title on the plot
plotTitle = '';
for i=1:k
    tVal = ['C(',num2str(i),')= ',num2str(centroids(i)),'];
    plotTitle = [plotTitle tVal];
end;
title(plotTitle);
xlabel('Scaliness (mm)','FontSize',labelFontSize,'fontweight','b')
ylabel('Membership degree','FontSize',labelFontSize,'fontweight','b')
title('Membership function of clustered
dataset','FontSize',labelFontSize,'fontweight','b')
grid on
axis([miX mxX 0 1.2]);
% =====
% ===== End of SHOWING THE CLUSTERED DATASET & MEMBERSHIP FUNCTIONS =====
% =====

% =====
% ===== CLASSIFY AND INPUT INTO A CLUSTER =====
% =====

clc;
xVal = input('Input Roughness value ');
nLn = 5;
xLn = xVal*ones(nLn);
yLn = linspace(0,1,nLn);
line(xLn,yLn,'Color','k','LineWidth',3);

for i=1:k
    fitR_sq = rsquareCls(i).data.rsquare;
    if fitR_sq >= 0.9
        a1 = cfunCls(i).data.a1;
        b1 = cfunCls(i).data.b1;
        c1 = cfunCls(i).data.c1;

        a2 = cfunCls(i).data.a2;
        b2 = cfunCls(i).data.b2;
        c2 = cfunCls(i).data.c2;

        probX(i) = a1*exp(-((xVal-b1)/c1).^2) + a2*exp(-((xVal-b2)/c2).^2);
    end;
end;

```



## APPENDIX H: LIST OF PUBLICATIONS

### Journals

1. Ahmad Fadzil M.H., **Esa Prakasa**, Vijanth S.A., H. Nugroho, Suraiya H.H., Azura M.A., "3D Surface Roughness Measurement for Scaliness Scoring of Psoriasis Lesions", *Computers in Biology and Medicine*, (Accepted to be published: 16 August 2013). Elsevier. (Impact Factor in 2012: **1.162**).
2. Ahmad Fadzil M.H., **Esa Prakasa**, H. Fitriyah, H. Nugroho, Suraiya H.H., Azura M.A., "Validation on 3D Surface Roughness Algorithm for Measuring Roughness of Psoriasis Lesion", *International Journal of Biological and Life Sciences* 8:4 2012, WASET Journal. (Indexed by Scopus).
3. Ahmad Fadzil M.H., **Esa Prakasa**, Vijanth S.A., H. Nugroho, C.H. Chong, Azura M.A., Suraiya H.H., "Development of Body Surface Area Measurement using Multi-View Imaging for Psoriasis Area Assessment", *Australasian Physical and Engineering Sciences in Medicine Journal*, Springer Verlag, Volume 34, Number 4, 559-637, 2011 (Impact Factor in 2012: **0.885**).
4. Ahmad Fadzil M.H., H. Nugroho, **Esa Prakasa**, Vijanth S.A., Azura M.A., Suraiya H.H., "Soft Clustering of Lesion Erythema for Psoriasis Assessment", *Journal of Investigative Dermatology* 2012, Volume 132, Nature Publishing Group. (Impact Factor in 2012: **6.193**).

### Book Chapter

1. Ahmad Fadzil M.H., **Esa Prakasa**, H. Fitriyah, H. Nugroho, Azura M.A., Suraiya H.H., "High Order Polynomial Surface Fitting for Measuring Roughness of Psoriasis Lesion". The paper is published as Book Chapter in *Lecture Notes in Computer Science* Volume 7066, Springer Verlag.
2. Ahmad Fadzil MH, **Esa Prakasa**, "Skin Surface Roughness Measurement for Assessing Scaliness of Psoriasis Lesion". The paper is published as Book Chapter in *Surface Imaging for Biomedical Applications*. Published: April 15, 2014 by CRC Press.
3. Ahmad Fadzil MH, **Esa Prakasa**, "Determination of Lesion Colour for Clustering Psoriasis Erythema". The paper is published as Book Chapter in *Surface Imaging for Biomedical Applications*, Published: April 15, 2014 by CRC Press.
4. Ahmad Fadzil MH, **Esa Prakasa**, "Body Surface Area Measurement for Lesion Area Assessment". The paper is published as Book Chapter in *Surface Imaging for Biomedical Applications*, Published: April 15, 2014 by CRC Press.

## Conferences

1. Ahmad Fadzil M.H., **Esa Prakasa**, "Digital Image Analysis-Assessment of Scaliness and Thickness for PASI Scoring", presented at The National Postgraduate Conference on Engineering, Science, and Technology (NPC) 2009. Universiti Teknologi PETRONAS. Seri Iskandar, Malaysia.
2. Ahmad Fadzil M.H., **Esa Prakasa**, H. Nugroho, H. Fitriyah, Suraiya H.H., Azura M.A., "Parallel Lines Extraction Approach to 3D Image Skin Surface for Roughness Characterization", presented at The WACBE World Congress on Bioengineering 2009, Hong Kong, China.
3. Ahmad Fadzil M.H., **Esa Prakasa**, H. Fitriyah, H. Nugroho, Suraiya H.H., Azura M.A., "Validation on 3D Surface Roughness Algorithm for Measuring Roughness of Psoriasis Lesion", presented at the International Conference on Medical Informatics and Biomedical Engineering (ICMIBE) 2010, Rio de Janeiro, Brazil.
4. Ahmad Fadzil M.H., **Esa Prakasa**, Vijanth S.A, H. Nugroho, Chi H.C, Azura M.A, Suraiya H.H, "Development of Body Surface Area Measurement using Multi-View Imaging for Psoriasis Area Assessment", presented at the Engineering and Physical Sciences in Medicine and the Australian Biomedical Engineering Conference (EPSM-ABEC) 2011, Darwin, Australia.
5. Ahmad Fadzil M.H., **Esa Prakasa**, H. Fitriyah, H. Nugroho, Azura M.A. S.H Hussein, "High Order Polynomial Surface Fitting for Measuring Roughness of Psoriasis Lesion", presented at The 2nd International Visual Informatics Conference (IVIC) 2011, Kuala Lumpur, Malaysia.
6. Ahmad Fadzil M.H., **Esa Prakasa**, H. Nugroho, Azura M.A, Suraiya H.H. " Sample Area for Surface Roughness Determination of Skin Surfaces", presented at The 4th International Conference on Intelligent and Advanced System (ICIAS) 2012, Kuala Lumpur, Malaysia.
7. Ahmad Fadzil M.H., **Esa Prakasa**, H. Nugroho, Azura M.A, Suraiya H.H, " Body Surface Area Measurement and Soft Clustering for PASI Area Assessment", presented at the 34th Annual International Conference of the IEEE Engineering in Medicine and Biology Society (EMBC 2012), San Diego, USA.
8. Ahmad Fadzil M.H., H. Nugroho, **Esa Prakasa**, Vijanth S.A., Azura M.A, Suraiya H.H, "Soft Clustering of Lesion Erythema for Psoriasis Assessment", presented at The 42nd Annual Meeting of the European Society for Dermatological Research (ESDR) 2012, Venice, Italy.
9. Ahmad Fadzil M.H., **Esa Prakasa**, H. Nugroho, Vijanth S.A., "Implementation of Fuzzy C-Means Clustering for Psoriasis Assessment on Lesion Erythema", presented at The 2012 IEEE Symposium on Industrial Electronics and Applications (ISIEA 2012), Bandung, Indonesia.

10. Azura M.A., Suraiya H.H., R. Baba, H. Nugroho, **Esa Prakasa**, Ahmad Fadzil MH. "Objective Evaluation of Psoriasis Severity using a Computerized PASI Scoring System", presented at The 4th Congress of The Psoriasis International Network (PSORIASIS) 2013, Paris, France.

### **Conferences, contributing as co-author**

1. Ahmad Fadzil M.H., H. Nugroho, **Esa Prakasa**, Azura M.A., Suraiya H.H., "Skin Roughness Measurement for Lesion Classification", presented at The WACBE World Congress on Bioengineering 2009, Hong Kong, China.
2. Ahmad Fadzil M.H., H. Fitriyah, **Esa Prakasa**, H. Nugroho, Suraiya H.H., Azura M.A., "Reference Line Construction Approach for Thickness Characterization in 3D Skin Surface Images" , presented at The WACBE World Congress on Bioengineering 2009, Hong Kong, China.
3. Ahmad Fadzil M.H., H. Fitriyah, **Esa Prakasa**, H. Nugroho, Suraiya H.H., Azura M.A., "Thickness Characterization of 3D Skin Surface Images Using Reference Line Construction Approach", presented at The 1st International Visual Informatics Conference (IVIC) 2009, Kuala Lumpur, Malaysia. The paper is published as Book Chapter published in Lecture Notes in Computer Science Volume 5857, Springer Verlag.
4. Ahmad Fadzil M.H., H. Fitriyah, **Esa Prakasa**, H. Nugroho, Suraiya H.H., Azura M.A., "Objective Assessment of Psoriasis Lesion Thickness for PASI Scoring using 3D Digital Imaging", presented at The International Conference on Medical Informatics and Biomedical Engineering (ICMIBE) 2010, Rio de Janeiro, Brazil.
5. Ahmad Fadzil M.H., H. Nugroho, **Esa Prakasa**, H. Fitriyah, Azura M.A., Suraiya H.H., "3D-based Skin Roughness Measurement for Lesion Classification", IEEE Symposium on Industrial Electronics & Applications (ISIEA) 2009, Kuala Lumpur, Malaysia.
6. Ahmad Fadzil M.H., H. Fitriyah, **Esa Prakasa**, Vijanth S.A., Suraiya H.H., Azura M.A., "In vivo 3D Thickness Measurement of Skin Lesion", IEEE EMBS Conference on Biomedical Engineering and Sciences (IECBES) 2010, Kuala Lumpur, Malaysia.

### **Technical Documents**

1. Prof. Ir. Dr. Ahmad Fadzil M.H., Dr. Azura M.A., Dr. Chong Yew Thong, Puan Sri Dr. Suraiya H.H., Dr. Roshidah Baba, **Esa Prakasa**, Hurriyatul Fitriyah, Hermawan Nugroho, "Protocol for the Clinical Study: Objective Evaluation of Psoriasis Severity using A New Computerised Psoriasis Area and Severity Index ( $\alpha$ -PASI)". The protocol was approved by Malaysian Research and Ethics Committee (MREC), Ministry of Health on 4 April 2010 (NMRR-09-1098-4863).
2. Dr. Azura M.A., Dr. Chong Yew Thong, Puan Sri Dr. Suraiya H.H., Prof. Ir. Dr. Ahmad Fadzil M.H., **Esa Prakasa**, H. Nugroho, H. Fitriyah, "Technical Report: Observational Clinical Study on Computerised System for Monitoring and

Scoring of Psoriasis Area and Severity Index". Centre for Intelligent Signal & Imaging Research and Department of Dermatology, Hospital Kuala Lumpur. October 2011. The clinical study was conducted from March to October 2010.

3. Prof. Ir. Dr. Ahmad Fadzil M.H., F.A.Sc. FIEM, **Esa Prakasa**, H. Nugroho. "TechnoFund Completion Report: Computerised System for Monitoring and Scoring of Psoriasis Area and Severity Index (TF 0308 C041)", 26 October 2011.

# APPENDIX I: PATENT DOCUMENT OF SCALINESS ALGORITHM



(19) **United States**  
 (12) **Patent Application Publication** (10) **Pub. No.: US 2012/0308096 A1**  
 Mohamad Hani et al. (43) **Pub. Date: Dec. 6, 2012**

(54) **METHODOLOGY AND APPARATUS FOR OBJECTIVE, NON-INVASIVE AND IN VIVO ASSESSMENT AND RATING OF PSORIASIS LESION SCALINESS USING DIGITAL IMAGING**

(86) PCT No.: **PCT/MY11/00643**  
 § 371 (c)(1),  
 (2), (4) Date: **Apr. 2, 2012**  
 (30) Foreign Application Priority Data  
 Nov. 8, 2010 (MY) PI 2010005221

(75) Inventors: **Abmad Fadzil Mohamad Hani, Irenoh (MY), Esa Prakasa, Irenoh (MY)**

Publication Classification

(73) Assignee: **INSTITUTE OF TECHNOLOGY PETRONAS SDN BHD, Irenoh, Perak (MY)**

(51) Int. Cl.: **G06K 9/00 (2006.01)**

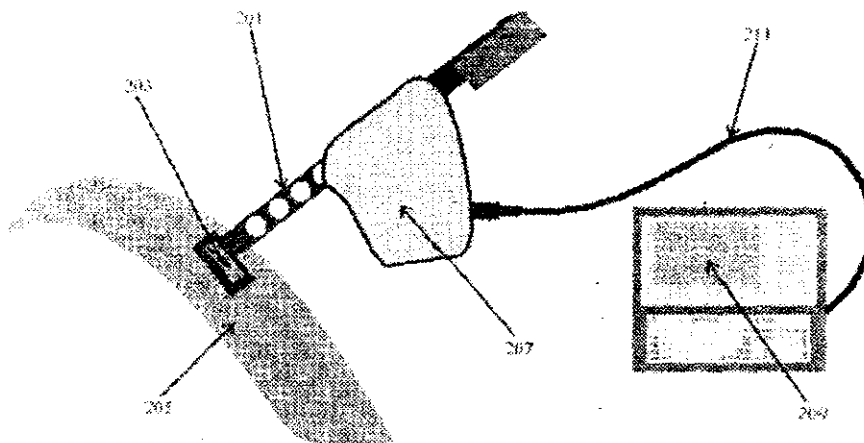
(52) U.S. Cl.: **382/128**

(57) **ABSTRACT**

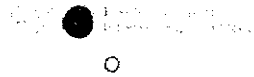
(21) Appl. No.: **13/499,784**

The present invention relates generally to a method and apparatus for assessing data from digital images of psoriasis lesion for said psoriasis lesion scaliness by utilizing a developed computer vision system to obtain Psoriasis Area and Severity Index (PASI) parameters in particular.

(22) PCT Filed: **May 9, 2011**



APPENDIX J: CERTIFICATE OF AWARD (ITEX 2009)



*Certificate of Award*

*This is to certify that*

**PROF IR DR AHMAD FADZIL M HANIFF, DANI IHTATHO,  
HERMAWAN NUGROHO, HURRIYATUL FITRIYAH,  
ESA PRAKASA**

*has been awarded the*

**ITEX GOLD MEDAL**

*for the invention*

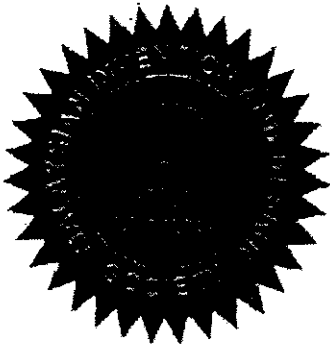
**COMPUTERISED PSORIASIS AREA SEVERITY INDEX (PASI)  
SCORING FOR PSORIASIS LESION**

*at the*

**20<sup>th</sup> International Invention, Innovation & Technology Exhibition  
ITEX 2009, Kuala Lumpur, Malaysia**

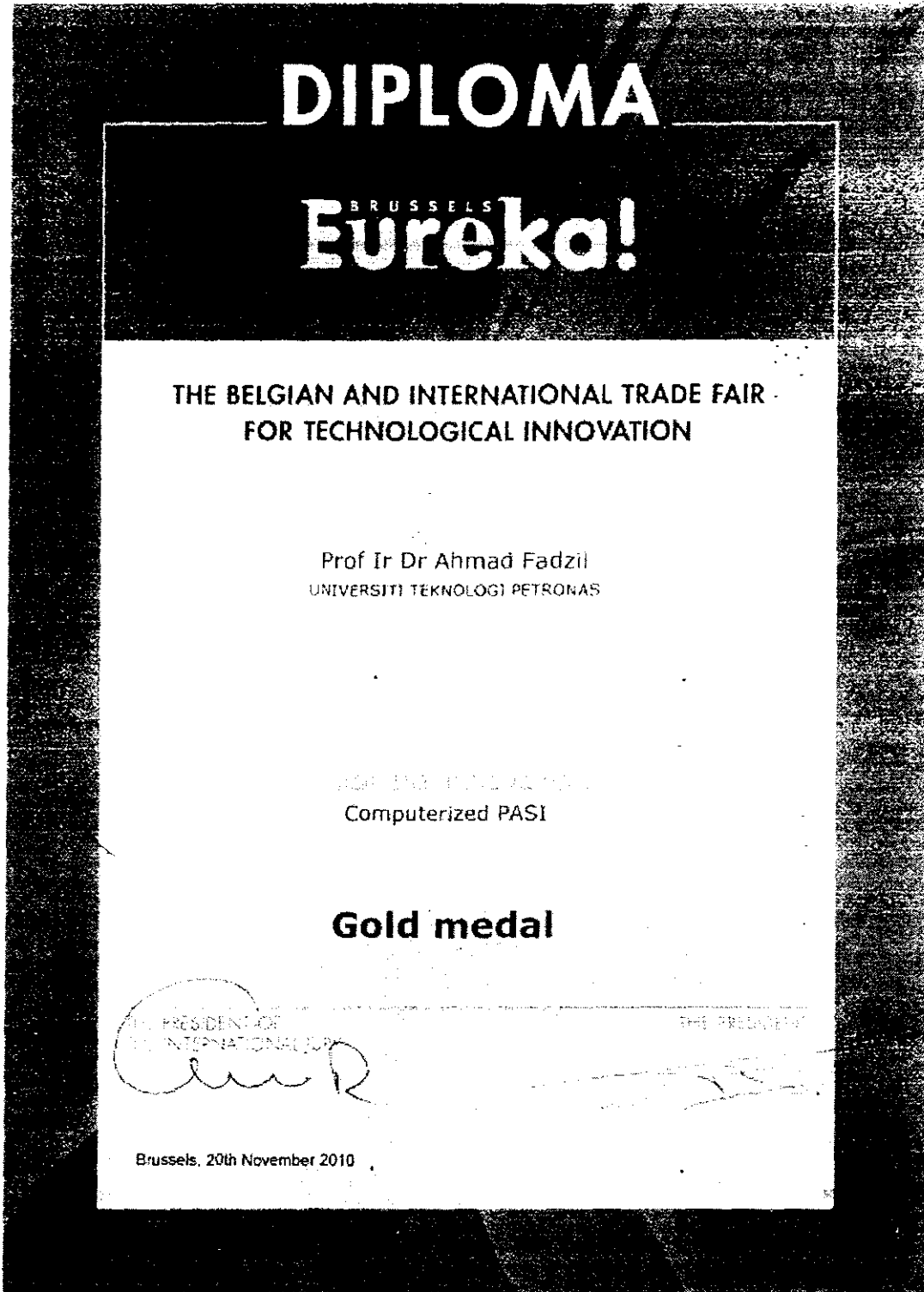
*held from*

**15<sup>th</sup> - 17<sup>th</sup> May 2009**



  
Academician Tan Sri Emeritus Professor  
Dato' Dr Augustine S. H. Ong  
President  
Malaysian Invention and Design Society

APPENDIX K: CERTIFICATE OF AWARD (INNOVA 2010)



APPENDIX L: CERTIFICATE OF AWARD (MTE 2012)



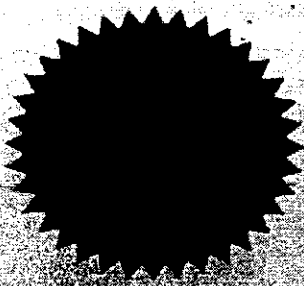
This Certificate of Award is presented to

**Ahmad Fadzil M. Hani**  
**Esa Prakasa**  
**Hermawan Nugroho**  
**Hurriyatul Fitriyah**

For the invention/innovation of

**Computerised System for Monitoring and Scoring  
of Psoriasis Area and Severity Index (PASI)**

Malaysia Technology Expo 2012  
16 - 18 February 2012  
Kuala Lumpur



  
Ahmad Fadzil bin Hani  
Secretary General  
Malaysia Association of Research Scientists

  
Dr. Wan Roszaid bin W Zaini  
Chairman  
Organising Committee MTE 2012